IL
NUOVO CIMENTO
ORGANO DELLA SOCIETÀ ITALIANA DI FISICA
SOTTO GLI AUSPICI DEL CONSIGLIO NAZIONALE DELLE RICERCHE

VOL. II, N. 3 *Serie decima* 1° Settembre 1955

Analytical Method for Obtaining Phase Shifts from Experimental Data on Pion-Proton Scattering.

E. CLEMENTEL, G. POIANI and C. VILLI

Istituti di Fisica delle Università di Padova e di Trieste
Istituto Nazionale di Fisica Nucleare - Sezione di Padova

(ricevuto il 6 Giugno 1955)

Summary. — An analytical method is outlined for obtaining phase shifts from experimental data on pion-proton scattering. As an example phase shifts for $\pi^+ \to \pi^+$ scattering at 120, 135 and 300 MeV are calculated. The graphical translation of this method reveals the working principle of a mechanical phase shift analyzer.

The purpose of this note is to describe a convenient analytical method for finding the pion-nucleon phase shifts, which gives, with small amount of numerical calculations and in a more direct way than the Ashkin and Vosko graphical method [1], a clear insight into the mathematical structure of the phase shift fitting problem.

The method has been developed according to the basic assumption of the charge independence of nuclear forces, and limiting the contributions to the scattering to S and P waves only [2]. For easy reference we list in the Appendix the formulas of the differential cross sections for pion-proton scattering and of the coefficients in terms of phase shifts.

---

[1] J. ASHKIN and S. H. VOSKO: *Phys. Rev.* **91** 1248 (1953).

[2] H. L. ANDERSON, E. FERMI, D. E. NAGLE and G. B. YODH: *Phys. Rev.*, **86**, 793 (1952); E. FERMI, N. METROPOLIS and E. F. ALEI: *Phys. Rev.*, **95**, 1581 (1954); F. DE HOFFMANN, N. METROPOLIS, E. F. ALEI and H. A. BETHE: *Phys. Rev.*, **95**, 1586 (1954).

Although solutions of the phase shift equations have been searched by means of electronic computers, the suspicion arised that the method used by Fermi *et al.* could miss some solutions, fitting the data equally well. Therefore, it was thought of interest to study the problem on analytical ground, which so far has never been considered in the literature.

The application of this method, which takes the clue from a parametrization method applied to the analysis of proton-proton scattering ([3]), depends on first obtaining the nine experimental quantities $A_{\pm}$, $B_{\pm}$, $C_{\pm}$ and A_0, B_0, C_0 fiitting, within experimental errors, the data.

To make the determination of the phase shifts consistent with such experimental numbers, the phases α_{33} and α_{31}, occurring with α_3 in the process (*a*) $\pi^+ \to \pi^+$, are expressed as functions of α_3, and then α_3, is determined using the known value of B_+. In this way, the P-wave phase shifts for the $T=\frac{3}{2}$ state depend, for a fixed value of α_3, on the experimental numbers A_+ and C_+, which are involved in the total cross-section $\sigma_T(\pi^+)$. It is clear that this analytical procedure is particularly suitable for testing the stability of the phase shifts against variations of the coefficients A_+, B_+, and C_+.

Once the sets of the three phase shifts for the $T=\frac{3}{2}$ state are determined, the solution for the process (*b*) $\pi^- \to \pi^-$ can be evaluated. To disentagle the mathematical problem of finding, for any given set α_3, α_{33}, α_{31}, the three phase shifts for the $T=\frac{1}{2}$ state, we use the optical theorem and therefore, because of exchange scattering, the determination of the phase shifts α_{11}, α_{13} and α_1 depends also on the experimental numbers A_0 and C_0, which appear in the total cross-section for the process (*c*) $\pi^- \to \pi^0$. Selection among all sets of the six phase shifts is provided by fitting the experimental values A_- and B_0 and by the continuity condition of all the phase shifts versus pion energy.

First we consider the process (*a*). The complex quantities $\boldsymbol{a}_+$, $\boldsymbol{b}_+$ and $\boldsymbol{c}_+$ are expressed as functions of α_3, A_+ and C_+ by

$$(1) \qquad \begin{cases} |\boldsymbol{a}_+|^2 = 2(1 - \cos 2\alpha_3) \equiv r_+(\alpha_3), \\ |\boldsymbol{b}_+|^2 = 4(A_+ + C_+) - r_+(\alpha_3), \\ |\boldsymbol{c}_+|^2 = 4A_+ - r_+(\alpha_3). \end{cases}$$

Taking into account the optical theorem (A,10), we derive

$$(2) \qquad 2\cos 2\alpha_{33} + \cos 2\alpha_{31} = 3 + \tfrac{1}{2}r_+ - 2[A_+ + \tfrac{1}{3}C_+] \equiv p_+(\alpha_3),$$

and from the third of Esq. (1) we have

$$(3) \qquad \cos 2(\alpha_{33} - \alpha_{31}) = 1 + \tfrac{1}{2}r_+ - 2A_+ \equiv q_+(\alpha_3).$$

([3]) L. BERETTA, E. CLEMENTEL and C. VILLI: *Nuovo Cimento*, **1**, 739 (1955); *Phys. Rev.*, **98**, 1596 (1955).

It follows that

$$\cos 2\alpha_{33}^{(\pm)} = \lambda_+^2 \pm (\lambda_+^2 - \mu_+)^{\frac{1}{2}}, \qquad \cos 2\alpha_{31}^{(\pm)} = p_+ - 2\cos 2\alpha_{33}^{(\pm)}, \tag{4}$$

where

$$\lambda_+(\alpha_3) = p_+(2 + q_+)(5 + 4q_+)^{-1}, \qquad \mu_+(\alpha_3) = (p_+^2 + q_+^2 - 1)(5 + 4q_+)^{-1}. \tag{5}$$

Once the dependence of $\alpha_{33}^{(\pm)}$ and $\alpha_{31}^{(\pm)}$ on α_3, consistent with the experimental value of $\sigma_T(\pi^+)$ is known, α_3 is determined by means of the following equation

$$4B_+ = \pi_+(3 - q_+) + 2\sin 2\alpha_3 (2\sin 2\alpha_{33}^{(\pm)} + \sin 2\alpha_{31}^{(\pm)}), \tag{6}$$

which solves the problem completely for given values of A_+, B_+ and C_+.

The problem of determining the phase shifts for the $T = \frac{1}{2}$ state according to the previous procedure would be exceedingly difficult because of the dependence of the complex quantities $\boldsymbol{a}_-$, $\boldsymbol{b}_-$ and $\boldsymbol{c}_-$, involved in the process (b), on the corresponding quantities involved in the process (a). Inspection of the following relations, corresponding to Eqs. (1) for the process (a),

$$\left.\begin{aligned} |\boldsymbol{a}_-|^2 &= r_+ - 4[\mathrm{Re}\,(\boldsymbol{a}_+) - 2](1 - \cos 2\alpha_1) + 4\,\mathrm{Im}\,(\boldsymbol{a}_+)\sin 2\alpha_1 \equiv r_-(\alpha_1), \\ |\boldsymbol{b}_-|^2 &= 36(A_- + C_+) - r_-(\alpha_1), \qquad |\boldsymbol{c}_-|^2 = 36A_- - r_-(\alpha_1), \end{aligned}\right\} \tag{7}$$

has suggested as more convenient to determine from the optical theorem (A.11) the following equation

$$\begin{aligned} &2\cos 2\alpha_{13} + \cos 2\alpha_{11} = \\ &\quad = 4 + (k^2/4\pi)\sigma_T(\pi^+) - 3(A_0 + A_-) - (C_0 + C_-) - \cos 2\alpha_1 \equiv p_-(\alpha_1), \end{aligned} \tag{8}$$

and from the definition of B_-

$$2\sin 2\alpha_{13} + \sin 2\alpha_{11} \equiv q_-(\alpha_1), \tag{9}$$

where

$$\begin{aligned} q_-(\alpha_1) = {} & [2\,\mathrm{Im}\,(\boldsymbol{a}_-)]^{-1} \cdot \\ & \cdot [18B_- - 2\,\mathrm{Re}\,(\boldsymbol{a}_-)(p_- - 3) - \mathrm{Re}\,(\boldsymbol{a}_-)\,\mathrm{Re}\,(\boldsymbol{a}_+) - \mathrm{Im}\,(\boldsymbol{a}_-)\,\mathrm{Im}\,(\boldsymbol{a}_+)]. \end{aligned} \tag{10}$$

In this way the problem becomes analytically very simple, and one gets

$$\cos 2\alpha_{11}^{(\pm)} = \lambda_-^2 \pm (\lambda_-^2 - \mu_-)^{\frac{1}{2}}, \qquad \cos 2\alpha_{13}^{(\pm)} = \tfrac{1}{2}(p_- - \cos 2\alpha_{11}^{(\pm)}), \tag{11}$$

where

$$(12) \qquad \begin{cases} \lambda_-(\alpha_1) = \frac{1}{2}p_-(p_-^2 + q_-^2 - 3)(p_-^2 + q_-^2)^{-1}, \\ \mu_-(\alpha_1) = \frac{1}{4}[4q_-^2 - (p_-^2 + q_-^2 - 3)^2]. \end{cases}$$

Eqs. (11), for any given set α_3, α_{33}, α_{31}, express the P-wave phase shifts for the $T=\frac{1}{2}$ state as functions of α_1, which is finally determined by solving the equation

$$(13) \quad 36A_- = r_- + [\mathrm{Re}\,(\boldsymbol{c}_+) + p_- - 3\cos 2\alpha_{11}^{(\pm)}]^2 + [\mathrm{Im}\,(\boldsymbol{c}_+) + q_- - 3\sin 2\alpha_{11}^{(\pm)}]^2.$$

The application of this procedure, according to the assumption made by MARTIN [4] in his analysis of the scattering of negative pions on hydrogen, is very simple. In fact, if the P-wave phase shifts for isotopic spin $\frac{1}{2}$ are assumed to be zero, it follows that $p_-(\alpha_1) = 3$ and $q_-(\alpha_1) = 0$. Then, taking into account the relations between the experimental quantities B_+ and C_+ with the corresponding of the processes (b) and (c), following from the assumption $\alpha_{11} = \alpha_{13} = 0$, it is easy to see that α_1 and therefore, according to Eq. (13), A_+ can be expressed as a function of α_3. In this way the determination of the FERMI and YANG sets for positive pion scattering and the phase shift α_s can be obtained through Eqs. (4) and (6), using only the negative scattering data. An analysis on these lines of the process $\pi^- \rightarrow \pi^-$ will be presented soon (*).

To test the method, we analyze the scattering data for the process (a) at 120 MeV [5], 135 MeV [2] and 300 MeV [6]. The input parameters are given in Table I. Calculations for 135 MeV have been carried out using mean values of A_+ and C_+.

TABLE I. – *Input parameters, Yang* (+) *and Fermi* (—) *phase shifts for* 120, 135 *and* 300 MeV $\pi^+ \rightarrow \pi^+$ *scattering.*

E (MeV)	A_+	B_+	C_+	α_3	$\alpha_{33}^{(+)}$	$\alpha_{31}^{(+)}$	$\alpha_{33}^{(-)}$	$\alpha_{31}^{(-)}$
120	0.34	— 0.31	0.74	— 12.2	10.7	43.9	31.5	— 1.6
135	0.35	— 0.63 ± 0.25	1.6	— 14.0	18.9	51.4	39.6	6.9
300	0.52	0.55	2.55	— 12.0	152.6	108.7	126.3	— 9.8

[4] R. L. MARTIN: *Phys. Rev.*, **95**, 1606 (1954).

(*) *Note added in proof.* - This analysis has already appeared in the August issue of *Nuovo Cimento*, while this paper was in press.

[5] L. FERRETTI, E. MANARESI, G. PUPPI, G. QUARENI and A. RANZI: *Nuovo Cimento*, **1**, 1238 (1955).

[6] R. S. MARGULIES: *Bull. of Am. Phys. Soc.*, **30**, 73 (1955).

From the third of Eqs. (1), it follows that solutions for the phase shift equations exist provided α_3 satisfies the condition $4A_+ \geq r_+(\alpha_3)$. For 120 MeV scattering α_3 varies within the interval $|\alpha_3| \leq 35°.85$, while for 135 MeV scattering $|\alpha_3| \leq 36°.3$ and $|\alpha_3| \leq 46°.15$ for 300 MeV scattering.

Assuming a repulsive interaction in the S state ($\alpha_3 < 0$), it is seen from Eq. (6) that the selection among the eight possible combinations in the expression $2 \sin 2\alpha_{33}^{(\pm)} + \sin 2\alpha_{13}^{(\pm)}$ (four for the the (—)-type and four for the (+)-type solutions) is fixed both in sign and magnitude by the quantity

$$s_+(\alpha_3) = (2 \sin 2\alpha_3)^{-1}[4B_+ - r_+(3 - p_+)] . \tag{14}$$

In each case it has been found only one (+)-type solution, corresponding to the Yang solution, and only one (—)-type solution, corresponding to the Fermi solution. Both solutions belong to the same value of α_3. For 120 MeV and 135 MeV scattering the two solutions satisfy the conditions $\alpha_{33}^{(+)} < \alpha_{31}^{(+)}$, $\alpha_{33}^{(-)} > \alpha_{31}^{(-)}$ and $\alpha_{33}^{(+)} - \alpha_{31}^{(+)} = \alpha_{31}^{(-)} - \alpha_{33}^{(-)}$, whereas for 300 MeV scattering it is found, $\alpha_{33}^{(\pm)} > \alpha_{31}^{(\pm)}$ and $\alpha_{33}^{(+)} - \alpha_{31}^{(+)} = \pi - (\alpha_{33}^{(-)} - \alpha_{31}^{(-)})$, if one assumes, somewhat arbitrarily, that the Fermi α_{31} phase shift is the smallest one and has to be chosen negative [7]. The sets with all the phase shifts reversed in sign represent of course also a possible solution.

In particular, at 135 MeV, because of the limitation of α_3, no solutions are found for $|B_+| > 0.72$; the value $\alpha_3 = -14°$ corresponds to $B_+ = -0.42$. As an example we give in Table II $\cos 2\alpha_{ij}^{(\pm)}$ as function of α_3 for 300 MeV scattering. Since in the region of α_3, where solutions satisfying Eq. (6) are found, it is $\cos 2\alpha_{33}^{(+)} > 0$ and $\sin 2\alpha_{33}^{(+)} < 0$, it follows that $2\alpha_{33}^{(+)}$ is either positive and larger than 270° or negative and smaller than 90°: we reject the latter possibility which would lead to a repulsion in the $P_{\frac{3}{2}}$, $T=\frac{3}{2}$ state.

TABLE II. — *Dependence of* $\cos 2\alpha_{ij}^{(\pm)}$ *on* α_3 *for* 300 MeV $\pi^+ \to \pi^+$ *scattering.*

$\lvert\alpha_3\rvert$	$\cos 2\alpha_{33}^{(+)}$	$\cos 2\alpha_{31}^{(+)}$	$\cos 2\alpha_{33}^{(-)}$	$\cos 2\alpha_{31}^{(-)}$
46.15°	0.433	0.433	0.433	0.433
30°	0.598	— 0.436	— 0.051	0.863
20°	0.593	— 0.569	— 0.140	0.897
12°	0.570	— 0.794	— 0.296	0.939
5°	0.559	— 0.842	— 0.337	0.949
0°	0.556	— 0.852	— 0.347	0.951

[7] Since these calculations are intended to be of an illustrative nature only, we shall not discuss the positive sign for the Fermi phase shift α_{31} at 135 MeV, which is bound to a particular set, most likely unsatisfactory, of values of the input coefficients.

For all energies, the Fermi and Yang sets become identical, at the upper and lower limit of variability of α_3. The possible solutions for the considered energies are listed in Table I, where the phase shifts are given in degrees.

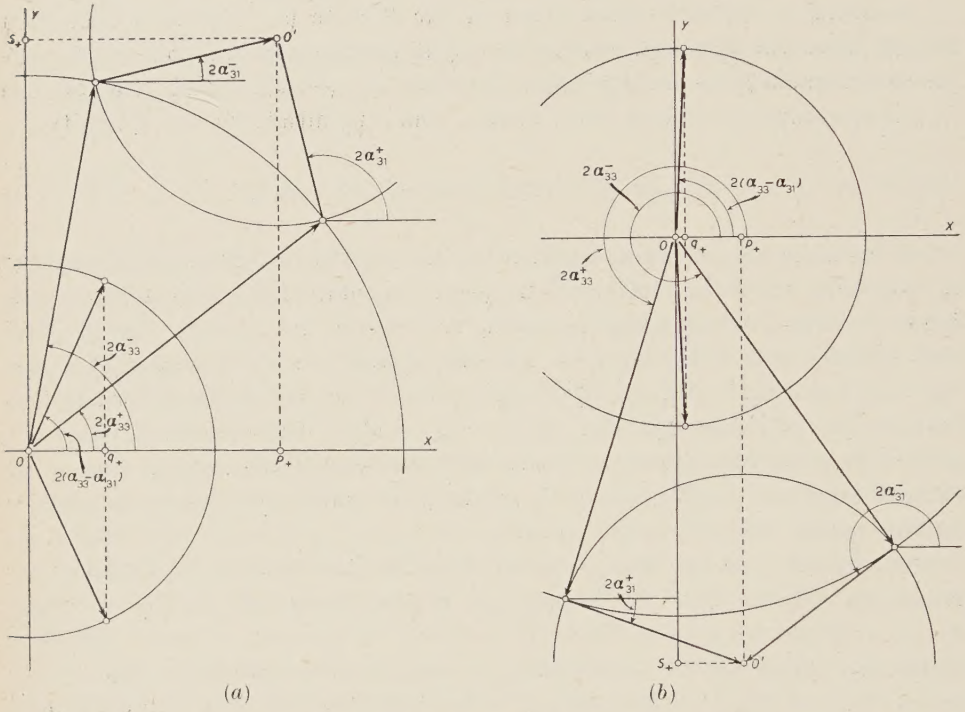

Fig. 1. – Graphical check of the analytical solutions for 135 MeV (*a*) [$\alpha_3 = -14°$] and 300 MeV (*b*) [$\alpha_3 = -12°$] pion-proton scattering. Solutions labelled with (+) and (—) correspond to Yang and respectively Fermi solutions. [In Fig. 1*b* the labels (+) and (—) of the phase shifts have to be interchanged].

To verify the consistency of the sets obtained using this analytical method, we outline its graphical translation based on Eqs. (2), (3) and (6). A self explaining example is given in Fig. 1 for 135 MeV scattering (*a*) and for 300 MeV scattering (*b*).

Chosen a system of orthogonal axes (X, Y), erect, at a distance p_+ from the origin O, a vector of modulus s_+, perpendicular to the X axis. Draw a circle of radius 2 with center in O and a second circle of radius 1 with center in O'. Joining the two intersections with O and O', two sets are found consistent with Eqs. (2) and Eq. (6). To check if also Eq. (3) is satisfied, draw a circle of radius 1 with center in O and erect a line perpendicular to the X axis at a distance q_+ from the origin O. Joining O with the intersection of this line with the latter circle, the values $\alpha_{33}^{(\pm)} - \alpha_{31}^{(\pm)}$ so determined must be consistent with the values obtained in the first step.

Inspection of the geometrical features of the graphical check shows the working principle of a simple mechanical analyzer, which allows a quick determination of the Fermi and Yang solutions with only the knowledge of α_3, $\sigma_T(\pi^+)$ and the differential cross-section at 90°. Such a mechanical analyzer, would be particularly useful when $\sigma_T(\pi^+)$ is known and the scattering data of negative pions alone are used, assuming zero the two P-wave phase shifts for isotopic spin $\frac{1}{2}$. In fact, if as an alternative to the simplified analytical procedure previously outlined, α_1 is evaluated directly from equation (8), using the knowledge of $\sigma_T(\pi^+)$ and of the total cross-section for elastic and charge exchange scattering, the determination of the experimental quantities A_+, B_+ and C_+ is straightforward and Eq. (13) may be used to determine α_3. Finally, taking into account that $p_+ - q_+ = 2[1 - \frac{1}{3}C_+]$, the analyzer gives directly $\cos 2\alpha_{ij}^{(\mp)}$ as function of α_3, solving entirely the analytical problem involved by $\pi^+ \to \pi^+$ scattering up to Eq. (5).

* * *

We thank Dr. L. BERETTA for help in numerical calculations.

APPENDIX

$$\text{(A.1)} \qquad \left\{ \begin{array}{l} \pi^+ + \mathrm{P} \to \pi^+ + \mathrm{P} \\ k^2 \dfrac{\mathrm{d}\sigma(\pi^+)}{\mathrm{d}\Omega} = |(1/2i)\boldsymbol{a}_+ + (1/2i)\boldsymbol{b}_+ \cos\vartheta|^2 + |(1/2i)\boldsymbol{c}_+ \sin\vartheta|^2 \\ \qquad\qquad = A_+ + B_+ \cos\vartheta + C_+ \cos^2\vartheta\,, \end{array} \right.$$

$$\text{(A.2)} \qquad \left\{ \begin{array}{l} \pi^- + \mathrm{P} \to \pi^- + \mathrm{P} \\ k^2 \dfrac{\mathrm{d}\sigma(\pi^-)}{\mathrm{d}\Omega} = |(1/2i)\boldsymbol{a}_- + (1/2i)\boldsymbol{b}_- \cos\vartheta|^2 + |(1/2i)\boldsymbol{c}_- \sin\vartheta|^2 \\ \qquad\qquad = A_- + B_- \cos\vartheta + C_- \cos^2\vartheta\,, \end{array} \right.$$

$$\text{(A.3)} \qquad \left\{ \begin{array}{l} \pi^- + \mathrm{P} \to \pi^0 + \mathrm{N} \\ k^2 \dfrac{\mathrm{d}\sigma(\pi^0)}{\mathrm{d}\Omega} = |(1/2i)\boldsymbol{a}_0 + (1/2i)\boldsymbol{b}_0 \cos\vartheta|^2 + |(1/2i)\boldsymbol{c}_0 \sin\vartheta|^2 \\ \qquad\qquad = A_0 + B_0 \cos\vartheta + C_0 \cos^2\vartheta\,, \end{array} \right.$$

$$\text{(A.4)} \qquad \left\{ \begin{array}{l} \boldsymbol{a}_+ = \exp[2i\alpha_3] - 1 \\ \boldsymbol{b}_+ = 2\exp[2i\alpha_{33}] + \exp[2i\alpha_{31}] - 3 \\ \boldsymbol{c}_+ = \exp[2i\alpha_{33}] - \exp[2i\alpha_{31}]\,, \end{array} \right.$$

$$\text{(A.5)} \qquad \begin{cases} A_+ = (1/4)(|\boldsymbol{a}_+|^2 + |\boldsymbol{c}_+|^2) \\ B_+ = (1/4)(\boldsymbol{a}_+^* \boldsymbol{b}_+ + \boldsymbol{a}_+ \boldsymbol{b}_+^*) \\ C_+ = (1/4)(|\boldsymbol{b}_+|^2 - |\boldsymbol{c}_+|^2)\,, \end{cases}$$

$$\text{(A.6)} \qquad \begin{cases} \boldsymbol{a}_- = \boldsymbol{a}_+ + 2\exp[2i\alpha_1] - 2 \\ \boldsymbol{b}_- = \boldsymbol{b}_+ + 4\exp[2i\alpha_{13}] + 2\exp[2i\alpha_{11}] - 6 \\ \boldsymbol{c}_- = \boldsymbol{c}_+ + 2\exp[2i\alpha_{13}] - \exp[2i\alpha_{11}]\,, \end{cases}$$

$$\text{(A.7)} \qquad \begin{cases} A_- = (1/36)(|\boldsymbol{a}_-|^2 + |\boldsymbol{c}_-|^2) \\ B_- = (1/36)(\boldsymbol{a}_-^* \boldsymbol{b}_- + \boldsymbol{a}_- \boldsymbol{b}_-^*) \\ C_- = (1/36)(|\boldsymbol{b}_-|^2 - |\boldsymbol{c}_-|^2)\,, \end{cases}$$

$$\text{(A.8)} \qquad \begin{cases} \boldsymbol{a}_0 = (3/2)\boldsymbol{a}_+ - (1/2)\boldsymbol{a}_- \\ \boldsymbol{b}_0 = (3/2)\boldsymbol{b}_+ - (1/2)\boldsymbol{b}_- \\ \boldsymbol{c}_0 = (3/2)\boldsymbol{c}_+ - (1/2)\boldsymbol{c}_- \end{cases}$$

$$\text{(A.9)} \qquad \begin{cases} A_0 = (1/18)(|\boldsymbol{a}_0|^2 + |\boldsymbol{c}_0|^2) \\ B_0 = (1/18)(\boldsymbol{a}_0^* \boldsymbol{b}_0 + \boldsymbol{a}_0 \boldsymbol{b}_0^*) \\ C_0 = (1/18)(|\boldsymbol{b}_0|^2 - |\boldsymbol{c}_0|^2)\,, \end{cases}$$

$$\text{(A.10)} \qquad \sigma_T(\pi^+) = -(2\pi/k^2)\ Re(\boldsymbol{a}_+ + \boldsymbol{b}_+) = (4\pi/k^2)(A_+ + C_+/3)$$

$$\text{(A.11)} \qquad \sigma_T(-) = \sigma_T(\pi^-) + \sigma_T(\pi^0) = -(2\pi/3k^2) Re(\boldsymbol{a}_- + \boldsymbol{b}_-) = \\ = (4\pi/k^2)[A_+ + A_0 + (C_- + C_0)/3]\,.$$

RIASSUNTO

Si sviluppa un metodo analitico per il calcolo delle fasi in base ai dati sperimentali sullo scattering pione-protone. A titolo di esempio si esegue il calcolo per il processo $\pi^+ \to \pi^+$ a 120, 135 e 300 MeV. La traduzione grafica del metodo analitico rivela il principio di funzionamento di un analizzatore meccanico delle fasi.

On the Yang-Feldman Formalism.

S. S. Schweber

Brandeis University - Waltham, Massachusetts

(ricevuto il 6 Giugno 1955)

Summary. — The connection between the in- and out-fields and the interaction representation fields is established. The commutation rules for these as well as the symmetric field are obtained. The formulation of scattering theory in terms of these fields is rederived from their connection with the interaction representation.

Introduction.

Much consideration has recently been given to the use of the Heisenberg representation in field theory. Perhaps the basic motivating reason for this has been the hope that a formulation of relativistic field theories which does not use perturbation theory, but still permits practical calculations, might be developed. The work of Yang and Feldman [1], and especially that of Källén [2,3] has contributed much toward that end. Thus Källén, using the Heisenberg representation, has been able to formulate renormalization theory without recourse to perturbation theory and also to establish some properties of the magnitude of the renormalization constants. More recently, it has been shown by Goldberger [4], Low [5], Nambu [6], and others that the

(1) C. N. Yang and D. Feldman: *Phys. Rev.*, **79**, 972 (1950).
(2) G. Källén: *Ark. för Phys.*, **2**, no. 37, 371 (1950).
(3) G. Källén: *Helv. Phys. Acta*, **26**, 755 (1953).
(4) M. L. Goldberger: *Phys. Rev.*, **97**, 508 (1955).
(5) F. Low: *Phys. Rev.*, **96**, 1428 (1954).
(6) Y. Nambu: **98**, 803 (1955).

matrix element for scattering can easily and succinctly be written down in terms of the Heisenberg variables describing the system. Low ([7]) has further extended this work and made it the basis of a new approach to field theoretic scattering problems ([8]).

The present paper rederives some of the results mentioned above starting from the Yang-Feldman formalism. The methods here described were originally developed by the author in the Fall of 1954 (see reference ([4])) for a proof indicating the general validity of certain analytic properties of the scattering matrix element as a consequence of the causality condition as formulated by Gell-Mann, Goldberger and Thirring ([9]). This proof was also given by Goldberger ([4]). Section 1 derives the connection between the in- and out-fields and the interaction representation fields and establishes from the latter the scattering matrix elements in terms of the in- and out-fields. Section 2 derives the commutation rules between the in- and out-fields; and in Section 3 we obtain the closed form for the scattering matrix element. Section 4 gives a preliminary account of some work on the symmetric field.

1. – The Yang-Feldman Formalism.

We shall here briefly recall the basic formulae of the Yang-Feldman formalism. For simplicity, we shall deal with a neutral meson theory for which the equations of motion of the Heisenberg operators are given by (*)

$$(i\gamma^\mu \partial_\mu - M)\boldsymbol{\psi}(x) = -\delta M \boldsymbol{\psi}(x) + G\gamma(x)\boldsymbol{\varphi}(x)\boldsymbol{\psi}(x) \tag{1.1}$$

$$(\Box + \mu^2)\boldsymbol{\varphi}(x) = -G\bar{\boldsymbol{\psi}}(x)\gamma(x)\boldsymbol{\psi}(x) + \delta\mu^2\boldsymbol{\varphi}(x) + \lambda\boldsymbol{\varphi}^3(x)\,. \tag{1.2}$$

The in- and out-meson fields in the present situation are defined by the equations

$$\boldsymbol{\varphi}(x) = \boldsymbol{\varphi}_{\text{in}}(x) - \int_{-\infty}^{-\infty} \Delta_R(x - x')\boldsymbol{j}(x')\,\mathrm{d}^4x' \tag{1.3}$$

$$\boldsymbol{\varphi}(x) = \boldsymbol{\varphi}_{\text{out}}(x) - \int_{-\infty}^{+\infty} \Delta_A(x - x')\boldsymbol{j}(x')\,\mathrm{d}^4x' \tag{1.4}$$

([7]) F. Low: *Phys. Rev.*, **97**, 1392 (1955).

([8]) See also H. Lehmann, K. Symanzik and W. Zimmermann: *Nuovo Cimento*, **1**, 205 (1955).

([9]) M. Gell-Mann, M. L. Goldberger and W. Thirring: *Phys. Rev.*, **95**, 1612 (1954).

(*) Boldface letters are used to denote the Heisenberg variables whereas light-faced ones will indicate interaction representation quantities.

where an adiabatic hypothesis is implied in going to the limits $t \to \pm\infty$ in the integrations of (3) and (4), and where

$$\boldsymbol{j}(x) = +G\bar{\boldsymbol{\psi}}(x)\gamma(x)\boldsymbol{\psi}(x) - \delta\mu^2\boldsymbol{\varphi}(x) - \lambda\boldsymbol{\varphi}^3(x)\,. \tag{1.5}$$

Since

$$\Delta_A(x) - \Delta_R(x) = \Delta(x)\,, \tag{1.6}$$

we may relate the in- and out-fields as follows:

$$\boldsymbol{\varphi}_{\text{out}}(x) = \boldsymbol{\varphi}_{\text{in}}(x) + \int_{-\infty}^{+\infty} \Delta(x - x')\boldsymbol{j}(x')\,\mathrm{d}^4x'. \tag{1.7}$$

The S-matrix in the Heisenberg representation has been shown by YANG and FELDMAN [1] to be that matrix which relates the in- and out-fields:

$$\boldsymbol{\varphi}_{\text{out}}(x) = S^{-1}\boldsymbol{\varphi}_{\text{in}}(x)S\,. \tag{1.8}$$

Using (1.7) and (1.8), the following commutation rules are easily derived [2]:

$$[\boldsymbol{\varphi}_{\text{in}}(x), S] = S\int_{-\infty}^{+\infty} \Delta(x - x')\boldsymbol{j}(x')\,\mathrm{d}^4x' \tag{1.9}$$

$$[\boldsymbol{\varphi}_{\text{out}}(x), S] = \int_{-\infty}^{+\infty} \Delta(x - x')\boldsymbol{j}(x')\,\mathrm{d}^4x' S\,. \tag{1.10}$$

We shall now establish the connection between the in- and out-fields and the interaction representation operators. To this end, we recall that the Heisenberg field variables and the interaction representation ones are related by the following unitary transformation:

$$\boldsymbol{\varphi}(x) = U^{-1}(t, 0)\varphi(x)U(t, 0) \tag{1.11}$$

with $x_0 = t$. We have taken the Heisenberg and interaction representations to coincide at time $t = 0$. We may rewrite Eq. (1.11) as

$$\boldsymbol{\varphi}(x) = \varphi(x) + U^{-1}(t, 0)[\varphi(x), U(t, 0)]\,, \tag{1.12}$$

so that the desired relation will be obtained upon evaluating the commutator

of $\varphi(x)$ with $U(t, 0)$. This task is facilitated if we note that the commutator

$$[\varphi(x), \varphi(y)] = ihc\Delta(x - y) , \tag{1.13}$$

implies that the following operational formula may be written down for the commutator of $\varphi(x)$ with any other operator (denoted by $\bullet$):

$$[\varphi(x), \bullet] = ihc\int \mathrm{d}^4x' \Delta(x - x') \frac{\delta}{\delta\varphi(x')} \bullet \tag{1.14}$$

where $\delta/\delta\varphi(x')$ denotes functional differentiation, with

$$\frac{\delta}{\delta\varphi(x')} \varphi(x) = \delta^{(4)}(x - x') , \tag{1.15}$$

so that

$$[\varphi(x), U(t, 0)] = ihc\int_{-\infty}^{+\infty} \Delta(x - x') \frac{\delta}{\delta\varphi(x')} U(t, 0) . \tag{1.16}$$

Now the Dyson ([10]) expansion of $U(t, 0)$ is given by

$$U(t', t) = \sum_{n=0}^{\infty} \left(-\frac{i}{hc}\right)^n \frac{1}{n!} \int_t^{t'} \mathrm{d}^4x_1 \int_t^{t'} \mathrm{d}^4x_2 \ldots \int_t^{t'} \mathrm{d}^4x_n P(H_1(x_1)H_1(x_2) \ldots H_1(x_n)) \tag{1.16a}$$

$$H_1(x) = G\bar{\psi}(x)\gamma(x)\psi(x)\varphi(x) - \tfrac{1}{2}\delta\mu^2\varphi^2(x) - \delta M\bar{\psi}(x)\psi(x) - \tfrac{1}{4}\lambda\varphi^4(x) , \tag{1.16b}$$

so that

$$[\varphi(x), U(t, 0)] = \int_0^t \mathrm{d}^4x \Delta(x - x') \cdot$$

$$\cdot \sum_{n=0}^{\infty} \left(-\frac{i}{hc}\right)^n \frac{1}{n!} \int_0^t \mathrm{d}^4x_1 \ldots \int_0^t \mathrm{d}^4x_n P(H_1(x_1) \ldots H_1(x_n)j(x')) =$$

$$= \int_0^t \mathrm{d}^4x' \Delta(x - x') P(U(t, 0)j(x')) . \tag{1.17}$$

We now note that Eq. (1.11) may, for times $x_0 = t > 0$, be rewritten in the

([10]) F. J. Dyson: *Phys. Rev.*, **75**, 486 (1949).

form [11]

$$\begin{aligned}(1.18)\qquad \boldsymbol{\varphi}(x) &= U^{-1}(\infty,0)U(\infty,0)U(0,t)\varphi(x)U(t,0) = \\ &= U^{-1}(\infty,0)U(\infty,0)\varphi(x)U(t,0) = \\ &= U^{-1}(\infty,0)P\big(U(\infty,t)\varphi(x)U(t,0)\big) = \\ &= U^{-1}(\infty,0)P\big(U(\infty,0)\varphi(x)\big) \qquad \text{for } x_0 > 0.\end{aligned}$$

Similarly, in Eq. (1.17*b*) (since $0 \leqq x_0' \leqq t$) we may rewrite the chronological operator appearing therein as follows:

$$\begin{aligned}(1.19)\qquad P\big(U(t,0)j(x')\big) &= U^{-1}(\infty,t)U(\infty,t)P\big(U(t,0)j(x')\big) = \\ &= U^{-1}(\infty,t)P\big(U(\infty,0)j(x')\big)\,,\end{aligned}$$

so that Eq. (1.12) finally reads

$$\begin{aligned}(1.20)\qquad \boldsymbol{\varphi}(x) &= \varphi(x) + \int_0^t \mathrm{d}^4x'\,\Delta(x-x')U^{-1}(t,0)P\big(U(t,0)j(x')\big) = \\ &= \varphi(x) + \int_0^t \mathrm{d}^4x'\,\Delta(x-x')\boldsymbol{j}(x')\,,\end{aligned}$$

which relates the Heisenberg to the interaction representation operators. Using this last equation, and the fact that

$$\Delta_R(x) = -\theta(x)\Delta(x)\,,$$

we may rewrite Eq. (1.3) as follows:

$$(1.21)\qquad \boldsymbol{\varphi}_{\mathrm{in}}(x) + \int_{-\infty}^0 \Delta(x-x')\boldsymbol{j}(x')\,\mathrm{d}^4x' = \boldsymbol{\varphi}(x) - \int_0^t \Delta(x-x')\boldsymbol{j}(x')\,\mathrm{d}^4x' = \varphi(x)\,,$$

which gives the connection between the in-field and the interaction representation operator:

$$(1.22)\qquad \boxed{\varphi(x) = \boldsymbol{\varphi}_{\mathrm{in}}(x) - \int_{-\infty}^0 \Delta(x-x')\boldsymbol{j}(x')\,\mathrm{d}^4x'}\,.$$

[11] Compare F. J. Dyson: *Phys. Rev.*, 82, 428 (1951).

It is clear from this formula that $\boldsymbol{\varphi}_{\text{in}}$ satisfies the homogeneous Klein-Gordon equation since $\varphi(x)$ and $\Delta(x)$ do. Using Eq. (1.4) we obtain the relation between $\varphi(x)$ and $\boldsymbol{\varphi}_{\text{out}}(x)$, namely

$$\boxed{\varphi(x) - \boldsymbol{\varphi}_{\text{out}}(x) = \int_0^\infty \Delta(x - x')\boldsymbol{j}(x')\,\mathrm{d}^4x'} \tag{1.23}$$

Using a procedure similar to that which we used for arriving at Eq. (1.17), we now find that

$$[\varphi(x),\, U(\infty, 0)] = \int_0^\infty \mathrm{d}^4x' \Delta(x - x') P\big(U(\infty, 0)j(x')\big) = \tag{1.24}$$

$$= U(\infty, 0)\int_0^\infty \mathrm{d}^4x' \Delta(x - x')\boldsymbol{j}(x')\,,$$

where in the second line of Eq. (1.24) we have used Eq. (1.18). It follows from (1.24) that

$$U^{-1}(\infty, 0)\varphi(x)U(\infty, 0) = \varphi(x) + \int_0^\infty \mathrm{d}^4x' \Delta(x - x')\boldsymbol{j}(x') = \boldsymbol{\varphi}_{\text{out}}(x)\,. \tag{1.25}$$

Thus $\boldsymbol{\varphi}_{\text{out}}(x)$ and $\varphi(x)$ are related by a similarity transformation. Similarly we have

$$U(0, -\infty)\varphi(x)U^{-1}(0, \infty) = \varphi(x) - [\varphi(x),\, U(0, -\infty)]\,U^{-1}(0, -\infty) = \tag{1.26}$$

$$= \varphi(x) - \int_{-\infty}^0 \mathrm{d}^4x' \Delta(x - x') P\big(U(0, -\infty)j(x')\big)\, U(0, -\infty)\,.$$

Consider now Eq. (1.11) in the case that $t = x_0$ is earlier than the time 0 for which all the representations coincide. In this case we may write

$$\boldsymbol{\varphi}(x) = U^{-1}(t, 0)\varphi(x)U(t, 0) = U(0, t)\varphi(x)U(t, 0)U(0, -\infty)U^{-1}(0, -\infty) = \tag{1.27}$$

$$= P\big(U(0, -\infty)\varphi(x)\big)\,U^{-1}(0, -\infty) \qquad \text{for } x_0 < 0,$$

so that from (1.26) and (1.27) it follows that

$$U(0, -\infty)\varphi(x)U^{-1}(0, -\infty) = \varphi(x) - \int_{-\infty}^0 \Delta(x - x')\boldsymbol{j}(x')\,\mathrm{d}^4x' = \boldsymbol{\varphi}_{\text{in}}(x)\,. \tag{1.28}$$

Equations (1.25) and (1.28) are explicit verification of general formulae of the formal theory of scattering ([12]). Thus both $\boldsymbol{\varphi}_{\text{in}}(x)$ and $\boldsymbol{\varphi}_{\text{out}}(x)$ are related to the interaction representation operator by a similarity transformation and therefore they all satisfy the same commutation rules, viz.,

$$[\boldsymbol{\varphi}_{\text{in}}(x), \boldsymbol{\varphi}_{\text{in}}(y)] = [\boldsymbol{\varphi}_{\text{out}}(x), \boldsymbol{\varphi}_{\text{out}}(y)] = [\varphi(x), \varphi(y)] = i\hbar c\Delta(x-y)\,. \tag{1.29}$$

We can now also derive some well known properties of the vacuum of the interacting fields. This state can be shown ([13]) to be given, apart from an (infinite) phase factor, by

$$\boldsymbol{\Psi}_0 = U(0, \pm\infty)\boldsymbol{\Phi}_0\,, \tag{1.30}$$

where $\boldsymbol{\Phi}_0$ is the bare vacuum state vector. Now $\varphi^{(+)}(x)\boldsymbol{\Phi}_0 = 0$ defines the bare vacuum. It follows from it that

$$U(0,-\infty)\varphi^{(+)}(x)U(0,-\infty)^{-1}\boldsymbol{\Psi}_0 = \boldsymbol{\varphi}_{\text{in}}^{(+)}(x)\boldsymbol{\Psi}_0 = U(0,-\infty)\varphi^{(+)}(x)\boldsymbol{\Phi}_0 = 0\,, \tag{1.31}$$

where $\boldsymbol{\varphi}_{\text{in}}^{(+)}(x)$ is the positive frequency part of $\boldsymbol{\varphi}_{\text{in}}^{(+)}(x)$. That $\boldsymbol{\varphi}_{\text{in}}(x)$ can be split into a positive and negative frequency part

$$\boldsymbol{\varphi}_{\text{in}}(x) = \boldsymbol{\varphi}_{\text{in}}^{(+)}(x) + \boldsymbol{\varphi}_{\text{in}}^{(-)}(x)\,, \tag{1.32}$$

follows from the fact that $\boldsymbol{\varphi}_{\text{in}}(x)$ satisfies the homogeneous Klein-Gordon equation

$$(\Box + \mu^2)\boldsymbol{\varphi}_{\text{in}}(x) = 0\,. \tag{1.33}$$

We may therefore write

$$\boldsymbol{\varphi}_{\text{in}}^{(+)}(x) = \int_\sigma \mathrm{d}\sigma_\mu(x)\left\{\frac{\partial\Delta^{(+)}(x-x')}{\partial x'_\mu} \overleftrightarrow{\partial x'_\mu} - \Delta^{(+)}(x-x') \overleftrightarrow{\partial x'_\mu}\right\}\boldsymbol{\varphi}_{\text{in}}(x')\,, \tag{1.34}$$

where σ is a space-like surface which goes through the point x. Equation (1.31) now indicates that the vacuum may be characterized as the state of lowest energy for which

$$\boldsymbol{\varphi}_{\text{in}}^{(+)}(x)\boldsymbol{\Psi}_0 = 0 = \boldsymbol{\psi}_{\text{in}}^{(+)}(x)\boldsymbol{\Psi}_0 = \boldsymbol{\psi}_{\text{in}}^{(+)}(x)\boldsymbol{\Psi}_0 = 0\,. \tag{1.35}$$

([12]) See, for example, M. GELL-MANN and M. GOLDBERGER: *Phys. Rev.*, **91**, 398 (1953); eqs. (3.26) and (3.27).

([13]) M. GELL-MANN and F. LOW: *Phys. Rev.*, **84**, 350 (1951).

From a consideration of the equation

$$U^{-1}(0,+\infty)\Psi_0 = \Phi_0 , \tag{1.36}$$

one readily verifies that identical equations to (1.35) hold for the out-field. Thus we may regard the positive frequency parts of the in- (out) fields as destruction operators. That the negative frequency parts are indeed creation operators can be inferred from a consideration of the state vector (*)

$$\Psi_{(1)}(p) = \frac{1}{(2\pi)^{\frac{3}{2}}} \int_{\sigma} \bar{\psi}_{\text{in}}(x)\gamma_\mu w(\boldsymbol{p}) \exp\,[ip\cdot x]\, \mathrm{d}\sigma^\mu(x)\Psi_0 , \tag{1.37}$$

where $p^2 = m^2$, $p_0 > 0$, and $w(\boldsymbol{p})$ is a free particle positive energy spinor. An analysis similar to that which established Eq. (1.30) [see the appendix of reference ([13])] indicates that $\Psi_{(1)}(p)$ is an eigenfunction of the total energy momentum of the field system, $\boldsymbol{P}_\mu$,

$$\boldsymbol{P}_\mu \Psi_{(1)}(p) = p_\mu^{(1)} \Psi_{(1)}(p) , \tag{1.38}$$

with $p_\mu{}^{(1)} = \{\sqrt{\boldsymbol{p}^2 + M^2}, \boldsymbol{p}\}$ and

$$p_\mu{}^{(1)} p^{\mu(1)} = M^2 . \tag{1.39}$$

Thus $\Psi_{(1)}(p)$ is the physical one-nucleon state.

Similar statements hold for the operator $\varphi_{\text{in}}^{(-)}(x)$. Thus the vector $\varphi_{\text{in}}^{(-)}(x)\Psi_0$ is a one-meson state. In fact, an n-meson « incoming » state is given by

$$(n\,!)^{-\frac{1}{2}} \varphi_{\text{in}}^{(-)}(x_1) \ldots \varphi_{\text{in}}^{(-)}(x_n)\Psi_0 = (n\,!)^{-\frac{1}{2}} N(\varphi_{\text{in}}(x_1) \ldots \varphi_{\text{in}}(x_n))\Psi_0 , \tag{1.40}$$

where N denotes the fact that the normal product of the operators is to be taken. Similarly

$$(n\,!)^{-\frac{1}{2}} \varphi_{\text{out}}^{(-)}(x_1) \ldots \varphi_{\text{out}}^{(-)}(x_n)\Psi_0 = (n\,!)^{-\frac{1}{2}} N(\varphi_{\text{out}}(x_1) \ldots \varphi_{\text{out}}(x_n))\Psi_0 , \tag{1.41}$$

(*) One readily verifies that the vector $\Psi_{(1)}(p)$ is independent of the space-like surface σ, since ψ_{in} and $w(\boldsymbol{p}) \exp(-ip\cdot x)$ satisfy the free particle Dirac equation. We may therefore choose the space-like surface to be flat and that it is normal in the direction of t. Then $\gamma^\mu \ldots \mathrm{d}\sigma_\mu(x) \to \gamma^0 \ldots \mathrm{d}^3x$. The fact that we are taking the scalar product with a *positive* energy spinor is then equivalent to taking the negative frequency part of $\psi_{\text{in}}(x)$. In (37) we are picking that part of $\bar{\psi}_{\text{in}}(x)\Psi_0$ which has a momentum $\boldsymbol{p}$ and energy $p_0 > 0$, with $p_0 = \sqrt{\boldsymbol{p}^2 + M^2}$.

is an n-meson «incoming» state. It is easy to see how this can be generalized to incoming and outgoing states containing arbitrary numbers of mesons and nucleons. The elements of the S-matrix are now given by the scalar products of incoming and outgoing states ([12])

$$S_{ab} = (\Psi_a^{\text{out}}, \Psi_b^{\text{in}}) . \tag{1.42}$$

Eq. (1.42) is easily verified for a particular case starting from the definition of Dyson of the S-matrix in the interaction representation. Consider, for example, the case of meson-meson scattering. The scattering matrix element for this process is given in the IR by

$$\frac{1}{\sqrt{2!}} \frac{1}{\sqrt{2!}} (\varphi^{(-)}(y_1)\varphi^{(-)}(y_2)\Phi_0, S\varphi^{(-)}(x_1)\varphi^{(-)}(x_2)\Phi_0) = \tag{1.43}$$

$$= \frac{1}{\sqrt{2!}\,2!} (U(\infty,0)\boldsymbol{\varphi}_{\text{out}}^{(-)}(y_1)\,\boldsymbol{\varphi}_{\text{out}}^{(-)}(y_2)\Psi_0, U(\infty,-\infty)U^{-1}(0,-\infty)\boldsymbol{\varphi}_{\text{in}}^{(-)}(x_1)\,\boldsymbol{\varphi}_{\text{in}}^{(-)}(x_2)\Psi_0) =$$

$$= \left(\frac{1}{\sqrt{2!}} N(\boldsymbol{\varphi}_{\text{out}}(y_1)\boldsymbol{\varphi}_{\text{out}}(y_2))\,\Psi_0, \frac{1}{\sqrt{2!}} N(\boldsymbol{\varphi}_{\text{in}}(x_1)\boldsymbol{\varphi}_{\text{in}}(x_2)\Psi_0)\right) .$$

Clearly the proof will go through for an arbitrary initial and final state so that the scattering matrix will be obtained from Eq. (1.42).

The physical interpretation of the incoming and outgoing states is simple. For example, the state $\boldsymbol{\varphi}_{\text{in}}(\boldsymbol{k}_1, x_0 = 0)\,\boldsymbol{\varphi}_{\text{in}}(\boldsymbol{k}_2, x_0 = 0)\Psi_0$, where

$$\boldsymbol{\varphi}_{\text{in}}(\boldsymbol{k}, x_0) = \int \mathrm{d}^3x \exp\,[-i\boldsymbol{k}\cdot\boldsymbol{x}]\boldsymbol{\varphi}_{\text{in}}(\boldsymbol{x}, x_0), \tag{1.44}$$

is a stationary state describing two beams of free mesons (of momentum $\boldsymbol{k}_1$ and $\boldsymbol{k}_2$) colliding and producing outgoing waves of scattered particles (mesons, nucleon pairs, etc.) provided that these reactions are consistent with the conservation laws. In such states, bound subsystems can occur but only in the outgoing waves. By the adiabatic hypothesis (which is here made in order to give meaning to the integrals in (1.3), (1.4) and (1.16b) at $x_0 = \pm -\infty$), the incoming beams will consist of dressed (physical) particles but all initial bound states are made to vanish. Similarly the state $\boldsymbol{\varphi}_{\text{out}}(\boldsymbol{k}_1, x_0 = 0)\boldsymbol{\varphi}_{\text{out}}(\boldsymbol{k}_2, x_0 = 0)\Psi_0$ will consist of two outgoing (plane wave) beams of dressed mesons together with incoming waves of all possible reaction products all adjusted in phase to give a stationary state. Eq. (1.42) therefore does not allow the computation of the scattering matrix element between initial and final states containing bound states.

2. – The Commutation Rules.

In order to make use of Eq. (1.42) expressing the S-matrix in terms of the in- and out-field, we shall need the commutation rules for these field operators. We shall now derive these commutation rules. Consider the commutator

$$(2.1)\qquad [\boldsymbol{\varphi}_{\text{out}}(x), \boldsymbol{\varphi}_{\text{in}}(y)] = \left[\boldsymbol{\varphi}_{\text{in}}(x) + \int_{-\infty}^{+\infty} \mathrm{d}^4x' \Delta(x - x')\boldsymbol{j}(x'), \boldsymbol{\varphi}_{\text{in}}(y)\right] =$$

$$= i\hbar c \Delta(x - y) - \int_{-\infty}^{+\infty} \mathrm{d}^4x' \int_{-\infty}^{0} \mathrm{d}^4y' \Delta(x - x')\Delta(y - y')[\boldsymbol{j}(x'), \boldsymbol{j}(y')] +$$

$$+ \int_{-\infty}^{+\infty} \mathrm{d}^4x' \Delta(x - x')[\boldsymbol{j}(x'), \varphi(y)] ,$$

where to arrive at the last line of Eq. (2.1), we have used Eqs. (1.7) and (1.29). In order to compute the commutator of the interaction representation operator $\varphi(y)$ and the Heisenberg operator $\boldsymbol{j}(x)$, we note that we may write

$$(2.2)\qquad \boldsymbol{j}(x) = U^{-1}(t, 0)\boldsymbol{j}(x)U(t, 0) =$$

$$= U^{-1}(\infty, 0)U(\infty, 0)U(0, t)j(x)U(t, 0)U(0, -\infty)U^{-1}(0, -\infty) =$$

$$= U^{-1}(\infty, 0)P\big(Sj(x)\big)U^{-1}(0, -\infty) ,$$

an expression which is valid for arbitrary times x_0 (i.e., for both $t = x_0 \geqslant 0$ and $t = x_0 \leqslant 0$).

We shall therefore have to evaluate the commutator of $\varphi(y)$ with $U^{-1}(\infty, 0)$ and $U^{-1}(0, -\infty)$. Now we may express the inverse of $U(t, t_0)$, $U^{-1}(t, t_0)$ in a Dyson series involving the anti-chronological operator, $\bar{P}$, which orders the operators in a chronological sequence such that the *latest* one stands to the right of all earlier ones, i.e.,

$$(2.3)\qquad U^{\dagger}(t, t_0) = U^{-1}(t, t_0) = \sum_{n=0}^{\infty} \frac{1}{n!} \left(\frac{i}{\hbar c}\right)^n \int \mathrm{d}^4x_1 \ldots \int \mathrm{d}^4x_n P\big(H_{\text{I}}(x_1) \ldots H_{\text{I}}(x_n)\big) ,$$

so that an analysis similar to that of Eq. (1.17) now yields

$$(2.4)\qquad [\varphi(y), U^{-1}(t_2, t_1)] = -\int_{t_1}^{t_2} \Delta(y - y')\bar{P}\big(U^{-1}(t_2, t_1)j(y')\big) .$$

The commutator of $\varphi(y)$ and $\boldsymbol{j}(x')$ is therefore given by

$$
\begin{aligned}
(2.5)\qquad [\varphi(y), \boldsymbol{j}(x')] &= [\varphi(y),\, U^{-1}(\infty, 0) P\big(S j(x')\big)\, U^{-1}(\infty, 0)] \\
&= -\int_0^{+\infty} \mathrm{d}^4y'\, \Delta(y - y') \bar{P}\big(U(0, \infty) j(y')\big) P\big(S j(x') \big(U^{-1}(0, -\infty) + \\
&+ \int_{-\infty}^{+\infty} \mathrm{d}^4y'\, \Delta(y - y')\, U^{-1}(\infty, 0) P\big(S j(x') j(y')\big)\, U^{-1}(0, -\infty) - \\
&- \int_{-\infty}^{0} \mathrm{d}^4y'\, \Delta(y - y') U^{-1}(\infty, 0) P\big(S j(x')\big) \bar{P}\big(U(-\infty, 0) j(y')\big) - \\
&- i\hbar c \int_{-\infty}^{+\infty} \mathrm{d}^4y'\, \delta(y - y') \Delta(y' - x') \big(3\lambda \boldsymbol{\varphi}^2(x') + \delta\mu^2\big)\ ,
\end{aligned}
$$

where the last line is the contribution of the commutator of $\varphi(y)$ with $j(x)$. This expression can be simplified further if we note that we may also write, if $y_0 > 0$,

$$
\begin{aligned}
(2.6a)\qquad \boldsymbol{j}(y) &= U(0, t) j(y)\, U(t, 0)\, U(0, \infty) U^{-1}(0, \infty) = \\
&= U(0, t) j(y)\, U(t, \infty) U^{-1}(0, \infty) = \\
&= \bar{P}\big(U(0, \infty) j(y)\big)\, U^{-1}(0, \infty) \qquad \text{for } y_0 > 0.
\end{aligned}
$$

Similarly, if $y_0 < 0$

$$
\begin{aligned}
(2.6b)\qquad \boldsymbol{j}(y) &= U(0, -\infty) U^{-1}(-\infty, 0) U(0, t) j(y)\, U(t, 0) = \\
&= U(0, -\infty) \bar{P}\big(U(-\infty) j(y)\big) \qquad \text{for } y_0 < 0,
\end{aligned}
$$

so that

$$
\begin{aligned}
(2.7)\qquad [j(x'), \varphi(y)] &- \int_0^{+\infty} \mathrm{d}^4y'\, \Delta(y - y') \boldsymbol{j}(y') \boldsymbol{j}(x') - \int_{-\infty}^{+\infty} \mathrm{d}^4y'\, \Delta(y - y') P\big(\boldsymbol{j}(x') \boldsymbol{j}(y')\big) \\
&+ \int_{-\infty}^{0} \mathrm{d}^4y'\, \Delta(y - y')\, \boldsymbol{j}(x') \boldsymbol{j}(y') + 3i\lambda\hbar c \int_{-\infty}^{+\infty} \mathrm{d}^4y'\, \delta(y' - y') \Delta(x' - y') \boldsymbol{\varphi}^2(x')\ .
\end{aligned}
$$

Hence, combining terms, we obtain finally

$$(2.8)\qquad [\boldsymbol{\varphi}_{\text{out}}(x), \boldsymbol{\varphi}_{\text{in}}(y)] = i\hbar c\Delta(x-y) + \int_{-\infty}^{+\infty} \mathrm{d}^4x' \int_{-\infty}^{+\infty} \mathrm{d}^4y' \Delta(x-x')\Delta(y-y') \cdot$$

$$\cdot \{ \boldsymbol{j}(y')\boldsymbol{j}(x') - P(\boldsymbol{j}(x')\boldsymbol{j}(y')) \} + i\hbar c \int_{-\infty}^{+\infty} \mathrm{d}^4x' \int_{-\infty}^{+\infty} \mathrm{d}^4y' \delta(y-y')\Delta(x-x')\Delta(x'-y') \cdot$$

$$\cdot \{ 3\lambda\boldsymbol{\varphi}^2(x) + \delta\mu^2 \} = i\hbar c\Delta(x-y) -$$

$$- \int_{-\infty}^{+\infty} \mathrm{d}^4x' \int_{-\infty}^{+\infty} \mathrm{d}^4y' \Delta(x-x')\Delta(y-y')\theta(x'-y')[\boldsymbol{j}(x'), \boldsymbol{j}(y')] +$$

$$+ i\hbar c \int_{-\infty}^{+\infty} \mathrm{d}^4x' \int_{-\infty}^{+\infty} \mathrm{d}^4y' \delta(y-y')\Delta(x-x')\Delta(x'-y') \cdot \{ 3\lambda\boldsymbol{\varphi}^2(x) + \delta\mu^2 \} .$$

3. – Scattering Matrix Elements.

We are now in a position to obtain in a very simple fashion the matrix elements for scattering in closed form. Consider, for example, the case of meson-nucleon scattering. According to Eq. (1.42), the S-matrix element for this situation will be given by

$$(3.1)\qquad S_{ab} = (\boldsymbol{\varphi}_{\text{out}}^{(-)}(x)\boldsymbol{\Psi}_a, \boldsymbol{\varphi}_{\text{in}}^{(-)}(y)\boldsymbol{\Psi}_b) = (\boldsymbol{\Psi}_a, \boldsymbol{\varphi}_{\text{out}}^{(+)}(x)\boldsymbol{\varphi}_{\text{in}}^{(-)}(y)\boldsymbol{\Psi}_b) ,$$

where

$$(3.2)\qquad \boldsymbol{\Psi}_a = \bar{\boldsymbol{\psi}}_{\text{out}}^{(-)}(z_1)\boldsymbol{\Psi}_0 ,$$

and

$$(3.3)\qquad \boldsymbol{\Psi}_b = \boldsymbol{\psi}_{\text{in}}^{(-)}(z_2)\boldsymbol{\Psi}_0 .$$

Using the commutation rules (2.7), we may now write

$$(3.4)\qquad S_{ab} = (\boldsymbol{\Psi}_a, \boldsymbol{\varphi}_{\text{in}}^{(-)}(y)\boldsymbol{\varphi}_{\text{out}}^{(+)}(x)\boldsymbol{\Psi}_b) + (\boldsymbol{\Psi}_a, [\boldsymbol{\varphi}_{\text{out}}^{(+)}(x), \boldsymbol{\varphi}_{\text{in}}^{(-)}(y)]\boldsymbol{\Psi}_b) .$$

If, furthermore, we express in the first line of Eq. (3.4), $\boldsymbol{\varphi}_{\text{out}}^{(+)}(x)$ in terms of $\boldsymbol{\varphi}_{\text{in}}^{(+)}(x)$, namely,

$$(3.5)\qquad \boldsymbol{\varphi}_{\text{out}}^{(+)}(x) = \boldsymbol{\varphi}_{\text{in}}^{(+)}(x) + \int_{-\infty}^{+\infty} \Delta^{(+)}(x-x')\boldsymbol{j}(x')\,\mathrm{d}^4x'$$

and notice that $\boldsymbol{\varphi}_{\text{in}}$ and $\boldsymbol{\psi}_{\text{in}}$ commute, then by virtue of the definition of the vacuum, it follows that:

$$\boldsymbol{\varphi}_{\text{in}}^{(+)}(x)\boldsymbol{\Psi}_b = 0 \,. \tag{3.6}$$

Similarly expressing $\boldsymbol{\varphi}_{\text{in}}^{(-)}(y)$ in terms of $\boldsymbol{\varphi}_{\text{out}}^{(-)}(y)$ and again noting that

$$\boldsymbol{\varphi}_{\text{out}}^{(+)}(y)\boldsymbol{\Psi}_a = 0 \,, \tag{3.7}$$

we therefore obtain, using (2.8),

$$\begin{aligned} S_{ab} = {} & ihc\Delta^{(+)}(x-y)\delta_{ab} - \int_{-\infty}^{+\infty} \mathrm{d}^4x' \int_{-\infty}^{+\infty} \mathrm{d}^4y' \Delta^{(+)}(x-x')\Delta^{(-)}(y-y') \cdot \\ & \cdot (\boldsymbol{\Psi}_a, \{\boldsymbol{j}(y')\boldsymbol{j}(x') + \theta(x'-y')[\boldsymbol{j}(x'), \boldsymbol{j}(y')]\}\boldsymbol{\Psi}_b) + \\ & + ihc \int \mathrm{d}^4x' \int \mathrm{d}^4y' \Delta(x-x')\Delta(x'-y')\delta(y-y')\{3\lambda(\boldsymbol{\Psi}_a, \boldsymbol{\varphi}^2(x')\boldsymbol{\Psi}_b) + \delta\mu^2\delta_{ab}\} = \\ = {} & ihc\Delta^{(+)}(x-y)\delta_{ab} - \int_{-\infty}^{+\infty} \mathrm{d}^4x' \int_{-\infty}^{+\infty} \mathrm{d}^4y' \Delta^{(+)}(x-x')(\boldsymbol{\Psi}_a, P(\boldsymbol{j}(x')\boldsymbol{j}(y'))\boldsymbol{\Psi}_b)\Delta^{(-)}(y-y') + \\ & + ihc \int \mathrm{d}^4x' \int \mathrm{d}^4y' \Delta(x-x')\Delta(x'-y')\delta(y-y')\{3\lambda(\boldsymbol{\Psi}_a, \boldsymbol{\varphi}^2(x')\boldsymbol{\Psi}_b) + \delta\mu^2\delta_{ab}\} \,. \end{aligned} \tag{3.8}$$

To obtain the matrix element for scattering from some initial state p_1, k_1 to some final state p_2, k_2 (p is the nucleon coordinate with $p_0 = \sqrt{\boldsymbol{p}^2 - M^2}$ and includes the specification of the spin and k is that of the meson, $k_0 = \sqrt{\boldsymbol{k}^2 + \mu^2}$), replace $\boldsymbol{\Psi}_b$ by the state vector (1.37) and $\boldsymbol{\Psi}_a$ by a similar one with $\boldsymbol{\psi}_{\text{in}}$ replaced by $\boldsymbol{\psi}_{\text{out}}$. Similarly, we must also include the meson wave functions: $(2(2\pi)^3k_0)^{-\frac{1}{2}} \exp[-ik\cdot x]$ in the incoming and outgoing states. The correct initial incoming state is therefore given by

$$\begin{aligned} \boldsymbol{\Psi}_{\text{in}} = \frac{1}{i}\int \mathrm{d}\sigma_\mu(y) \Bigg(& \frac{\partial \boldsymbol{\varphi}_{\text{in}}^{(-)}(y)}{\partial y_\mu} \frac{1}{\sqrt{2(2\pi)^3}} \exp[-ik\cdot y] - \\ & - \boldsymbol{\varphi}_{\text{in}}^{(-)}(y) \frac{\partial}{\partial y_\mu} \frac{1}{\sqrt{2(2\pi)^3}} \exp[-ik\cdot y] \Bigg) \cdot \int \mathrm{d}\sigma_\mu(z) \bar{\boldsymbol{\psi}}_{\text{in}}^{(-)}(z_1)\gamma^\mu u(p_1) \exp[-ip_1\cdot z]|\boldsymbol{\Psi}_0 \end{aligned} \tag{3.9}$$

with a similar state vector for the outgoing state, expressed in terms of the outgoing field operators.

Note that we may choose the times x_0 and y_0 of the outgoing and incoming field operators as $+\infty$ and $-\infty$, respectively. This, because in (3.10) the choice of the space-like surface σ is arbitrary as the operators and wave functions

satisfy free field equations. If we do so, then (3.9) may be rewritten in a slightly different form by using the properties of the Δ_F function as follows:

$$S_{ab} = \frac{\hbar c}{2}\,\Delta_F(x-y)\,\delta_{ab} - \int_{-\infty}^{+\infty} \mathrm{d}^4x' \int_{-\infty}^{+\infty} \mathrm{d}^4y'\, \frac{1}{2}\,\Delta_F(x-x') \cdot \tag{3.10}$$

$$\cdot (\Psi_a,\, P(\boldsymbol{j}(x')\boldsymbol{j}(y'))\Psi_b)\, \frac{1}{\Omega}\,\Delta_F(y-y')\,,$$

where we have omitted the renormalization counter terms.

The consequences of causality (*) can now easily be imposed on the matrix element (3.10) and one in fact proceeds in a manner similar to the proof of Section III of Gell-Mann, Goldberger, and Thirring by comparing the matrix element of the commutator of $\boldsymbol{\varphi}_{\mathrm{in}}(x)$ and $\boldsymbol{\varphi}_{\mathrm{out}}(x)$, i.e. Eq. (2.8) with Eq. (3.10).

Causality requires that the commutator of the Hermitian operators $\boldsymbol{\varphi}_{\mathrm{out}}(x)$, $\boldsymbol{\varphi}_{\mathrm{in}}(y)$ vanish for $(x-y)^2$ spacelike. Writing

$$P(A(x)B(y)) = \theta(x-y)A(x)B(y) + \theta(y-x)B(y)A(x)\,, \tag{3.11}$$

the time integrations in Eq. (3.10) can be carried out by introducing a complete set of state vectors for the Fermion-Boson system. The time integration can similarly be carried out in the matrix element of the commutator of $\boldsymbol{\varphi}_{\mathrm{in}}(x)$, $\boldsymbol{\varphi}_{\mathrm{out}}(y)$. One then concludes that the second order perturbation theory results of Gell-Mann, Goldberger, and Thirring are in fact correct to all orders of perturbation theory provided that the operators and states are interpreted as Heisenberg ones.

The methods outlined above can also be applied to more complicated processes (e.g. meson-meson scattering), though computationally it is somewhat easier to revert to the interaction representation and use the commutation rules for the interaction representation operator

$$[\varphi(x), S] = ihc \int \mathrm{d}^4x'\, \Delta(x-x')P(Sj(x'))\,, \tag{3.12}$$

as well as the equations (1.30) and (1.36) connecting the true with the bare vacuum.

(*) M. L. Goldberger has since given a much simpler proof of the dispersion relation. The author wishes to thank Professor Goldberger for communicating this proof to him.

4. – The Symmetric Field.

In addition to the in- and out-field, we may define the symmetric field through the relation

$$\varphi(x) = \varphi_{\text{sym}}(x) - \int_{-\infty}^{+\infty} \mathrm{d}^4x' \Delta(x - x') \boldsymbol{j}(x') \,, \tag{4.1}$$

where

$$\bar{\Delta}(x) = \tfrac{1}{2}(\Delta_A(x) + \Delta_R(x)) \,, \tag{4.2}$$

whence

$$\varphi_{\text{sym}}(x) = \tfrac{1}{2}(\varphi_{\text{in}}(x) + \varphi_{\text{out}}(x)) \,. \tag{4.3}$$

Note, therefore, that $\varphi_{\text{sym}}(x)$ satisfies a free field equation. It is related to the interaction representation operators by the equation

$$\varphi(x) = \varphi_{\text{sym}}(x) - \frac{1}{2}\int_{-\infty}^{+\infty} \Delta(x - x') \boldsymbol{j}(x') \, \mathrm{d}^4x' \,. \tag{4.4}$$

Also

$$\varphi_{\text{sym}}(x) = \varphi_{\text{out}}(x) - \frac{1}{2}\int_{-\infty}^{+\infty} \Delta(x - x') \boldsymbol{j}(x') \, \mathrm{d}^4x' \,, \tag{4.5}$$

$$\varphi_{\text{sym}}(x) = \varphi_{\text{in}}(x) + \frac{1}{2}\int_{-\infty}^{+\infty} \Delta(x - x') \boldsymbol{j}(x') \, \mathrm{d}^4x' \,, \tag{4.6}$$

so that the commutation rules for the symmetric field read (*)

$$[\varphi_{\text{sym}}(x), \varphi_{\text{sym}}(y)] = \tag{4.7}$$

$$= i\hbar c \Delta(x - y) - \frac{1}{4}\int_{-\infty}^{+\infty} \mathrm{d}^4x' \int_{-\infty}^{+\infty} \mathrm{d}^4y' \Delta(x - x') \Delta(y - y') [\boldsymbol{j}(x'), \boldsymbol{j}(y')] \,,$$

where we have again omitted the contribution from the renormalization counter terms. The symmetric operators build up the standing wave solutions

(*) Compare this result with the discussion following Eq. (52) of reference [2].

of the scattering problem ([14]). The properties of these solutions and its consequences for the reactance matrix K will be dealt with in a future publication.

([14]) See in this coneection M. L. GOLDBERGER: *Phys. Rev.*, **84**, 929 (1951).

RIASSUNTO (*)

Si stabilisce la relazione tra i campi *in* e *out* e il campo della rappresentazione per interazione. Si ottengono le regole di commutazione sia per questi campi che per il campo simmetrico. Dalla loro connessione con la rappresentazione per reazione si deriva nuovamente la formulazione della teoria dello scattering in termini di questi campi.

(*) *Traduzione a cura della Redazione.*

IL NUOVO CIMENTO Vol. II, N. 3 1° Settembre 1955

On Bloch and Nordsieck's divergence.

R. Ascoli

Istituto di Fisica dell'Università - Torino
Istituto Nazionale di Fisica Nucleare - Sezione di Torino

(ricevuto il 10 Giugno 1955)

Summary. — The convergence of the expectation value $\bar{N}$ of the number of soft photons emitted by a given classical current is studied, using Bloch and Nordsieck's approximation. It is found that $\bar{N}$ is finite, whenever the particles producing the field are moving in a finite volume of space. Therefore in every experiment that can really be done the number of emitted photons is finite. Bloch and Nordsieck's divergence, which arises in the case of a charged particle undergoing a transition between two definite momentum states, corresponds to experimental conditions which can not be reached in nature (an infinite volume of space is necessary). In the Appendix a less stringent condition for the convergence of $\bar{N}$ is derived.

We know that, according Bloch and Nordsieck's treatment, a charged particle which undergoes a transition from a definite momentum state to another definite momentum state emits an infinite number of photons.

This divergence does not lead to serious difficulties, because it is not a divergence in a transition probability, such as the infrared divergence of perturbation theory, but it is a divergence of the number of photons emitted in a transition whose probability still remains finite.

Infinite, however, must always be the limit of a finite quantity, and in physics this limit may arise if we use in our theories some schematisation which corresponds to a limit which cannot be reached in nature.

Thus we are led to investigate whether Bloch and Nordsieck's divergence depends on having assumed a transition between two definite momentum states as the source of the electromagnetic field. It is clear, indeed, that not any source gives rise to the emission of an infinite number of photons. This

does not happen for example in the case of an armonic oscillator in quantum theory.

Thus we try to get a condition for the source of the field so that the expectation value of the number of emitted photons is finite.

We use Thirring and Touschek's formalism [1], and we limit our investigation to the field produced by a classical distribution of current. Then the field operators $A_\mu(x)$ in the Heisenberg picture satisfy the equation [2] $\Box A_\mu(x) = -j_\mu(x)$, where $j_\mu(x)$ is a given function of the point in space-time. Defining in- and outgoing fields in the usual way, we have:

$$A_\mu^{\text{out}}(x) = A_\mu^{\text{in}}(x) - \int \mathrm{d}x' D(x-x') j_\mu(x') \,, \tag{1}$$

where

$$D(x) = D^{\text{av}}(x) - D^{\text{ret}}(x) = -\frac{i}{(2\pi)^3}\int \mathrm{d}k \exp\left[i(kx)\right] \delta(k^2)\varepsilon(k) \,, \tag{2}$$

with $\varepsilon(k) = 1$ for $k_0 > 1$, $\varepsilon(k) = -1$ for $k_0 < 1$. Defining $A_\mu(k)$ and $j_\mu(k)$ by

$$A_\mu(x) = \frac{1}{(2\pi)^3}\int \mathrm{d}k \exp\left[i(kx)\right] \delta(k^2) A_\mu(k) \,, \tag{3}$$

$$j_\mu(x) = \frac{1}{(2\pi)^4}\int \mathrm{d}k \exp\left[i(kx)\right] j_\mu(k) \,, \tag{4}$$

it follows from (1), (2), (3), (4):

$$A_\mu^{\text{out}}(k) = A_\mu^{\text{in}}(k) + i j_\mu(k)\varepsilon(k) \,. \tag{5}$$

This expression shows that in the field state $|X\rangle$ we are concerned with, the difference $A_\mu^{\text{out}}(k) - A_\mu^{\text{in}}(k)$ is definite. We are interested to the case in which no photon is present in the ingoing field: $A_\mu^{\text{in}}(k)\,|X\rangle = 0$. We call N_Δ the number of outgoing photons with momentum k_μ in a given volume Δ of k_μ space and with polarisation $e_\mu(k)$. Then the expectation value of N_Δ in state $|X\rangle$ is given by:

$$\overline{N}_\Delta = \langle X | N_\Delta | X \rangle = \langle X | \frac{1}{(2\pi)^3}\int_\Delta \mathrm{d}k\, \delta(k^2) \left(A^{\text{out}*}(k)e(k)\right)\left(A^{\text{out}}(k)e(k)\right) | X\rangle = \tag{6}$$

$$= \frac{1}{(2\pi)^3}\int_\Delta \mathrm{d}k\, \delta(k^2) \left| \left(j(k)e(k)\right)\right|^2$$

making use of (5).

[1] W. Thirring and B. Touschek: *Phil. Mag.*, 42, 245 (1951).

[2] We use natural units $\hbar = 1$, $c = 1$.

The expectation value of the total number of photons is obtained by extending the integration to the whole region of k_μ space with $k_0 > 0$, and summing over the polarisation vectors $e_r(k)$ $(r = 1, 2)$:

$$\overline{N} = \frac{1}{(2\pi)^3} \int_{k_0>0} \mathrm{d}k\, \delta(k^2) \sum_r |(j(k) e_r(k))|^2 . \tag{7}$$

From here on we renounce to the covariant formalism, and we take $A_0 = 0$ in the reference system in which we perform the calculation. We obtain:

$$\overline{N} \quad \frac{1}{(2\pi)^3} \int \frac{\mathrm{d}\boldsymbol{k}}{2|\boldsymbol{k}|} \sum_r |\boldsymbol{j}(k)\cdot\boldsymbol{e}_r(k)|^2 = \frac{1}{2(2\pi)^3} \int \mathrm{d}\Omega_k \int_0^\infty \mathrm{d}|\boldsymbol{k}|\, |\boldsymbol{k}| \sum_r |\boldsymbol{j}(k)\cdot\boldsymbol{e}_r(k)|^2 , \tag{8}$$

where $k_0 = |\boldsymbol{k}|$ and $\mathrm{d}\Omega_k$ is the element of solid angle in $\boldsymbol{k}$ space.

We observe that $\sum_r |\boldsymbol{j}(k)\cdot\boldsymbol{e}_r(k)|^2 \leq |\boldsymbol{j}(k)|^2$, so that $\overline{N}$ satisfies the inequality:

$$\overline{N} < \frac{1}{2(2\pi)^3} \int \mathrm{d}\Omega_k \int_0^\infty \mathrm{d}|\boldsymbol{k}|\, |\boldsymbol{k}|\, |\boldsymbol{j}(k)|^2 . \tag{9}$$

Therefore a sufficient condition to assure the convergence of $\overline{N}$ for small $|\boldsymbol{k}|$ is $|\boldsymbol{j}(k)|$ to be finite or to be infinite of an order lesser than $\alpha < 1$, as $|\boldsymbol{k}|$ approaches zero, for any direction of $\boldsymbol{k}$.

We assume that the current is produced by a set of particles of charge e_i and the positions $\boldsymbol{x}_i$ of these particles are given functions of time x_0: $\boldsymbol{x}_i = \boldsymbol{x}_i(x_0)$. Then:

$$\boldsymbol{j}(x) = \sum_i e_i \frac{\mathrm{d}\boldsymbol{x}_i}{\mathrm{d}x_0} \delta(\boldsymbol{x} - \boldsymbol{x}_i) , \tag{10}$$

and the inverse of (4) gives:

$$\boldsymbol{j}(k) = \int \mathrm{d}x \exp[-i(kx)] \boldsymbol{j}(x) = i \sum_i e_i \int \mathrm{d}x_0 \exp[-i(kx_i)] \frac{\mathrm{d}\boldsymbol{x}_i}{\mathrm{d}x_0} , \tag{11}$$

where $x_i = (\boldsymbol{x}_i, ix_0)$.

We easily see that a sufficient condition for the convergence of $\overline{N}$ is $\mathrm{d}\boldsymbol{x}_i/\mathrm{d}x_0$ to be a function of bounded variation in the neighbourhood of $x_0 = \pm\infty$ and $\int \mathrm{d}x_0 (\mathrm{d}\boldsymbol{x}_i/\mathrm{d}x_0) = \int \mathrm{d}\boldsymbol{x}_i$ to exist and to be finite for each particle in some reference system, so that the particles are always confined in a given finite volume of space. In fact the latter condition assures that $\boldsymbol{j}(k)$ is finite for $\boldsymbol{k} = 0$ and the former that $\boldsymbol{j}(k)$ is finite in the neighbourhood of $\boldsymbol{k} = 0$.

Therefore we conclude that in every experiment which can really be done the number of emitted photons is finite. Bloch and Nordsieck's divergence corresponds to experimental conditions that cannot be reached in nature.

In the Appendix a less stringent condition for the convergence of $\overline{N}$ is derived (no. 1), and the relativistic invariance of the result is verified (no. 2).

APPENDIX

1. – The condition deduced above for the convergence of $\overline{N}$ is obtained requiring $\boldsymbol{j}(k)$ to be finite for $\boldsymbol{k} = 0$. A condition of a more general kind can be deduced requiring only $|\boldsymbol{j}(k)|$ to be infinite of an order lesser than $\alpha < 1$.

We show that the number of emitted photons is certainly finite if, in some reference system, the velocity of each particle goes to zero at least with $C|x_0|^{-\varepsilon}$, as $x_0 \to \pm\infty$ ([3]), where $\varepsilon > 0$ and C is a constant.

We have in fact:

$$(12)\qquad \boldsymbol{j}_i(k) = ie_i \int \mathrm{d}x_0 \exp\left[-i(kx_i)\right] \frac{\mathrm{d}\boldsymbol{x}_i}{\mathrm{d}x_0} =$$

$$= ie_i \int_{-a}^{+a} \mathrm{d}x_0 \exp\left[-i(kx_i)\right] \frac{\mathrm{d}\boldsymbol{x}_i}{\mathrm{d}x_0} +$$

$$+ ie_i \left(\int_{-\infty}^{-a} + \int_{a}^{\infty} \right) \mathrm{d}x_0 \exp\left[i|\boldsymbol{k}| \left(x_0 - \frac{\boldsymbol{k}}{|\boldsymbol{k}|} \cdot \boldsymbol{x}_i \right) \right] \frac{\mathrm{d}\boldsymbol{x}_i}{\mathrm{d}x_0} ,$$

where a is a positive number.

The first integral is finite. In the last two integrals we put $x_0 - (\boldsymbol{k}/|\boldsymbol{k}|)\cdot\boldsymbol{x}_i = u$. According to the assumption about the velocity, we have $\lim_{x_0 \to \pm\infty} \mathrm{d}\boldsymbol{x}_i/\mathrm{d}x_0 = 0$, so that $\lim_{x_0 \to \pm\infty} \mathrm{d}u/\mathrm{d}x_0 = \lim_{x_0 \to \pm\infty} (1 - (\boldsymbol{k}/|\boldsymbol{k}|)\cdot(\mathrm{d}\boldsymbol{x}_i/\mathrm{d}x_0)) = 1$. Therefore, on choosing $|x_0|$ large enough, $\mathrm{d}u/\mathrm{d}x_0$ is close to one, so that $|u|$ steadily increases with $|x_0|$, and, if a is large enough, the last two integrals become:

$$\left(\int_{-\infty}^{-b_1} + \int_{b_2}^{\infty} \right) \mathrm{d}u \exp\left[i|\boldsymbol{k}|u \right] \frac{\mathrm{d}\boldsymbol{x}_i}{\mathrm{d}u} = \int_{-\infty}^{+\infty} \mathrm{d}u \exp\left[i|\boldsymbol{k}|u \right] \boldsymbol{f}_i(u) ,$$

where $\boldsymbol{f}_i(u)$ goes to zero at least with $\boldsymbol{c}|u|^{-\varepsilon}$ $(\varepsilon > 0)$ as $x_0 \to \pm\infty$, for $\boldsymbol{f}_i(u) = (\mathrm{d}\boldsymbol{x}_i/\mathrm{d}u) = (\mathrm{d}\boldsymbol{x}_i/\mathrm{d}x_0)(\mathrm{d}x_0/\mathrm{d}u)$ when $u_i < -b_1$ or $u_i > b_2$, and $\mathrm{d}x_0/\mathrm{d}u \sim 1$.

([3]) More exactly it must be possible to put $\mathrm{d}\boldsymbol{x}_i/\mathrm{d}x_0$ into the form: $\mathrm{d}\boldsymbol{x}_i/\mathrm{d}x_0 = \boldsymbol{\varphi}(x_0)|\boldsymbol{x}_0|^{-\varepsilon}$, where $\boldsymbol{\varphi}(x_0)$ is of bounded variation in the neighbourhood of $\pm\infty$.

Then from a theorem about the onedimensional Fourier transform (4) we have that $|\boldsymbol{j}_i(k)|$ is not infinite of an order larger than $1-\varepsilon$, as $|\boldsymbol{k}$ tends to zero, so that the convergence of the integral of formula (9) for small $|\boldsymbol{k}$ is assured, provided $\varepsilon > 0$.

If $\varepsilon = 0$ no general conclusion can be driven about the convergence of $\overline{N}$. Two important examples are the following (we consider one single particle):

1) $\mathrm{d}\boldsymbol{x}/\mathrm{d}x_0 = \boldsymbol{v}$ if $x_0 < 0$, $\mathrm{d}\boldsymbol{x}/\mathrm{d}x_0 = \boldsymbol{v}'$ if $x_0 > 0$ (where $\boldsymbol{v} \neq \boldsymbol{v}'$ are constant velocities). This is the case studied by BLOCH and NORDSIECK: $\boldsymbol{j}(k)$ has a singularity of the type of $\delta_1(|\boldsymbol{k}|)$ function, so that it is infinite of order 1, as $|\boldsymbol{k}| \to 0$, and $\overline{N}$ diverges.

2) $\mathrm{d}\boldsymbol{x}/\mathrm{d}x_0 = \boldsymbol{v}$, constant. This is the case of the uniform motion of a charged particle, which gives rise to no emission of radiation: in fact $\boldsymbol{j}(k)$ has a $\delta(|\boldsymbol{k}|)$ singularity and $\overline{N}$ (formula (9)) converges to zero (5).

2. – Let one of the previous conditions for the convergence of $\overline{N}$ be satisfied by the velocities $\mathrm{d}\boldsymbol{x}_i/\mathrm{d}x_0$ in some reference system. One of the remarks of the last example may be used to see how $\overline{N}$ still converges in any other reference system. In fact it is easy to see that the velocities $\mathrm{d}\boldsymbol{x}'_i/\mathrm{d}x'_0$ of the particles in another reference system are each the sum of two terms: the first satisfies the same condition as $\mathrm{d}\boldsymbol{x}_i/\mathrm{d}x_0$, the second is the constant velocity $\boldsymbol{v}$ of system x' with respect to system x. Therefore the substitution of $\mathrm{d}\boldsymbol{x}'_i/\mathrm{d}x'_0$ into (9) gives rise only to convergent integrals.

(4) We use here the following theorem: let $f(x) = \varphi(x)|x|^{-\varepsilon}$, where $0 < \varepsilon < 1$ and $\varphi(x)$ is of bounded variation. Then the Fourier transform $F(k)$ of $f(x)$ behaves like $C(|k|^{\varepsilon}/k)$, as $k \to 0$. (Here C is a complex constant). The theorem can be proved similarly to the theorem 126 of E. C. TITCHMARSCH: *Introduction to the theory of Fourier Integrals* (Oxford, 1937), p. 172.

(5) In these two examples the formula (9) includes an integral of the form $\int \mathrm{d}|\boldsymbol{k}|\,|\boldsymbol{k}|\,\delta^2(|\boldsymbol{k}|)$. The symbol $\delta^2(x)$ has in general no meaning (see L. SCHWARTZ: *Théorie des distributions* (Paris, 1950), vol. I, p. 115). It is easy to see however, that all the rules of calculation can be applied to $f(x)\delta^2(x)$, provided $f(0) = 0$.

RIASSUNTO

Si studia qui la convergenza del numero medio N di fotoni di bassa energia emesso da una assegnata distribuzione classica di corrente, usando l'approssimazione di Bloch e Nordsieck. Si sono ricavate condizioni sufficienti perchè N sia finito. La più immediata assicura che $\overline{N}$ è finito ogniqualvolta le cariche che producono il campo si muovono in un volume finito di spazio. Perciò in ogni esperimento realmente effettuabile il numero di fotoni emessi è finito. Un'altra condizione sufficiente per la convergenza di $\overline{N}$, dedotta nell'Appendice, è che la velocità delle cariche tenda a 0 con una potenza $-\varepsilon < 0$ del tempo, quando questo tende a $\pm\infty$. Se $\varepsilon = 0$ la convergenza di N non è più garantita: ricade in questo caso il moto di una carica che passa da uno stato ad un altro di impulsi determinati. In quest'esempio, studiato da Bloch e Nordsieck, è noto che $\overline{N}$ diverge. Però esso corrisponde a condizioni sperimentali che non possono essere realizzate in natura (volume infinito dello spazio necessario).

On the Possible Existence of Degenerate Charged States of Heavy Unstable Bosons in the Gell-Mann-Pais Theory.

N. Dallaporta and L. Taffara

Istituto di Fisica dell'Università - Padova
Istituto Nazionale di Fisica Nucleare - Sezione di Padova

(ricevuto il 12 Giugno 1955)

Summary. — It is studied under what assumption degenerate charged states of heavy unstable bosons may exist in the framework of the Gell-Mann-Pais theory which should be invariant with opposite parities under combined operations of charge conjugation and charge symmetry, so that they should undergo different and mutually exclusive decay processes. It is found that such degenerate states may exist only if one assumes the third scheme of hyperonic levels of Gell-Mann-Pais, which postulates more Λ and Σ charged states than are up to now experimentally known, and moreover only if one postulates that reactions between nucleons, which should give associated production of hyperons, are always forbidden.

Recent experimental data in the field of heavy unstable particles have increased the evidence that many of the most peculiar features of the processes connected with these particles may be accounted for within the framework of the Gell-Mann-Pais theory [1]. In particular, according to their general idea of inner quantum numbers of the particles which, in many cases, forbid strong and electromagnetic interaction between them and, in this way, reconcile their relative copious production with their long mean life [2], these authors have recently shown that one should expect that a heavy neutral boson would not coincide with its charge conjugate partner [3]; so only linear

[1] M. Gell-Mann and A. Pais: *Proceedings of the 1954 Glasgow Conference on Nuclear and Meson Physics* (London), p. 342.

[2] N. Dallaporta: *Nuovo Cimento*, **1**, 962 (1955).

[3] M. Gell-Mann and A. Pais: *Phys. Rev.*, **97**, 1387 (1955).

combinations of these two bosons states should be invariant under the charge conjugation operation and the selection rules due to charge conjugation should only apply to these linear combinations.

In this way it turns out that only one of those two combined states (which correspond to particles of the same spin, parity and about the same mass) should be allowed by charge conjugation to decay into two pions while the other could possibly decay into three pions. However, this interesting result has been deduced only for neutral particles, while now the most evident experimental data concerning the simultaneous existence of both these kinds of decay are found for charged particles [4] (especially positive ones). Therefore, one feels that the result of Gell-Mann-Pais would be of wider interest if it could also be extended to all states of charge.

Of course, this cannot be achieved only by applying charge conjugation, under whose operation only neutral states can be invariant. Therefore, one is induced to try also charge symmetry and see if, in this case, one can find charged states which remain invariant under a given operation. This is the aim of the present study, and as a first step it will be shown that, under a definite assumption of the Gell-Mann-Pais theory, if one applies the combined operations of charge conjugation and charge symmetry, such charged states may exist. We shall then discuss what are the limits imposed on this possibility by its physical consequences.

One of the most important ideas contained in the Gell-Mann-Pais theory which up to now possesses the strongest experimental evidence is that of associated production, i.e., the fact that strong interactions can take place between heavy unstable particles only if they involve both a hyperon and a heavy boson.

According to this idea, processes ruled by strong interactions should always be of the following kind:

$$(1) \qquad \begin{cases} N \to Y + K & K \to N + \bar{Y} \\ Y \to N - \bar{K} & \bar{K} \to Y - \bar{N} \end{cases}$$

plus any number of pions. In these processes, N means nucleon, Y hyperon, K a heavy boson which gives rise to a nucleon plus an antihyperon and $\bar{K}$ its

[4] The evidence for the decay $\chi^{\pm} \to \pi^{\pm} + \pi^0$ may be found in: M. G. K. Menon and C. O'Ceallaigh: *Proc. Roy. Soc.*, A **221**, 292 (1954); A. L. Hodson, J. Ballam, W. H. Arnold, D. R. Harris, R. Ronald Rau, Geo. T. Reynolds and S. B. Treiman: *Phys. Rev.*, **96**, 1089 (1954); M. V. K. Appa Rao and S. Mitra: *Proc. Indian Academy of Sciences*, A **41**, n. 1 (1955); H. S. Bridge, H. De Staebler, B. Rossi and B. V. Sreekantan: *Nuovo Cimento*, **1**, 874 (1955); M. Baldo, G. Belliboni, M. Ceccarelli, M. Grilli, B. Sechi, B. Vitale and G. T. Zorn: *Nuovo Cimento*, **1**, 1180, (1955).

conjugate, which give rise to an antinucleon plus a hyperon. We shall, for the moment, assume that the K and the $\overline{\mathrm{K}}$-particles are different and may be distinguished.

Let us now for our further considerations assume for the hyperon and nucleon states the third of the schemes proposed by PAIS and GELL-MANN:

(2)

$$\begin{array}{cccc} \Sigma^- & \Sigma^0 & \Sigma^+ & \Sigma^{++} \\ (-1,-\frac{1}{2}) & (-1,+\frac{1}{2}) & (+1,-\frac{1}{2}) & (+1,+\frac{1}{2}) \\ & \Sigma'^0 & \Sigma'^+ & \\ & (0,-\frac{1}{2}) & (0,+\frac{1}{2}) & \\ & \downarrow & \downarrow & \\ & \Lambda^0 & \Lambda^+ & \\ & (0,-\frac{1}{2}) & (0,+\frac{1}{2}) & \end{array} \qquad \begin{array}{cc} \mathrm{N} & \mathrm{P} \\ (-\frac{1}{2},0) & (+\frac{1}{2},0) \end{array}$$

Each level is marked by two values of the two isotopic spin quantum numbers I and K, and each state by two values (in brackets) of I_z and K_z.

Two of these states Σ'^0, Σ'^+ have the same quantum numbers as the Λ states and are supposed to decay immediately into them through gamma radiation. We are left, therefore, with only six hyperonic states. Of these six, for reasons that will appear later, we shall mark the triplet related to $K_z = -\frac{1}{2}$ with an index « o », and the triplet related to $K_z = +\frac{1}{2}$ with an index « u ».

The charge conjugate levels will be obtained by reversing the sign of the charges and the sign of both components of I_z and K_z.

We thus obtain:

(3)

$$\begin{array}{cccc} \overline{\Sigma}^{--} & \overline{\Sigma}^- & \overline{\Sigma}^0 & \overline{\Sigma}^+ \\ (-1,-\frac{1}{2}) & (-1,+\frac{1}{2}) & (+1,-\frac{1}{2}) & (+1,+\frac{1}{2}) \\ & \overline{\Sigma}'^- & \overline{\Sigma}'^0 & \\ & (0,-\frac{1}{2}) & (0,+\frac{1}{2}) & \\ & \downarrow & \downarrow & \\ & \overline{\Lambda}^- & \overline{\Lambda}^0 & \\ & (0,-\frac{1}{2}) & (0,+\frac{1}{2}) & \end{array} \qquad \begin{array}{cc} \overline{\mathrm{N}} & \overline{\mathrm{P}} \\ (+\frac{1}{2},0) & (-\frac{1}{2},0) \end{array}$$

If we now consider all possible virtual pairs of type (1), we find for the boson states the following schemes and quantum numbers:

$$(\mathrm{K}_o^-)_{(-\frac{3}{2},+\frac{1}{2})} \rightarrow \mathrm{N} + \overline{\Sigma}^- \qquad \mathrm{K}_{o\,(-\frac{1}{2},+\frac{1}{2})}^0 \begin{array}{l} \nearrow \mathrm{N} + \overline{\Lambda}^0 \\ \searrow \mathrm{P} + \overline{\Sigma}^- \end{array} \qquad \mathrm{K}_{o\,(+\frac{1}{2},+\frac{1}{2})}^+ \begin{array}{l} \nearrow \mathrm{N} + \overline{\Sigma}^0 \\ \searrow \mathrm{P} + \overline{\Lambda}^0 \end{array}$$

$$\overline{\mathrm{K}}_{o\,(-\frac{1}{2},-\frac{1}{2})}^- \begin{array}{l} \nearrow \overline{\mathrm{N}} + \Sigma^- \\ \searrow \overline{\mathrm{P}} + \Lambda^0 \end{array} \qquad \overline{\mathrm{K}}_{o\,(+\frac{1}{2},-\frac{1}{2})}^0 \begin{array}{l} \nearrow \overline{\mathrm{N}} + \Lambda^0 \\ \searrow \overline{\mathrm{P}} + \Sigma^+ \end{array} \qquad (\overline{\mathrm{K}}_{o\,(+\frac{3}{2},-\frac{1}{2})}^+) \rightarrow \overline{\mathrm{N}} + \Sigma^+$$

$$\mathrm{K}_{u\,(-\frac{1}{2},-\frac{1}{2})}^- \begin{array}{l} \nearrow \mathrm{N} + \overline{\Lambda}^- \\ \searrow \mathrm{P} + \overline{\Sigma}^{--} \end{array} \qquad \mathrm{K}_{u\,(+\frac{1}{2},-\frac{1}{2})}^0 \begin{array}{l} \nearrow \mathrm{N} + \overline{\Sigma}^0 \\ \searrow \mathrm{P} + \overline{\Lambda}^- \end{array} \qquad (\mathrm{K}_{u\,(+\frac{3}{2},-\frac{1}{2})}^+) \rightarrow \mathrm{P} + \Sigma^0$$

$$(\mathrm{K}_{u\,(-\frac{3}{2},+\frac{1}{2})}^-) \rightarrow \mathrm{P} + \Sigma^0 \qquad \mathrm{K}_{u\,(-\frac{1}{2},+\frac{1}{2})}^0 \begin{array}{l} \nearrow \overline{\mathrm{N}} + \Sigma^0 \\ \searrow \mathrm{P} + \Lambda^+ \end{array} \qquad \mathrm{K}_{u\,(+\frac{1}{2},+\frac{1}{2})}^+ \begin{array}{l} \nearrow \mathrm{P} + \Sigma^+ \\ \searrow \overline{\mathrm{N}} + \Lambda^+ \end{array}$$

It is seen that, if we except the states written in brackets, we obtain two degenerate levels each corresponding to the quantum numbers $I = \frac{1}{2}$, $K = \frac{1}{2}$ (as already suggested in [1]) and containing each a quadruplet of states. The other bracketed states should correspond (if they exist) to a higher level $I = \frac{3}{2}$, $K = \frac{1}{2}$.

We may now apply the charge conjugation and charge symmetry operations to our different bosonic levels. To do this, we apply the operation to the levels of hyperons and nucleons (2), (3) and, through the definition (1) get the corresponding relation between bosons.

In this way, we get, for the charge conjugation operation, the following obvious transformations:

$$\begin{array}{lll} \mathrm{K}_o^+ \to \overline{\mathrm{K}}_o^- & \mathrm{K}_o^0 \to \overline{\mathrm{K}}_o^0 & (\mathrm{K}_o^- \to \overline{\mathrm{K}}_o^+) \\ (\mathrm{K}_u^+ \to \overline{\mathrm{K}}_u^-) & \mathrm{K}_u^0 \to \overline{\mathrm{K}}_u^0 & \mathrm{K}_u^- \to \overline{\mathrm{K}}_u^+ \end{array}$$

For charge symmetry, as we have now two different isotopic spin quantum numbers I and K, we may distinguish the following three operations:

operation P': K_z is left unaltered, while the sign of I_z is reversed;

operation P'': inversion of the sign of K_z while the I_z quantum number is left unaltered;

operation $P = P' \cdot P''$: the product of the two preceding operations: both the signs I_z and K_z are reversed.

In this last case we obtain:

$$(4) \qquad \begin{cases} \mathrm{K}_o^+ \rightharpoonup \mathrm{K}_u^- & \mathrm{K}_o^0 \to \mathrm{K}_u^0 \quad (\mathrm{K}_o^- \to \mathrm{K}_u^+) \\ (\overline{\mathrm{K}}_o^+ \to \overline{\mathrm{K}}_u^-) & \overline{\mathrm{K}}_o^0 \to \overline{\mathrm{K}}_u^0 \quad \overline{\mathrm{K}}_o^- \to \overline{\mathrm{K}}_u^+ \end{cases}$$

Let us also consider, as has been done by RADICATI [5], the product operation V of charge symmetry P and charge conjugation C.

As we have in this case three different charge symmetries, we shall also get three different V operations:

$$\text{operation } V' = C \cdot P'$$

$$\text{operation } V'' = C \cdot P''$$

and finally,

$$\text{operation } V = C \cdot P = C \cdot P' \cdot P'' .$$

[5] L. RADICATI: unpublished result.

For this last case we get:

$$(5) \qquad \begin{cases} K_o^+ \to \overline{K}_u^+ & K_o^0 \to \overline{K}_u^0 & (K_o^- \to \overline{K}_u^-) \\ (\overline{K}_o^+ \to K_u^+) & \overline{K}_o^0 \to K_u^0 & \overline{K}_o^- \to K_u^- \end{cases}$$

If we look in the preceding tables for the operations which conserve charge, we see that this is achieved for neutral particles by either the C, the P and the V operations, but for charged particles by the V operation only. Therefore let us, for a moment, concentrate on this last one (V).

We may exactly reproduce for it and for charged states the same line of reasoning used by Gell-Mann-Pais for the neutral particles under charge conjugation. Let us suppose, for example, that the K_o^+ state is represented by the complex wave function $\psi_{K_o^+} = A + iB$ and that the $\overline{K}_u^+$ state is represented by another complex wave function $\psi_{\overline{K}_u^+} = C + iD$. Then, under the V operation we have:

$$(6) \qquad V\psi_{K_o^+}V^{-1} = \psi_{\overline{K}_u^+} \qquad V\psi_{\overline{K}_u^+}V^{-1} = \psi_{K_o^+} .$$

We see immediatly that the new complex wave functions:

$$(7) \qquad \psi^+ = \frac{\psi_{K_o^+} + \psi_{\overline{K}_u^+}}{\sqrt{2}} \qquad \psi^- = \frac{\psi_{K_o^+} - \psi_{\overline{K}_u^+}}{\sqrt{2}}$$

are invariant under V operation, the first one corresponding to an eigenvalue $+1$ and the second to an eigenvalue -1 of the V quantum number.

This could mean, as has been recently pointed out for the neutral case [3], that, from the point of view of decay, these new states are the observable ones, as the conservation of the V quantum number should give rise to selection rules which oblige these states to decay according to different patterns: in fact although not as absolute as the conservation of the C number, the V number conservation should also be effective for the weak interaction decays of heavy bosons, since electromagnetic interactions as well as strong ones are forbidden by Gell-Mann-Pais selection rules.

In particular it is easy to see that if decay into two pions is allowed for one of the states, let us say ψ^+, then it will be forbidden for the other which instead could decay into three pions.

Generally, we may say that the assumptions we have made allow the existence of a number of degenerate states for heavy bosons (of about the same mass). This number may be increased if we also include the possibility of existence of bracketed states (corresponding to the $\frac{3}{2}$, $\frac{1}{2}$ levels); moreover we could also consider the possibility that differences for the bosons could

arise according to the difference between the Σ and Λ hyperons into which they can transform: for example, K_0^0 can be considered as $N + \overline{\Lambda}^0$ or $P + \overline{\Sigma}^-$; and we could conceive that two different bosons would corrispond to these two possible virtual states. For neutral states the degeneracy is still higher, as it is apparent from the preceding considerations that the formalism gives rise to the possibility of the existence of four different states of the same spin, parity and approximatively mass. Therefore this kind of scheme seems fit to accomodate a number of different K-meson decay schemes for which there is now much more definite experimental evidence ([6]).

This possibility, however, is strictly dependent on two assumptions which have been made in the foregoing and which we would now like to discuss.

The first is that there are two kinds of bosons, the K and the $\overline{K}$ that are physically different; and the second is that all the hyperonic states of scheme (2) exist.

The first point has been deduced by Pais and Gell-Mann from the fact that reactions giving associated production of heavy hyperons are forbidden. In fact, if we assume that:

$$N + N \neq Y + Y , \tag{8}$$

then $N + \overline{Y} \neq Y + \overline{N}$ and therefore $K \neq \overline{K}$.

Instead, according to the scheme (2), not all reactions of type (8) are forbidden by the Pais-Gell-Mann selection rules. One can easily see that reactions giving two hyperons of the same kind (both of « *o* » type or « *u* » type) are effectively forbidden, while those giving a « *o* » hyperon and a « *u* » hyperon are allowed.

It would immediatly follow that transitions of the kind:

$$K_o \to \overline{K}_u ,$$

are allowed and, as a consequence, K_o and $\overline{K}_u$ (owing to the great probability of each one going into the other) cannot be distingushed, and this would destroy the possibility of having alternative mode of decay of similar bosons of type ψ^+ and ψ^-. If we still want to preserve a difference between the K and $\overline{K}$-particles, we should assume either that they are intrinsically different (for example, if they have spin, they could have opposite or different magnetic momenta), or that, for some other reason, the Pais-Gell-Mann reactions of type (8) should always be forbidden.

We are led to the same conclusion, that is to a possible reduction of the

([6]) Report on the work of the Bristol-Dublin-Milan-Padua collaboration: *Pisa Conference, Nuovo Cimento,* in press.

number of degenerate bosonic states, if we also consider the second point, that is the question whether all the hyperonic states of scheme (2) exist. It is well known that actually only three hyperonic states, the « *o* » states, have been observed, while, for the three « *u* » states, (« unobserved ») there is no experimental evidence.

Therefore we are faced with the possibility that, for some reason, the « *u* » states can not exist, and in order to suppress them, we must return from the third scheme of Gell-Mann-Pais to the more simple second one which, although theoretically less complete, is, at present, more in agreement with experimental data.

In this case, by suppressing the « *u* » states, we should havei mmediatly the suppression of one of the quadruplets of bosonic states and the loss of degeneracy.

We see, therefore, that in both cases the result is the same; either by reduction of the number of hyperonic states, or the fusion of the two kinds of K and $\overline{\mathrm{K}}$ bosons, the two different degenerate quadruplets of bosonic states are reduced to only one.

Therefore the high degeneracy of bosonic levels, which favours the possibility of different K-decay schemes, is dependent on the scheme (2) for the hyperonic levels and on the fact that all the reactions (8) are forbidden. This makes, up to now, the possibility of this kind of explanation for the degenerate states of charged bosons somewhat hypotetical.

Of course, many different interesting implications should automatically follow if the two kinds of K and $\overline{\mathrm{K}}$ bosons exist. Therefore all experimental evidence which could prove or disprove the existence of the « *u* » hyperonic states should be of the greatest importance.

* * *

We are indebted to Prof. L. RADICATI for a discussion on some interesting points of the problem, and for allowing us to quote his unpuhlished results.

RIASSUNTO

Si cerca di stabilire sotto quali condizioni nell'ambito della teoria di Pais e Gell-Mann possano esistere degli stati degenerati di bosoni pesanti instabili carichi che siano invarianti ed abbiano parità opposte rispetto alle operazioni combinate di coniugazione di carica e simmetria di carica in modo che possano dare luogo a decadimenti diversi e reciprocamente incompatibili. Si trova che tali stati degenerati possono esistere solamente assumendo il cosiddetto terzo schema di livelli iperonici di Pais e Gell-Mann (che, oltre agli stati sperimentalmente osservati dei livelli Σ e Λ, presuppone l'esistenza di altri stati di carica non ancora osservati) ed inoltre escludendo la possibilità di qualunque reazione tra nucleoni che porti alla produzione associata di due iperoni.

Zur Vertexfunktion in quantisierten Feldtheorien.

H. Lehmann, K. Symanzik und W. Zimmermann

Max-Planck-Institut für Physik - Göttingen

(ricevuto il 12 Giugno 1955)

Summary. — It is shown that the vertex function $\Gamma(p_1, p_2)$ in quantized field theories has to satisfy a condition which implies that it vanishes for large momenta. This condition follows from the requirement that no abnormal states (with negative norm) exist.

Es ist der Zweck dieser Note, eine Bedingung aufzuzeigen, die die Vertexfunktion Γ in quantisierten Feldtheorien erfüllen muß, falls diese Theorien exakte Lösungen besitzen. Betrachten wir z.B. die pseudoskalare Mesontheorie, so wird sich zeigen, daß $\Gamma_5(p_1, p_2)$ für den Fall freier Nukleonenimpulse ($i\gamma p_1 = i\gamma p_2 = -M$) und eines Mesonenimpulses $k = p_1 - p_2$ einer Integralbedingung zu genügen hat die — grob gesagt — zum Ausdruck bringt, daß Γ_5 für große Werte von $-k_\mu^2$ verschwindet. Dies gilt unabhängig vom speziellen Kopplungstyp. Die erste störungstheoretische Näherung $\Gamma_5(p_1, p_2) = g\gamma_5$ und ebenso die höheren Näherungen besitzen nicht diese Eigenschaft. Es ist also notwendig, daß Γ_5 asymptotisch kleiner ist als seine erste Näherung.

Mit diesem Umstand hängt es zusammen, daß das von Lee [1] betrachtete Modell einer Feldtheorie bei fehlendem Abschneidefaktor keine physikalisch sinnvolle Lösung besitzt [2]. Denn dort ist die Wechselwirkung so gewählt worden, daß $\Gamma(p_1, p_2) = g$, d.h. die erste Näherung bereits den exakten Ausdruck darstellt.

Es bleibt die Frage offen, ob in den üblichen relativistischen Feldtheorien (Mesontheorie oder Quantenelektrodynamik) die Kopplung ein Abfallen von Γ für große Impulswerte bewirkt.

[1] T. D. Lee: *Phys. Rev.*, **95**, 1329 (1954).
[2] G. Källén und W. Pauli: *Dan. Mat. Fys. Medd.* Im Druck.

Wir führen unsere Betrachtung am Beispiel der Wechselwirkung neutraler pseudoskalarer Mesonen der Masse m mit Nukleonen der Masse $M > 2m$ durch; eine Übertragung auf andere Fälle bereitet keine Schwierigkeiten. Benutzt werden folgende Bezeichnungen und Definitionen (3):

$$(1)\quad \begin{cases} \langle TA(x)A(y)\rangle_0 = \Delta_F'(x-y); \ \langle T\psi(x)\bar{\psi}(y)\rangle_0 = -S_F'(x-y)\,, \\ \langle T\psi(x)A(y)\bar{\psi}(z)\rangle_0 = \int S_F'(x-\xi)\Delta_F'(y-\eta)\Gamma_5(\xi,\eta,\zeta)S_F'(\zeta-z)\,\mathrm{d}^4\xi\,\mathrm{d}^4\eta\,\mathrm{d}^4\zeta\,. \end{cases}$$

Weiterhin Δ_F', S_F', Γ_5, in deren Definitiongleichungen die T-Ordnung durch die antichronologische Ordnung $\overline{T}$ ersetzt ist, also

$$(1')\quad \langle T\psi(x)A(y)\bar{\psi}(z)\rangle_0 = \int \overline{S}_F'(x-\xi)\Delta_F'(y-\eta)\overline{\Gamma}_5(\xi,\eta,\zeta)\overline{S}_F'(\zeta-z)\,\mathrm{d}^4\xi\,\mathrm{d}^4\eta\,\mathrm{d}^4\zeta.$$

Wie man leicht nachweist, ist

$$(2)\quad \Gamma_5(x,y,z) = \gamma_4\Gamma_5^+(z,y,x)\gamma_4 \qquad (\Gamma_5^+ \text{ hermitisch adjungiert zu } \Gamma_5)$$

Für die Δ_F'-Funktion verwenden wir im Impulsraum die Formel (4)

$$(3)\quad \Delta_F'(k^2) = \Delta_F(k^2) - i\int \frac{\sigma(\lambda^2)\,\mathrm{d}(\lambda^2)}{k^2+\lambda^2-i\varepsilon}; \qquad \sigma(\lambda^2) \geqslant 0$$

Zur Herleitung einer Integralbeziehung zwischen Δ_F' und Γ_5 gehen wir von der Identität (Ω ist der Vakuumzustand)

$$(4)\quad (\Omega, A(x)A(y)\Omega) = \sum_{(\chi)} (\Omega, A(x)\Phi_{\text{in}}^{\chi})(\Phi_{\text{in}}^{\chi}, A(y)\Omega)\,,$$

aus. Auf der rechten Seite wird über ein vollständiges System einlaufender Zustände summiert. Nach einer früher angegebenen Reduktionsformel (5) kann man die rechte Seite durch Vakuumerwartungswerte zeitlich geordneter Operatoren (τ-Funktionen) ausdrücken, sowie über alle Zustände summieren, die zu einer festen Teilchenzahl (n) gehören (6). (n) bezeichnet dabei die Anzahl und Art (Nukleonen, Antinukleonen, Mesonen usw.) der einlaufenden Teilchen.

(3) A und ψ sind die renormierten Feldoperatoren, demnach Δ_F', S_F' die renormierten Funktionen. Die in (1) definierte Funktion Γ_5 unterscheidet sich um einen Faktor g von der üblichen Vertexfunktion.

(4) Vgl. z.B. H. LEHMANN: *Nuovo Cimento*, **11**, 342 (1954).

(5) H. LEHMANN, K. SYMANZIK und W. ZIMMERMANN: *Nuovo Cimento*, **1**, 205 (1955).

(6) Die Existenz gebundener Zustände ändert nichts am Ergebnis dieser Überlegungen.

So liefert die Summation über alle Zustände, in denen ein Nukleon-Antinukleon-paar vorhanden ist:

$$(5)\qquad \sum_{\alpha_1,\alpha_2} (\Omega, A(x)\Phi_{\text{in}}^{\alpha_1,\alpha_2})(\Phi_{\text{in}}^{\alpha_1,\alpha_2} A(x)\Omega) =$$

$$= -\int \Delta_F'(x-\xi_2)\,\mathrm{Sp}\{\Gamma_5(\xi_1,\xi_2,\xi_3)S^+(\xi_3-\eta_1)\Gamma_5(\eta_1,\eta_2,\eta_3)S^-(\eta_3-\xi_1)\bar{\Delta}_F'(\eta_2-y)\}\,\mathrm{d}^4\xi_1 \ldots \mathrm{d}^4\eta_3$$

Γ_5 und $\bar{\Gamma}_5$ entstehen dabei gemäß (1) und (1′) aus dem nach Anwendung der Reduktionsformel zunächst auftretenden T- bzw. $\bar{T}$-Produkt.

Allgemein erhält man auf diese Weise eine Beziehung der Form

$$(6)\qquad (\Omega, A(x)A(y)\Omega) = \int \Delta_F'(x-\xi)F(\xi-\eta)\bar{\Delta}_F'(\eta-y)\,\mathrm{d}^4\xi\,\mathrm{d}^4\eta$$

mit

$$F(\xi-\eta) = \sum_{(n)} F_{(n)}(\xi-\eta)$$

Die Funktionen $F_{(n)}$ lassen sich auf die oben erwähnten τ-Funktionen und Δ^+, S^+, S^--Funktionen zurückführen. Wesentlich ist für unsere Zwecke nur, daß die Fouriertransformierten $F_{(n)}(k) \geqslant 0$ sind. Dies folgt unmittelbar aus (4). Ausserdem enthält $F_{(n)}(k)$ nur positive Frequenzen; wir setzen $F_{(n)}(k) = \theta(k_0)F_{(n)}(-k^2)$. Wegen des positiven Charakters der $F_{(n)}(k)$ ist also $F(k) \geqslant F_{(2)}(k)$, [7] wenn $F_{(2)}$ den Beitrag der Zustände mit einem Paar bedeutet.

Durch Übergang zum Impulsraum folgt [8] aus (6)

$$(7)\qquad 2\pi\sigma(-k^2) = |\Delta_F'(k^2)|^2\, F(-k^2)$$

und mit Gl. (3) ($\varkappa^2 = -k^2$)

$$(8)\qquad \sigma(\varkappa^2) = \frac{1}{2\pi} F(\varkappa^2)\left\{\pi^2\sigma^2(\varkappa^2) + \left[\frac{1}{\varkappa^2 - m^2} + P\int_{(3m)^2}^{\infty} \frac{\sigma(\lambda^2)\,\mathrm{d}(\lambda^2)}{\varkappa^2-\lambda^2}\right]^2\right\}.$$

Dies ist eine Integralgleichung für $\sigma(\varkappa^2)$, welche die nicht explizit bekannte Funktion $F(\varkappa^2)$ enthält.

Zur bequemeren Diskussion von Gl. (8) führen wir die Bezeichnungen ein:

$$\frac{\varkappa^2 - 9m^2}{8m^2} \equiv t\,, \qquad 8m^2\sigma(\varkappa^2) \equiv \varrho(t)\,, \qquad \frac{1}{2\pi}\frac{F(\varkappa^2)}{8m^2} \equiv k(t)\,.$$

[7] Dieser Umstand ist bereits von Källén zur Abschätzung von Renormierungskonstanten benutzt worden. G. Källén: *Dan. Mat. Fys. Medd.*, **27**, n. 12 (1953).

[8] Zunächst folgt Gl. (7) nur für $k_0 > 0$. Durch Vertauschung von x und y in Gl. (4) sieht man jedoch, daß (7) für alle Frequenzen gilt.

Damit lautet Gl. (8):

$$\varrho(t) = k(t)\left\{\pi^2\varrho^2(t) + \left[\frac{1}{t+1} + P\int_0^\infty \frac{\varrho(t')\,\mathrm{d}t'}{t-t'}\right]^2\right\}. \tag{8'}$$

Diese Gleichung wird durch

$$\varrho(t) = \frac{1}{(t+1)^2}\cdot\frac{k(t)}{\left[1-(t+1)\int_0^\infty \frac{k(t')\,\mathrm{d}t'}{(t-t')(t'+1)^2}\right]^2 + \pi^2\frac{k^2(t)}{(t+1)^2}} \tag{9}$$

gelöst, sofern

$$I = \int_0^\infty \frac{k(t)\,\mathrm{d}t}{(t+1)^2} \leqslant 1 \tag{10}$$

ist. (Für $I = 1$ ist (9) nur dann Lösung, wenn $\int_0^\infty \frac{k(t)}{t+1}\,\mathrm{d}t = \infty$.)

Im Anhang werden wir zeigen, daß die Lösbarkeitsbedingung (10) nicht nur für den (physikalisch wohl allein sinnvollen) Ausdruck (9), sondern für alle Lösungen von (8') notwendig ist.

Somit folgt aus der Existenz von $\Delta_F'(k^2)$ die Bedingung

$$I = \frac{1}{2\pi}\int_{(3m)^2}^\infty \frac{F(\varkappa^2)\,\mathrm{d}(\varkappa^2)}{(\varkappa^2-m^2)^2} \leqslant 1\,. \tag{11}$$

Wegen $F \geqslant F_2$ folgt aus (18):

$$I_2 = \frac{1}{2\pi}\int_{(3m)^2}^\infty \frac{F_2(\varkappa^2)\,\mathrm{d}(\varkappa^2)}{(\varkappa^2-m^2)^2} \leqslant 1\,. \tag{12}$$

Hieraus erhalten wir sofort ein Bedingung für Γ_5, denn es ist nach (5) und (6)

$$F_2(k) = -\frac{1}{(2\pi)^4}\int \mathrm{Sp}\{\Gamma_5(q-k,q)S^+(q)\bar{\Gamma}_5(q,q-k)S^-(q-k)\}\mathrm{d}^4q$$

mit

$$\Gamma_5(x,y,z) = \frac{1}{(2\pi)^8}\int \Gamma_5(p_1,p_2)\exp\left[ip_1(x-y) + ip_2(y-z)\right]\mathrm{d}^4p_1\,\mathrm{d}^4p_2\,.$$

Die Vertexfunktion $\Gamma_5(p_1,p_2)$ wird natürlich nur für den Fall benötigt,

daß p_1, p_2 Impulse freier Teilchen sind, d.h. $i\gamma p_1 = i\gamma p_2 = -M$. Dann ist

$$\Gamma_5(p_1, p_2) \equiv \gamma_5 f(-(p_1 - p_2)^2)$$
$$\bar{\Gamma}_5(p_1, p_2) \equiv -\gamma_5 f^*(-(p_1 - p_2)^2) .$$

Hiermit folgt

$$F_2(\varkappa^2) = \frac{1}{4\pi}\,\theta(\varkappa^2 - 4M^2)\varkappa\sqrt{\varkappa^2 - 4M^2}\,|f(\varkappa^2)|^2 \tag{13}$$

und damit

$$I_2 = \frac{1}{8\pi^2}\int_{4M^2}^{\infty} \frac{\varkappa\sqrt{\varkappa^2 - 4M^2}}{(\varkappa^2 - m^2)^2}\,|f(\varkappa^2)|^2\,\mathrm{d}(\varkappa^2) \leqslant 1 . \tag{14}$$

Diese Bedingung für die Vertexfunktion impliziert unter anderem, daß Γ_5 asymptotisch abfällt.

Abschliessend einige Bemerkungen:

1) Man kann durch analoge Betrachtung der S'_F-Funktion eine weitere Bedingung für Γ_5 ableiten. Sie gilt für den Fall, daß $\Gamma_5(p_1, p_2)$ sich auf ein freies Nukleon und ein freies Meson bezieht (d.h. $i\gamma p_2 = -M$; $(p_1 - p_2)^2 = -m^2$) und besagt, daß Γ_5 verschwindet für $-p_1^2 \to \infty$.

2) Unsere Betrachtung resultierte aus der Frage, ob die von Källén und Pauli beim Leeschen Modell aufgefundenen abnormen Zustände (negativer Norm) auch in den üblichen relativistischen Feldtheorien zu erwarten sind. Diese Frage ist hier (für Zustände der Nukleonenzahl Null) zurückgeführt worden auf die Bedingung (11). Wenn diese erfüllt ist, also Gl. (8) eine Lösung besitzt, liegen keine abnormen Zustände vor.

3) Die Renormierungskonstante Z_3^{-1} ist nach (3) und (9)

$$Z_3^{-1} = 1 + \int_{\cdot}^{\infty} \varrho(t)\,\mathrm{d}t = \frac{1}{1 - I}$$

sie ist also endlich für $I < 1$, unendlich für $I = 1$.

4) Wenn man in Gl. (8) $F = F_2$ und — im Widerspruch zur Bedingung (14) — $\Gamma_5 = g\gamma_5$ setzt, so erhält man bei einer formalen Entwicklung nach Potenzen von g^2 eine geometrische Reihe mit der Summe

$$\Delta'_F(k) = \Delta_F(k)[1 - \Delta_F(k)\pi(k)]^{-1}$$

($\pi(k)$ entspricht dem renormierten Mesonselbstenergiegraphen niedrigster Näherung; der angegebene Ausdruck für $\Delta_F'(k)$ entsteht durch Summation über alle Iterationen dieses Graphen). Diese Funktion ist keine Lösung unserer Integralgleichung (vgl. hierzu Anhang). Man verifiziert leicht, daß sie einen Pol mit negativem Residuum besitzt, also physikalisch unzulässig ist. Dasselbe gilt für die entsprechende Näherung zur S_F'-Funktion ([9]).

Anhang

Die Iterationslösung (9) ist im Allgemeinen nicht die einzige Lösung von (8′). Zur Gewinnung der allgemeinen Lösung bemerken wir, daß (8′) sich auch schreiben läßt

$$k(t) = \frac{1}{\pi} \lim_{\varepsilon \to 0} \operatorname{Im} \frac{1}{\dfrac{1}{t+1} + \displaystyle\int_0^\infty \frac{\varrho(t')\,\mathrm{d}t'}{t - t' + i\varepsilon}} \,. \tag{A.1}$$

Hiermit bilden wir

$$\int_0^\infty \frac{k(t)\,\mathrm{d}t}{(t+1)^2(z-t)} = \frac{1}{2\pi i} \int \frac{\mathrm{d}t}{(t-z)(t+1)\left[1 + (t+1)\displaystyle\int_0^\infty \frac{\varrho(t')\,\mathrm{d}t'}{t-t'}\right]}$$

wobei rechts der Integrationsweg im Gegenzeigersinn um den von $t = 0$ bis $t = +\infty$ verlaufenden Verzweigungsschnitt ([10]) herumführt. Zur Auswertung schliessen wir den Weg im Unendlichen. Für Nullstellen $t_0 = x_0 + iy_0$ des letzten Faktors im Nenner folgt aus

$$\frac{1}{x_0 + iy_0 + 1} = -\int_0^\infty \frac{\varrho(t')\,\mathrm{d}t'}{x_0 + iy_0 - t'}$$

([9]) Solche Ausdrücke sind des öfteren benutzt worden, z.B. von N. Hu: *Phys. Rev.*, **80**, 1109 (1950); R. Karplus *et al.*: *Phys. Rev.*, **90**, 1072 (1953); K. A. Brueckner *et al.*, *Phys. Rev.*, **90**, 476 (1953); G. Feldman, *Proc. Roy. Soc. London*, A **223**, 112 (1954).

([10]) Über das analytische Verhalten der Stieltjestransformierten $\displaystyle\int_0^\infty \frac{\varrho(t')\,\mathrm{d}t'}{t-t'}$ vgl. D. V. Widder: *The Laplace Transform* (Princeton, 1946), Chapt. VIII.

([11]) Zur Vereinfachung machen wir die unwesentliche Voraussetzung, daß $\varrho(t)$ für $t > 0$ nicht verschwindet.

wegen $\varrho(t') \geqslant 0$ zunächst $y_0 = 0$, und man findet [11] bei

$$\int_0^\infty \frac{\varrho(t)}{t}\,\mathrm{d}t \begin{cases} < 1 & \text{keine Nullstelle} \\ > 1 & \text{eine Nullstelle } -1 < x_0 < 0 \\ = 1 & \text{die Nullstelle } x_0 = 0. \end{cases}$$

So erhalten wir

$$\int_0^\infty \frac{k(t)\,\mathrm{d}t}{(t+1)^2(z-t)} = \frac{1}{z+1} - \frac{1}{z+1}\cdot \frac{1}{1 + (z-1)\int_0^\infty \frac{\varrho(t')\,\mathrm{d}t'}{z-t'}} -$$

$$- \frac{1}{(z-x_0)}\cdot \frac{1}{\left[1 - (1-x_0)^2 \int_0^\infty \frac{\varrho(t')\,\mathrm{d}t'}{(x_0-t')^2}\right]} -$$

$$- \frac{1}{2\pi i}\lim_{R\to\infty} \int_{-R}^{+R} \frac{\mathrm{d}t}{(z-t)(t-1)\left[1 - (t-1)\int_0^\infty \frac{\varrho(t')\,\mathrm{d}t'}{t-t'}\right]}.$$

wobei das letzte Integral verschwindet und der vorletzte Term nur bei $\int_0^\infty \frac{\varrho(t)}{t}\,\mathrm{d}t \geqslant 1$ vorhanden ist.

Damit ergibt sich

$$\text{(A.2)}\quad \frac{1}{z+1} + \int_0^\infty \frac{\varrho(t')\,\mathrm{d}t'}{z-t'} = \frac{1}{z+1}\cdot \frac{1}{1 - (z-1)\int_0^\infty \frac{k(t)\,\mathrm{d}t}{(z-t)(t+1)^2} - c\cdot\frac{z+1}{z-x_0}}$$

oder

$$\text{(A.3)}\quad \varrho(t) = \frac{1}{(t+1)^2}\cdot \frac{k(t)}{\left[1 - (t+1)\int_0^\infty \frac{k(t')\,\mathrm{d}t'}{(t'+1)^2(t-t')} - c\cdot\frac{t+1}{t-x_0}\right]^2 + \pi^2 k^2(t)}$$

wobei c und x_0 den Bedingungen

$$-1 < x_0 \leqslant 0$$

$$(-x_0)\left[1 + \int_0^\infty \frac{k(t)\,\mathrm{d}t}{t(t+1)^2}\right] \leqslant c \leqslant 1 - \int_0^\infty \frac{k(t)\,\mathrm{d}t}{(t+1)^2}$$

$$\int_0^\infty \frac{k(t)\,\mathrm{d}t}{t+1} = \infty \quad \text{bei} \quad c = 1 - \int_0^\infty \frac{k(t)\,\mathrm{d}t}{(t+1)^2}$$

genügen. (A.3) ist die allgemeine Lösung von (8′). Nur bei $c = 0$, was die Lösung (9) gibt, erfüllt die Entwicklung von $\varrho(t)$ nach Potenzen von $K(t)$ die Gleichung (8′) auch gliedweise.

Schließlich sei bemerkt, daß sich (10) durch Einsetzen von (A.1) auch direkt verifizieren läßt.

RIASSUNTO (*)

Si dimostra che la funzione di vertice $\Gamma(p_1, p_2)$ nelle teorie di campo quantistiche deve soddisfare una condizione per la quale la funzione deve annullarsi per quantità di moto elevate. Tale condizione è conseguenza della esigenza che non esistano stati abnormi (con norma negativa).

(*) *Traduzione a cura della Redazione.*

IL NUOVO CIMENTO Vol. I, N. 3 1° Settembre 1955

A Field Theoretical Model for S-Wave Pion-Nucleon Scattering.

B. Bosco

Istituto di Fisica dell'Università - Torino
Istituto Nazionale di Fisica Nucleare - Sezione di Torino

R. Stroffolini

Istituto di Fisica dell'Università - Ferrara
Istituto Nazionale di Fisica Nucleare - Sezione di Padova

(ricevuto il 14 Giugno 1955)

Summary. — A field theoretical model is discussed which can be solved exactly. This model corresponds to a *ps-ps* Hamiltonian, in which only those terms are retained which correspond to the creation of one nucleon-antinucleon pair and to the destruction of one meson together with the inverse process. With this reduced Hamiltonian a finite number of particles are present also in the virtual state. For the pion-nucleon scattering only a single pair can exist in the intermediate states, and the low energy s-wave phase-shifts are evaluated. The agreement with experiments is rather good.

1. – Introduction.

Some efforts have been recently devoted to the investigation of field theoretical Hamiltonians which allow the exact solution of the scattering problem.

As an example Lee[1] and, subsequently Thirring and Haber-Schaim[2] have discussed non relativistic Hamiltonians in which many different fermion types are coupled with a boson field in such a way that the total number of bosons is limited.

These examples, devised with the purpose of studying the meson cloud of the nucleon, have been used to obtain indications on the physical problem of p-Wave pion-nucleon scattering.

(1) T. D. Lee *Phys. Rev.*, **95**, 1329 (1954).
(2) U. Haber-Schaim and W. Thirring: Private communication.

It may be of interest to investigate the complementary problem of the nucleon-antinucleon cloud of the meson, which is intimately connected with the *s*-wave pion-nucleon scattering. This will be done by using a field theoretical model whose scattering matrix can be deduced exactly and in which a single pair is allowed in the physical pion state. The interaction Hamiltonian of this model is simply that part of the fully relativistic *ps-ps* Hamiltonian, which corresponds to the process

$$\pi \rightleftarrows \mathrm{N} + \overline{\mathrm{N}} .$$

Clearly the neglected pair effect in the Hamiltonian

$$\text{Vacuum} \rightleftarrows \pi + \mathrm{N} + \overline{\mathrm{N}}$$

would give rise to an indefinite increase in the number of particles.

Pair-creation is essentially a relativistic effect. On the other hand DYSON [3] has given some arguments, suggesting that in a fully relativistic theory the number of virtual particles cannot be finite. Nevertheless we will show that it is possible in the frame-work of a cut-off theory to take into account in a satisfactory way the relativistic effects for meson momenta smaller than M.

2. – Ground State.

The *ps-ps* charge simmetrical interaction Hamiltonian H^{ps} is [4]:

$$H^{ps} = ig \sum_{s=1}^{3} \int (\psi^{+}\beta\gamma^{5}\tau^{s}\psi)\Phi^{s}\,\mathrm{d}^{3}r$$

where Ψ is the nucleon wave field, Φ the meson field; β, γ^{5} are the well known Dirac matrices; τ^{s} are the free isotopic spin matrices. Expanding the fields in the usual way into creation and destruction operators and retaining only the terms which give rise to the process:

$$\pi \rightleftarrows \mathrm{N} + \mathrm{N}$$

[3] F. J. DYSON: Advanced Quantum Mechanics 2nd ed.

[4] A system of units in which $\hbar = c = 1$ is used throughout this paper, together with following conventions and notations: the volume of the-system has been chosen equal to 1; α_k^{s+} and α_k^{s} are the creation and destruction operators of mesons of momentum k respectively; a_p^{-} and a_p, b_p^{-} and b_p the analogous operators for the nucleons and antinucleons.

adding the renormalization term $\frac{1}{2}\delta\mu^2 \sum \int \Phi^{s+}\Phi^s \mathrm{d}^3r$ - we obtain the interaction Hamiltonian H' of our system:

$$(1)\quad H' = g\sum_{s=1}^{3}\sum_{pp'k}\{a_p^+ b_{p'}^+ \varkappa_k^s \Gamma^s(p, p', k) + \text{complex conjugate}\} + \tfrac{1}{2}\delta\mu^2 \sum_{s=1}^{3}\int \Phi^{s-}\Phi^s \mathrm{d}^3r,$$

where

$$\Gamma^s(p, p', k) = \frac{1}{\sqrt{2\omega_k}}\int \Psi_+(\boldsymbol{p}, \boldsymbol{r})(i\beta\gamma^5\tau^s)\Psi_-(-\boldsymbol{p}', \boldsymbol{r}) \exp[i\boldsymbol{k}\cdot\boldsymbol{r}]\, \mathrm{d}^3r\,.$$

$\Psi_+(\boldsymbol{p}, \boldsymbol{r})$ and $\Psi_-(-\boldsymbol{p}, \boldsymbol{r})$ are eigenfunctions of the Dirac equation with positive and negative energy respectively and momentum, spin and isotopic spin specified by p.

Therefore, the total hamiltonian of our system H can be written:

$$(2)\quad H = H_0 + H'\,,$$

where H_0 is the hamiltonian of free fields.

We define a state of the « physical » meson, which we shall indicate by $|\Pi_k^s\rangle$, where the indices s and k specify the charge and momentum respectively. This state can be expressed by the component states of the « bare » meson $|\pi_k^s\rangle$ and the nucleon-antinucleon state by the following relation:

$$(3)\quad |\Pi_k^s\rangle = N^{\frac{1}{2}}(k)[\,|\pi_k^s\rangle + \sum f^s(p_1p_2)\,|a_{p_1}^+ b_{p_2}^+\rangle\,,$$

where $N(k)$ is a normalization constant for a given K and $f^s(p_1p_2)$ is proportional to the probability amplitude for finding a nucleon-antinucleon pair specified by the quantum numbers p_1 and p_2 in a « physical » meson state.

The physical meson state is an eigenfunction of H.

$$(4)\quad H\,|\Pi_k^s\rangle = w_k\,|\Pi_k^s\rangle\,.$$

From (4) making use of (1), (2) and (3) we obtain:

$$(5)\quad f^s(p_1p_2) = g\,\frac{\Gamma^s(p_1, p_2, k)}{w_k - E_{p_1} - E_{p_2}}$$

$$(6)\quad \left(w_k - \omega_k - \frac{\delta\mu^2}{\omega_k}\right) = g^2\,\frac{\mathrm{Tr}(\tau^s\tau^s)}{2\omega_k}\sum_q \frac{\langle \boldsymbol{q}^+|\,i\beta\gamma^5\,|\boldsymbol{q}-\boldsymbol{k}^-\rangle\langle \boldsymbol{q}-\boldsymbol{k}^-|\,i\beta k^5\,\boldsymbol{q}^-}{(w_k - E_q - E_{q-k})}\,,$$

$$(7)\quad N^{-1}(k) = 1 + g^2\,\frac{\mathrm{Tr}(\tau^s\tau^s)}{2\omega_k}\sum_q \frac{\langle \boldsymbol{q}^+|\,i\beta\gamma^5\,|\boldsymbol{q}-\boldsymbol{k}^-\rangle\langle \boldsymbol{q}-\boldsymbol{k}^-|\,i\beta\gamma^5\,|\boldsymbol{q}^+}{(w_k - E_q - E_{q-k})^2}$$

where $|\boldsymbol{q}^+\rangle$ and $|\boldsymbol{q}^-\rangle$ represent nucleon states with momentum $\boldsymbol{q}$ and positive and negative energy respectively. Since we use a cut-off on the momenta equal to ξM where ξ is smaller than unity, we can neglect the nucleon recoil and then write for (6) and (7):

$$\left(w_k - \omega_k - \tfrac{1}{2}\frac{\delta\mu^2}{\omega_k}\right) = \frac{g^2}{\pi^2}\frac{1}{\omega_k}\frac{1}{(w_k - 2M)}\frac{M^3\xi^3}{3} \tag{6'}$$

$$N^{-1}(k) = 1 + \frac{g^2}{\pi^2}\frac{1}{\omega_k}\frac{1}{(w_k - 2M)^2}\frac{M^3\xi^3}{3}\,. \tag{7'}$$

It is well known ([5]) that the charge renomalization can be done in several ways. Therefore we define the constant of charge renormalization Z_3 by means of the equation

$$Z_3 = \lim_{k\to 0} N(k)\,. \tag{8}$$

In this way we get for the renormalized coupling constant

$$g_c^2 = Z_3 g^2\,, \tag{9}$$

$$g_c^2 = \frac{g^2}{1 + g^2 A(0)} \tag{10}$$

where

$$A(k) = \frac{M^3\xi^3}{3\pi^2\omega_k}\frac{1}{(w_k - 2M)^2}\,.$$

Developping eq. (6') in power series of $w_k/2M$ and retaining only the terms not higher than the second, we get

$$w_k - \omega_k = \tfrac{1}{2}\frac{\delta\mu^2}{\omega_k} - \frac{a}{\omega_k}\left[1 + bw_k + b^2 w_k^2\right], \tag{11}$$

where

$$a = \frac{g^2}{\pi^2}\frac{M^2\xi^3}{6} \quad \text{and} \quad b = \frac{1}{2M}\,.$$

It is easy to see that equation (11) gives for w_k:

$$w_k = \omega_k + \Delta + \varepsilon\omega_k\,, \tag{12}$$

([5]) G. KÄLLÉN: *Nuovo Cimento*, **12**, 217 (1954).

provided that mass renormalization is done in the following way:

$$\frac{1}{2}\delta\mu^2 = a + ab\Delta - ab^2\Delta^2 . \tag{13}$$

and Δ and ε are given by

$$\varepsilon = -\frac{ab^2}{1 + 2ab}$$

$$\Delta = -\frac{ab(1 + \varepsilon)}{1 + 2ab^2(1 + \varepsilon)} \qquad \text{if} \quad \varepsilon \ll 1 . \tag{14}$$

The definition (13) of the mass renormalization term is chosen in such a way that the kinetic energy of the meson results equal (apart from the small term $\varepsilon\omega_k$) to the kinetic energy of a relativistic meson of mass μ. It is not possible however, in the framework of a non relativistic theory to have a meson with the correct total energy: the constant term Δ in eq. (12) represents the difference between the total energy of our meson and the correct relativistic total energy of a meson of mass μ. Such constant term, however does not introduce incosistencies as long a we do not consider relativistic effects of the kind of the creation of new mesons. For our purposes it is sufficient that the kinetic energy has, with good approximation, the correct expression according to relativity.

Equations (10) and (12) and (14) together can be solved using a method of successive approximations for any given pair of values of g_r^2 and ξ.

3. – Pion-Nucleon Scattering.

The scattering state will be denoted by $|N - \Pi\rangle$ and satisfies the Schrödinger equation

$$H|N + \Pi\rangle = E_0|N + \Pi\rangle . \tag{15}$$

On the other hand this eigenfunction can be written in terms of « physical » particles:

$$|N + \Pi\rangle = \sum_{s=1}^{3}\sum_{p,k}\chi_s(p, k)a_p^+|\Pi_k^s\rangle + \sum_{p_1p_2p_3}\varphi(p_1, p_2, p_3)|a_{p_1}^+a_{p_2}^+b_{p_3}^+\rangle . \tag{16}$$

Taking only the components of equation (15) on the states of three nucleons and of a « bare » meson, using eqs. (16), (3) and (5) and solving for the χ_s function

we obtain in the centre of mass system:

$$(17)\quad \left[1 - g^2 \frac{\mathrm{Tr}(\tau^i\tau^i)}{2\omega_p} \sum_q \frac{\langle \boldsymbol{q}^+ | i\beta\gamma^5 | \boldsymbol{q} + \boldsymbol{p}^- \rangle \langle \boldsymbol{q} + \boldsymbol{p}^- | i\beta\gamma^5 | q^+ \rangle}{(w_p - E_q - E_{p+q})(E_p + E_q + E_{p+q} - E_0)}\right] \cdot$$

$$\cdot (E_p + W_p - E_0)\chi_s(p) = -\sum_{r=1}^{3}\sum_q \frac{g^2\tau^r\tau^s}{2\sqrt{\omega_p\omega_q}} \frac{\boldsymbol{p}^+ \, i\beta\gamma^5 \, \boldsymbol{p}+\boldsymbol{q} \quad \boldsymbol{p}-\boldsymbol{q}^- \, i\beta\gamma^5 \, q^+\rangle\chi_r(\boldsymbol{q})}{(E_p + E_q + E_{p+q} - E_0)}$$

By making use of eq. (7) in the centre of mass system; we get:

$$(18)\qquad (E_p + w_p - E_0)h(p)\chi_s(p) = -\frac{g^2 N(p)}{16\pi^3}\sum_{r=1}^{3}\tau^r\tau^s \int k(\boldsymbol{p},\boldsymbol{q})\chi_r(\boldsymbol{q})\,\mathrm{d}^3q\,,$$

where

$$K(\boldsymbol{p},\boldsymbol{q}) = \frac{\langle \boldsymbol{p}^+ | i\beta\gamma^5 | \boldsymbol{p} + \boldsymbol{q}^- \rangle \langle \boldsymbol{p} + \boldsymbol{q}^- | i\beta\gamma^5 | \boldsymbol{q}^+ \rangle}{\sqrt{\omega_p}\sqrt{\omega_q}(E_p + E_q + E_{p+q} - E_0)}$$

and

$$h(p) = 1 - \frac{N(p)g^2}{8\pi^3}\int \frac{(E_p + W_p - E_0)\langle \boldsymbol{q}^+ | i\beta\gamma^5 | \boldsymbol{p}+\boldsymbol{q}^- \rangle \langle \boldsymbol{p} + \boldsymbol{q}^- | i\beta\gamma^5 | \boldsymbol{q}^+ \rangle}{\omega_p(W_p - E_q - E_{p+q})^2(E_p + E_q + E_{p+q} - E_0)} \cdot \mathrm{d}^3q$$

Neglecting the nucleon recoil we obtain:

$$(19)\qquad (M + W_p - E_0)h(p)\chi_s(p) = -\frac{g^2 N(p)}{4\pi^2}\sum_{r=1}^{3}\tau^r\tau^s \int \frac{q^2\chi_r(q)\,\mathrm{d}^3q}{\sqrt{\omega_p}\sqrt{\omega_q}(3M - E_0)}$$

and

$$h(p) = 1 - \frac{g^2 N(p)}{\pi^2}\frac{(M + w_p - E_0)}{\omega_p(w_p - 2M)^2(3M - E_0)}\frac{\xi^3 M^3}{3}\,.$$

Separating the isotopic spin variables [6] we obtain the following equations for isotopic spins $\frac{3}{2}$ and $\frac{1}{2}$ respectively:

$$(20a)\qquad (M + w_p - E_0)h(p)\chi_{\frac{3}{2}}(p) = -\frac{g^2 N(p)}{2\pi^2}\int \frac{q^2\chi_{\frac{3}{2}}(q)\,\mathrm{d}q}{\sqrt{\omega_q}\sqrt{\omega_p}(3M - E_0)}$$

$$(20b)\qquad (M + w_p - E_0)h(p)\chi_{\frac{1}{2}}(p) = \frac{g^2 N(p)}{4\pi^2}\int \frac{q^2\chi_{\frac{1}{2}}(q)\,\mathrm{d}q}{\sqrt{\omega_q}\sqrt{\omega_p}(3M - E_0)}\,.$$

[6] S. Fubini: *Nuovo Cimento*, **10**, 564 (1953).

Remembering the definitions (8) and (9) of Z_3 and g_c^2 we have:

$$g^2 N(p) = \frac{g_c^2}{1 + g_c^2[A(p) - A(0)]} . \tag{21}$$

We can therefore write equations (20) in the following form:

$$(M + w_p - E_0)h(p)\chi_{\frac{3}{2}}(p) = -\int \frac{g_c^2}{2\pi^2} \frac{q^2 \chi_{\frac{3}{2}}(q)\,dq}{\sqrt{\omega_q}\sqrt{\omega_p}(3M - E_0)\{1 + g_c^2[A(p) - A(0)]\}} \tag{22a}$$

$$(M + w_p - E_0)h(p)\chi_{\frac{1}{2}}(p) = \frac{g_c^2}{4\pi^2}\int \frac{q^2 \chi_{\frac{1}{2}}(q)\,dq}{\sqrt{\omega_p}\sqrt{\omega_q}(3M - E_0)\{1 + g_c^2[A(p) - A(0)]\}} \tag{22b}$$

and

$$h(p) = 1 - \frac{g_c^2}{\pi^2}\frac{\xi^3 M^3}{3} \frac{M + w_p - E_0}{\omega_p (w_p - 2M)^2 (3M - E_0)\{1 + g_c^2[A(p) - A(0)]\}} .$$

Let k be the value of p for which $M + w_p - E_0$ vanishes, then equation (22) can be written in the form:

$$\chi_{\frac{3}{2}} = \delta(p - k) - \frac{g_c^2}{2\pi^2}\int G(p, q)\chi_{\frac{3}{2}}(q)\,dq \tag{23a}$$

$$\chi_{\frac{1}{2}}(p) = \delta(p - k) + \frac{g_c^2}{4\pi^2}\int G(p, q)\chi_{\frac{3}{2}}(q)\,dq , \tag{23b}$$

where

$$G(p, q) = \frac{q^2}{\sqrt{\omega_p}\sqrt{\omega_q}(3M - E_0)} \frac{1}{h(p)(w_p - w_k)\{1 + g_c^2[A(p) - A(0)]\}} .$$

The Schmidt method ([6]) for integral equations gives the solution in the form:

$$\chi_p = \delta(p - k) + \int \frac{\Delta(k; p, q)}{D(k)} \delta(q - k)\,dq = \delta(p - k) + \frac{\Delta(k; p, k)}{D(k)} . \tag{24}$$

The phase shifts are given by the formula ([7]):

$$\operatorname{tg} \eta = \pi \frac{1}{D(k)} \lim_{p \to q} [(p - k)\Delta(k; p, k)] . \tag{25}$$

In the Appendix are deduced the expressions of $\Delta(k; p, k)$ and $D(k)$ for the values of $T = \frac{1}{2}$ and $T = \frac{3}{2}$.

([7]) W. Kohn: *Phys. Rev.*, **84**, 495 (1951).

We get in this way:

$$(26a) \qquad \operatorname{tg}\alpha_1 = \frac{g_c^2}{4\pi}\,2M\,\frac{k}{-w_k}\,\frac{1}{1+g_c^2[A(k)-A(0)]}\,\frac{1}{(1+\varepsilon)D_{\frac{1}{2}}(k)}\,,$$

$$(26b) \qquad \operatorname{tg}\alpha_3 = -\frac{g_c^2}{2\pi}\,\frac{k}{2M-w_k}\,\frac{1}{1+g_c^2[A(k)-A(0)]}\,\frac{1}{(1+\varepsilon)D_{\frac{3}{2}}(k)}\,.$$

4. – Discussion and numerical results.

From the experimental point of view the situation of s-wave pion-nucleon scattering is not quite clear, however at present time the signs of α_1 and α_3 at low energy seem to be out of discussion (8); that is α_1 must be positive and α_3 must be negative, and their difference of the order of $(0.23 \div 0.27)\eta$.

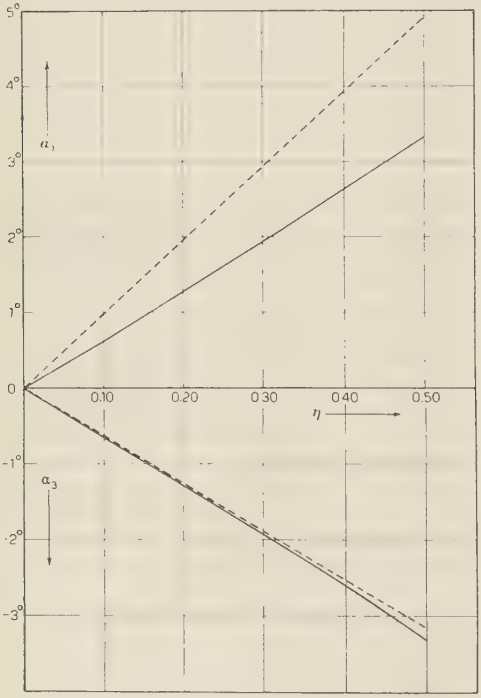

Fig. 1.

We can easily see that the signs of our phase-shifts are the correct ones and that they do not depend on the assumed values of $g_c^2/4\pi$ provided ξ is chosen in a reasonable way.

Moreover, we can see from eq. (26) that $g_c^2/4\pi$ is determined uniquely by a given set of values for the phase-shifts. The most recent pion-nucleon scattering phase-shifts analysis at low energy has been given by OREAR (8,9); with his values $g_c^2/4\pi$ has to be taken equal to 1. If we assume $\xi = 0.7$ we obtain the lines of the fig. 1. (The dotted lines are the phases of Orear).
With these values of the parameters we get for w_k:

$$w_k = \omega_k - 44.45 - 0.024\omega_k \text{ MeV}\,,$$

and we see in this way that the correction ε introduced by our mass renormalization procedure is very small.

(8) *Proceeding of Fifth Annual Rochester Conference on high energy nuclear Physics.*
(9) J. OREAR: *Phys. Rev.*, **96**, 176 (1954).

Finally it is worth white to spend a few words about the magnitude of $g_c^2/4\pi$. First we notice that its value is of the same order of the renormalized constant deduced in the frame-work of GOLDBERGER-DESER-THIRRING [10]. This leads to the conclusion that the nucleon-antinucleon cloud of the pion seems to be coupled with the pion much more weakly than the pion cloud is coupled to the nucleon. Moreover, since the s-scattering results of our model agree with the experimental ones, it does not seem unlikely that this scattering at very low energy is mainly due to the production of only one virtual pair in the cloud of the meson.

* * *

The problem was suggested to the authors by Prof. M. CINI and Dr. S. FUBINI, whose constant assistance is gratefully acknowledged. We are also indebted to Prof. G. WATAGHIN for his kind interest in this work. One of us (R.S.) would like to express his gratitude to Prof. G. WATAGHIN for the kind hospitality in his Institute.

APPENDIX

The Kernel of equation (23) is of the type $G(p, q) = M(p)N(q)$ and therefore it follows immediately:

$$\text{(27)} \qquad \begin{cases} D_{\frac{1}{2}}(k) = 1 - \dfrac{g_c^2}{4\pi^2}\displaystyle\int_0^{\xi_M} M(q)N(q)\,\mathrm{d}q \\ D_{\frac{3}{2}}(k) = 1 + \dfrac{g_c^2}{2\pi^2}\displaystyle\int_0^{\xi_M} M(q)N(q)\,\mathrm{d}q \end{cases}$$

and

$$\text{(28)} \qquad \begin{cases} \Delta_{\frac{1}{2}}(k; p, k) = \dfrac{g_c^2}{4\pi^2}\, M(p)N(k) \\ \Delta_{\frac{3}{2}}(k; p, k) = -\dfrac{g_c^2}{2\pi^2}\, M(q)N(k) \end{cases}$$

From equation (28) and eq. (25) we get directly eqs. (26). Using some trivial approximation, the integral

$$\text{(29)} \qquad I = \int_0^{\xi_M} M(q)N(q)\,\mathrm{d}q$$

---

[10] See reference [5]. This range is 0.3-2.

can be written in the form:

$$(30) \qquad I = -\frac{12\pi^2}{g_c^2\xi^3(1+\varepsilon)^3}\int_0^{\xi_M}\frac{q^2\,\mathrm{d}q}{(\omega_q-\omega_k)\{\omega_q^2-2B\omega_q-A\}}\,.$$

where:

$$2B = [2M - w_k]\left\{\frac{12\pi^2}{(1+\varepsilon)^2 g_c^2\xi^3} - \frac{M+\Delta}{\mu(1+\varepsilon)^2}\right\} - \frac{M+\Delta}{1+\varepsilon} + \omega_k$$

$$A = \frac{\omega_k}{1+\varepsilon}[M+\Delta] + [2M - w_k]\frac{M+\Delta}{(1+\varepsilon)^2}\,.$$

The evaluation of integral (30) is straightforward, and retaining the only relevant terms we obtain:

$$(31) \qquad I = \frac{1}{\alpha}\frac{12\pi^2}{g_c^2\xi^3(1+\varepsilon)^3}\left\{\omega_k \log\left[\xi\frac{M}{\mu} + \sqrt{1+\xi^2\frac{M^2}{\mu^2}}\right] + \mu\sqrt{1+\xi^2\frac{M^2}{\mu^2}} - \right.$$

$$\left. - k\log\left[\frac{\xi\,(M/\mu)\,k + \omega_k\sqrt{1+\xi^2 M^2/\mu^2} - \mu}{\mu\sqrt{1+\xi^2 M^2/\mu^2} - \omega_k}\right]\right\}.$$

Where α is the positive root of the following equation:

$$\alpha^2 - 2B\alpha - A = 0\,.$$

In the energy range of our problem α is given by

$$\alpha = 2B\,.$$

RIASSUNTO

Si discute un modello di teoria dei campi che può essere risolto esattamente. Questo modello si ottiene ritenendo nell'hamiltoniana *ps-ps*, i soli termini che corrispondono alla creazione di una coppia di nucleoni e distruzione di un mesone assieme al processo inverso. Con questa hamiltoniana ridotta anche negli stati virtuali è presente un numero finito di particelle. Per lo scattering pione-nucleone soltanto una coppia può esistere negli stati intermedi e si possono dedurre le fasi *s* a bassa energia. Il confronto con l'esperienza è soddisfacente.

The Low Energy Nuclear Mechanics and the Independent Particle Model.

A. Kind

Istituto di Fisica dell'Università - Padova
Istituto Nazionale di Fisica Nucleare - Sezione di Padova

(ricevuto il 16 Giugno 1955)

Summary. — The author analizes the independent particle model of the nucleus in its definition as an approximation to *week incoherent interaction* and its applicability to general problems of low energy nuclear mechanics. In zero approximation, defined by a condition of selfconsistency, the potential wells which determine the states of the single nucleons in the nucleus have a mean depth of the order of twice the mean potential energy per nucleon. It results, for instance, that direct emission and evaporation processes of nucleons have different thresholds. It is emphasized that the optical model for nuclear reactions can be directly derived from the model considered.

Different models, according to the interval of energy to be considered, show themselves differently adapted for describing the mechanics of the nucleus.

The idea formulated by Serber in his article of 1947 (1), that in the nucleon-nucleus high energy impact the interaction occurs predominantly between only two particles at a time, has been particularly profitable.

In recent years, the well known theory of multiple scattering has been developed, based on this idea, and consisting in the formulation of a method with which, by starting from the approximation of the two particles interaction, it is possible, at least partially, to take into account the contemporary participation of the other particles in the interaction, by way of perturbation (2).

(1) R. Serber: *Phys. Rev.*, **72**, 1114 (1947).

(2) For literature on the subject see: G. Takeda and K. M. Watson: *Phys. Rev.*, **97**, 1336 (1955).

In these terms, the multiple scattering formalism seems to be applicable only in the cases where the hypothesis of the two particles interaction represents a good starting approximation. The limit of the energy E of the incident nucleon, below which its application should not be justified, is about 50 MeV.

Even so, this formalism has also been applied to low energy problems, giving some apparently interesting results. It is not easy to explain their real significance, but it is certain that some of them are essentially due to fortuituous circumstances.

KIND and PATERGNANI ([3]) have calculated, in the approximation of the two nucleons interaction, the mean free path for nucleons in nuclear matter for E ranging from 50 MeV down to the values corresponding to the nucleons bounded in the nucleus; and for $E = 0$ they have obtained a result in good accord with that determined empirically by FESHBACH, PORTER and WEISSKOPF ([1]). This result however depends strongly on the configuration that is assumed for nuclear matter ([5]), and the accord is obtained only if this coincides with that of a Fermi gas, absolutely without interaction.

Still with the multiple scattering model, BRUECKNER, LEVINSON and MAHMOUD ([6]) have found an apparently satisfactory value for the nuclear binding energy. The correctness of their method is not, however, shown by the fact that in the second order approximation they obtain a small correction with respect to the first, since this result is closely tied to the structure of their starting approximation (Fermi degenerated gas) which is extremely resistent to any perturbative process, justified or not as the case may be.

On the other hand, a model, which seems to be suggested in a particularly natural way from our current knowledge about the structure of nuclear matter, for describing nuclear reactions in the limit case of low energy, is that according to which a nucleon in the interior of the nucleus interacts in a predominant way only with the whole of the other nucleons, behaving in their field of forces as an independent particle. This is the independent particle model.

In this note, it is intended to place in evidence the essential points of a correct formulation of this model, mentioning some particular characteristics for nuclear mechanics in general, which derive from it.

The idea of the independent particle model can be defined in the following way: In the description of a nuclear system at low energy (nucleus in the fundamental state, nucleon-nucleus interaction, etc.) it is possible to select a

---

([3]) A. KIND and G. PATERGNANI: *Nuovo Cimento*, **10**, 1375 (1953).

([1]) H. FESHBACH, C. E. PORTER and V. F. WEISSKOPF: *Phys. Rev.*, **96**, 448 (1954).

([5]) A. KIND and G. PATERGNANI: *Nuovo Cimento*, **11**, 106 (1954).

([6]) K. A. BRUECKNER, C. A. LEVINSON and H. M. MAHMOUD: *Phys. Rev.*, **95**, 217 (1954).

complete set of orthogonal functions Φ_k (antisymmetrized products of functions φ_i of single nucleons) so that, if in the representation generated from it we divide the total hamiltonian into a diagonal part H^0 and a non-diagonal part H^1, the H^1 part can be treated as a perturbation.

In these terms, the independent particle model is a *weak incoherent interaction* approximation.

Rigorous solution of this iterative procedure would require the solution of the problem of its convergence and, in particular, that of the saturation of nuclear forces. If, however, as is done here, we base the independent particle model on experimental evidence, these delicate problems which even today are still not resolved, can, at least up to a certain point, be left aside. It will only be necessary, in the development of the iterative procedure, to stop where they begin to gain importance.

We are thus content with a reduced solution of the problem.

In this, we must choose the system of the Φ_k functions, which, in our formalism, are solutions of zero order in H^1.

In principle, every such system is equivalent.

We restrict our choice so as to obtain the best possible starting approximation and, for this purpose, we require (and this will be realized only by iterative means) that the selfconsistency, which has to be satisfied for the rigorous solution ψ, is already so, at least on an average, in the zero order approximation. It will be generally only approximately possible to reconcile this condition with that of orthogonality of the Φ_k functions, and, in this sense, we introduce an inconsistency in the solution of the problem. Every function φ_i of the Φ_k describes the state of a single nucleon in the field of forces generated by all the others. If we want to build it as a solution of a potential well V_i, this should have a mean value $\bar{V}_i$ equal to the mean potential energy that the φ_i has effectively in that field. Indicating this with v_i^0, the condition of selfconsistency is written

$$\bar{V}_i = v_i^0 . \tag{1}$$

Let us admit that nuclear forces are given by the interaction hamiltonian

$$H_{\text{int}} = \tfrac{1}{2} \sum_{ij} V(i,j) .$$

The total mean potential energy of the nucleus in zero order approximation is

$$U^0 = \tfrac{1}{2} \sum_m \sum_n I_{mn} , \tag{2}$$

where

$$I_{mn} = \int \varphi_m^*(1)\varphi_n^*(2) V(1,2)[\varphi_m(1)\varphi_n(2) - \varphi_n(1)\varphi_m(2)] ,$$

is the mean interaction energy relative to the pair of states φ_m and φ_n. The mean potential energy v_i^0 of the state φ_i is equal to the work (negative) that nuclear forces accomplish by the extraction from the nucleus of the particle occupying the state φ_i, when the configuration of the other states remains unaltered. Thence (fixing alternatively in the two summations of (2) the index i) one has

$$v_i^0 = \sum_n I_{in} .$$

In this way

$$U^0 = \tfrac{1}{2} \sum_m v_m^0$$

and from (1)

$$\tfrac{1}{2} \sum_m \overline{V}_m = U^0 .$$

Similarly, indicating with t_i^0 the mean kinetic energy of the state φ_i, for the total energy of the system in zero approximation, we have

$$E^0 = \sum_m (\tfrac{1}{2} v_m^0 + t_m^0)$$

and, in order to satisfy (1),

$$E^0 = \sum_m (\tfrac{1}{2} V_m + t_m^0) . \tag{3}$$

If the considered system is a nucleus of A nucleons, we can write

$$v_i^0 = (A-1) I_i ,$$

defining in this way the mean interaction energy I_i of a generical pair which can be built with the state φ_i.

Averaging over all the A states φ_i of the nucleus, one obtains for the mean potential energy of a generical one of these, the value

$$v^0 = (A-1) I ,$$

where I represents the mean interaction energy for a generical pair of states φ.

From (1) we then have for the mean value of the potential well relative to a generical state φ

$$\overline{V} = v^0 . \tag{4}$$

For the total mean potential energy we finally have

$$U^0 = \tfrac{1}{2} A (A-1) I$$

and for the fraction of potential energy $u^0 = U^0/A$

$$u^0 = \tfrac{1}{2}(A-1)I = \tfrac{1}{2}v^0 , \tag{5}$$

from which, by means of (4),

$$V = 2u^0 .$$

If it is admitted that the radius of the nucleus is proportional to $A^{\frac{1}{3}}$, one obtains for u^0, (by neglecting surface effects) a value independent of A. On the contrary, on A depend the quantities I, and, if we indicate this dependence by a prime, from (5) we have

$$\frac{I^{A-1}}{I^A} = \frac{A-1}{A-2} . \tag{6}$$

Although the so defined zero order approximation of the independent particle model must usually be corrected by the introduction of the perturbation H^1 in order to give satisfactory results, it already contains the essential characteristics of the low energy nuclear mechanics (see, for instance, the shell model).

As an example, we want to calculate, for the two extreme cases of direct emission and evaporation, the threshold value Q of the energy that is to be transfered to a nucleon of a nucleus of weight A, so that its emission occurs.

Direct emission: By definition, in this case, the nucleon receiving the energy Q leaves the nucleus without interacting anelastically with it. To simplify the example, one can admit, without affecting the rigorousness of the reasoning, that the struck nucleon belongs to the generical state φ with mean potential and kinetic energies v^0 and t^0.

Thence one will have

$$Q = -(v^0+t^0) .$$

Once the nucleon is emitted, the residual nucleus must take itself into a new equilibrium state. Let us admit that this is the fundamental state corresponding to $A-1$ nucleons. In the contraction from the initial volume to the final one, the energy liberated (by γ emission) is

$$\Delta E = \tfrac{1}{2}(A-1)(A-2)(I^A - I^{A-1})$$

and from (6)

$$\Delta E = -\tfrac{1}{2}(A-1)I^A = -u^0 .$$

The difference

$$Q - \Delta E = -(u^0 + t^0) \equiv b^0$$

is, as it has to be, equal to the binding fraction for a nucleon in zero order approximation.

Evaporation: In this case, the nucleon is emitted while the nucleus is going into the equilibrium state corresponding to $A - 1$ nucleons. The energy ΔE developed in the contraction can be totally absorbed by the emitted nucleon and the threshold for the reaction is

$$Q = b^0 .$$

The difference between the two various thresholds is a measurable effect (angular distribution of the emitted nucleons). It is however essential that, in the analysis of the experimental data, one considers as direct emission only those events in which it is possibel to admit, at least to a good approximation, that the emission mechanism has not involved the whole of the nucleus.

When we consider the case of nucleon-nucleus collisions, we can see that the application of the independent particle picture leads directly to a description in terms of the optical model (7). While in the zero order approximation, one obtains a real optical potential of a mean depth equal to the mean potential energy v_i^0 of the state φ_i which describes the scattered nucleon, in the first order approximation in H^1 one obtains, by means of the determination of the mean life of the zero order solution, an expression for the imaginary part of it.

Finally, it is to be emphasized that only indirectly it is possible to describe a nuclear system in the independent particle approximation by means of the solution (eigenfunction and eigenvalue) of a Schrödinger equation, in which one has simply substituted for the correct interaction hamiltonian H_{int} a system of potential walls V_i, each acting on the co-ordinates of a single nucleon.

In fact, describing the system with the equation

$$\left(\sum_i - \frac{\hbar^2}{2M} \nabla^2 + \sum_i V_i \right) \Phi = E^0 \Phi$$

(where M is the nucleon mass) for its total energy one would have

$$E^0 = \sum_i (V_i + t_i^0) . \tag{7}$$

(7) A. KIND and C. VILLI: *Nuovo Cimento*, **1**, 749 (1955).

If however the single potential V_i has to describe the interaction of the nucleon i with all the others, when one sums over the index i from 1 to A, the potential energy is counted twice, and (7) does not give the energy of the system. This should be obviously equivalent, in the case of an atomic system, to adding to the interaction energy of the electrons with the nucleus, that of the nucleus with the electrons. On the contrary, the energy of the system is given in the correct way by (3).

If, however, we want to satisfy (7), it is necessary to impose on the potentials the condition

$$\sum_i V_i = U^0$$

which does not satisfy that of selfconsistency (1).

* * *

The author wishes to thank Dr. C. Villi for useful discussions about the subject.

RIASSUNTO

Il modello a particelle indipendenti del nucleo è analizzato nella sua definizione di approssimazione ad « interazione incoerente debole » e nella sua applicabilità ai problemi di bassa energia della meccanica del nucleo in genere. Nell'approssimazione di ordine 0, definita da una condizione di autoconsistenza, le buche di potenziale che determinano gli stati dei singoli nucleoni hanno una profondità media dell'ordine di 2 volte l'energia potenziale del nucleo divisa per il numero dei nucleoni. Ne risulta, per es., che i processi di emissione diretta ed evaporazione di un nucleone hanno soglie diverse. Si mette in evidenza come il modello ottico per le reazioni nucleari si deduca direttamente da quello considerato.

Osservazioni sull'interferenza coulombiana nello scattering $\pi^+ + P$.

E. Pedretti e A. Stanghellini
Istituto di Fisica dell'Università - Bologna

G. Quareni
Istituto di Fisica dell'Università - Padova

(ricevuto il 16 Giugno 1955)

Riassunto. — Basandoci sui dati sperimentali finora disponibili, abbiamo tracciato l'andamento con l'energia, fino a 150 MeV, delle fasi α_3 ed α_{33}, che intervengono nello scattering. Si assume che α_{31} sia trascurabile in questo intervallo energetico. Con queste fasi è stata determinata l'energia più favorevole per un esperimento che permetta di rivelare l'interferenza coulombiana e quindi che permetta di determinare il segno delle fasi. Il valore optimum dell'energia risulta intorno a 120 MeV. Esistono finora due determinazioni sperimentali a 113 e a 120 MeV ottenute con emulsioni fotografiche. Abbiamo sommato i risultati dei due esperimenti. La sezione d'urto differenziale risultante, basata su un totale di 782 eventi, corrisponde all'energia di 117 MeV. Essa indica chiaramente che l'interferenza coulombiana deve essere distruttiva. Le fasi trovate, secondo la soluzione di Fermi, sono: $\alpha_3 = -(11{,}1 \pm 1{,}0)^\circ$, $\alpha_{33} = (31{,}5 \pm 2{,}1)^\circ$, $\alpha_{31} = -(0{,}6 \pm 1{,}8)^\circ$. Questa soluzione, rispetto a quella che si ottiene scambiando tutti i segni delle fasi, è statisticamente preferita per un fattore 1360.

Nell'analisi in onde parziali delle sezioni d'urto di scattering pione-nucleone, si assume che intervengano solamente le onde S e P di cui si determinano gli sfasamenti. Il loro andamento con l'energia è abbastanza ben conosciuto nell'intervallo che va da poche decine di MeV a 250 MeV circa. Se si analizzano le sezioni d'urto totali e differenziali, tenendo conto delle forze nucleari e trascurando quelle coulombiane, il segno delle fasi rimane indeterminato. L'effetto d'interferenza di questi due tipi di forze rende possibile la determinazione del segno. Se si trascurano le forze coulombiane e si descrive lo scattering con le

sole onde S e P, la sezione d'urto differenziale risulta, come è noto, del tipo:

$$\sigma(\vartheta) = a + b \cos\vartheta + c \cos^2\vartheta .$$

L'interferenza produce rispetto a questo andamento un'alterazione in quella regione angolare dove le sezioni d'urto coulombiana e nucleare sono confrontabili. Essa sarà tanto più importante, quanto più piccolo è l'angolo di scattering, come si comprende facilmente se si tien presente che lo scattering coulombiano è regolato dalla formula di Rutherford. Al crescere dell'energia questa regione si restringe sempre più verso gli angoli più piccoli; anche questo comportamento rientra nelle proprietà dello scattering coulombiano.

Sperimentalmente la determinazione della sezione d'urto di scattering ai piccoli angoli è in genere piuttosto difficile: le ragioni risiedono nella scarsa frequenza di questi eventi dovuta alla piccolezza dell'angolo solido e alle difficoltà di rivelazione e di riconoscimento dei singoli scattering. Con la tecnica delle lastre, a cui ci riferiremo, la possibilità di rivelare gli scattering sull'idrogeno è ricondotta all'osservazione dei protoni di rinculo, le cui tracce possono essere osservate con buona efficienza se la loro lunghezza non scende al di sotto di 10μ. Ciò comporta, negli esperimenti intorno a 120 MeV d'energia, un taglio dell'intervallo angolare a circa 15° nel sistema del baricentro.

Le precedenti considerazioni indicherebbero che per mettere in luce l'interferenza coulombiana dovrebbero essere preferiti gli esperimenti ad energie molto basse. Qui però intervengono altre difficoltà: in primo luogo le sezioni d'urto sono assai piccole, in secondo luogo le forze nucleari che intervengono nello scattering $\pi^+ + P$ se sono repulsive nello stato S, sono attrattive nello stato P (o viceversa), così da compensare i loro effetti. Più precisamente ad energie intorno a 50 MeV, a cui sono stati eseguiti i primi esperimenti [1,2], α_3 è dell'ordine di α_3 in valore assoluto, e, considerato che α_{31} è praticamente nulla, le due sezioni d'urto che si possono calcolare scambiando i segni di tutte le fasi risultano praticamente indistinguibili, anche tenendo conto delle forze elettriche. Aumentando l'energia, l'interazione nello stato P diventa predominante e l'effetto d'interferenza può produrre un abbassamento od un innalzamento della sezione di urto a seconda che le forze nucleari sono attrattive o repulsive in questo stato.

Allo scopo di determinare l'optimum d'energia per un esperimento inteso a risolvere il problema dell'interferenza, abbiamo calcolato la quantità:

$$\Delta = 2\pi \int_{15^\circ}^{90^\circ} |\sigma_1(\vartheta) - \sigma_2(\vartheta)| \sin\vartheta \, d\vartheta$$

---

(1) I. P. Perry e C. E. Angell: *Phys. Rev.*, **91**, 1289 (1953); J. Orear, Lord and Weaver: *Phys. Rev.*, **93**, 575 (1954).

(2) D. Bodanski, A. Sachs e J. Steinberger: *Phys. Rev.*, **93**, 1367 (1954).

dove $\sigma_1(\vartheta)$ e $\sigma_2(\vartheta)$ sono le due sezioni d'urto differenziali come risultano scambiando i segni delle fasi. I limiti d'integrazione sono suggeriti: il primo di 15° dalle considerazioni sopra accennate sul taglio imposto dall'osservabilità degli eventi, il secondo di 90° dal fatto che già a quest'angolo le due soluzioni sicuramente si sovrappongono. Δ ha perciò il significato di differenza delle sezioni d'urto secondo le due possibili scelte dei segni delle fasi. Per questo calcolo abbiamo adottato, quale espressione della $\sigma(\vartheta)$ la formula data da SOLMITZ [3], trascurando i termini dell'ordine di $(v_P/c)^2$:

$$\sigma(\vartheta) = \left| \frac{1}{2ik}(P + Q\cos\vartheta) + f^{(nf)}(\vartheta) \right|^2 + \left| \frac{1}{2ik} R \sin\vartheta + f^{(f)})\vartheta) \right|^2$$

In questa formula P, Q, R sono le seguenti espressioni delle fasi:

$$P = \exp(2i\alpha_3) - 1; \qquad Q = \exp(2i\alpha_{31}) + 2\exp(2i\alpha_{33}) - 3;$$
$$R = \exp(2i\alpha_{33}) - \exp(2i\alpha_{31}).$$

Le forze coulombiane sono rappresentate dai termini:

$$f^{(nf)} = -\frac{e^2}{2p(v_\pi + v_P)\sin^2\vartheta/2}\left[1 + \frac{v_\pi v_P}{2c^2}(1 + \cos\vartheta)\right]$$

$$f^{(f)} = \frac{e^2}{2p(v_\pi + v_P)\sin^2\vartheta/2}\frac{\mu_P v_\pi v_P}{2c^2}$$

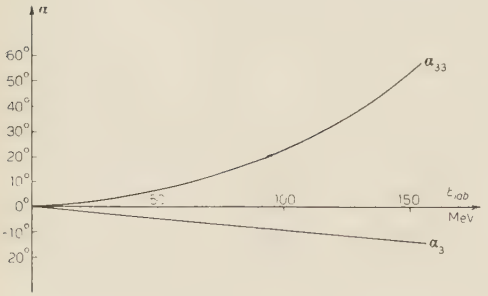

Fig. 1.

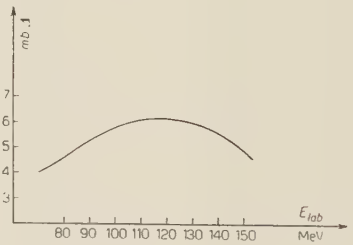

Fig. 2.

dove v_π è la velocità del mesone π, mentre μ_P e v_P sono rispettivamente il momento magnetico e la velocità del protone nel centro di massa.

La quantità Δ è stata calcolata per diverse energie, introducendo nell'espressione della sezione d'urto i valori delle fasi dedotti dalle curve di fig. 1, che abbiamo tracciate basandoci sui dati sperimentali finora disponibili. Nel calcolo abbiamo assunto che α_{31} sia zero nell'intervallo energetico considerato.

In fig. 2 è mostrato l'andamento di Δ in funzione dell'energia; esso presenta un massimo piuttosto appiattito intorno all'energia di ~ 120 MeV. Riteniamo

[3] F. T. SOLMITZ: *Phys. Rev.*, **94**, 1799 (1954).

dunque che questa sia l'energia più conveniente per una ricerca sperimentale dell'interferenza coulombiana. Finora sono stati eseguiti due esperimenti in questa regione di energia: a 113 MeV da J. Orear [4] e a 120 MeV da L. Ferretti *et al.* [5]. Entrambi indicano come più attendibile una interferenza distruttiva.

Allo scopo di ottenere un'indicazione più forte abbiamo sommato i due risultati (*) in un'unica distribuzione angolare da 15° a 150° nel centro di massa, basata su un totale di 782 eventi. L'energia media di interazione, pesata sul numero di eventi trovati nei due esperimenti, risulta 117 MeV. Per passare dalla distribuzione angolare alla sezione d'urto differenziale, che è rappresentata in fig. 3, abbiamo assunto quale valore della sezione d'urto totale a questa energia 90 mb, come suggerisce l'insieme dei dati sperimentali finora ottenuti.

Gli eventi sono stati distribuiti in gruppi di 15° in 15° nel centro di massa. Gli errori sono quelli standard e si riferiscono alle incertezze statistiche. I punti sperimentali tra 45° e 150° sono stati usati per determinare, col metodo dei minimi quadrati, l'andamento della sezione d'urto con le sole forze nucleari. Essa è risultata:

$$\sigma(\vartheta) = (4\ 17 \pm 0.39) - (3.86 \pm 0.84)\cos\vartheta + (10.54 \pm 1.25)\cos^2\vartheta \quad \text{mb}$$

Fig. 3.

ed è rappresentata in fig. 3 dalla curva punteggiata. Col metodo di Ashkin e Vosko [6] abbiamo calcolato le fasi corrispondenti alla soluzione di Fermi. Esse sono:

1) $\alpha_3 = -(11.1 \pm 1.0)^\circ \quad \alpha_{33} = (31.5 \pm 2.1)^\circ \quad \alpha_{31} = -(0.6 \pm 1.8)^\circ,$

2) $\alpha_3 = (11.1 \pm 1.0)^\circ \quad \alpha_{33} = -(31.5 \pm 2.1)^\circ \quad \alpha_{31} = (0.6 \pm 1.8)^\circ.$

[4] J. Orear: *Phys. Rev.*, **96**, 1417 (1954).

[5] L. Ferretti E. Manaresi, G. Puppi, G. Quareni e A. Ranzi: *Nuovo Cimento*, **1**, 1238 (1955).

(*) Ringraziamo il dr. J. Orear per averci fornito l'elenco completo degli angoli di scattering osservati nel suo esperimento.

[6] J. Ashkin e S. H. Vosko: *Phys. Rev.*, **91**, 1248 (1953).

Le due serie corrispondono alle due diverse possibilità di scelta dei segni; esse costituiscono due soluzioni che si differenziano se si tiene conto delle forze coulombiane. Alla soluzione 1) corrisponde infatti in fig. 3 la curva a tratto continuo, mentre alla 2) quella tratteggiata.

Si vede che la soluzione 1) fornisce un miglior accordo con i dati sperimentali. In particolare il basso valore della sezione d'urto sperimentale tra 15° e 30° richiede, per essere interpretata, un'interferenza distruttiva delle forze nucleari con quelle del campo coulombiano. Di conseguenza le forze nucleari devono essere in prevalenza attrattive e ciò è in accordo con la soluzione 1), dove la fase α_{33} è positiva. Le due soluzioni 1) e 2) permettono di calcolare il numero di eventi attesi nell'intervallo angolare tra 15° e 30°. Secondo la soluzione 1) questo numero risulta 47.5; secondo la soluzione 2) esso è 70. In realtà in questo intervallo compaiono 38 eventi. Le probabilità dei due scarti sono date dalla legge di Poisson, ed il loro rapporto è 1360 in favore dell'interferenza distruttiva.

Facciamo osservare che la conclusione a cui siamo giunti è condizionata dall'ipotesi che in questo processo di scattering intervengano le onde S e P solamente, ovvero che sia trascurabile il contributo delle onde superiori. Gli andamenti delle sezioni d'urto sperimentali a queste energie parrebbero confermare questa ipotesi anche se nessun esperimento finora eseguito presenta un'accuratezza tale da poter escludere il contributo di onde superiori. D'altra parte la conclusione cui si giunge dall'analisi dell'interferenza coulombiana nello scattering dei π^+ è in accordo con i risultati dello scattering dei π^- ([2]), se si assume il principio d'indipendenza rispetto alla carica. Anche per questi processi la soluzione più attendibile è quella che porta ad una fase α_{33} grande e positiva.

***

Ringraziamo il Prof. G. Puppi per l'interesse con cui ha seguito questa ricerca e per gli utili consigli da lui ricevuti.

SUMMARY

Referring to the experimental data, available so far, we have traced the behaviour with the energy up to 150 MeV, of the phase shifts α_3 and α_{33} which concern the scattering. α_{31} is considered negligable in this energy interval. From these phase shifts, the most favorable energy for an experiment which could reveal the Coulomb inter-

ference, and therefore the signs of the phase shift, has beendetermined. The optimum value of the energy is around 120 MeV. Up to now, two experimental determinations exist at 113 and 120 MeV, obtained with photographic plates. We added up the results of the two experiments. The differential cross-section obtained, based on a total of 782 events, corresponds to an average energy of 117 MeV; it clearly shows that the Coulomb interference must be destructive The phase shifts found, according to Fermi's solution, are: $\alpha_3 = -(11{,}1 \pm 1{,}0)^\circ$, $\alpha_{33} = (31{,}5 \pm 2{,}1)^\circ$, $\alpha_{31} = -(0{,}6 \pm 1{,}8)^\circ$. This solution in comparison to the one obtained by changing all the signs of the phase shifts, is statistically preferable by a factor of 1 360.

Sul moto di un elettrone finito e la corrispondenza con l'elettrone puntiforme nella meccanica classica relativistica (1).

E. Bellomo

Dublin Institute for Advanced Studies

(ricevuto il 30 Giugno 1955)

Riassunto. — Si studia dapprima un particolare modello di elettrone esteso, ricavandone le equazioni del moto. Si mostra l'origine del comportamento singolare delle soluzioni quando esso è piccolo a sufficienza. Ci si sofferma sui dettagli con particolare riguardo alla conservazione dell'energia e delle quantità di moto. Il parallelismo con l'elettrone puntiforme è messo in evidenza.

---

1. – Come si sa, l'equazione per l'elettrone puntiforme (2)

$$m\dot{v}^\mu(s) - \tfrac{2}{3}e^2[\ddot{v}^\mu(s) + (\dot{\boldsymbol{v}}(s)\cdot\dot{\boldsymbol{v}}(s))v^\mu(s)] = ev_\nu(s)F^{\mu\nu}_{\text{est.}} \equiv f^\mu_{\text{est.}}, \tag{1}$$

dovuta a Dirac (3), porta a soluzioni inaccettabili fisicamente (4), malgrado che il termine fra parentesi quadra, apparentemente responsabile di questi risultati,

---

(1) Lavoro svolto in gran parte presso l'Istituto di Fisica dell'Università di Pavia. Per un calcolo analogo in forma non covariante si veda D. Bohm and M. Weinstein: *Phys. Rev.*, **74**, 305 (1949); risultati covarianti in D. Bohm, M. Weinstein and H. Kouts: *Phys. Rev.*, **78**, 346 (1950). Per un elettrone esteso in maniera relativisticamente invariante si veda pure H. McManus: *Proc. Roy. Soc.*, **195**, 323 (1948); M. Weinstein: *Tesi* (Princeton, 1953).

(2) Le notazioni tensoriali si intendono nello spazio a quattro dimensioni con metrica pseudo euclidea positiva per i vettori temporali. Anche le notazioni vettoriali vanno intese nello stesso spazio. $F^{\mu\nu}_{\text{est.}}$ è il campo elettromagnetico esterno. Per le altre notazioni si veda il numero seguente.

(3) P. A. M. Dirac: *Proc. Roy. Soc.*, A **167**, 148 (1938).

(4) C. J. Eliezer: *Rev. Mod. Phys.*, **19**, 147 (1947).

debba considerarsi soddisfacente, dal punto di vista sperimentale, per quanto riguarda l'emissione della radiazione.

Con l'intenzione di cercare le cause di tale comportamento, l'autore considera dapprima un modello di elettrone finito a simmetria sferica, rigido secondo una definizione Lorentz-invariante introdotta da BORN [5]. Viene sempre considerato il caso di elettrone non soggetto a forze esterne, limitandosi a cercare sotto quali ipotesi l'elettrone tenda in breve tempo a muoversi di moto uniforme qualunque siano le condizioni iniziali.

Si fa uso soltanto dei potenziali ritardati, ottenendo un'equazione integrale per il moto dell'elettrone del tipo di quelle dell'ereditarietà: funzioni incognite le accelerazioni senza alcuna ipotesi di continuità per i valori assunti in funzione del tempo proprio. Condizioni iniziali: le accelerazioni subite dall'elettrone durante un intervallo di tempo pari a quello impiegato dalla luce per attraversarlo.

Questa equazione, dalla quale si può ottenere l'equazione di Dirac come caso limite se si ammette l'ulteriore derivabilità delle soluzioni, è approssimata a meno di termini svanenti con le dimensioni dell'elettrone.

2. – Si denoti con $\boldsymbol{z}(s)$ le coordinate spaziali e temporali di un punto dell'elettrone (s è il tempo proprio e la velocità della luce è posta uguale ad uno), con $\boldsymbol{v}(s) = \mathrm{d}\boldsymbol{z}(s)/\mathrm{d}s$ la sua velocità ($\boldsymbol{v}(s)\cdot\boldsymbol{v}(s) = 1$) e con $\dot{\boldsymbol{v}}(s) = \mathrm{d}\boldsymbol{v}(s)/\mathrm{d}s$ la sua accelerazione. Useremo una definizione di elettrone rigido che consiste nell'assumere che tutti i suoi punti sono in quiete quando uno di essi è in quiete, cioè che tutte le loro linee di universo sono ortogonali ad un qualunque spazio che sia ortogonale alla linea $\boldsymbol{z}(s)$.

In altre parole la funzione che esprime la densità di carica dell'elettrone è la stessa in quegli spazi.

Se $\boldsymbol{z}(s) + \boldsymbol{\gamma}$ e $\boldsymbol{z}(s + \Delta s) + \boldsymbol{\gamma}^*$ (con $\boldsymbol{\gamma}\cdot\boldsymbol{v}(s) = 0$ e $\boldsymbol{\gamma}^*\cdot\boldsymbol{v}(s + \Delta s) = 0$) sono le intersezioni della linea di universo di un punto dell'elettrone con due tali spazi corrispondenti ai tempi propri s e $s + \Delta s$, $\boldsymbol{\gamma}^*$ è il quadrivettore che risulta dall'applicare a $\boldsymbol{\gamma}$ una trasformazione di Lorentz corrispondente a un cambiamento di velocità da $\boldsymbol{v}(s)$ a $\boldsymbol{v}(s + \Delta s)$.

L'aumento del tempo proprio s' del punto $\boldsymbol{z}(s) + \boldsymbol{\gamma}$ è legato a quello di s da $\mathrm{d}s'/\mathrm{d}s = 1 - \boldsymbol{\gamma}\cdot\dot{\boldsymbol{v}}(s)$, così che in questo punto l'accelerazione è $\mathrm{d}\boldsymbol{v}(s)/\mathrm{d}s' = \dot{\boldsymbol{v}}(s)/(1 - \boldsymbol{\gamma}\cdot\dot{\boldsymbol{v}}(s))$. Assumeremo sempre

$$\boldsymbol{\gamma}\cdot\dot{\boldsymbol{v}}(s) \ll 1 \tag{2}$$

per tutti i punti dell'elettrone.

---

[5] M. BORN: *Ann. d. Phys.*, **30**, 1 (1909).

Non è necessario assumere che $\dot{\boldsymbol{v}}(s)$ sia differenziabile, anzi possiamo supporre che discontinuità di prima specie possano esistere.

Dobbiamo ora valutare la forza a cui l'elettrone è soggetto al tempo s a causa del proprio campo elettromagnetico: tale campo dipende dall'immediato passato dell'elettrone.

Il campo elettromagnetico prodotto al punto $\boldsymbol{x}$ da una carica puntiforme de' posta nel punto $\boldsymbol{x}'$ è rigorosamente dato dalla formula [3]

$$(3) \qquad \mathrm{d}F^{\mu\nu}_{\text{rit.}} = \frac{de'}{(\boldsymbol{r}\cdot\boldsymbol{v}')^3}\{(v'^{\nu}r^{\mu} - v'^{\mu}r^{\nu})(1 - \dot{\boldsymbol{v}}'\cdot\boldsymbol{r}) + (\dot{v}'^{\nu}r^{\mu} - \dot{v}'^{\mu}r^{\nu})(\boldsymbol{v}'\cdot\boldsymbol{r})\},$$

dove $\boldsymbol{r} = \boldsymbol{x} - \boldsymbol{x}'$, $\boldsymbol{r}\cdot\boldsymbol{r} = 0$ e $\boldsymbol{v}'$ e $\dot{\boldsymbol{v}}'$ rappresentano la velocità e l'accelerazione della carica de'. Il campo al tempo s nel punto $\boldsymbol{x} = \boldsymbol{z}(s) + \boldsymbol{\gamma}(\boldsymbol{\gamma}\cdot\boldsymbol{v}(s) = 0)$ è ottenuto integrando la precedente formula rispetto a tutti gli elementi di carica de' le cui coordinate soddisfano la relazione $\boldsymbol{r}\cdot\boldsymbol{r} = 0$: lo si denoti con $F^{\mu\nu}_{\text{rit.}}$.

La forza di Lorentz $\mathrm{d}f^{\mu}$ agente sull'elemento di carica de posto nel punto $\boldsymbol{x}$ è allora

$$(4) \qquad \mathrm{d}f^{\mu} = de F^{\mu\nu}_{\text{rit.}} v_{\nu}(s) =$$

$$= de \int \frac{de'}{(\boldsymbol{r}\cdot\boldsymbol{v}')^3}\{[r'^{\mu}_{\perp}(\boldsymbol{v}'\cdot\boldsymbol{v}(s)) - r'^{\mu}_{\perp}(\boldsymbol{r}\cdot\boldsymbol{v}(s))](1 - \dot{\boldsymbol{v}}'\cdot\boldsymbol{r}) -$$

$$+ (\boldsymbol{v}'\cdot\boldsymbol{r})[(\dot{\boldsymbol{v}}'\cdot\boldsymbol{v}(s))r^{\mu}_{\perp} - (\boldsymbol{r}\cdot\boldsymbol{v}(s))\dot{v}'^{\mu}_{\perp}]\},$$

dove il segno $_{\perp}$ indica la sola parte ortogonale a $\boldsymbol{v}(s)$, e quindi genericamente $\boldsymbol{p}_{\perp}$ sta per $\boldsymbol{p} - (\boldsymbol{p}\cdot\boldsymbol{v}(s))\boldsymbol{v}(s)$.

Si ponga $\boldsymbol{x}' = \boldsymbol{z}(s - \Delta s) + \boldsymbol{\gamma}'$ $(\boldsymbol{\gamma}'\cdot\boldsymbol{v}(s - \Delta s) = 0)$ e si indichi con $\boldsymbol{\gamma}^*$ il trasformato di $\boldsymbol{\gamma}'$ per il cambiamento di velocità da $\boldsymbol{v}(s - \Delta s)$ a $\boldsymbol{v}(s)$.

Si noti ora che $\boldsymbol{v}'^{\mu}_{\perp}$ è dell'ordine di Δs, cioè di $|\boldsymbol{\gamma} - \boldsymbol{\gamma}^*|$, e che lo stesso si può dire di $\dot{\boldsymbol{v}}(s - \Delta s)\cdot\boldsymbol{v}(s)$. Inoltre nell'integrando precedente sono i termini di ordine pari in $|\boldsymbol{\gamma} - \boldsymbol{\gamma}^*|$ che cambiano di segno quando $\boldsymbol{\gamma}$ e $\boldsymbol{\gamma}^*$ sono scambiati e perciò danno un contributo nullo se si integra la precedente espressione rispetto a de. Eseguiamo l'integrazione trascurando per un momento una leggera modificazione [6] a cui ci obbligherebbe la definizione di rigidità adottata.

Il solo termine importante così ottenuto è quello avente in (4) potenza -1

---

[6] In realtà l'ipotesi di rigidità assunta ci costringerebbe a considerare l'impulso e l'energia cedute dal campo elettromagnetico alla massa meccanica dell'elettrone in funzione del tempo proprio s, cioè su spazi ortogonali alle linee di universo, e quindi in generale non paralleli fra loro. Prima di eseguire l'integrazione $\mathrm{d}f^{\mu}$ dovrebbe essere moltiplicato per il fattore $1 - \boldsymbol{\gamma}\cdot\dot{\boldsymbol{v}}(s)$.

in $|\boldsymbol{\gamma} - \boldsymbol{\gamma}^*|$. Sostituendo a $1/(\boldsymbol{r}\cdot\boldsymbol{v}')^3$ l'espressione

$$\frac{1}{(\boldsymbol{r}\cdot\boldsymbol{v}(s))^3}\left(1 - 3\,\frac{\boldsymbol{r}\cdot\boldsymbol{v}_\perp(s-\Delta s)}{\boldsymbol{r}\cdot\boldsymbol{v}(s)}\right),$$

esso può essere scritto:

$$(5)\qquad \iint \frac{de\,de'}{(\boldsymbol{r}\cdot\boldsymbol{v}(s))^3}\Big\{ - v_\perp^\mu(s-\Delta s)(\boldsymbol{r}\cdot\boldsymbol{v}(s)) - (\dot{\boldsymbol{v}}(s-\Delta s)\cdot\boldsymbol{r})r_\perp^\mu - (\boldsymbol{v}(s)\cdot\boldsymbol{r})^2\dot{v}_\perp^\mu(s-\Delta s) - 3\,\frac{(\boldsymbol{r}\cdot\boldsymbol{v}_\perp(s-\Delta s))r_\perp^\mu}{(\boldsymbol{r}\cdot\boldsymbol{v}(s))}\Big\}.$$

L'ipotesi di simmetria sferica per l'elettrone intorno al punto di coordinate $\boldsymbol{z}(s)$ non è stata finora usata, mentre si è scelto $\boldsymbol{z}(s)$ in modo che valga $\iint(\boldsymbol{\gamma}'/|\boldsymbol{\gamma}^* - \boldsymbol{\gamma}|)\,de\,de' = 0$, così da trascurare completamente il fattore $1/(1 - \boldsymbol{\gamma}'\cdot\dot{\boldsymbol{v}}(s-\Delta s))$ per $\dot{\boldsymbol{v}}'(x')$ e le correzioni di ordine superiore per Δs, che deve dunque intendersi uguale a $|\boldsymbol{\gamma}^* - \boldsymbol{\gamma}|$ nella formula precedente.

Assumendo tale ipotesi, e con dipendenza radiale della densità di carica qualsiasi, il primo termine si cancella esattamente col quarto, mentre il secondo diventa $-\frac{1}{3}$ del terzo termine.

In assenza di forze esterne l'equazione del moto è allora

$$(6)\qquad m_0\dot{v}^\mu(s) = -\frac{2}{3}\iint\frac{de\,de'}{\xi}\,\dot{v}_\perp^\mu(s-\xi),$$

dove $\xi = |\boldsymbol{\gamma} - \boldsymbol{\gamma}^*| \cong \boldsymbol{r}\cdot\boldsymbol{v}(s)$, e m_0 denota una massa inerte di origine non elettromagnetica che diremo massa meccanica.

Aggiungendo ai due lati dell'equazione la quantità

$$\frac{4}{3}\,\dot{v}^\mu(s)\iint\frac{de\,de'}{2\xi},$$

si ottiene

$$(7)\qquad \left(m_0 + \frac{4}{3}\iint\frac{de\,de'}{2\xi}\right)\dot{v}^\mu(s) = \frac{2}{3}\iint\frac{\dot{v}^\mu(s) - \dot{v}_\perp^\mu(s-\xi)}{\xi}\,de\,de'.$$

Si può vedere facilmente che quando le dimensioni dell'elettrone tendono a zero questa espressione si riduce all'equazione di Dirac

$$m\dot{v}^\mu(s) = \tfrac{2}{3}\,e^2[\ddot{v}^\mu(s) + (\dot{v}(s)\cdot\dot{v}(s))v^\mu(s)] \equiv \tfrac{2}{3}\,e^2\ddot{v}_\perp^\mu,$$

purchè si identifichi la quantità $m_0 + \frac{4}{3}\iint de\,de'/2\xi$ con la massa sperimentale m e $\dot{\boldsymbol{v}}(s)$ sia pensato differenziabile.

Con l'introduzione del fattore $1 - \boldsymbol{\gamma}\cdot\dot{\boldsymbol{v}}(s)$, di cui si è detto in nota, si otterrebbe allora in (5) il termine addizionale $-\iint[\boldsymbol{\gamma}\cdot\dot{\boldsymbol{v}}(s)/(\boldsymbol{r}\cdot\boldsymbol{v}(s))^3]r_\perp^\mu\,de\,de'$ che in

virtù della simmetria sferica si ridurrebbe a $\frac{1}{3}\dot{v}^{\mu}(s)\iint \mathrm{d}e\,\mathrm{d}e'/2\xi$. Esso riporterebbe ad 1 il fattore 4/3 nel contributo elettromagnetico, ma sarebbe dello stesso carattere di m_0 nell'equazione (6), cioè « istantaneo » (7). E ciò a causa dell'ipotesi di rigidità adottata. Lo potremmo conglobare in m_0 scrivendo $m_0 = m_{\text{mecc.}} - \frac{1}{3} m_{\text{e.m.}}$.

Consideriamo ora al posto della (6) l'equazione

$$m_0\dot{v}^{\mu}(s) = -\frac{2}{3}\iint \frac{\mathrm{d}e\,\mathrm{d}e'}{\xi}\,\dot{v}^{*\mu}(s-\xi), \tag{8}$$

dove l'asterisco ha ancora il solito significato. Questo significa sostituire a $\dot{v}^{\mu}_{\perp}(s-\xi)$ un vettore parallelo e concorde con esso, ma di modulo $|\dot{\boldsymbol{v}}(s-\xi)|$; la differenza è del secondo ordine colle dimensioni dell'elettrone.

Se ora nei due spazi ortogonali alla linea di universo nei generici punti $s - \Delta s$ e s noi costruiamo due sistemi di coordinate i cui vettori unitari sono trasformati l'uno nell'altro dalla trasformazione di Lorentz corrispondente al cambiamento di velocità da $\boldsymbol{v}(s-\Delta s)$ a $\boldsymbol{v}(s)$, e se indichiamo con $\dot{v}^k(s)$ $(k = 1, 2, 3)$ le componenti dell'accelerazione nel nuovo sistema corrispondente al punto s, l'equazione precedente diventa

$$m_0\dot{v}^k(s) = -\frac{2}{3}\iint \frac{\mathrm{d}e\,\mathrm{d}e'}{\xi}\,\dot{v}^k(s-\xi)\,. \tag{9}$$

Queste equazioni sono sempre relativisticamente invarianti; esse hanno in più il vantaggio di essere lineari e valide separatamente per ogni k.

Si deve insistere sul fatto che questa *non* è un'approssimazione non relativistica. Le (9) e le (8) sono perfettamente equivalenti.

Le equazioni (9) hanno soluzioni del tipo $\dot{v}^k = g^k e^{\alpha s}\cos(\beta s + \varphi^k)$, con g^k e φ^k costanti arbitrarie.

Sostituendo infatti si ottiene

$$m_0 g^k e^{\alpha s}\cos(\beta s+\varphi^k) = -\frac{2}{3}\,g^k e^{\alpha s}\Big\{\cos(\beta s+\varphi^k)\iint \frac{\mathrm{d}e\,\mathrm{d}e'}{\xi}\,e^{-\alpha\xi}\cos(\beta\xi) +$$

$$+\sin(\beta s+\varphi^k)\iint \frac{\mathrm{d}e\,\mathrm{d}e'}{\xi}\,e^{-\alpha\xi}\sin(\beta\xi)\Big\}\,.$$

Questo richiede che

$$m_0 = -\frac{2}{3}\iint \frac{\mathrm{d}e\,\mathrm{d}e'}{\xi}\,e^{-\alpha\xi}\cos(\beta\xi) \qquad \text{e} \qquad \iint \frac{\mathrm{d}e\,\mathrm{d}e'}{\xi}\,e^{-\alpha\xi}\sin(\beta\xi) = 0\,. \tag{10}$$

(7) Con ciò si vuol dire che esso dà un contributo all'inerzia contenente la sola accelerazione al tempo s.

I possibili valori di α e β sono determinati da queste equazioni. Le soluzioni divergenti corrispondono ad $\alpha > 0$, e le convergenti ad $\alpha < 0$.

Il primo caso necessariamente implica $|m_0| < (4/3)m_{\text{e.m.}}$. Se anche $\beta = 0$ si hanno le cosiddette soluzioni « fuggenti » (8) per le quali perciò $-(4/3)m_{\text{e.m.}} < < m_0 < 0$, cioè

$$0 < m_0 + \frac{4}{3} m_{\text{e.m.}} < \frac{4}{3} m_{\text{e.m.}} , \tag{11}$$

e viceversa c'è sempre una soluzione della data forma se questa condizione e soddisfatta.

L'equazione (7) può suggerire l'uso dell'equazione approssimata

$$m\dot{v}^{\mu}(s) - \frac{2}{3} e^2 \frac{\dot{v}^{\mu}(s) - \dot{v}^{\mu}_{\perp}(s - \varrho)}{\varrho} = e v_{\nu}(s) F^{\mu\nu}_{\text{est.}} , \tag{12}$$

inveee dell'equazione di Dirac (9).

Le soluzioni della

$$m\dot{v}^{k}(s) - \frac{2}{3} e^2 \frac{\dot{v}^{k}(s) - \dot{v}^{k}(s - \varrho)}{\varrho} = 0 \qquad (k = 1, 2, 3), \tag{13}$$

sono $\dot{v}^{k}(s) = c^{k}(s) \left(\frac{\frac{2}{3}(e^2/\varrho)}{\frac{2}{3}(e^2/\varrho) - m} \right)^{s/\varrho}$ che sono convergenti a zero se $(4/3)(e^2/\varrho) < m$ $(m > 0)$.

Qui i $c^{k}(s)$ sono funzioni periodiche di periodo ϱ arbitrarie. Al limite per ϱ tendente a zero si ha $\dot{v}^{k}(s) = c^{k} e^{\frac{3}{2}(m/e^2)s}$ con c^{k} constanti. In definitiva si ottengono le conclusioni precedenti leggermente semplificate. Le soluzioni divergenti non oscillanti si avrebbero per $0 < m < \frac{2}{3}(e^2/\varrho)$, limitazione che coincide con la (11) interpretando $e^2/2\varrho$ come massa elettromagnetica.

3. – Per quanto riguarda i teoremi di conservazione, l'energia e la quantità di moto sono certamente conservate su iperpiani ortogonali alla linea di universo dell'elettrone per il modo stesso in cui le equazioni sono state scritte.

Inoltre si può dimostrare (vedi appendice) che anche i momenti quadridimensionali di tali grandezze calcolati sui detti iperpiani possono considerarsi

---

(8) Le soluzioni singolari con $\beta \neq 0$ non hanno corrispondente nell'equazione di Dirac, perchè come risulta dalla seconda delle (10) la lunghezza d'onda delle oscillazioni si aggira sulle dimensioni dell'elettrone. Non si tratta di condizioni che diremo in seguito di regime.

(9) Equazioni alle differenze sono state anche usate da altri autori: P. Caldirola: *Nuovo Cimento*, **10**, 1747 (1953); P. Caldirola e F. Duimio: *Nuovo Cimento*, **12**, 699 (1954).

conservati nel modello adottato (a meno di quantità infinitesime con le dimensioni) se si assume la simmetria sferica anche per la densità di massa meccanica.

Dette conservazioni sono valevoli pure per l'elettrone di Dirac, anche senza la restrizione ad iperspazi ortogonali ([10,11]).

Si sa anzi che il termine addizionale nell'equazione di Dirac è dovuto ad un effetto complessivo dell'emissione della radiazione e dell'inerzia elettromagnetica, e precisamente si attribuisce la seconda parte alla reazione della radiazione emessa ([12]), mentre la prima (differenziale esatto ([13]) della cosiddetta « energia di accelerazione » ([3,14])), non è altro che un effetto di ritardo nell'inerzia elettromagnetica, come risulta dalla corrispondenza con l'elettrone finito.

Veramente nel caso di elettrone finito tanto la forza di inerzia che la reazione del campo, cioè l'intero termine a secondo membro della (6), sono un risultato delle interazioni tra i diversi punti dell'elettrone e perciò il fenomeno dell'emissione e la conseguente reazione non può essere considerato un fenomeno istantaneo; la precedente separazione dei termini è valida in quanto per l'elettrone puntiforme siamo per così dire in condizioni di « regime », il che avviene quando le accelerazioni sono derivabili e l'elettrone è così piccolo che accelerazioni e derivate possono considerarsi costanti in tempi corrispondenti a quelli impiegati dalla luce per attraversarlo. Questo, e il fatto che i termini supplementari non sono indipendenti dal termine di inerzia elettromagnetica, ricevono conferma osservando che il secondo membro della (6) è suddiviso in (7) in modo artificioso: per es., dall'intero termine in (6) si può vedere, che se l'elettrone fosse bruscamente sottoposto ad accelerazione costante esso non reagirebbe subito, ma gradualmente in un tempo dell'ordine di quello impie-

---

([10]) H. J. Bhabha: *Proc. In. Acad. Sci.*, A **10**, 329 (1939).

([11]) Si veda anche, per la conservazione dell'energia e quantità di moto, M. H. L. Pryce: *Proc. Roy. Soc.*, A **168**, 389 (1398).

([12]) Ciò può esser visto direttamente calcolando il flusso di energia e impulso attraverso un tubo circondante la linea di universo della particella. Usando i campi ritardati (cioè la formula (3)), il modo più semplice e preciso consiste nell'usare il tubo definito dalle equazioni $(\boldsymbol{r}\cdot\boldsymbol{r})=0$, $(\boldsymbol{r}\cdot\boldsymbol{v}(s))=k$, con $\boldsymbol{r}=\boldsymbol{x}-\boldsymbol{z}(s)$ e $k>0$, che per ogni s definiscono una sezione nella parte del futuro del cono $|r|=0$ con vertice in $\boldsymbol{z}(s)$. In tal modo in corrispondenza ad un dato intervallo ds della linea di universo, anche dopo aver integrato su tutte le direzioni spaziali, non si ottengono termini contenenti potenze positive di k, cioè del raggio del tubo. L'unico termine non svanente quando k tende all'infinito risulta $ds\frac{2}{3}e^2(\dot{\boldsymbol{v}}(s)\cdot\dot{\boldsymbol{v}}(s))\boldsymbol{v}(s)$, che rappresenta pertanto la radiazione emessa. Vedi anche i lavori citati in note ([10,11]).

([13]) Con questo si vuol dire che l'integrale lungo ogni linea di universo tra due estremi fissi, e con ivi gli stessi valori per le derivate fino all'ordine necessario per l'espressione integranda, assume sempre lo stesso valore.

([14]) G. A. Schott: *Phil. Mag.*, **29**, 49 (1915).

gato dalla luce per attraversarlo, cosicchè in un primo momento solo la massa meccanica avrebbe un effetto ([15]).

* * *

Una illustrazione intuitiva della parte che le varie grandezze giocano nell'equazione del moto può aversi scrivendo per l'energia e l'impulso totale della particella l'espressione approssimata

$$m_0 \boldsymbol{v}(s) + \frac{4}{3} m_{\text{e.m.}} \boldsymbol{v}(s - \varrho),$$

essendo ϱ una costante dell'ordine delle dimensioni dell'elettrone.

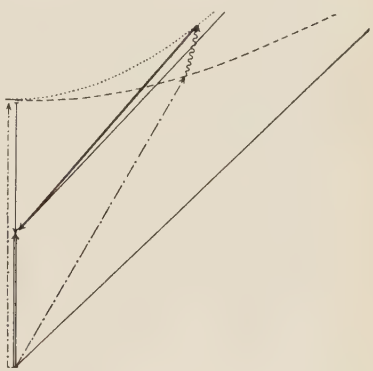

Fig. 1. – Energia e quantità di moto nelle soluzioni fuggenti nel sistema in quiete con la particella al tempo $-\infty$:

⟹ energia e impulso totali;

⟶ energia e impulso meccanici della particella;

⟶ · – · → energia e impulso elettromagnetici della particella.

⟿ energia e impulso della radiazione.

Come abbiamo visto in ogni intervallo di tempo infinitesimo ds la radiazione emessa chiude il bilancio tra energia e impulso ceduti dal campo esterno, ed energia ed impulso assunti dall'elettrone; nell'ipotesi di regime ammetteremo che l'ammontare di queste grandezze emesso sotto forma di radiazione costituisca un quadrivettore tangente alla linea di universo nel punto s.

La fig. 1 mostra allora la possibilità della conservazione nelle soluzioni fuggenti in assenza di campo esterno.

Le figure seguenti mostrano in un sistema in quiete con la particella il bilancio dell'energia e quantità di moto in un tempo molto breve δs, a meno del fattore δs (e di grandezze dell'ordine di ϱ^2).

Nella fig. 2 si ha ancora il caso di soluzioni fuggenti in assenza di campo esterno ([16]).

([15]) Osservazione dovuta a M. Marcov: *Journ. Phys. USSR*, **10**, 159 (1946) Vedi anche G. Morpurgo: *Nuovo Cimento*, **9**, 808 (1952).

([16]) Con considerazioni semplici ci si potrebbe anche render conto che, fissate le masse, l'angolo iperbolico fra i due vettori energia-impulso nelle soluzioni fuggenti

Le figg. 3*a* e 3*b* rappresentano il caso in cui vale la relazione $m\dot{\boldsymbol{v}}(s) \approx \boldsymbol{f}_{\text{est.}}$, rispettivamente per $m_0 > 0$ e $m_0 < 0$.

Nelle condizioni della fig. 3*a*, fissato il valore di ϱ cioè del ritardo, si ha anzi stabilità: se $\boldsymbol{f}_{\text{est}}$ aumenta, subito $\dot{\boldsymbol{v}}(s)$ aumenta, ma il rapporto tra i vettori $m_0\dot{\boldsymbol{v}}(s)$ e $(4/3)m_{\text{e.m.}}\dot{\boldsymbol{v}}(s-\varrho)$ tende a ristabilirsi col tempo, quando anche $\dot{\boldsymbol{v}}(s-\varrho)$ dovrà aumentare obbligando $\dot{\boldsymbol{v}}(s)$ a diminuire; la somma $m_0\dot{\boldsymbol{v}}(s) + (4/3)m_{\text{e.m.}}\dot{\boldsymbol{v}}\ (s-\varrho)$ deve infatti mantenersi uguale alla forza esterna, a meno di differenze dell'ordine di ϱ^2 [17].

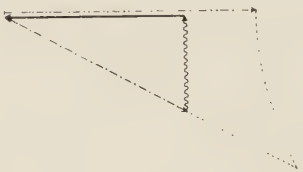

Fig. 2. – Rappresentazione differenziale delle conservazioni dell'energia e quantità di moto nelle soluzioni fuggenti, in un sistema in quiete con la particella:

- $\frac{4}{3}m\dot{\boldsymbol{v}}(s-\varrho)$;
- $\frac{4}{3}m_{\text{e.m.}}\dot{\boldsymbol{v}}_{\text{e.m.}}(s)$;
- $m_0\dot{\boldsymbol{v}}(s)$;
- energia e quantità di moto irradiate nell'unità di tempo.

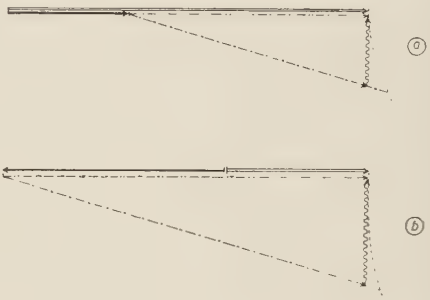

Fig. 3. – Rappresentazione come in fig. 2 nel caso di moto « regolare » in presenza di campo esterno: *a*) caso stabile; *b*) caso instabile.

⟹ forza esterna.

Invece il caso della fig. 3*b* è instabile: se $\boldsymbol{f}_{\text{est}}$ aumenta $\dot{\boldsymbol{v}}(s)$ diminuisce; questo porta col tempo ad una diminuzione di $\dot{\boldsymbol{v}}(s-\varrho)$ che a sua volta causa una ulteriore diminuzione di $\dot{\boldsymbol{v}}(s)$. Infine $\dot{\boldsymbol{v}}(s)$ inverte il segno e cresce nel senso opposto oltre ogni limite, causando l'arresto e l'inversione del moto della particella se la sua velocità era nel senso della forza agente. Questo si sa accadere secondo l'equazione di Dirac per un elettrone lanciato contro una carica posi-

---

aumenta col tempo oltre ogni limite, e che il medesimo, fissato il valore del tempo proprio, tende a zero quando le masse tendono all'infinito pur rimanendo la loro somma costante ed uguale alla massa sperimentale. Da notare così che la somma dei due contributi all'energia e all'impulso dell'elettrone deve diventare, in dette soluzioni, un vettore di tipo spaziale. Un controllo può esser fatto con un bilancio, osservando che l'energia e l'impulso in totale ceduti alla radiazione (un vettore temporale) aumentano col tempo oltre ogni limite.

[17] Le soluzioni dell'equazione $m_0\dot{\boldsymbol{v}}(s) + \frac{4}{3}m_{\text{e.m.}}\dot{\boldsymbol{v}}_{\perp}(s-\varrho) = \boldsymbol{f}_{\text{est.}}$ (cfr eq. (12)) devono soddisfare anche la condizione $(\dot{\boldsymbol{v}}_{\perp}(s-\varrho)/|\dot{\boldsymbol{v}}(s-\varrho)|)\cdot|\dot{\boldsymbol{v}}(s)| \approx \dot{\boldsymbol{v}}(s)$. Ciò porta alla sola soluzione $\dot{\boldsymbol{v}}(s) = 0$ per $\boldsymbol{f}_{\text{est}} = 0$ e $m_0 > 0$.

tiva fissa ([1,18]); anche un elettrone in quiete disturbato da un campo costante ([19]) fuggirebbe nella direzione opposta alla forza agente, e così via.

Un ritardo anche nella massa meccanica costringerebbe a qualche altra modificazione, perchè tutti gli altri contributi sono ortogonali alla linea di universo della particella.

Non volendo alterare l'espressione dell'energia irradiata ([20]) o quella della forza esterna, o il valore della massa, in condizioni di regime detto ritardo non può esser preso in considerazione.

Per l'elettrone puntiforme l'imposizione delle conservazioni per l'energia gli impulsi e i loro momenti non lascia altra possibilità che aggiungere alla equazione di Dirac un differenziale esatto ([13]) $\dot{A}$ tale che $r_\mu \dot{A}^\mu = 0$ e $r_\lambda A_\mu - r_\mu A_\lambda$ sia differenziale esatto ([10,21]).

Quanto alle condizioni iniziali per l'elettrone di Dirac, esse sono una semplificazione di quelle per l'elettrone finito considerato, caso in cui risultano una infinità e possono essere assegnate, come si è visto, dando le accelerazioni subite dall'elettrone in un breve intervallo di tempo, e in più la posizione e la velocità iniziali, oppure dando queste ultime e i valori iniziali del campo elettromagnetico.

Appendice

Per il tensore densità-flusso di energia e impulso totali $T^{\mu\nu} = T^{\mu\nu}_{\text{e.m.}} + T^{\mu\nu}_{\text{mecc.}}$ in una teoria esatta dovrebbero valere le equazioni $\partial T^{\mu\nu}/\partial x^\nu = 0$.

Le equazioni del moto per il modello adottato si scrivono invece

$$\frac{\partial}{\partial s}\int \mathrm{d}\sigma_\omega T^{\mu\omega} = \int \mathrm{d}\sigma(1 - \boldsymbol{\gamma}\cdot\dot{\boldsymbol{v}}(s))\frac{\partial T^{\mu\nu}}{\partial x^\nu} = 0\,, \tag{A.1}$$

([18]) G. Zin: *Nuovo Cimento*, **6**, 1 (1949).

([19]) Veramente dovremmo supporre il campo introdotto con continuità, ma l'obbiezione è superabile per l'elettrone puntiforme.

([20]) L'equazione $m\dot{\boldsymbol{v}}(s) - \frac{2}{3}e^2\ddot{\boldsymbol{v}}(s) - k\ddot{\boldsymbol{v}}(s) + [-\frac{2}{3}e^2\dot{v}^2 - k\dot{v}^2]\boldsymbol{v}(s) = \boldsymbol{f}_{\text{est.}}$ non dà il termine necessario di radiazione. Essa corrisponde per esempio ad una particella di cui una parte della massa meccanica negativa è dovuta ad un campo lineare attrattivo (tra sorgenti uguali) *ritardato* propagantesi con la velocità della luce, se $k < 0$. In questo caso si avrebbe un'effettiva duplice radiazione, di cui una di energia negativa.

([21]) Partendo dal considerare infiniti termini soddisfacenti queste condizioni, C. J. Eliezer (*Proc. Roy. Soc.*, **194**, 543 (1948)), elimina le soluzioni singolari sostituendo al ritardo della massa elettromagnetica (e alla corrispondente potenza irradiata) un anticipo nell'intensità della forza esterna di un tempo pari al raggio classico dell'elettrone (lav. cit. formula (52)).

dove $d\sigma_\omega$ sono le componenti e $d\sigma$ è il modulo dell'elemento di volume dell'iperpiano ortogonale alla linea di universo nel punto generico s; $T^{\mu\nu}_{\text{mecc.}} = \varrho_{\text{mecc.}} v^\mu(s) v^\nu(s)$, essendo $\varrho_{\text{mecc.}}$ la densità di massa meccanica su tale iperpiano.

Similmente il momento angolare (x_0 è un punto qualsiasi fisso nello spazio-tempo)

$$\text{(A.1)} \qquad \int d\sigma_\omega M^{\mu\nu\omega} = \int d\sigma_\omega \left[(x^\mu - x_0^\mu) T^{\nu\omega} - (x^\nu - x_0^\nu) T^{\mu\omega}\right],$$

può essere conservato solo su detti iperpiani.

Infatti per la simmetria di $T^{\mu\nu}$

$$\text{(A.3)} \qquad \frac{\partial M^{\mu\nu\omega}}{\partial x^\omega} = (x^\mu - x_0^\mu) \frac{\partial T^{\nu\omega}}{\partial x^\omega} - (x^\nu - x_0^\nu) \frac{\partial T^{\mu\omega}}{\partial x^\omega},$$

quindi

$$\frac{\partial}{\partial s} \int d\sigma_\omega M^{\mu\nu\omega} = \int d\sigma (1 - \boldsymbol{\gamma}\cdot\dot{\boldsymbol{v}}(s)) \left[(x^\mu - x_0^\mu) \frac{\partial T^{\nu\omega}}{\partial x^\omega} - (x^\nu - x_0^\nu) \frac{\partial T^{\mu\omega}}{\partial x^\omega}\right] =$$

$$= \int d\sigma (1 - \boldsymbol{\gamma}\cdot\dot{\boldsymbol{v}}(s)) \left[\gamma^\mu \frac{\partial T^{\nu\omega}}{\partial x^\omega} - \gamma^\nu \frac{\partial T^{\mu\omega}}{\partial x^\omega}\right],$$

per le equazioni del moto.

Il solo termine importante in $d\sigma \frac{\partial T^{\nu\omega}_{\text{e.m.}}}{\partial x^\omega}$ è ora $de \int \frac{de' v'_\perp}{(\boldsymbol{r}\cdot\boldsymbol{v}(s))^3} - de \int \frac{de'(\gamma'^\nu - \gamma^{*\nu})}{|\boldsymbol{\gamma} - \boldsymbol{\gamma}^*|^3}$.

Poichè $d\sigma (1_{\text{mecc.}} \boldsymbol{\gamma}\cdot\dot{\boldsymbol{v}}(s)) \frac{\partial T^{\nu\omega}}{\partial x^\omega} = dm_{\text{mecc.}} \dot{v}^\nu(s)$, per l'ipotesi della simmetria sferica il precedente integrale svanisce, quando le dimensioni dell'elettrone tendono a zero.

SUMMARY

The author studies a special relativistic model of an extended electron and gets its equations of motion. The reason for its unphysical solutions is later shown. They happen, roughly, if the electron is smaller than its classical radius. Details are also studied, especially with respect to the conservations of energy and momenta. The point-electron limit is emphasized.

IL NUOVO CIMENTO Vol. II, N. 3 1° Settembre 1955

Arrangement for Precise Scattering Measurements in Nuclear Emulsions.

W. Stodiek

Max-Planck-Institut für Physik - Göttingen

(ricevuto il 30 Giugno 1955)

Summary. — An arrangement is described whereby, employing a simple microscope, the magnitude of the stage-noise is reduced, independent of the cell-length, such that it has no influence any longer on the determination of the scattering angle. The unsensitivity to shock or vibration permits the use of an ocular-eye-piece screw-micrometer. An auxiliary device for convenient alignment of the nuclear plates is also described.

Measurement of the scattering of high energy particles in nuclear photographic emulsions demands considerable precision from the measuring microscope. Data on the magnitude of the stage-noise of several microscopes frequently employed for scattering measurements or specially developed for this purpose (1) are contained in different papers (2).

In measuring the scattering by the coordinate method, the distance between the nuclear track and a reference line is measured; this line is generally the guide curve of the microscope stage, and its linearity is determined by the precision of the guide rails and also by elastic and inelastic deformations undergone during its motion. The guiding mechanism has two tasks. First, to bring the various points of the nuclear track into view and, secondly, to produce the comparison curve relative to which the scattering is measured.

(1) M. G. E. Cosyns: *Bulletin du Centre de Physique Nucléaire de l'Université libre de Bruxelles*, no. 30 (1951); J. E. C. Plainevaux: *Nuovo Cimento*, **10**, 1451 (1952); **11**, 626 (1954); **12**, 37 (1954).

(2) K. Gottstein: *Nuovo Cimento*, **12**, 619 (1954); J. K. Bøggild and M. Scharf: *Suppl. Nuovo Cimento*, **12**, 374 (1954).

If a high linearity and constancy of the comparison curve is required, i.e. a small « stage-noise », it is more favorable to separate these two tasks and leave only the function of a comparator to the stage while measuring the scattering against a special reference body.

Fig. 1 shows the corresponding arrangement. The reference body, e.g. a glass plate, is mounted on the microscope parallel to the stage guide. Its surface (a) represents a plane of high precision. The microscope objective is fastened to the end of the tube by means of a leaf-spring pair and through a feeler arm it rests upon the surface. This surface and the nuclear track move together with the stage, and all errors in the stage motion due to the guide occur only as parallax errors. The accuracy of the instrument is therefore, in the first approximation, determined by the planarity of the reference surface, which can be made very high.

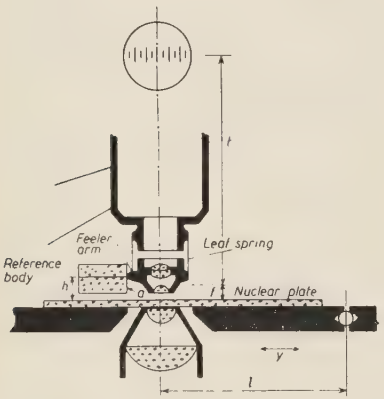

Fig. 1. – Arrangement of microscope stage, reference body and objective. Stage deviations in the y direction, perpendicular to the track, are reduced in proportion to f/t; stage tip in proportion to h/l.

Considering fig. 1, the amount by which the stage-noise can be reduced is easily estimated. Motion of the stage in the y-direction enters in inverse proportion to the magnification of the objective, say 1/100. Tipping of the stage contributes an amount proportional to h/l, which is about 1/20 on the usual microscopes, but which may easily be decreased to 1/100 on large stages. By a slight inclination of the stage to the optical axis, h could be brought to zero. Stage tip is then entirely without influence. Inaccuracies in the vertical motion of the tube resulting in a displacement or tip of the optical axis with respect to the stage correspond to those of the stage.

We estimate the errors caused by deformation of the feeler arm and of the reference surface using the formulae of Hertz.

For a radius of curvature of 1 cm the following values are obtained:

	Steel		Glass	
Load	1 g	0.1 g	1 g	0.1 g
Approach of Sphere and Plate	7 mμ	1.5 mμ	14 mμ	3 mμ
Radius of Circle of Contact	8.7 μm	0.4 μm	12.5 μm	0.6 μm
Maximum Occurring Surface Pressure	750 kg/cm²	300 kg/cm²	375 kg/cm²	150 kg/cm²

The approach of the bodies under load is thus so slight that changes in the load force have no influence on the measuring accuracy.

If a glass plate serves as the comparison body, it might be presumed that the feeler arm would scratch the glass. Because the motion is slow, no essential warming takes place; a scratch or tear formation will happen only when the static compressive limit is exceeded, which lies at about 10000 kg/cm² ([3]).

Lubrication of the feeler arm is in general not necessary, as shown by experiment. Nevertheless, lubrication with the solid lubricant molybdenum disulfide could be advantageous ([4]).

Dust particles on the reference surface are hardly disturbing, since even with a very dusty plate the feeler seldom strikes a grain of dust because of the very small bearing surface. If, however, the feeler does strike a dust particle, it is certain to be seen as a noticeable jump of the visual field. Simple fire-polished glass plates are useful for reference bodies at cell lengths up to 1000 μm. Ground plates with curvature radius of 50 km are available for the highest precision. The only elastic and thermal deformations that enter with their full values are those which effect a displacement of the reference body relative to the nuclear track; these can be estimated to a few mμ.

Because of the small motion of the objective, one must take care that only the objective diaphram limits the bundle of rays, not that of the condenser. With a good condenser this is easy to attain, particularly since the nuclear plate also scatters strongly. Objectives with a small principal plane separation are to be preferred since they produce less ray displacement if they are tipped.

By means of this auxiliary device the stage-noise is reduced to 1/10 to 1/20 of its value in the case of small and very simple stages, and easily to 1/50 to 1/100 in the case of larges ones. The employment of this device makes the microscope insensitive to shock and vibration. An ocular screw micrometer can be used.

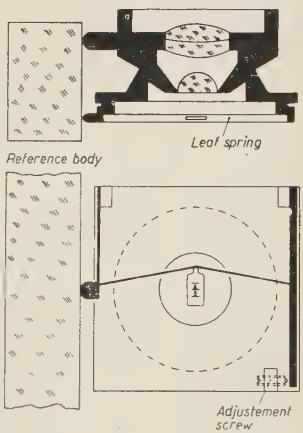

Fig. 2. – Arrangement for examination of stage-noise. With the adjustment screw the magnification ratio can be changed.

([3]) E. MADELUNG: *Naturwiss.*, **30**, 223 (1942).

([4]) G. SPENGLER: *Zeits. VDI*, **96**, 506, 683 (1954); K. NENTWIG: *Feinwerktechnik*, 58, 224 (1954).

A simple microscope (Leitz-B-Stativ) was fitted with the device described above, and the usual gear adjustment was replaced by a simple screw arrangement. For examination of the accuracy of the instrument, a device described in fig. 2 was installed at the objective; this device simulates actual operation conditions. Since the expected measurements are very small a premagnification is necessary and a leaf-spring is utilized as the measuring element. The sagitta increase gives then an indication of change in chordlength. The transformation ratio in this case was equal to 10. With the use of a comparison plate having a radius of curvature of approximately 2.5 km, stage noise was evident in the relative measurement with the above-described auxiliary apparatus; this stage noise was of a magnitude of about 0.01 μm independent of the cell lenght. In consideration of the plate curvature, the total stage noise was about

0.01 μm for a cell-length up to 2000 μm,

0.04 μm for a cell-length equal to 10000 μm.

Thus the stage noise is less than the microscopic inaccuracy of observation.

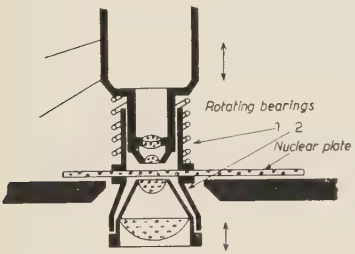

Fig. 3. – Arrangement for the alignment of the photoplate. The actual device contains ball bearings; the lower bearing centers itself on the axis of the upper one. A favorable magnification for this objective is 25 to 1. In normal use the upper bearing (1) is locked in a raised position.

The alignment of the nuclear track under the microscope parallel to the direction of stage is simplified by a little gadget; its operation can be seen in fig. 3. The microscope tube is lowered so far that the bearing 1, containing a spring, presses the plate against the stage. Then, with the help of the condenser drive and the bearing 2, the plate is raised slightly from the stage and can easily be rotated about the optical axis. The track remains visible during the rotation.

I am much indebted to Dr. K. Gottstein and Messrs. H. M. Mayer and H. Röhrs for valuable discussions.

RIASSUNTO (*)

Si descrive un dispositivo che permette, impiegando un semplice microscopio, di ridurre l'ampiezza dello « stage-noise » indipendentemente dalla lunghezza della cella, in modo che questa non ha più alcuna influenza sulla determinazione dell'angolo di scattering. L'insensibilità agli urti e alle vibrazioni permette l'uso di un oculare a vite micrometrica. Si descrive altresì un accessorio per il buon allineamento delle lastre nucleari.

(*) *Traduzione a cura della Redazione.*

IL NUOVO CIMENTO Vol. II, N. 3 1° Settembre 1955

A Precision Re-Measurement of the ^{60}Ni Gamma-Gamma Directional Correlation Function.

S. Colombo

Istituto Nazionale di Fisica Nucleare - Sezione di Milano

A. Rossi and A. Scotti

Istituto di Fisica dell'Università - Milano
Istituto Nazionale di Fisica Nucleare - Sezione di Milano

(ricevuto il 4 Luglio 1955)

Summary. — A precision re-measurement of the directional correlation function of the ^{60}Ni gamma-gamma cascade, obtained through beta decay of metallic ^{60}Co, has been performed. The experimental apparatus includes as scintillation counters Du Mont Type 6292 photomultipliers, coupled with $1'' \cdot 1''$ cylindrical Anthracene crystals, and a coincidence circuit with a resolving time of $4 \cdot 10^{-8}$ s. The experimental results are reported, with a discussion of the systematic errors involved and of the experimental corrections introduced. The comparison with the theoretical results, assuming the usual unperturbed 4(E2)2(E2)0 cascade, shows a very close agreement.

1. – Introduction.

The measurement of the directional correlation function of radiation emitted in cascade by excited nuclei, and the experimental study of the possible attenuation of the correlation due to the influence of extranuclear fields, have recently acquired great importance in the field of nuclear spectroscopy.

Frauenfelder [1,2] has published two review articles on this subject; Biedenharn and Rose [3] have summarized the theoretical aspects of the same.

A great precision is required in these measurements, especially in the case of attenuation due to extranuclear fields and in the investigation of mixed

multipole transitions, in order that the comparison with theoretical calculations be significant. To this end, in addition to increasing the statistical accuracy, it is necessary to minimize, or if possible to eliminate completely, those systematic errors, for which precise methods of correction are not available.

Following these criteria, we have built an apparatus for the measurement of gamma-gamma directional correlation functions, and have performed, as a calibration check, a re-measurement of the ^{60}Ni cascade.

A brief report of the results has been previously published ([4]).

2. – The ^{60}Ni Gamma-Gamma Directional Correlation Function.

The decay scheme of ^{60}Co, from which the second excited state of ^{60}Ni is obtained through beta decay, with following double gamma cascade (energy respectively 1.1715 and 1.3317 MeV) is known ([5]).

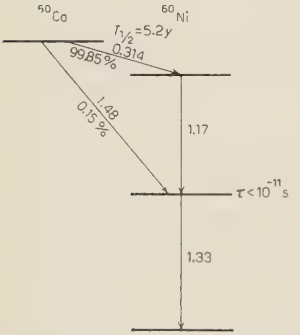

Fig. 1. – Decay scheme of ^{60}Co (all energies in MeV).

Recent measurements ([6]) report the existence of a weak intensity beta spectrum (maximum energy 1.48 MeV, percent abundance 0.15 %), directly leading to the first excited state of ^{60}Ni, according to fig. 1.

Owing to the very low abundance of this disturbing radiation, additional screens to stop it were not necessary.

With the assumption, also suggested by measurements of internal conversion ratios ([7]), that the ^{60}Ni cascade is of electric quadrupole-electric quadrupole character [4(E2)2(E2)0], the unperturbed directional correlation function is theoretically expressed ([8]) as proportional to

$$W(\theta) = 1 + \frac{1}{8}\cos^2\theta + \frac{1}{24}\cos^4\theta,$$

(where θ is the angle between the emissions direction of the two quanta), or, in an equivalent way ([3,9]), by

$$W'(\theta) = 1 + 0.1020 P_2(\cos\theta) + 0.0091 P_4(\cos\theta),$$

(where $P_2(\cos\theta)$ and $P_4(\cos\theta)$ are the Legendre polynomials of order 2 and 4 respectively).

The value of the anisotropy $A(\theta) = W(\theta)/W(\pi/2)$ for $\theta = \pi$, instead of the values of the coefficients in the expansions $W(\theta)$ or $W'(\theta)$, is often reported experimentally. This anisotropy has the theoretical value of 1.16667.

The mean life of the intermediate state of the cascade is extremely short. The Weisskopf formula ([10]) for the case of electric quadrupole radiation gives an estimate of $8 \cdot 10^{-12}$ s. Experimentally, upper limits have been obtained, having the following values: $3 \cdot 10^{-9}$ s ([11]), $2 \cdot 10^{-9}$ s ([12]), $7 \cdot 10^{-10}$ s ([13]), 10^{-10} s ([14]), and 10^{-11} s ([15]).

It seems probable, therefore, that an influence of extranuclear fields on the correlation should be negligible.

TABLE I.

Date and reference	$A(\pi) = W(\pi)/W(\pi/2)$	Error	Remarks
1946 ([18])	1.071	0.10	Geiger counters
1947 ([19])	1.19	0.04	$CoCl_2$ crystalline source
	1.20	0.04	$CoCl_2$ aqueous solution
	1.22	0.04	nitrosil carbonile, gaseous source
	1.21	0.025	average value
1948 ([20])	1.157 (*)	0.02 (*)	first measurement with scintillation counters
1950 ([21])	1.16 (*)	0.02 (*)	
([22])	1.1625 (*)	0.037 (*)	
([23])	1.169 (*)	0.015 (*)	
([24])	1.171 (*)	0.012 (*)	
1951 ([25])	1.45	0.12 (*)	$CoCl_2$ solution, Geiger counters
([26])	1.153	0.0135 (*)	
([27])	1.17	0.05	
1952 ([16])	1.148	0.003	metal source
	1.148	0.002	average from various sources
1953 ([28])	1.166	0.0116	
([17])	1.1557 (°)	0.0010	$CoCl_2$ solution in various concentrations
	1.1520 (°)	0.0038	
	1.1453 (°)	0.0023	possible chemical modification of the valence state of Co
([29])	1.163	0.012	
([30])	1.165	0.003	
([31])	1.166	0.002	in various conditions of discrimination and angular resolution
	1.168	0.003	
	1.167	0.001	average value
([32])	1.170	0.009	$CoCl_2$ solution in HCl, dried on film
1954 ([33])	1.167	0.005	
1955 ([34])	1.167	0.001	

(°) Values uncorrected for angular resolution to be compared with a corrected theoretical value of 1.1517 instead of 1.16667.

Experimental values of the anisotropy, obtained with metallic ^{60}Co, lower than the unperturbed theoretical value ([16]), or values depending on the chemical nature of the investigated compound ([17]), have sometimes however been reported. These results suggested the hypothesis of an attenuation due to strong magnetic fields produced at the nucleus by the atomic electron shells. These doubts have stimulated further and more accurate measurements, which have yielded again the unperturbed value. It is now believed that the deviating values were due to systematic reasons connected with the difficulties of such measurements, for which adequate correction was not provided ([2]).

In Table I we report, in chronological succession, the experimental data on the anisotropy of the ^{60}Ni cascade published, as far as we know, up to now: in the first column is the reference and the year of publication of the paper, in the second the reported anisotropy, in the third the quoted error, and finally the necessary remarks. We have marked with an asterisk (*) the numerical values of the anisotropy and (or) error, which we have taken from diagrams published by the authors, when numerical data were lacking. The exact nature of the quoted error is not always explicitly given.

3. – Experimental Apparatus.

3·1. *The support for counters and source.* – The support for counters and source has been made of a robust aluminium disk (76 cm in diametre, 0.8 cm in thickness), held in horizontal position by an independent frame. A material of low atomic number has been chosen in order to reduce scattering of γ-rays. The disk border has been divided in sections of 5°.

Two arms may rotate about the disk axis and be fixed at the border in any position by means of pressure screws. These arms support, through dovetail guides, the frames for scintillation counters and amplifiers.

A thin central aluminium pin bears at its pointed end the source, consisting of a small cylindrical piece of ^{60}Co, 0.8 mm in diametre, 1 mm in height, obtained from A.E.R.E., Harwell. The source activity was about 60 μc. The distance of the source from the disk surface was 14.5 cm.

Special care was paid to mechanical centering of the source, and to the strength of the counter supports.

3·2. *The scintillation counters.* – As γ-ray detectors we used Du Mont Type 6292 photomultipliers (erroneously quoted as Type 6291 in ([4])), coupled to Harschaw Anthracene crystals of cylindrical shape (1″ in thickness, 1″ in diametre). R.C.A. Type 5819 photomultipliers, first chosen for more favourable transit time properties, could not be used here, for they showed noticeable fatigue effect (decrease in the internal amplification during measuring time), at the high counting rate required by the experiment.

The internal electrostatic screen, with which Du Mont photomultipliers are provided, was given a potential, with respect to the cathode, which was individually adjusted for best electron collection. The overall working voltage was about 950 volt, in order not to overfatigue the counters.

The scintillating crystals have been enclosed, according to normal practice (see, for example ([35])), in an aluminium box provided with a thin glass wall, optically polished. MgO white powder surrounded the crystal, in order to increase photon collection by diffusion. Aluminium rings held the crystals accurately centered, a necessary requirement for good geometry and angular resolution correction (see Section 5). Optical contact was maintained by means of high viscosity Dow Corning Silicon Oil (10^6 centistokes).

A mu-metal cylindrical screen (0.7 mm thick) protected the photomultiplier from the influence of magnetic fields, and also provided light tightness and mechanical support for the scintillating head. No significant variations of single counting rate (that is, of the internal amplification) were then found changing in any way the position of the photomultiplier with respect to the magnetic field of the earth.

The head of the scintillation counter was surrounded by a lead screen, properly shaped, so that the background counting rate was reduced to a negligible value. The acceptance aperture was cone shaped, and had its vertex coincident with the chosen position of the source. This arrangement improves the definition of the effective solid angle, reducing the scattering of γ-rays from the inner wall. This might however cause noticeable variation of the acceptance solid angle, due to even small defects in centering or to vibration and displacements of the counter supports. The constancy of the single counting rate in different positions of the counters again proved the absence of this effect.

In fig. 2 the arrangement adopted for the counter head is sketched.

The geometrical solid angle, evaluated from the median section of the crystal, is about 0.25 sterad. This approximate value has been

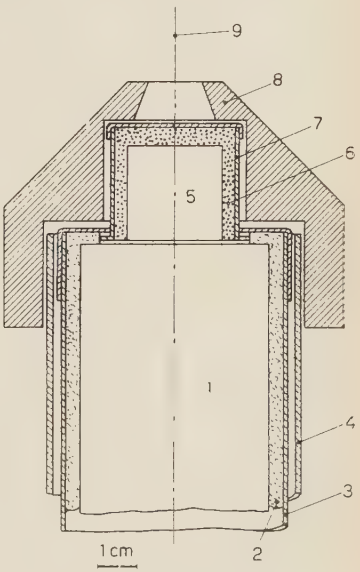

Fig. 2. – Detector head assembly: 1. Photomultiplier; 2. Black felt protection around the glass envelope; 3. Mu-metal screen; 4. Aluminium support for the lead screen; 5. Anthracene crystal; 6. MgO powder reflector; 7. Aluminium container with glass wall; 8. Lead screen; 9. Source position (3.2 cm apart from crystal surface).

used for a preliminary evaluation of the correction factors, in planning the experiment (see Section **5**).

3·3. *Electronic circuitry.* – The block scheme of the electronic apparatus utilized for the experiment is illustrated in fig. 3.

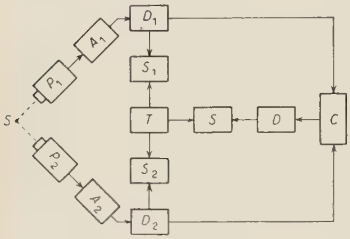

Fig. 3. – Block scheme of the electronic equipment: *S*) Source; P_1, P_2) Detectors and voltage dividers; A_1, A_2) Amplifiers; D_1, D_2) Fast discriminators and pulse formers; S_1, S_2) Single count scalers; *C*) Mixer circuit; *D*) Discriminator; *S*) Coincidence count scaler; *T*) Timing circuit for the three scalers.

The negative output pulses from the photomultiplier anodes are amplified about 10 times and reversed in sign, before being fed into the fast discriminators and pulse formers. The electronic scheme of the amplifier is reported in fig. 4. After amplification, the rise time of the pulses is about $5 \cdot 10^{-8}$ s. The saturation amplitude of these pulses is only about 3.5 volt, due to the low output impedance (125 ohm) used to match the impedance of the connection cables.

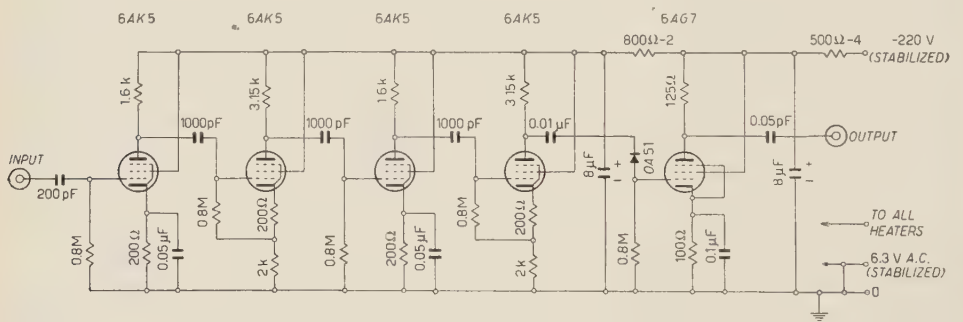

Fig. 4. – Electronic scheme of the amplifiers A_1 and A_2.

The circuit of the fast discriminators has been mounted according to MOODY *et al.* [36]; a Philips EFP60 tube is used in the trigger circuit (fig. 5). In order to form the pulses in the plate circuit, a short circuited delay cable (4 metres long) has been used, thus obtaining, after inversion through a pulse transformer, positive pulses of about $4 \cdot 10^{-8}$ s duration. The output pulses from the discriminators are counted after amplification by the scalers S_1 and S_2.

The coincidence circuit (fig. 6) uses a 6BN6 tube as a mixer, according to FISCHER and MARSHALL [37]; the output pulse amplitude from the mixer

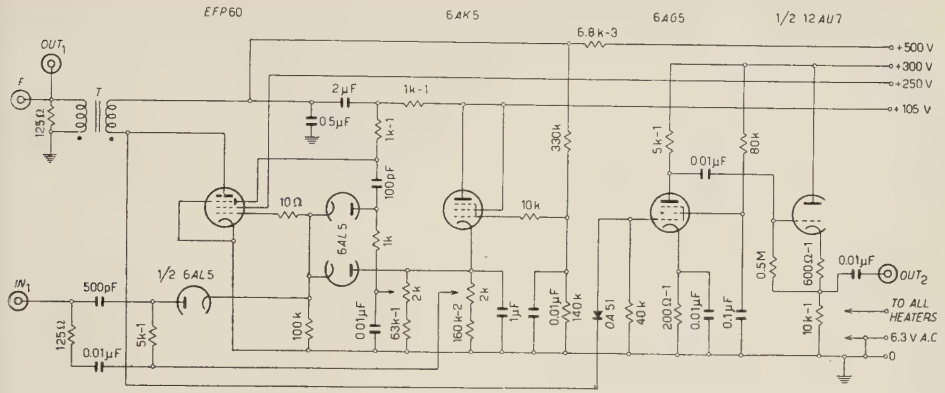

Fig. 5. – Electronic scheme of the fast discriminators D_1 and D_2 (all voltage supplies are electronically regulated).

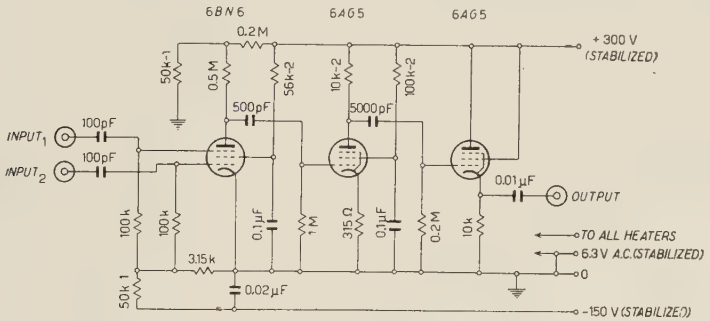

Fig. 6. – Electronic scheme of the mixer circuit C.

tube depends on the relative time delay between the input pulses, thus permitting adjustment of the resolving time by means of a discriminator D.

In fig. 7 the dependence of the resolving time on the discrimination bias, using forming cables 4 metres long (about $4 \cdot 10^{-8}$ s reflection time) is shown as a practically straight line. The resolving time was here measured with the method of two independent sources.

The output pulses from the coincidence mixer are counted after discrimination by the scaler S.

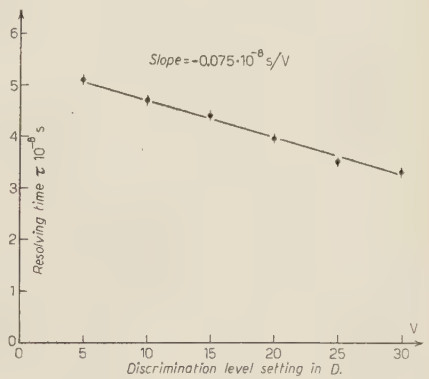

Fig. 7. – Dependence of resolving time of the coincidence circuit C on the discrimination level in D (see fig. 3).

The paralysis time of the three scalers was about $0.8 \cdot 10^{-6}$ s, with scaling factor of 10^4. No correction was needed for counting losses.

The three scalers are controlled for simultaneous starting and automatic stopping by the timer circuit T, described elsewhere ([28]).

All voltage supplies, including filament power supply, have been electronically regulated.

3·4. *Stability of the resolving time.* – The resolving time of the coincidence circuit has been often measured during the course of the experiment, inserting a sufficient delay cable in one of the channels and counting the remaining chance coincidences. Complete absence of true coincidences was previously checked by means of a ^{22}Na source. A comparison with the method of the two independent sources gave the same values. The advantage of the delay cable method is apparent when a frequent periodic check of the resolving time is needed during the experiment, because it avoids changes in the geometry and displacement of one of the counters. The resolving time has been measured for 15 minutes at 2 hours intervals, and has proved quite stable. In Table II the values of the resolving time obtained during a partial period, totalling 16 hours of counting, is reported as an illustration. In this Table T is the total time of measurement of chance coincidences, τ the average value of the resolving time at the end of T hours of counting, σ the corresponding standard deviation, τ' the average value of the resolving time in each period of two hours. The standard deviation of τ' is $0.014 \cdot 10^{-8}$ s. The results of Table II were collected during a run of 5 days.

TABLE II.

T (hours)	τ (10^{-8} s)	σ (10^{-8} s)	τ'(10^{-8} s)
2	3.9960	0.014	3.9960
4	4.0035	0.010	4.0111
6	4.0054	0.008	4.0093
8	4.0073	0.007	4.0130
10	4.0041	0.006	3.9913
12	4.0084	0.006	4.0295
14	4.0119	0.005	4.0331
16	4.0102	0.005	3.9981

3·5. *Genuine coincidence loss.* – Genuine coincidences (that is, genetically related counts) are lost, if the pulses from the formers do not arrive at the mixer tube within the resolving time τ. This can be due to fluctuations of the transit time of electrons in the photomultipliers and finite decay time of the scintillations, and to the different amplitudes of the pulses from the detectors

(Compton distribution of secondary electrons in the crystals). The fast discriminators are triggered when the input pulses reach about 1 volt amplitude, so that higher pulses have faster action (the total rise time being practically independent of pulse height).

We have determined the relative genuine coincidence loss measuring the genuine coincidence rate due to the γ-rays of the ^{60}Ni cascade, practically coincident in time ([10,15]), in function of the resolving time of the coincidence mixer, in the range from $1.5 \cdot 10^{-8}$ to $2 \cdot 10^{-7}$ s. The reported graphs (fig. 8) show that at $4 \cdot 10^{-8}$ s (the adopted resolving time) the coincidence loss amounts to about 65% at 950 volt high voltage supply, and to about 47% at 1300 volt (curves A and B respectively). The improvement at higher voltage is probably due to lower fluctuations of the transit time of the electrons in the photomultipliers.

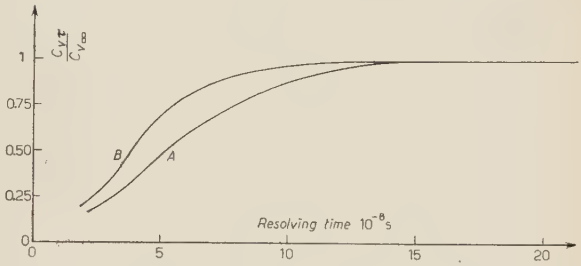

Fig. 8. – Genuine coincidence rate in function of resolving time: Overall applied voltage: curve A, 950 volt - curve B, 1300 volt.

4. – The Collection of Experimental Data.

One of the detectors was held at the position 0°; single counts Z_1 and Z_2, and total coincidence counts C_t during periods of $T = 900$ s were taken for positions of the mobile detector ranging in steps of 15° from 90° to 270°, corresponding to angles between the counter axes of 90°, 105°, 120°, 135°, 150°, 165° and 180° on both sides. The order of magnitude of the single counting rate was 800000 cpm, that of the total coincidence was 1600 cpm. The background counting rate in both detectors was about 80 cpm, a negligible rate.

The random coincidences C_c in the same period of time were calculated by means of the approximate formula:

$$C_c = 2\tau Z_1 Z_2 / T \,,$$

where τ is the resolving time of the coincidence circuit.

The application of the more accurate formula ([39-41]):

$$C_c = 2\tau (Z_1 - C_v)(Z_2 - C_v)/T \,,$$

which involves less straightforward calculations due to the presence of the unknown term C_r (true coincidence counts during T) was not necessary here. Given the very low ratio C_r/Z_1 and C_r/Z_2 (about 10^{-4}), due to the low efficiency of the detectors (Anthracene crystals and high discrimination), and to the rather high coincidence losses, the systematic error introduced in the final value $A(\theta)$ (see further) by the application of the approximate formula only affects the 5th decimal figure.

The number of genuine coincidences in the same period T was derived by subtraction:

$$C_r - C_t - C_c ,$$

and was divided by $Z_1 Z_2$ in order to eliminate, in first approximation, the effects of slow variations in the efficiencies, due to fatigue effect in the counters and drift in the electronics apparatus.

The activity of the source was chosen as to have $C_v/C_c \cong 1$.

The final formula then results:

$$C'_v = C_v/Z_1 Z_2 = \frac{2}{T}\left(\frac{TC_t}{2Z_1 Z_2} - \tau\right)$$

and the constant factor $2/T$ can be neglected for simplicity.

For every chosen angle θ we have formed the anisotropy ratio:

$$A(\theta) = C'_v(\theta)/C'_v(\pi/2) .$$

The measuring time was chosen long enough (about 300 hours) as to have a standard deviation on each value of $A(\theta)$ of about $2 \cdot 10^{-3}$.

5. – Correction of Systematic Errors.

The theoretical directional correlation function (see Sect. 2) is not to be compared directly to the experimental results, because it is calculated with the assumption of perfectly isolated point source (absence of scattering in the source and of spurious coincidences due to scattered quanta), infinitesimal solid angle subtended by the detectors, absence of accompanying spurious radiations, etc.

Our experimental arrangement allows us to consider as valid the assumptions of practically point source and negligible scattering in the source itself.

The effects of scattering on the counter heads and on the supporting disk have often been reduced by covering the scintillators with a thin lead screen ([12]), which absorbs the diffused softer radiation much more than direct quanta.

This procedure does not however permit exact evaluation of the residual correction. We have therefore preferred to eliminate completely this effect, using the detectors as energy discriminators, at an appropriate high level. In order also to avoid detection of annihilation quanta (which are strongly correlated in opposite directions and might alter considerably the experimental correlation even if present in small quantity), we have chosen the discrimination level just above 340 keV, corresponding to the most energetic Compton electron liberated in the scintillator by annihilation radiation. The level of discrimination was constantly checked during the experiment by means of a positron source, seeing that no coincidences due to annihilation radiation were counted.

This high discrimination has further diminished the efficiency of the detectors, thus making necessary a longer measuring time to obtain a given statistical accuracy. It however offers the advantage of eliminating a source of error, which is not easily accounted for with accuracy.

An error which is not possible to avoid is that due to the finite angular resolution of the detectors. Furthermore, it is practically necessary to chose the acceptance solid angle as large as geometry permits, in order to collect rapidly experimental data (the rate of genuine coincidences depends directly on the product of solid angles). This entails a smearing out of the theoretical correlation, which must be corrected for.

According to FRANKEL ([43]), the measured directional correlation function, with the assumption of centered point source and cylindrically symmetrical detectors, can be represented by:

$$W_s(\theta) = 1 + \alpha_2' P_2(\cos\theta) + \alpha_4' P_4(\cos\theta) .$$

The relationship between the experimental coefficients α_2' and α_4', and the theoretical ones α_2 and α_4, is of simple proportionality:

$$\alpha_2 = (Q_0/Q_2)\alpha_2' ; \qquad \alpha_4 = (Q_0/Q_4)\alpha_4' .$$

The coefficients Q_0, Q_2 and Q_4 depend on the detection efficiencies $\varepsilon^{\mathrm{I}}(\alpha)$ and $\varepsilon^{\mathrm{II}}(\alpha)$ of the two counters, expressed in terms of the angle α from the counter axis. As the energies of the two quanta are not very different, a single value of the detection efficiency for each counter may be assumed.

It results: $Q_0 = J_0^{\mathrm{I}} J_0^{\mathrm{II}} \qquad Q_2 = J_2^{\mathrm{I}} J_2^{\mathrm{II}} \qquad Q_4 = J_4^{\mathrm{I}} J_4^{\mathrm{II}}$

(the superscripts $^{\mathrm{I}}$ and $^{\mathrm{II}}$ refer to the two counters respectively) where

$$J_0 = \int \varepsilon(\alpha) |\sin\alpha| \, \mathrm{d}\alpha ,$$

$$J_2 = \int \varepsilon(\alpha) P_2(\cos\alpha) |\sin\alpha| \, \mathrm{d}\alpha ,$$

$$J_4 = \int \varepsilon(\alpha) P_4(\cos\alpha) |\sin\alpha| \, h\alpha$$

are calculated for counters I and II respectively (the superscripts have not been indicated here for simplicity).

Following LAWSON and FRAUENFELDER [31], we have measured experimentally, by means of a collimated beam of ^{60}Co radiation, the efficiencies $\varepsilon^{I}(\alpha)$ and $\varepsilon^{II}(\alpha)$, using the same geometrical and electronic conditions of the experiment. We have then calculated, by numerical integration, the appropriate correction factors.

This experimental procedure has the advantage, as was pointed out by LAWSON and FRAUENFELDER [31], over a similar theoretical method proposed by ROSE [41], of taking into account all the experimental conditions actually adopted in the experiment (efficiency of the scintillators, discrimination of the electronic equipment, scattering of quanta on the wall of the accepting cone, etc.).

A well collimated γ-ray beam has been obtained from a 3 mC ^{60}Co source through a channel (15.5 cm in lenght, 2 · 2 mm in section) bored in lead. The analysis of the angular aperture of the beam has been performed by means of a small NaI(Tl) crystal, coupled with a photomultiplier, at a distance of 95 cm from the exit hole, giving a profile reported in fig. 9. Taking into account the finite angular aperture of the exploring crystal (about 0.3° at the chosen distance), the angular spread of the beam at half intensity is about 1°.

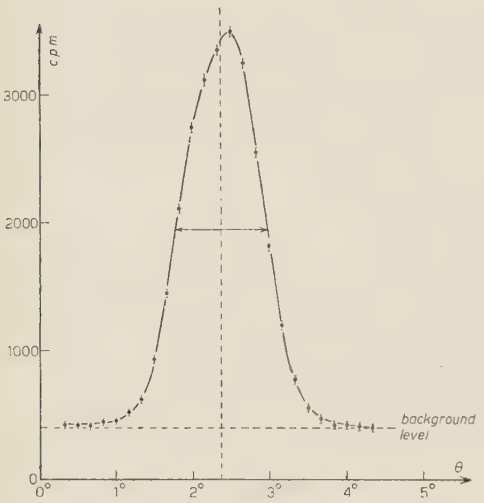

Fig. 9. - Profile of the gamma ray beam utilized for determination of detector efficiencies.

Exploring with this beam the scintillation counters we have obtained the relative efficiency curves $\varepsilon^{I}(\alpha)$ and $\varepsilon^{II}(\alpha)$ reported in fig. 10. Within the statistical accuracy (which was about 0.3% at the top), they are symmetrical, and present a flat top. This is probably due to a uniform redistribution on the photocathode of the produced photons, owing to the numerous internal flaws and opacities of the Anthracene crystals, rather than to effective uniformity of the photocatode response.

A similar measurement was performed along the perpendicular diametre of both counters, and gave coincident curves, thus assuring the good cylindrical symmetry necessary for the calculation of the correction factors.

The following values were obtained:

J_0/J_2:	(counter I)	1.0769	(counter II)	1.0771
J_0/J_4:	»	1.2872	»	1.2880

$$Q_0/Q_2 = 1.1599 \text{ (standard deviation } 2.3\cdot10^{-3})$$
$$Q_0/Q_4 = 1.6578 \quad \text{» } \quad \text{» } \quad 3.3\cdot10^{-3}) .$$

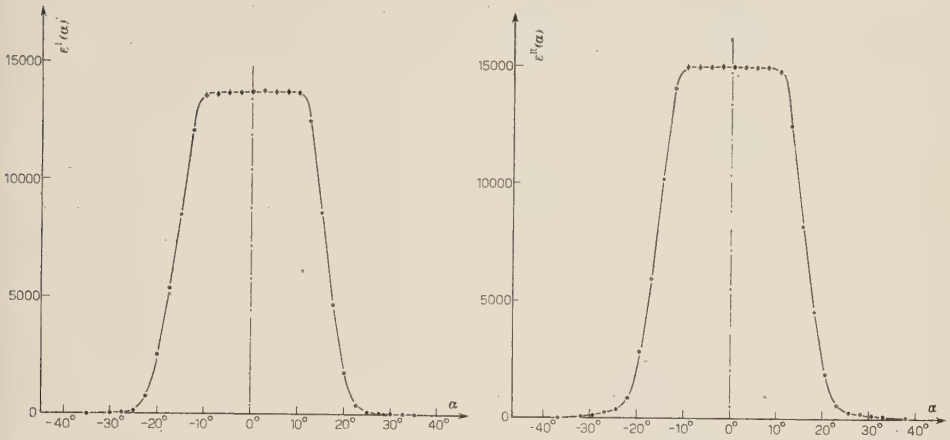

Fig. 10. – Experimentally determined efficiencies for counters I and II (arbitrary units, background subtracted).

An approximate evaluation of the same factors ([12,2]), which was used for a first planning of the experiment, gives satisfactory agreement:

$$Q_0/Q_2 = 1.13 \qquad Q_0/Q_4 = 1.65 .$$

6. – The Presentation of Corrected Experimental Data and the Comparison with Theoretical Results.

We report in Table III the experimental data obtained and their comparison with the theoretical values.

TABLE III.

θ	$A_1(\theta)$	$\sigma_1(\theta)$	$A_2(\theta)$	$\sigma_2(\theta)$	$A_3(\theta)$	$\sigma_3(\theta)$	$A_4(\theta)$	$\sigma_4(\theta)$	$A_5(\theta)$
90°	(1)	—	(1)	—	(1)	—	(1)	—	(1)
105°	1.0071	$2.2\cdot10^{-3}$	1.0077	$0.7\cdot10^{-3}$	1.00790	$1.0\cdot10^{-4}$	1.0083	$6\cdot10^{-4}$	1.00856
120°	1.0309	2.2	1.0300	0.8	1.03064	0.8	1.0329	5	1.03385
135°	1.0646	2.0	1.0636	1.0	1.06441	0.9	1.0717	6	1.07292
150°	1.0981	2.3	1.1006	0.9	1.10130	1.5	1.1163	8	1.11719
165°	1.1298	2.3	1.1300	1.1	1.13028	2.1	1.1526	10	1.15290
180°	1.1421	2.0	1.1412	2.2	1.14131	2.4	1.1667	12	1.16667

Values of the anisotropy $A(\theta) = W(\theta)/W(\pi/2)$.
$A_1(\theta)$: Experimental value, derived directly from measured data;
$A_2(\theta)$: Experimental value, after least square fit;
$A_3(\theta)$: Theoretical value, taking into account counter resolution;
$A_4(\theta)$: Experimental value, corrected for counter resolution;
$A_5(\theta)$: Theoretical value.

We denote by $A_1(\theta) = W_s(\theta)/W_s(\pi/2)$ the experimental value of the anisotropy at angle θ as directly derived from collected data (see Sect. **4**); $\sigma_1(\theta)$ is the standard deviation of $A_1(\theta)$, derived through the usual statistical rules from total number of counts.

By means of least square fit to the accepted form of the function:

$$W'_s(\theta) = 1 + \alpha'_2 P_2(\cos\theta) + \alpha'_4 P_4(\cos\theta),$$

we have obtained the best values of α'_2 and α'_4, and their standard deviations σ'_2 and σ'_4:

$$\alpha'_2 = 0.08766 \qquad \sigma'_2 = 0.8 \cdot 10^{-3} \qquad \alpha'_4 = 0.00614 \qquad \sigma'_4 = 1.5 \cdot 10^{-3}.$$

Hence the values $A_2(\theta)$ and the corresponding $\sigma_2(\theta)$ reported in the table.

The theoretical correlation function has been corrected for angular resolution, thus obtaining the values $A_3(\theta)$, with standard deviations $\sigma_3(\theta)$.

The comparison between $A_2(\theta)$ and $A_3(\theta)$ is quite satisfactory.

It is usually preferred to correct experimental results for angular resolution, thus obtaining the values $A_4(\theta)$. The standard deviation $\sigma_4(\theta)$ also includes the statistical uncertainty due to the correction factors.

The comparison of $A_4(\theta)$ with the theoretical values $A_5(\theta)$ is equivalent to the preceding one between $A_2(\theta)$ and $A_3(\theta)$.

The very close agreement between experimental values and theoretical calculations confirms that the influence of extranuclear fields is negligible, within experimental accuracy, in agreement with the last results obtained in similar conditions by the Illinois group ([30,31]), by LEMMER and GRACE at very low temperature ([33]), and recently by STEFFEN ([34]).

* * *

It is a pleasure to thank Miss R. SOMIGLIANA and Mr. R. GISLON for the help given in taking and reducing experimental data, and Mr. V. MANDL, who mounted and checked a great part of the electronic equipment.

REFERENCES

([1]) H. FRAUENFELDER: *Angular Correlation of Nuclear Radiation*, *Annual Review of Nuclear Science*, vol. 2, (1953).

([2]) H. FRAUENFELDER: *Angular Correlation*, a chapter from K. Siegbahn's book: *Beta and Gamma Ray Spectroscopy* (Amsterdam, 1955).

([3]) L. C. BIEDENHARN and M. E. ROSE: *Rev. Mod. Phys.*, **25**, 729 (1953).

([4]) S. COLOMBO, A. ROSSI and A. SCOTTI: *Nuovo Cimento*, **1**, 522 (1955).

([5]) J. M. HOLLANDER, I. PERLMAN and G. T. SEABORG: *Rev. Mod. Phys.*, **25**, 469 (1953).
([6]) G. L. KEISTER and F. H. SCHMIDT: *Phys. Rev.*, **93**, 140 (1954).
([7]) Y. F. CHANG: *Phys. Rev.*, **87**, 252 (1952).
([8]) D. R. HAMILTON: *Phys. Rev.*, **58**, 122 (1940).
([9]) H. FERENTZ and N. ROSENZWEIG: *Argonne National Laboratory Report* 5324 (1954).
([10]) J. M. BLATT and V. H. WEISSKOPF: *Theoretical Nuclear Physics* (New York, 1951) p. 627.
([11]) R. E. BELL and H. E. PETCH: *Phys. Rev.*, **76**, 1409 (1949).
([12]) T. C. ENGELDER: *Phys. Rev.*, **90**, 259 (1953).
([13]) S. GORODETZKY, A. KNIPPER, R. ARMBRUSTER and A. GALLMANN: *Journ. Phys. Rad.*, **14**, 550 (1953).
([14]) Z. BAY: *Phys. Rev.*, **90**, 371 (1953).
([15]) Z. BAY, V. P. HENRY and F. MC LERNON: *Phys. Rev.*, **97**, 561 (1955).
([16]) H. AEPPLI, H. FRAUENFELDER, E. HEER and R. RÜETSCHI: *Phys. Rev.*, **87**, 379 (1952).
([17]) E. D. KLEMA and F. K. MC GOWAN: *Phys. Rev.*, **91**, 616 (1953).
([18]) W. M. GOOD: *Phys. Rev.*, **70**, 978 (1946).
([19]) E. L. BRADY and M. DEUTSCH: *Phys. Rev.*, **72**, 870 (1947).
([20]) E. L. BRADY and M. DEUTSCH: *Phys. Rev.*, **74**, 1541 (1948).
([21]) E. L. BRADY and M. DEUTSCH: *Phys. Rev.*, **78**, 561 (1950).
([22]) A. H. WILLIAMS and M. L. WIEDENBECK: *Phys. Rev.*, **78**, 822 (1950).
([23]) J. R. BEYSTER and M. L. WIEDENBECK: *Phys. Rev.*, **79**, 411 (1950).
([24]) R. M. STEFFEN: *Phys. Rev.*, **60**, 115 (1950).
([25]) S. DAS and S. K. SEN: *Indian Jour. of Phys.*, **25**, 451 (1951).
([26]) E. K. DARBY: *Can. Journ. Phys.*, **29**, 569 (1951).
([27]) B. L. ROBINSON and L. MADANSKY: *Phys. Rev.*, **84**, 604 (1951).
([28]) S. CHATTERJE and A. K. SAHA: *Zeits. f. Phys.*, **135**, 141 (1953).
([29]) J. J. KRAUSHAAR and M. GOLDHABER: *Phys. Rev.*, **89**, 1081 (1953).
([30]) J. S. LAWSON, H. FRAUENFELDER and W. K. JENTSCHKE: *Phys. Rev.*, **91**, 484 (1953).
([31]) J. S. LAWSON and H. FRAUENFELDER: *Phys. Rev.*, **91**, 649 (1953).
([32]) R. M. KLOEPPER: *Phys. Rev.*, **91**, 1026 (1953).
([33]) H. R. LEMMER and M. A. GRACE: *Proc. Phys. Soc.*, A **67**, 1051 (1954).
([34]) R. M. STEFFEN: to be publiseed in *Amer. Journ. Phys.*
([35]) R. K. SWANK and J. S. MOENICH: *Rev. Scient. Instr.*, **23**, 502 (1952).
([36]) N. F. MOODY, G. J. R. MACLUSKY and M. O. DEIGHTON: *Electronic Eng.*, **24**, 214 (1952).
([37]) J. FISCHER and J. MARSHALL: *Rev. Scient. Instr.*, **23**, 417 (1952).
([38]) S. COLOMBO: *Nuovo Cimento*, **12**, 290 (1954).
([39]) J. C. STREET and R. H. WOODWARD: *Phys. Rev.*, **46**, 1029 (1934).
([40]) C. ECKART and F. R. SHONKA: *Phys. Rev.*, **53**, 752 (1938).
([41]) L. I. SCHIFF: *Phys. Rev.*, **50**, 88 (1936).
([42]) M. WALTER, O. HUBER and W. ZÜNTI: *Helv. Phys. Acta*, **23**, 697 (1950).
([43]) S. FRANKEL: *Phys. Rev.*, **83**, 673 (1951).
([44]) M. E. ROSE: *Phys. Rev.*, **91**, 610 (1953).

RIASSUNTO

È stata eseguita una misura di precisione della funzione di correlazione direzionale gamma-gamma del ^{60}Ni, ottenuta mediante decadimento beta di ^{60}Co in forma metallica. L'apparecchiatura sperimentale comprende contatori a scintillazione, costituiti da fotomoltiplicatori Du Mont tipo 6292, associati a cristalli di antracene in forma cilindrica da $1'' \times 1''$, e un circuito di coincidenza con tempo risolutivo di $4 \cdot 10^{-8}$ s. Si riportano i risultati sperimentali, con una discussione degli errori sistematici introdotti e delle correzioni sperimentali apportate. Il confronto con i risultati teorici relativi a una cascata 4(E2)2(E2)0 non perturbata mostra un ottimo accordo.

IL NUOVO CIMENTO Vol. II, N. 3 1° Settembre 1955

Operation Conditions of a Bubble Chamber.

(n-pentane, iso-pentane and diethyl ether).

L. Bertanza, G. Martelli and A. Zacutti

Istituto di Fisica dell'Università - Pisa
Istituto Nazionale di Fisica Nucleare - Sezione Aggregata di Pisa

(ricevuto il 6 Luglio 1955)

Summary. — A general criterion to calculate the operations conditions for a bubble chamber is deduced. Numerical tables are given for n-pentane, iso-pentane and diethyl ether.

---

1. – The aim of the present work is the calculation of the values of temperature and pressure for which a bubble chamber will operate, with particular regard to its « bias » conditions, i.e. the conditions for which only bubbles carrying *at least* a given number of ions are detected, so that the sensitivity of the device for particles having different specific ionization may be preset within large limits.

It is generally assumed that the mechanism of formation of bubbles along the path of ionizing particles in overheated liquids is somehow similar to the formation of droplets on the ions formed in supersaturated vapours. It has also been suggested that the nucleation of bubbles could instead be initiated on the path of the particles, by addition of a local triggering heat provided by the particles themselves. Probably, both phenomena are likely to contribute to the formation of bubbles, but so far no « thermal » theory has been worked out. On the other hand, the predictions of the « electrostatic » theory are in excellent agreement with experimental data: it seems therefore reasonable to assume that the contribution of the ions to the nucleation should largely prevail over other effects.

The present calculations are based on the « electrostatic » theory as it has been worked out in some recent papers [1-3].

In what follows we shall, first, recall briefly some points of this theory.

2. – For the sake of clarity, the symbols which will be used are summarized in the following list:

T	absolute temperature of the liquid;
P	hydrostatic pressure in the liquid;
R	radius of a bubble;
N	number of ions in a bubble;
n	number of molecules of vapour inside a bubble;
$p_n(R, N)$	internal vapour pressure in a bubble of radius R, containing n molecules and N ions;
$p_\infty(T)$	vapour pressure of the liquid at the temperature T;
e	elementary charge;
$\sigma(T)$	average value of the surface tension on a liquid-vapour surface, at the temperature T;
$\varepsilon(T)$	dielectric constant of the liquid, at the temperature T;
$C^2(N)$	a positive coefficient such that, for large N, $C^2(N)/R^4$ is the equivalent electrostatic pressure on the bubble surface, arising from the presence of the ions in the bubble itself;
μ_l	chemical potential per molecule in the liquid phase;
μ_b	chemical potential per molecule of vapour inside the bubble;
k	Boltzmann's constant.

3. – The nucleation theory states that sub-microscopic bubbles continuously form and collapse in every liquid, as a consequence of thermal fluctuations.

The condition for the mechanical equilibrium of one of such bubbles may be written as

$$p_n(R) = P + \frac{2\sigma}{R} . \tag{1}$$

For a bubble in thermodynamical equilibrium (hereafter referred to as « equilibrium nucleus »), i.e. for a bubble satisfying at the same time condition (1) and

$$\mu_b = \mu_l , \tag{2}$$

---

(1) G. MARTELLI: *Nuovo Cimento*, **12**, 250, (1954).

(2) L. BERTANZA and G. MARTELLI: *Nuovo Cimento*, **1**, 324 (1955).

(3) L. BERTANZA and G. MARTELLI: *Nucleation processes in liquids under negative pressures*. To be published in *Il Nuovo Cimento*.

the internal pressure

$$p_k = P + \frac{2\sigma}{R_k},$$

(hereafter all quantities referred to an equilibrium nucleus will be labelled with the subscript k), may be shown to be related to other thermodynamical parameters by

$$\ln \frac{p_\infty}{p_k} = \frac{M(p_\infty - P)}{d\mathcal{R}T},$$

where M is the molecular weight, d the density and $\mathcal{R}$ the gas constant.

These equations define, for each value of P and T, the size R_k of the equilibrium nucleus. *A liquid is overheated when* $P < p_k$.

In order to investigate the contribution of the ions to the formation of bubbles in overheated liquids, it will be convenient to consider first the case where ions are formed in a pre-existing bubble. Let us call $\overline{N}$ the critical value for which the repulsive force among the ions (proportional to $N(N-1) \sim N^2$) equals the force (proportional to N) tending to pull the dielectric into the bubble. Since the first prevails when $N > \overline{N}$, the presence of $N > \overline{N}$ charges prevents bubbles from collapsing. For most liquids is $\overline{N} \sim \varepsilon$ [2].

It may be shown that also clusters of $N > \overline{N}$ ions, formed inside a volume of the same order of magnitude as the average radius of a bubble, strongly favour the nucleation processes. This fact may be roughly described as though, pushed apart by their mutual repulsion, they were giving rise to « holes », which under suitable conditions may evolve into bubbles of macroscopic sizes.

In what follows we are obviously interested only in those cases where $N > \overline{N}$.

4. – For a N-charged bubble the equilibrium condition (1) may be rewritten as

$$p_n(R, N) = P + \frac{2\sigma}{R} - \frac{C^2}{R^4}. \tag{3}$$

The total energy $D_n(R, N)$ required for the reversible formation of a mechanically stable bubble containing n molecules of vapour, from an initial aggregate of n_a molecules of vapour is

$$D_n(R, N) = \sum_{n_a+1}^{n} (\mu_i - \mu_l) = kT \int_{n_a}^{n} \ln \frac{p_i}{p_k} \, di = W_n(R, N) - W_{n_a}(N), \tag{4}$$

where

$$W_n(R, N) = nkT \ln \frac{p_n}{p_k} + \frac{4}{3} \pi\sigma R^2 + \frac{16}{3} \pi \frac{C^2}{R}$$

and μ_i is the chemical potential per molecule of vapour in a bubble having i molecules. In fig. 1 the behaviour of the function $f(R) = p_n - P = (2\sigma/R) - (C^2/R^4)$, i.e. the radius dependent part of eq. (1), is shown for two different values of N (4).

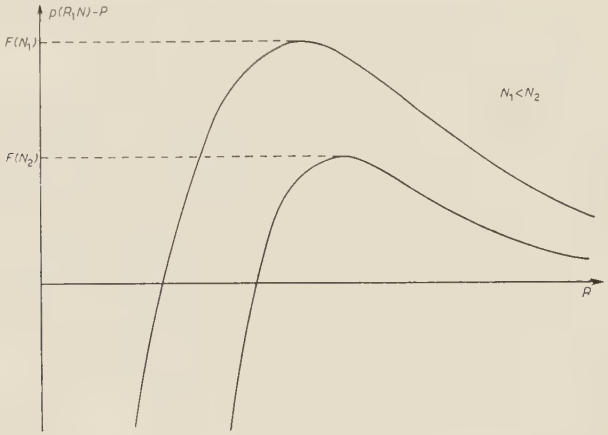

Fig. 1.

If we call $F(N)$ the maximum of $f(R, N)$, the thermodynamical conditions of the liquid may be such that either

(5) $$p_k - P < F(N) \qquad \text{(case } a\text{)},$$

or

(6) $$p_k - P = F(N) \qquad \text{(case } b\text{)}.$$

Case a). In this case the function $D_n(R, N)$ behaves as shown in fig. 2, and the initial aggregates require a certain amount of energy to reach the critical size R'. Beyond this size they will grow freely, i.e. with decrease of their total energy. This can happen only when a favourable chain of fluctuations (in which the bubbles exchange molecules with the liquid) bring them up to

(4) We consider here the case when $P > 0$, but the results of our calculations are valid also in the case when $P < 0$.

the critical size. The average time (or *waiting time*) required for the growth is given by

$$(7) \qquad t(N) = \text{const} \int_{n_a}^{s-1} \frac{1}{A'} \exp\left\{\frac{1}{kT}(W_n - W_{n_a})\right\} \mathrm{d}n =$$

$$= \text{const} \sqrt{\frac{2n_k\pi(3-L)}{L}} \exp\left\{\frac{1}{kT}(W_k - W_{n_a})\right\},$$

where

$$L = \frac{2\sigma}{R_k p_k} - \frac{4C^2}{R_k^4 p_k}\,; \qquad A' = 4\pi R^2\,,$$

and s is a particular value of n (2).

An important result which may be deduced from eq. (7) is the following one: if one chooses two N's, say N_1 and N_2 ($N_1 < N_2$), and if temperature and pressure are such as to satisfy the condition

$$p_k - P < F(N_2)\,,$$

then

$$t(N_2) < t(N_1)\,.$$

In this case the inequality $p_k - P < F(N_1)$ is obviously satisfied too.

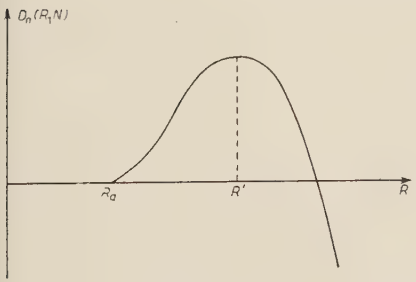

Fig. 2.

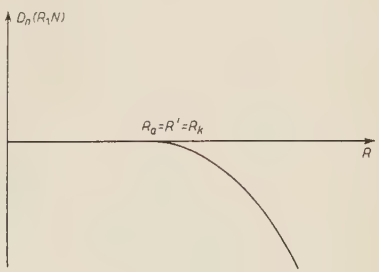

Fig. 3.

Case b). When $p_k - P = F(N)$, the function $D_n(R, N)$ decreases monotonically, with increasing R (fig. 3): the initial aggregates evolve spontaneously into macroscopic bubbles, and an eruptive boiling occurs in the liquid, as soon as this condition is satisfied.

If for a given N^*, $L(N^*) = 0$ (it may be easily verified that the condition (6) is the same as $L = 0$), the limits of the integral in eq. (7) coincide, and the

waiting time relative to bubbles with N^* ions becomes zero effectively. Bubbles carrying *at least* N^* ions require no appreciable time to evolve up to the critical size. (If aggregates containing at least N^* ions are pre-existing, bubbles nucleate on them as soon as the liquid is brought to these conditions).

5. – From the foregoing considerations the *bias conditions*, i.e. the values of temperature and pressure at which a bubble chamber has to operate in order to reveal bubbles carrying at least a given number of ions, may be deduced.

The equations

$$p_k(T) - P = F(T, N)\,,$$

have been solved with respect to P and T, for various liquids and for some

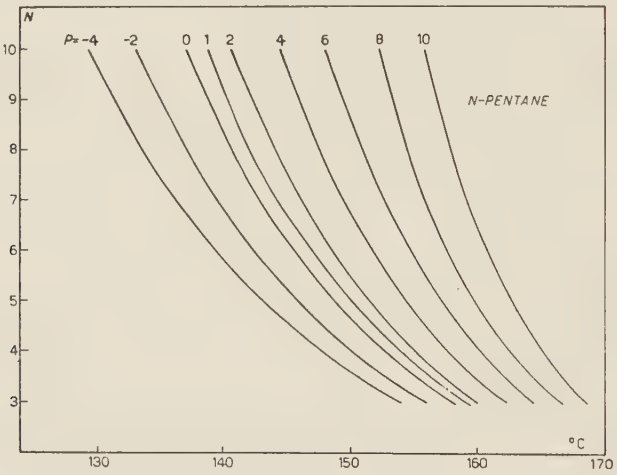

Fig. 4.

TABLE I. – *n-pentane.*

	$N = 3$	$N = 4$	$N = 6$	$N = 8$	$N = 10$
P (atm)	T (°C)	T	T	T	T
−4	154.2	148	139.6	133.8	129.4
−2	156.2	150.4	142.6	137.2	133.2
0	158.2	153	145.8	140.8	137.2
1	159.4	154.2	147.2	142.4	139
2	160.2	155.4	148.8	144.2	140.8
4	162.4	157.8	152	147.8	144.6
6	164.6	160.4	155	151.2	148.2
8	166.8	162.8	158	154.6	152.4
10	168.8	165.4	161	158.2	156

given values of N (5). The results are given in tables I, II and III, and plotted in the graphs of fig. 4, 5 and 6, for n-pentane, iso-pentane and diethyl ether respectively.

TABLE II. – *Iso-pentane.*

	$N = 3$	$N = 4$	$N = 6$	$N = 8$	$N = 10$
P (atm)	T (°C)	T	T	T	T
— 4	145	139	130.8	125	120.8
— 2	147	141.4	134	128.4	124.4
0	149.2	143.8	137.2	132	128.4
2	151	146.2	140.2	135.8	132.4
4	153	148.6	142.8	139.2	136
6	155.4	151,2	145.8	142.2	139.8
8	157.4	153.8	149.2	145.8	143.4
10	159.4	156.2	152	149.2	147.2

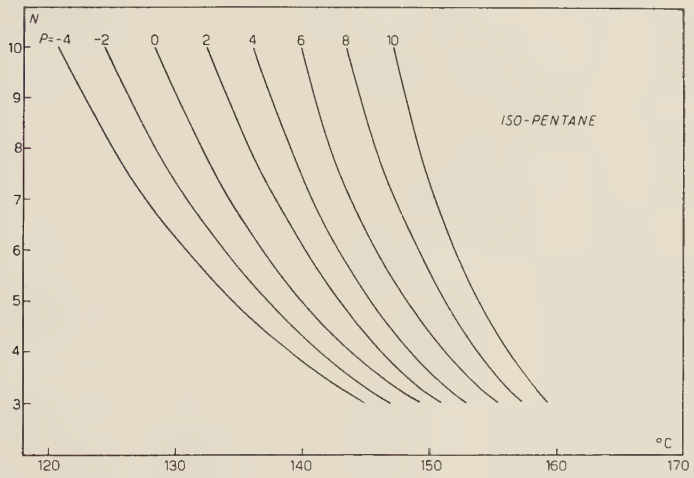

Fig. 5.

Good agreement is found with the experimental data available at present (6). In order to have the sensitive time of the bubble chamber as long as pos-

(5) The values of $\sigma(T)$ and $\varepsilon(T)$ given in the *International Critical Tables* have been used.

(6) Cfr., for instance, the figures given by D. A. GLASER: *Phys. Rev.*, **97**, 474 (1955).,

TABLE III. – *Diethyl ether.*

	$N = 3$	$N = 4$	$N = 6$	$N = 8$	$N = 10$
P (atm)	T (°C)	T	T	T	T
−4	157	149.2	140	134	130
−2	158.5	151	142.8	137	133
0	160.2	153	145.2	140	136.2
1	161	154	146.5	141.5	138
2	161.8	155	147.8	142.8	139.5
4	163	157	150.2	145.8	142.8
6	164.5	159	152.8	149	146
8	166	161	155.2	151.8	149
10	168	163	158	154.8	152.2

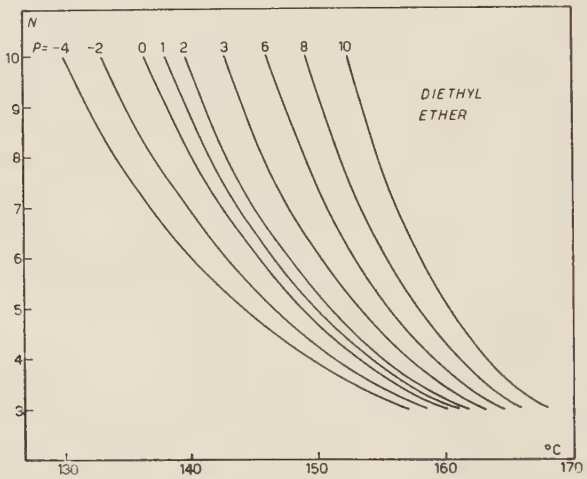

Fig. 6.

sible, among the infinite pairs of values of P and T deduced in this way, that particular pair must be chosen, for which the value of the waiting time which one would obtain if only bubbles with $N < N^*$ ions were present, is maximum.

RIASSUNTO

Si deduce un criterio generale per calcolare le condizioni termodinamiche di lavoro di una camera a liquido, sulla base della teoria della nucleazione di bolle di vapore sugli ioni presenti in un liquido surriscaldato. Si danno tabelle numeriche per l'n-pentano, l'iso-pentano e per l'etere etilico.

Assorbimento di ultrasuoni in sistemi di liquidi parzialmente miscibili.

M. Cevolani e S. Petralia

Istituto di Fisica dell'Università - Bologna

(ricevuto il 6 Luglio 1955)

Riassunto. — Col metodo degli impulsi si è misurato il coefficiente di assorbimento di ultrasuoni, di frequenza compresa tra 9 e 33 MHz, in fenolo fuso, anilina, cicloesano, nelle miscele fenolo-acqua e anilina-cicloesano a diverse concentrazioni dei componenti e per temperature al di sopra di quella critica di solubilità, come pure l'assorbimento in queste miscele nelle condizioni critiche. Nel fenolo e nell'anilina l'assorbimento diminuisce al crescere della temperatura, così come avviene per il loro assorbimento di viscosità, per cui l'eccesso di assorbimento rispetto al valore classico deve essere di origine strutturale; nel cicloesano l'assorbimento aumenta col crescere della temperatura. Le miscele presentano un massimo di assorbimento per quelle concentrazioni, alle quali la curva di solubilità corrispondente ha una regione piatta; tale massimo diminuisce col crescere della temperatura e non dipende in modo quadratico dalla frequenza ultrasonora. Al punto critico si ha un assorbimento notevole, che viene interpretato come dovuto a processi di rilassamento con frequenze diverse; nel caso della miscela anilina-cicloesano si mostra che le frequenze di rilassamento cadono nel campo di frequenze da noi esplorato.

È stato constatato da vari Autori [1-4] che, in vicinanza della temperatura critica di un gas o di un sistema di liquidi parzialmente miscibili, l'assorbimento degli ultrasuoni mostra un massimo pronunciato, sulla cui origine si

[1] R. Lucas: *Journ. Phys. et le Radium*, **8**, 41 (1937).

[2] A. G. Chynoweth e W. G. Schneider: *Journ. Chem. Phys.*, **19**, 1566 (1951); **20**, 1777 (1952).

[3] G. F. Alfrey e W. G. Schneider: *Discussion Farad. Soc.*, **15**, 218 (1953).

[4] S. Petralia e M. Cevolani: *Rend. Acc. Lincei*, **12**, 674 (1952).

possono prospettare varie ipotesi. Sostanzialmente si cerca di riportarsi alle teorie oggi correnti sulla parte non classica dell'assorbimento degli ultrasuoni nei fluidi, tenendo conto dello stato di aggregazione in cui il fluido viene a trovarsi nell'intorno del punto critico. Informazioni sulle condizioni del fluido allo stato critico si possono trarre dagli studi eseguiti con altri metodi di indagine e in particolare da misure sulla luce diffusa.

Onde arrecare un contributo alla conoscenza dei processi, che devono aver luogo in una mescolanza di liquidi in prossimità del punto critico di soluzione, noi, facendo seguito a precedenti determinazioni [4], abbiamo misurato l'assorbimento di ultrasuoni nelle miscele fenolo-acqua e anilina-cicloesano, entrambe caratterizzate da una temperatura critica superiore t_c, per valori della temperatura t del sistema variabili attorno a t_c.

Nel tentativo di interpretare i valori anomali dell'assorbimento al punto critico, ci occorreva conoscere, oltre l'assorbimento classico della miscela, quella parte dell'assorbimento che i liquidi puri o le miscele presentano, in generale, in conseguenza di vari meccanismi di rilassamento. Abbiamo perciò esteso le ricerche, misurando il coefficiente d'assorbimento in miscele fenolo-acqua e anilina-cicloesano, per diverse concentrazioni c dei costituenti e a temperature fisse al di sopra di quella critica, e così pure l'assorbimento nel fenolo, nell'anilina e nel cicloesano a varie temperature.

Data la particolare struttura delle miscele al punto critico, ci si può attendere che i processi, che determinano l'assorbimento anomalo, cadano entro limiti di frequenza facilmente realizzabili. Le misure, fatte in precedenza alla frequenza di 3 MHz, sono state perciò estese fino alla frequenza di 33 MHz, quest'ultimo limite essendo imposto dalla nostra apparecchiatura attuale.

1. – Tecnica sperimentale.

Il metodo di misura dell'assorbimento ultrasonoro, qui adottato, si basa sulla tecnica degli impulsi. Un generatore di impulsi di tensione rettangolari, di durata regolabile tra 2 e 10 μs, comanda un tubo oscillatore (tipo 6AG7), in guisa che questo lavori solo durante tale breve tempo. Il segnale elettrico prodotto è applicato, attraverso un adattatore di impedenza, a una piastrina di quarzo, la cui frequenza fondamentale è di 3 MHz. L'impulso elastico generato dal quarzo si propaga nel liquido sovrastante e raggiunge un secondo quarzo, che fa da ricevente e che può esser spostato, mediante vite micrometrica, rispetto al quarzo trasmittente. Al quarzo ricevente, dove l'impulso sonoro si trasforma in elettrico, fa seguito un adattatore, un attenuatore tarato, un amplificatore a larga banda e l'oscillografo catodico (fig. 1).

La piastrina di quarzo poteva esser eccitata sulla 3ª, 5ª, 9ª e 11ª armonica. La vaschetta contenente il liquido, il quarzo trasmittente e quello ricevente,

era adattata dall'interferometro precedentemente adoperato per le misure di velocità. Essa era disposta entro un bagno termostatico, la cui temperatura era regolata a $\pm$ 0.03 °C.

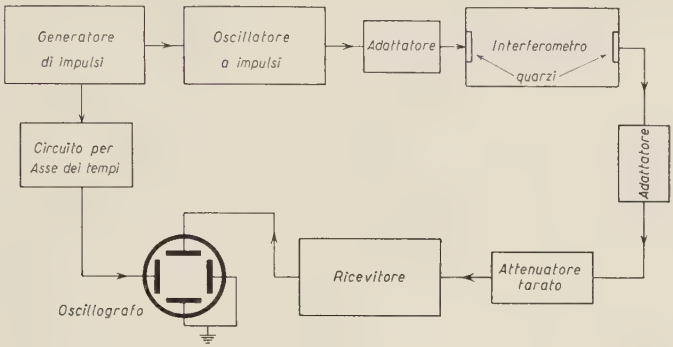

Fig. 1. – Schema della disposizione sperimentale.

La misura dell'assorbimento dell'impulso ultrasonoro era effettuata compensando la variazione dell'ampiezza dell'impulso elettrico osservato all'oscillografo, variazione conseguente a uno spostamento del pistone ricevente, mediante un'attenuazione nota. Il buon funzionamento del dispositivo è stato verificato con misure di assorbimento nell'acqua a varie temperature, misure che hanno permesso di ricostruire la curva di Hall ([5]), che dà il rapporto α/f^2, tra il coefficiente d'assorbimento dell'ampiezza sonora e il quadrato della frequenza f, in funzione della temperatura dell'acqua.

2. – Risultati sperimentali.

I risultati delle misure eseguite sono raccolti nelle tabelle I-IV e riportati nelle figg. 2-10. Essi sono espressi mediante la grandezza α/f^2, per i liquidi puri o per le miscele, in funzione della temperatura o della frequenza ultrasonora o della concentrazione delle miscele. Nel caso dell'anilina e sue miscele, alcune misure sono state scartate dai calcoli, perchè durante la loro esecuzione si era notata una alterazione del colore della sostanza, per quanto spesso i valori del coefficiente d'assorbimento determinati in tali condizioni non differivano molto dagli altri.

Quando è stato necessario, si è fatto il calcolo del parametro α/f^2 secondo la teoria classica, limitatamente al termine di questa teoria derivante dalla viscosità, dato che nei liquidi l'assorbimento dovuto alla conducibilità termica

([5]) L. Hall: *Phys. Rev.*, **73**, 773 (1948).

si può ritenere trascurabile rispetto al primo, per cui si è preso

$$\frac{\alpha_{cl}}{f^2} = \frac{2\pi^2}{\varrho V^3}\frac{4}{3}\eta \,. \tag{1}$$

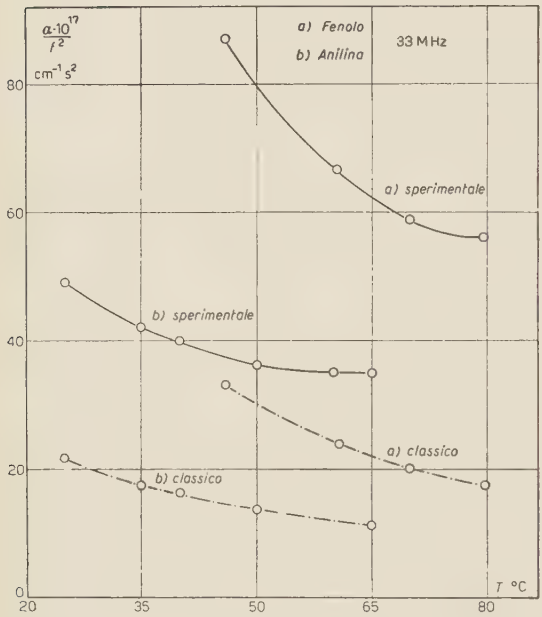

Fig. 2. – Valori classici e sperimentali del parametro α/f^2 per il fenolo e l'anilina a diverse temperature. Frequenza ultrasonora 33 MHz.

La velocità V e la densità ϱ sono state tratte da nostre precedenti determinazioni e la viscosità η che compare nella (1) è stata ricavata dalle International Critical Tables (1929).

3. – Liquidi puri.

Alcuni dati relativi ai liquidi puri fenolo, anilina e ciclo-

TABELLA I. – *Assorbimento classico e sperimentale nei liquidi fenolo, anilina, cicloesano, a diverse temperature e frequenze ultrasonore.*

Liquido	Temperatura °C	α_{cl}/f^2 10^{17} cm^{-1} s^2	$(\alpha_{sp}/f^2)10^{17}$ cm^{-1} s^2				$r = \alpha_{sp}/\alpha_{cl}$	$k \cdot 10^2$ g cm^{-1} s^{-1}
			9 MHz	15 MHz	27 MHz	33 MHz		
Fenolo	46.0	32.9	75	76	79	85	2.4	7.2
	60.7	23.7	63	62	62	67	2.7	5.6
	70.0	20.2	65	64	60	59	3.1	5.5
	79.7	17.4	58	57	56	56	3.3	4.8
Anilina	25	21.7	47	50	47	49	2.2	6.1
	35	17.3	47	46	43	43	2.6	5.7
	40	16.4	45	44	41	40	2.6	5.2
	50	13.6	41	39	37	36	2.8	4.6
	60	12.1	36	36	36	36	3.0	4.0
	65	11.6	36	35	35	35	3.0	3.8
Cicloesano	25	15.2	190	192	194	192		
	35	15.0	211	211	210	211		
	50	15.0	241	238	240	238		

TABELLA II. – *Assorbimento ultrasonoro nelle miscele fenolo-acqua e anilina-cicloesano in funzione della concentrazione molecolare, a diverse frequenze e temperature.*

Miscela	Conc. molec. del 1° comp. %	$\alpha_{cl}/f^2 \cdot 10^{17}$ $cm^{-1}\ s^2$	$(\alpha_{sp}/f^2) \cdot 10^{17}$ $cm^{-1}\ s^2$			
			9 MHz	15 MHz	27 MHz	33 MHz
Fenolo-Acqua 70 °C	0.0	2.9	—	8.1	7.8	7.7
	0.4	—	—	8.1	8.0	7.4
	0.8	—	—	7.7	8.1	7.7
	1.2	—	—	8.7	9.1	7.8
	1.6	—	—	11.0	10.5	9.5
	2.1	3.4	30	22.3	16.8	15.4
	3.3	—	46	41.6	29.7	28.5
	4.6	4.5	49	44.4	32.2	31.4
	6.0	—	50	45.1	33.4	32.1
	7.6	6.0	48	43.0	32.8	31.0
	16.1	8.5	32	31.0	23.9	23.5
	22.3	—	29	27.8	21.9	21.0
	30.9	—	31	29.8	23.3	22.0
	43.4	12.5	36	34.8	28.2	27.1
	63.3	—	46	44.0	38.7	37.7
	100.0	20.3	65	64.0	60.3	58.7
Anilina-Cicloesano 35 °C	0.0	15.0	211	211	210	211
	4.5	15.0	214	191	191	196
	9.1	15.0	218	195	191	193
	18.4	15.0	288	236	226	218
	27.9	15.2	448	345	275	258
	32.6	15.2	582	392	287	266
	37.6	15.3	600	395	281	263
	47.5	15.5	546	362	257	229
	57.5	15.6	412	256	190	182
	67.8	15.8	225	155	123	122
	78.3	16.0	101	81	73	73
	89.1	16.6	62	52	50	48
	100.0	17.3	47	46	43	43
Anilina-Cicloesano 50 °C	0.0	15.0	241	238	240	238
	9.1	14.7	210	203	197	195
	18.4	14.4	204	192	185	182
	32.6	14.1	235	204	186	176
	37.6	14.0	253	214	192	175
	47.5	13.7	226	195	172	157
	57.5	13.5	185	154	133	117
	78.3	13.2	80	66	57	54
	89.1	13.3	54	47	41	39
	100.0	13.6	41	39	37	36

TABELLA III. – *Assorbimento ultrasonoro nella miscela anilina-cicloesano in funzione della temperatura alla concentrazione critica e a varie frequenze.*

Temperatura °C	α_{sp}/f^2 10^{17} cm^{-1} s^2			
	9 MHz	15 MHz	27 MHz	33 MHz
		fase ricca di anilina		
21.6	189	163	136	130
27.6	311	248	170	149
29.2	428	308	197	174
30.0	673	399	279	226
		fase omogenea		
30.1	822	505	316	249
30.2	752	536	316	252
30.3	732	507	308	244
30.5	704	489	309	244
30.7	710	488	316	244
31.3	658	466	300	248
31.7	628	454	294	244
32.5	606	425	285	226
34.6	546	357	268	243
37.5	452	305	241	214
40.2	377	260	222	206
50.0	223	191	173	158
65.0	135	134	133	130

esano sono contenuti nella tabella I (vedi fig. 2). Si può osservare anzitutto che per i tre liquidi α_{sp}/f^2 sperimentale è superiore al valore classico. Per l'anilina e il cicloesano tale parametro risulta in buon accordo con i valori dati da J. KARPOVICH [6]. Le altre determinazioni, che si trovano nella letteratura per il cicloesano, sono alquanto discordanti; le misure di G. W. HAZZARD [7] danno $\alpha/f^2 = 330 \cdot 10^{-17}$ cm^{-1} s^2 a temperatura ambiente, mentre più recentemente T. KISHIMOTO e O. NOMOTO [8] trovano il valore di $510 \cdot 10^{-17}$ cm^{-1} s^2, a 25 °C. Per il fenolo non ci sono note misure di assorbimento. Osserviamo ancora che, per tutti i tre liquidi, $\alpha_{sp} f^2$ si può considerare indipendente dalla frequenza. Col crescere della temperatura, nel caso dell'anilina e del fenolo si ha una diminuzione di α_{sp}/f^2; nel cicloesano tale rapporto cresce col crescere della temperatura, d'accordo con i risultati ottenuti da Kishimoto e Nomoto, per quanto le variazioni relative del coefficiente d'assorbimento constatate da noi siano diverse da quelle di questi Autori. Il rapporto r, che compare nella tabella I, tra il coefficiente d'assorbimento osservato e quello classico, si può ritenere,

[6] J. KARPOVICH: *Journ. Acoust. Soc. Amer.*, **26**, 819 (1954).
[7] G. W. HAZZARD: *Journ. Acoust. Soc. Amer.*, **22**, 29 (1950).
[8] T. KISHIMOTO e O. NOMOTO: *Journ. Phys. Soc. Japan*, **9**, 620 (1954).

TABELLA IV. *Assorbimento ultrasonoro nelle miscele fenolo-acqua in funzione della temperatura alla concentrazione critica e a varie frequenze.*

Temperatura °C	α_{sp}/f^2 10^{17} cm^{-1} s^2			
	9 MHz	15 MHz	27 MHz	33 MHz
		fase ricca di fenolo		
50.0	56	51	36	34
60.0	52	48	33	32
62.0	53	48	33	31
65.0	—	50	33	31
		fase omogenea		
66.0	65	55.1	40.3	37.2
66.2	66	55.1	39.8	36.5
66.5	62	52.0	38.1	35.2
67.0	61	51.1	36.8	34.1
68.0	56	46.7	34.6	32.3
69.2	53	42.7	32.5	28.9
70.0	47	40.2	31.4	28.8
71.0	46	36.9	28.7	26.3
72.0	42	34.8	27.3	25.2
73.0	40	33.3	25.5	24.1
75.2	36	31.1	24.0	21.8
76.0	35	30.2	23.3	21.1
80.0	32	28.4	21.3	19.8

in prima approssimazione, costante al variare della temperatura per i primi due liquidi, e presumibilmente le sue oscillazioni sono da imputare agli errori sperimentali, sia su α_{sp} che sulla viscosità, che si trova riportata nelle tabelle. Il valore medio di r vale 2.9 per il fenolo e 2.7 per l'anilina.

Come è noto, i valori di α/f^2 superiori a quelli calcolabili classicamente per i liquidi puri, si interpretano mediante l'ipotesi di processi di rilassamento. Questi possono essere di varia natura. Nel caso nostro conviene ricordare i due seguenti, quelli cioè che si originano da cambiamenti strutturali nello stato quasi-cristallino del liquido, e quelli che implicano i modi interni molecolari. I primi comportano una compressibilità del liquido dipendente dalla frequenza, gli altri determinano un calore specifico anch'esso dipendente dalla frequenza ultrasonora. Col crescere della temperatura, nei liquidi che si rilassano secondo il primo meccanismo si ha una diminuzione dell'assorbimento e il rapporto r, tra il coefficiente d'assorbimento misurato e quello classico, risulta indipendente dalla temperatura e compreso tra 2 e 3, per cui assorbimento di rilassamento e assorbimento classico mostrano la stessa dipendenza da t; nei liquidi ad assorbimento molecolare si ha un aumento dell'assorbimento quando la temperatura cresce. La prima classe di liquidi comprende sostanze che sono associate, in cui l'assorbimento di origine molecolare deve ritenersi trascurabile,

perchè, date le forti interazioni molecolari, lo scambio energetico tra i vari gradi di libertà è altamente efficiente. Per tutte e due le classi di liquidi, la parte di assorbimento che rilassa varia con la frequenza ultrasonora secondo la relazione di H. O. Kneser (9)

$$\frac{\alpha}{f^2} = \frac{A}{1 + f^2/f_m^2}, \tag{2}$$

essendo f_m la frequenza di rilassamento per quel processo, che è interessato nella transizione tra due diversi stati del sistema.

Si può allora concludere che nel cicloesano, liquido costituito da molecole a struttura simmetrica, non polari, si ha un assorbimento di origine molecolare; nel fenolo, e probabilmente nell'anilina, prevalgono i processi dovuti all'aggregazione molecolare. È ben certo che il fenolo, solido o liquido, è una sostanza polare, associata per legami idrogeno. La questione della formazione di associazioni nell'anilina è stata discussa da vari Autori, e più recentemente da M. Davies (10) e da E. Fischer (11). Davies, in base a determinazioni spettroscopiche fatte nell'infrarosso su soluzioni di anilina in tetracloruro di carbonio, conclude per l'esistenza di associazioni. Secondo Fischer le misure di rilassamento dielettrico nelle stesse soluzioni forniscono dei dati, che non costituiscono nè conferma nè negazione dell'esistenza di associazione delle molecole di anilina tra di loro (almeno con formazione di complessi a lunga vita, superiore a 10^{-8} s); essi si lascerebbero piuttosto interpretare nell'ipotesi, che il momento di dipolo dell'anilina non sia rigidamente connesso con la compagine molecolare.

L'eccesso di assorbimento nei liquidi si può anche attribuire, secondo L. Tisza (12), a una viscosità di compressione o seconda viscosità, ponendo per il coefficiente d'assorbimento totale

$$\frac{\alpha}{f^2} = \frac{2\pi^2}{\varrho V^3}\left(\frac{4}{3}\eta + k\right), \tag{3}$$

dove k sta a indicare la seconda viscosità. Il coefficiente d'assorbimento osservato si può perciò dividere in due termini

$$\alpha_{sp} = \alpha_{cl} + \alpha_k \tag{4}$$

e da questa relazione si può ricavare α_k e quindi k

$$\alpha_k = \alpha_{sp} - \alpha_{cl} = k\,\frac{2\pi^2}{\varrho V^3} f^2 . \tag{5}$$

(9) H. O. Kneser: *Ann. der Phys.*, **32**, 277 (1938).
(10) M. Davies: *Zeits. Naturf.*, **9a**, 474 (1954).
(11) E. Fischer: *Zeits. Naturf.*, **9a**, 904 (1954).
(12) L. Tisza: *Phys. Rev.*, **61**, 531 (1942).

I valori di k per il fenolo e l'anilina sono elencati nella tabella I. Esprimendo le viscosità in termini di un'energia di attivazione, E_η e E_k rispettivamente, ponendo cioè

$$\eta = \eta_0 \exp [E_\eta/RT], \qquad k = k_0 \exp [E_k/RT]$$

con η_0 e k_0 assunte costanti, si determinano E_η e E_k. Si trova per il fenolo $E_\eta = 5.5$ Kcal/mole, $E_k = 2.7$ Kcal/mole e per l'anilina $E_\eta = 4.6$ Kcal/mole, $E_k = 2.8$ Kcal/mole.

4. – Miscele.

I valori sperimentali e classici di α/f^2 per le due miscele fenolo-acqua, anilina-cicloesano, in funzione della concentrazione molecolare del primo componente, sono riportati nella tabella II e nelle figg. 3, 4, 5. Le misure sono state eseguite alla temperatura di 70 °C per il primo sistema e di 35 °C, 50 °C e 65 °C per il secondo sistema, in ogni caso quindi a temperature superiori a quella critica di solubilità.

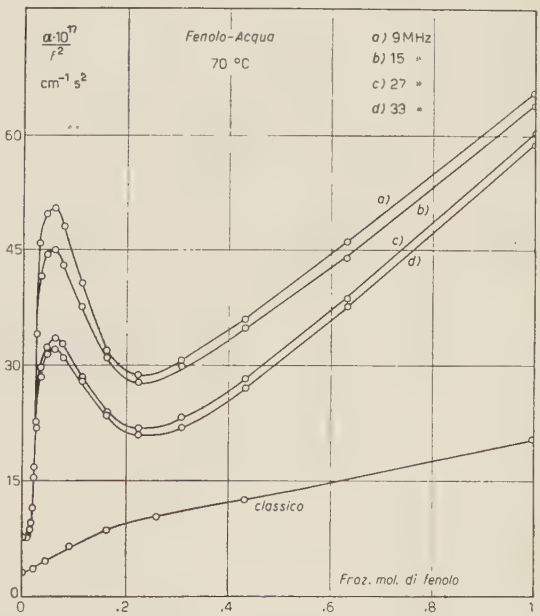

Fig. 3. – Parametro α/f^2 per la miscela fenolo-acqua, in funzione della frazione molecolare di fenolo. Temperatura 70 °C, frequenze ultrasonore 9, 15, 27 e 33 MHz.

Le curve di fig. 3, relative al sistema fenolo-acqua, mostrano un massimo abbastanza acuto nell'assorbimento, per una concentrazione molecolare di fenolo del 6%. È interessante confrontare l'andamento dell'assorbimento in questa miscela con quello della compressibilità ([13]). Questa, per piccola concentrazione di fenolo (0.8%) diminuisce rispetto al valore che compete all'acqua pura; aumentando la concentrazione infe nolo, la compressibilità cresce rapidamente al disopra dei valori che si dovrebbero avere per una miscela ideale, indicando che nella soluzione si formano associazioni di fenolo. Nelle

([13]) M. Cevolani e S. Petralia: *Nuovo Cimento*, **1**, 705 (1955).

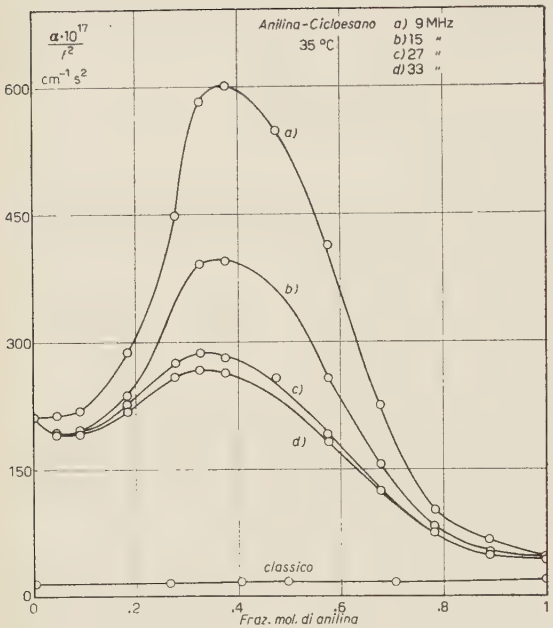

Fig. 4. – Parametro α/f^2 per la miscela anilina-cicloesano, in funzione della frazione molecolare di anilina. Temperatura 35 °C, frequenze ultrasonore 9, 15, 27 e 33 MHz.

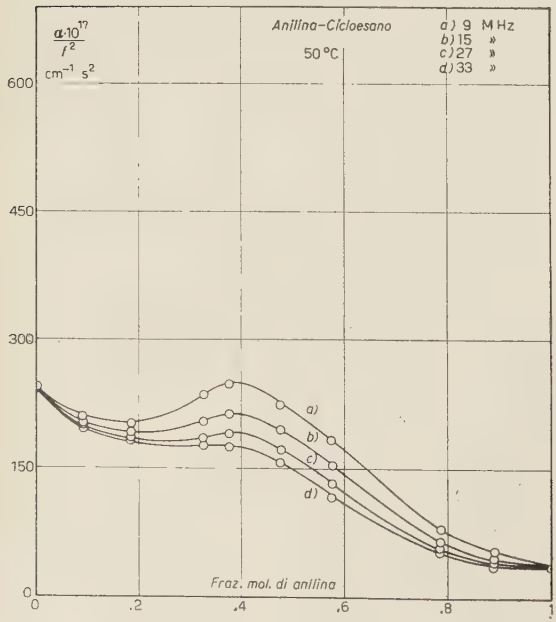

Fig. 5. – Parametro α/f^2 per la miscela anilina-cicloesano, in funzione della frazione molecolare di anilina. Temperatura 50 °C, frequenze ultrasonore 9, 15, 27 e 33 MHz.

curve di fig. 3 non si può affermare che ci sia un minimo alle piccole concentrazioni di fenolo, la nostra disposizione non permettendo di apprezzare, con errore inferiore al 5 %, le variazioni nell'assorbimento, e il minimo che può risultare nei valori tabulati in II, rientra probabilmente negli errori di misura. Il massimo pronunciato, che si nota successivamente, cade a quella concentrazione in fenolo per cui risulta massima la derivata della compressibilità rispetto alla concentrazione stessa. Al di là del massimo l'assorbimento cresce pressocchè linearmente col crescere del contenuto in fenolo della miscela. Dalle curve di fig. 8, dove, per una concentrazione di fenolo uguale a quella critica, sono riportati i valori di α/f^2, per le diverse frequenze, in funzione della temperatura, si può dedurre che l'assorbimento diminuisce rapidamente col crescere della temperatura.

Nelle curve di figg. 4 e 5, riferentesi alla miscela anilina-cicloesano, si nota una diminuzione iniziale dell'assorbi-

mento nel mezzo disperdente cicloesano per effetto dell'anilina, azione ben nota che le impurità esercitano sull'assorbimento molecolare dei fluidi. Tale azione è più rilevante alla temperatura superiore di 50 °C, ove si estende per un più ampio intervallo di concentrazioni in anilina. Col crescere della quantità di anilina subentra un nuovo processo di assorbimento, che dà origine a un largo massimo, la cui altezza decresce notevolmente passando dalla temperatura di 35 °C a 50 °C e tende a scomparire a 65 °C (fig. 6). I valori massimi di α/f^2, per le due temperature di 35 °C e 50 °C, sono riportati in funzione della frequenza in fig. 7: essi vanno attenuandosi col crescere della frequenza ultrasonora e della temperatura. Per questa miscela la curva di compressibilità, da noi precedentemente costruita, procede quasi monotona a tutte le concentrazioni.

Il comportamento delle miscele, per quanto riguarda l'assorbimento ultrasonoro, può quindi far pensare all'esistenza di processi di associazione, o comunque strutturali, in esse.

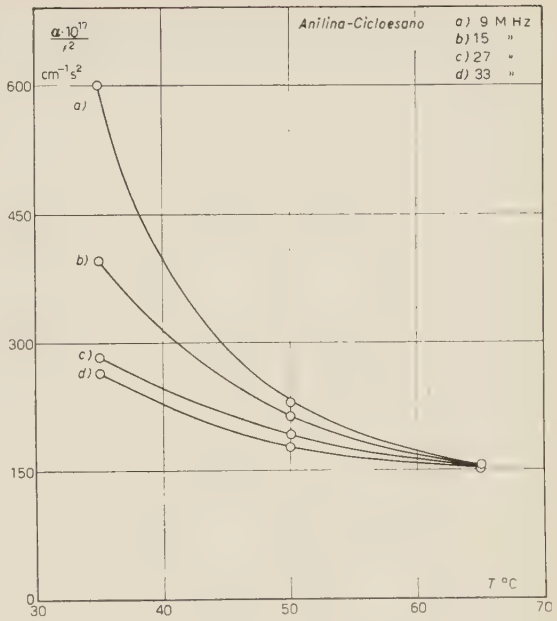

Fig. 6. – Valori massimi di α/f^2 per la miscela anilina-cicloesano a diverse frequenze ultrasonore, in funzione della temperatura.

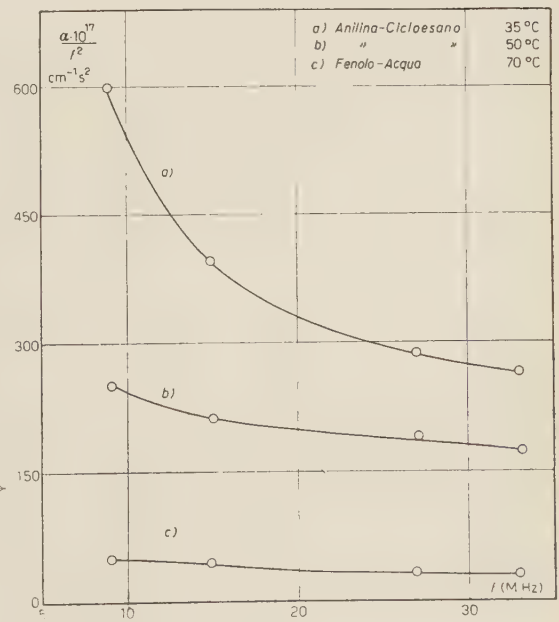

Fig. 7. – Valori massimi di α/f^2 per la miscela fenolo-acqua a 70 °C e per la miscela anilina-cicloesano a 35 °C e a 50 °C, in funzione della frequenza.

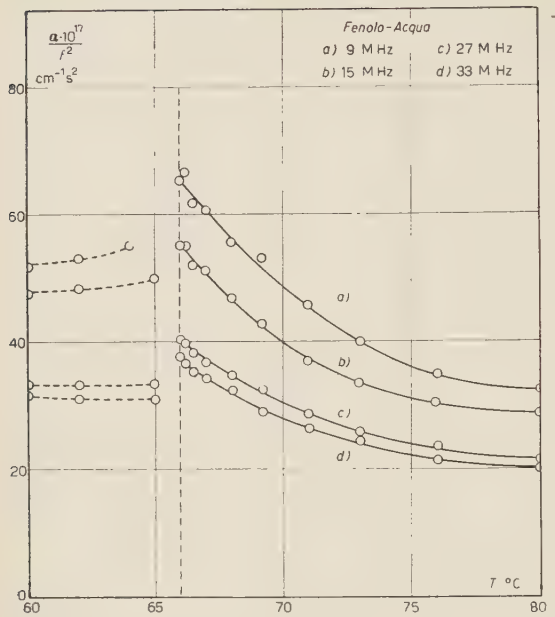

← Fig. 8. – Valori del parametro α/f^2 per la miscela fenolo-acqua, in funzione della temperatura. Concentrazione in fenolo 9% molecolare. Temperatura critica di soluzione 66 °C.

5. – Fenomeni al punto critico.

Nelle figg. 8 e 9 sono riportati i valori di α_{sp}/f^2 per le due miscele, in funzione della temperatura attorno al valore critico t_c. Come concentrazione critica si è presa, per il sistema fenolo-acqua 9.0% molecolare di fenolo e per l'altro sistema 6.47% di anilina.

Alle temperature inferiori a quella critica le misure sono state fatte nella regione ove il liquido è più denso (fenolo contenente acqua e anilina arricchita di cicloesano). Per il sistema fenolo-acqua non è stato possibile eseguire le misure per la parte della curva di assorbimento, che si svolge al disotto di t_c. Per temperature molto prossime a t_c, anche in fase omogenea, i valori osservati per il coefficiente d'assorbimento α scartano talvolta notevolmente gli uni dagli altri, forse a causa di piccole varia-

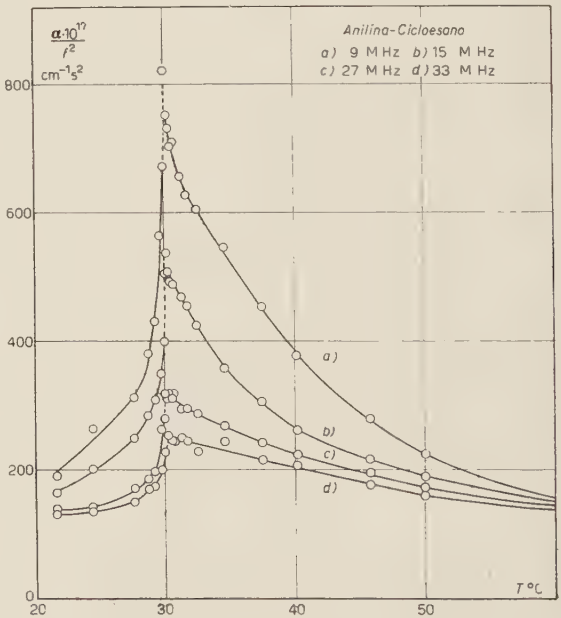

→ Fig. 9. – Valori del parametro α/f^2 per la miscela anilina-cicloesano, in funzione della temperatura. Concentrazione in anilina 47,6% molecolare. Temperatura critica di soluzione 30 °C.

(14) R. S. Krishnan: *Proc. Ind. Ac. Scien.*, **2**, 221 (1935).

zioni di temperatura, essendo il sistema molto sensibile a queste: i punti segnati nelle figg. 8 e 9 sono valori medi delle determinazioni ritenute più attendibili. Le curve di assorbimento sono caratterizzate da un massimo, che sale rapidamente per valori della temperatura inferiori a t_c, che è tanto più accentuato quanto più bassa è la frequenza, e che si estende per vari gradi al di sopra di t_c, cioè nella fase omogenea. Ciò costituisce un segno del persistere in questa fase dei processi, che determinano l'assorbimento anomalo al punto critico (d'accordo d'altronde con le osservazioni di R. S. KRISHNAN [14] in luce diffusa).

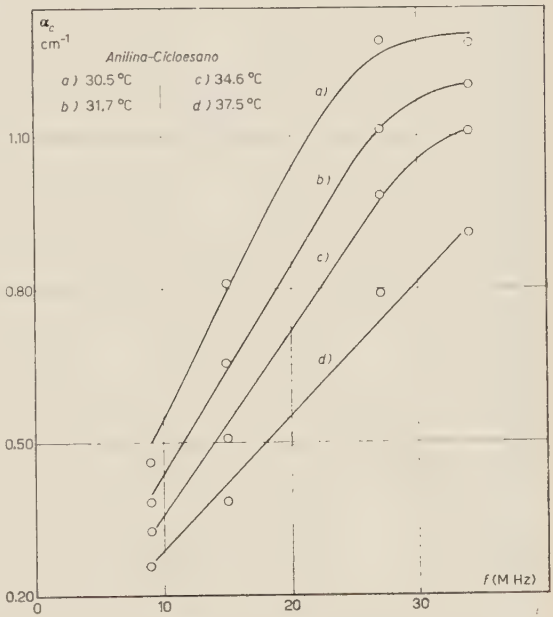

Fig. 10. - Coefficiente d'assorbimento critico della miscela anilina-cicloesano, a diverse temperature superiori a quella critica di soluzione, in funzione della frequenza ultrasonora.

Tali processi potrebbero essere:

1) una diffusione del fascio ultrasonoro negli aggregati molecolari, che si ensa esistano nella massa liquida al punto critico;

2) un accrescimento della viscosità della miscela nella regione critica, e fluttuazioni di densità nel sistema;

3) alterazioni dell'equilibrio tra stati delle configurazioni molecolari, con tempi di rilassamento finiti, causate dal passaggio dell'onda sonora.

Sembra molto improbabile che i processi elencati nei nn. 1) e 2) contribuiscano in modo apprezzabile all'attenuazione osservata. La cosa è stata discussa in via teorica e su base sperimentale da vari Autori. Gli aggregati molecolari devono avere dimensioni dell'ordine della lunghezza d'onda della luce visibile, circa un centinaio di volte più piccole della più corta lunghezza d'onda ultrasonora qui impiegata; essi partecipano quasi certamente ai moti dell'onda sonora e la diffusione da parte di essi non deve risultare importante; inoltre la dipendenza dell'assorbimento misurato dalla frequenza non risponde alla legge di assorbimento per diffusione (fig. 7). La viscosità di una miscela, del tipo che qui ci interessa, assumerebbe secondo W. OSTWALD [15], in vici-

[15] W. OSTWALD: *Trans. Farad. Soc.*, **29**, 1002 (1933).

nanza del punto critico, valori elevati: in corrispondenza l'assorbimento di tipo classico dovrebbe crescere. Secondo altri Autori [16,17] però, l'andamento della viscosità al punto critico sarebbe del tutto o quasi regolare. In una misura fatta da noi sul sistema anilina-cicloesano a concentrazione critica e temperatura di 30.6 °C, cioè di qualche decimo di grado superiore a t_c, abbiamo ottenuto un valore della viscosità che altera il rapporto αf^2, classicamente calcolato, di qualche unità di 10^{-17}: risulta infatti $\alpha/f^2 = 20 \cdot 10^{-17}$ cm^{-1} s^2. R. Lucas [1] ha considerato anche l'assorbimento per viscosità in un liquido presentante fluttuazioni di densità. Egli trova che il coefficiente di assorbimento è composto di tre termini, di cui uno è quello di Stokes e gli altri due derivano dal supporre nel liquido regioni di densità locale ϱ diversa dalla densità media ϱ_0. Essi sono termini di correzione, e lo stesso Lucas pensa che il loro contributo all'assorbimento totale non sia rilevante. Ciò risulta anche da calcoli semplici che si possono fare, almeno se ci si preoccupa dell'ordine di grandezza. Così pure A. Odajima [18] e Schneider [3] ritengono che l'attenuazione dovuta alla viscosità e alla diffusione sia di secondaria importanza.

Pertanto l'elevato assorbimento, che si constata al punto critico delle miscele qui studiate, va attribuito al rilassamento che si ha nelle alterazioni strutturali e di configurazione del liquido che accompagnano il passaggio dell'onda sonora. Anzi, data la complessità degli sciami molecolari presenti, si dovrà avere più di un tempo di rilassamento, e qualcuno di essi potrà risultare dell'ordine del periodo dell'onda sonora. Probabilmente tale rilassamento implicherà e una compressibilità funzione della frequenza (processi di Hall [5]) e un calore specifico dipendente dalla frequenza (processi di L. R. O. Storey [19]).

Può essere utile, seguendo Schneider, di separare il coefficiente di assorbimento misurato in vicinanza del punto critico α_{sp} in due termini α_s e α_c, porre cioè

$$\alpha_{sp} = \alpha_s + \alpha_c \,. \tag{7}$$

Qui α_s sarebbe il coefficiente di assorbimento delle miscele lontano da t_c, dove le curve delle figg. 8 e 9 assumono andamento asintotico, e rappresenta quindi l'assorbimento caratteristico delle miscele per quella data concentrazione e temperatura, comprendente l'assorbimento classico ed altri tipi di assorbimento, probabilmente di origine strutturale. È certo che il fenolo in soluzione tende ad associarsi, più o meno a seconda del solvente, come risulta da ricerche spettroscopiche [20], di carattere elettrico [21] e da misure di assorbimento [22]

[16] H. Schlegel: *Journ. Chim. Phys.*, **31**, 668 (1934).
[17] D. G. Dervichian e R. S. Titchen: *Compt. Rend.*, **230**, 1165 (1950).
[18] A. Odajima: *Res. Inst. Appl. Electr.*, **4**, 125 (1954).
[19] L. R. O. Storey: *Proc. Phys. Soc.*, **65** B, 943 (1952).
[20] R. Mecke: *Discussion Farad. Soc.*, **9**, 161 (1950).
[21] R. Mecke, A. Reuter and L. Schupp: *Zeits. Naturf.*, **4**a, 182 (1949).
[22] W. Maier e A. Mez: *Zeits. Naturf.*, **10**a, 166 (1955).

e di velocità di ultrasuoni ([13]). Allo scopo di vedere se, anche nelle miscele contenenti anilina, possono aver luogo processi dello stesso tipo, stiamo attualmente eseguendo misure di assorbimento ultrasonoro sopra soluzioni di anilina in tetracloruro di carbonio. Per le miscele qui studiate, si può aggiungere che esse hanno un calore specifico che non è funzione lineare della concentrazione, e un calore di mescolamento finito (negativo ([16,23])). Il termine α_c si riferisce ai processi che intervengono nello stato critico; esso sarà esprimibile in funzione della frequenza con una relazione analoga alla (2).

Data la larghezza dei massimi di figg. 8 e 9, il meccanismo di assorbimento, espresso dal coefficiente α_c, deve intervenire a determinare l'assorbimento che abbiamo misurato nel sistema fenolo-acqua a 70 °C e nel sistema anilina-cicloesano, certamente almeno alla temperatura di 35 °C. Il massimo, che si nota nelle curve che danno il rapporto αf^2 in funzione di c (figg. 3, 4), potrebbe quindi essere determinato dal persistere, alla temperatura di misura, delle condizioni strutturali della miscela che si hanno al punto critico. Tale massimo è tutto compreso nella regione piana della curva di solubilità per il sistema fenolo-acqua, quale è riportata nelle I.C.T. (1928); risulta un poco spostato rispetto alla porzione piatta della curva di solubilità del sistema anilina-cicloesano, costruita da R. W. Rowden e O. K. Rice ([24]), ma ciò può essere determinato da impurità presenti nei prodotti da noi adoperati.

L'andamento di α_c in funzione della frequenza è rappresentato dalle curve di fig. 10 per la miscela anilina-cicloesano: ogni curva si riferisce a una data temperatura al di sopra di t_c. Si vede che, tenendo conto degli errori di misura, α_c cresce linearmente per un buon intervallo di frequenze. Per il sistema fenolo-acqua tale variazione lineare di α_c con la frequenza non è senz'altro evidente; si può piuttosto notare una dipendenza quadratica.

La variazione lineare di α_c con la frequenza per il sistema anilina-cicloesano, si può porre in relazione con la (2), valevole per una transizione tra due stati caratterizzati da una frequenza di rilassamento f_m. Se è $f_m \gg f$, α_c secondo la (2) risulta funzione quadratica di f; se $f_m \ll f$, α_c si può considerare indipendente dalla frequenza. Nel punto di flesso della curva rappresentativa della (2), α_c varierà linearmente con f e ivi risulta f_m dello stesso ordine di grandezza di f. Poichè, nella fig. 10, il tratto rettilineo di tale curva risulta piuttosto lungo, si deve concludere che più meccanismi di rilassamento intervengono, come avevamo sopra predetto, con frequenze di rilassamento, che cadono nell'ambito delle frequenze ultrasonore da noi esplorato. Si può ancora osservare che, secondo la curva di fig. 10 costruita con le misure fatte alla temperatura di 30.5 °C, di poco superiore a t_c, α_c tende a divenire indipendente dalla frequenza

([23]) J. B. Ferguson: *Journ. Phys. Chem.*, **31**, 757 (1927).
([24]) R. W. Rowden e O. K. Rice: *Changements de Phases* (Paris, 1952).

per valori di questa superiori a 27 MHz. Una tendenza a procedere in modo analogo mostrano anche le curve costruite per le temperature di 31.7 °C e 34.6 °C; ciò non appare invece nella curva relativa alla temperatura di 37.5 °C, già lontana da t_c. Da qui si può dedurre che, coll'avvicinarsi alle condizioni critiche, i tempi di rilassamento τ vanno aumentando. Questo è d'accordo con quanto si ricava da un'espressione trovata da ODAJIMA [18], la quale dà la dipendenza di τ dalla temperatura assoluta T:

$$\tau = h \frac{T_c}{T - T_c} \frac{\exp [W/kT]}{\alpha_0}, \tag{8}$$

ed è d'accordo con quanto si può prevedere sul comportamento dei granuli molecolari al punto critico.

SUMMARY (*)

By the pulse method the absorption coefficient for ultrasonics of frequency between 9 and 33 MHz has been measured in molten phenol, aniline, cyclohexane, in the mixtures phenol-water and phenol-cyclohexane at different concentrations of the components and at temperatures above the critical solubility temperature; also the absorption in these mixtures in critical conditions has been measured. In phenol and aniline the absorption diminishes with increasing temperature, so as it happens with their viscosity absorption and therefore the excess of absorption as compared to the classical value ought to be ascribed to structural reasons; in cyclohexane the absorption increases with increasing temperature. The mixtures show an absorption maximum for the concentrations at which the corresponding solubility curve has a flat region; this maximum diminishes with increasing temperature and does not depend quadratically from the ultrasonic frequency. At the critical point there is a considerable absorption which is interpreted as due to relaxing processes with different frequencies; in the case of the mixture aniline-cyclohexane we show that the relaxing frequencies fall in the field of frequencies explored in this work.

(*) *Editor's translation.*

Un'analogia fra l'elettrodinamica quantistica e l'elettrodinamica classica della descrizione corpuscolare.

A. Loinger

Istituto di Fisica dell'Università - Pavia

(ricevuto il 6 Luglio 1955)

Riassunto. — Si dimostra che per un elettrone (puntiforme) non relativistico, interagente col campo elettromagnetico e soggetto a forze esterne, l'operatore posizione della particella obbedisce ad una equazione formalmente analoga all'equazione classica di Dirac-Lorentz.

1. – È stato dimostrato da Morpurgo [1] che, *nell'approssimazione di dipolo*, esiste una stretta corrispondenza tra l'elettrodinamica classica e quella quantistica di un elettrone non relativistico, nel senso che l'equazione classica del terzo ordine di Dirac-Lorentz è valida anche pei valori di aspettazione dei corrispondenti termini quantistici.

Mostreremo in questa nota come, per un elettrone puntiforme, tale risultato sia di validità affatto generale, cioè non ristretta all'approssimazione di dipolo; e precisamente faremo vedere come per un elettrone (puntiforme) non relativistico, soggetto a forze esterne ed interagente col campo elettromagnetico, sia possibile: *a*) scrivere delle equazioni di moto esatte della descrizione di Heisenberg, in cui figura la massa sperimentale; *b*) eliminare da tali equazioni i gradi di libertà del campo elettromagnetico e dimostrare che l'operatore posizione della particella obbedisce ad un'equazione formalmente analoga all'equazione classica di Dirac-Lorentz.

Esporremo infine, nel § 3, i motivi che non consentono una estensione covariante di questi risultati.

2. – L'operatore hamiltoniano del nostro problema è dato, supposto che i potenziali del campo elettromagnetico della particella obbediscano al « gauge »

[1] G. Morpurgo: *Nuovo Cimento*, **9**, 808 (1952).

coulombiano, dalla seguente espressione:

$$H = \frac{1}{2m_0}\left\{\boldsymbol{p} - \frac{e}{c}\boldsymbol{A}(\boldsymbol{z}, t) - \frac{e}{c}\boldsymbol{A}_{\text{est}}(\boldsymbol{z}, t)\right\}^2 + e\Phi_{\text{est}}(\boldsymbol{z}, t) + \\ + \frac{1}{8\pi}\int \mathrm{d}_3\boldsymbol{x}\left\{\frac{1}{c^2}\left(\frac{\partial \boldsymbol{A}(\boldsymbol{x}, t)}{\partial t}\right)^2 - (\nabla \wedge \boldsymbol{A}(\boldsymbol{x}, t))^2\right\} ;$$

in essa: m_0, $\boldsymbol{z} \equiv (z_1, z_2, z_3)$ e $\boldsymbol{p}$ rappresentano rispettivamente la massa « meccanica », la posizione e la quantità di moto totale dell'elettrone; $\boldsymbol{A}_{\text{est}}$, Φ_{est} sono i potenziali e.m. del campo esterno; $\boldsymbol{A}(\boldsymbol{x}, t)$ il potenziale vettore del campo e.m. dipendente dal moto dell'elettrone (nella generica posizione $\boldsymbol{x}$, all'istante t), soddisfacente alla condizione (« gauge » coulombiano):

$$\nabla \cdot \boldsymbol{A}(\boldsymbol{x}, t) = 0 .$$

Teniamo conto di tale condizione assumendo delle parentesi di Poisson quantistiche (≡ commutatori divisi per ih) per $\boldsymbol{A}$ ed $\dot{\boldsymbol{A}}$ uguali a:

$$[A_j(\boldsymbol{x}, t), \dot{A}_k(\boldsymbol{x}', t)] = 4\pi c^2 \delta_{jk}\delta(\boldsymbol{x} - \boldsymbol{x}') - \frac{c^2\partial^2}{\partial x_j \partial x'_k}\frac{1}{\boldsymbol{x} - \boldsymbol{x}'} .$$

Useremo costantemente la descrizione del moto di Heisenberg; pertanto tutte le nostre equazioni saranno valide anche classicamente, ove eventualmente si interpreti il simbolo [..., ...] come parentesi di Poisson classica.

Procedendo con metodi ben noti, si può facilmente rendersi conto che le equazioni di moto del sistema si scrivono:

$$(1)\quad \begin{cases} \Box \boldsymbol{A}(\boldsymbol{x}, t) = -\dfrac{2\pi e}{c}\,\mathrm{Tr}\,\{\dot{\boldsymbol{z}}(t)\,\delta(\boldsymbol{x} - \boldsymbol{z}(t)) + \delta(\boldsymbol{x} - \boldsymbol{z}(t))\dot{\boldsymbol{z}}(t)\} ; \\ m_0\ddot{\boldsymbol{z}} = -\dfrac{e}{c}\dfrac{\partial}{\partial t}\boldsymbol{A}(\boldsymbol{z}, t) + \dfrac{e}{2c}\{\dot{\boldsymbol{z}} \wedge \nabla \wedge \boldsymbol{A}(\boldsymbol{z}, t) - \nabla \wedge \boldsymbol{A}(\boldsymbol{z}, t) \wedge \dot{\boldsymbol{z}}\} + \\ \qquad + e\boldsymbol{E}_{\text{est}}(\boldsymbol{z}, t) + \dfrac{e}{2c}\{\dot{\boldsymbol{z}} \wedge \boldsymbol{B}_{\text{est}}(\boldsymbol{z}, t) - \boldsymbol{B}_{\text{est}}(\boldsymbol{z}, t) \wedge \dot{\boldsymbol{z}}\} ; \end{cases}$$

ove Tr {...} sta ad indicare la parte trasversale (o solenoidale) del vettore {...} (²), ed $\boldsymbol{E}_{\text{est}}$, $\boldsymbol{B}_{\text{est}}$ è il campo e.m. esterno.

(²) Si osservi che:

$$\mathrm{Tr}[\boldsymbol{c}f(\boldsymbol{x})] = \boldsymbol{c}f(\boldsymbol{x}) - (\boldsymbol{c} \cdot \nabla)\nabla\varphi(\boldsymbol{x}); \qquad \nabla^2\varphi(\boldsymbol{x}) = f(\boldsymbol{x}) .$$

Poniamo ora [3]:

$$\boldsymbol{A} = \boldsymbol{A}_0 + \boldsymbol{A}_1 \; ; \tag{2}$$

ove $\boldsymbol{A}_0$ soddisfa alle equazioni:

$$\left\{ \begin{array}{l} \nabla^2 \boldsymbol{A}_0(\boldsymbol{x}, t) = -\dfrac{2\pi e}{c} \operatorname{Tr} \{\boldsymbol{z}(t)\, \delta(\boldsymbol{x} - \boldsymbol{z}(t)) + \text{con. herm.}\} = \\ \quad = -\dfrac{2\pi e}{c} \left\{ \dot{\boldsymbol{z}}(t)\, \delta(\boldsymbol{x} - \boldsymbol{z}(t)) + \dfrac{1}{4\pi} (\dot{\boldsymbol{z}}(t) \cdot \nabla) \nabla \dfrac{1}{|\boldsymbol{x} - \boldsymbol{z}(t)|} + \text{con. herm.} \right\} ; \\ \nabla \cdot \boldsymbol{A}_0(\boldsymbol{x}, t) = 0 ; \end{array} \right. \tag{3}$$

ossia $\boldsymbol{A}_0$ fornisce (nell'approssimazione non relativistica) il potenziale vettore (a divergenza nulla) di quell'elettrone che si muove di moto rettilineo ed uniforme e che all'istante t ha la stessa posizione e la stessa velocità dell'elettrone vero. $\boldsymbol{A}_0$ è cioè un potenziale « legato » all'elettrone o da esso « trasportato », mentre $\boldsymbol{A}_1$ è, per così dire, un potenziale « esterno ».

La soluzione delle (3), come si vede senza difficoltà, è:

$$\begin{aligned} \boldsymbol{A}_0(\boldsymbol{x}, t) &= \frac{e}{2c} \operatorname{Tr} \{\dot{\boldsymbol{z}} |\boldsymbol{x} - \boldsymbol{z}|^{-1} + \text{con. herm.}\} = \\ &= \frac{e}{4c} \{\dot{\boldsymbol{z}} |\boldsymbol{x} - \boldsymbol{z}|^{-1} + [\dot{\boldsymbol{z}} \cdot (\boldsymbol{x} - \boldsymbol{z})] |\boldsymbol{x} - \boldsymbol{z}|^{-3} (\boldsymbol{x} - \boldsymbol{z}) + \text{con. herm.}\} ; \end{aligned} \tag{4}$$

la valutazione di $\boldsymbol{A}_0(\boldsymbol{z}, t)$ si può fare in maniera analoga a quella seguita nell'elettrodinamica classica del modello puntiforme; si ottiene (v. appendice I):

$$\frac{e}{c} \boldsymbol{A}_0(\boldsymbol{z}, t) = \frac{4}{3} \frac{W_0}{c^2} \dot{\boldsymbol{z}}(t) = \mu \dot{\boldsymbol{z}}(t) \; ; \tag{5}$$

ove $W_0 = \lim\limits_{\boldsymbol{x} \to \boldsymbol{z}'} \dfrac{e^2}{2} \dfrac{1}{|\boldsymbol{x} - \boldsymbol{z}'|}$ $(= +\infty)$ è l'energia del campo coulombiano della particella e $\mu = (4/3)(W_0/c^2)$ è la massa elettromagnetica di essa.

[3] Tale scomposizione è stata introdotta, nell'elettrodinamica classica, da KRAMERS (*Rep. Solvay Conference* 1948 (Bruxelles 1950), p. 241; *Hand- und Jahrbuch d. Chem. Physik* (Leipzig, 1938), voll. 1-2, §§ 89, 90; v. anche N. G. VAN KAMPEN: *Dan. Mat. Fys. Medd.*, **26**, n. 15 (1951)).

Le equazioni (13), (14) del lavoro di Kramers sono esattamente le corrispondenti classiche, per un elettrone puntiforme, delle nostre (6).

Tenendo conto di (2), (4), le (1) forniscono (v. appendice II):

$$(6)\qquad \begin{cases} \Box\, \boldsymbol{A}_1(\boldsymbol{x}, t) = \dfrac{e}{2c^3}\,\mathrm{Tr}\,\dfrac{\partial^2}{\partial t^2}\,\{\dot{\boldsymbol{z}}(t)\,|\,\boldsymbol{x} - \boldsymbol{z}(t)\,|^{-1} + \text{con. herm.}\}\ ; \\ m\ddot{\boldsymbol{z}} = -\dfrac{e}{c}\dfrac{\partial}{\partial t}\boldsymbol{A}_1(\boldsymbol{z}, t) + \dfrac{e}{2c}\,\{\dot{\boldsymbol{z}}\ \wedge\nabla\wedge\boldsymbol{A}_1(\boldsymbol{z}, t) + \text{con. herm.}\} + \\ \qquad\qquad + e\boldsymbol{E}_{\text{est}}(\boldsymbol{z}, t) + \dfrac{e}{2c}\,\{\dot{\boldsymbol{z}}\wedge\boldsymbol{B}_{\text{est}}(\boldsymbol{z}, t) + \text{con. herm.}\}\ ; \end{cases}$$

ove si è posto $m_0 + \mu = m$, massa sperimentale.

Abbiamo così ottenuto delle equazioni di moto del sistema elettrone — campo e.m., nella descrizione di Heisenberg, in cui figura la massa sperimentale m e non la fittizia m_0.

Osserviamo ora che, di solito, interessa studiare il moto dell'elettrone (ci vogliamo sempre riferire, naturalmente, alla descrizione di Heisenberg) nello spazio libero sotto l'azione delle forze esterne, e quindi $\boldsymbol{A}(\boldsymbol{x}, t) = \boldsymbol{A}_{\text{rit}}(\boldsymbol{x}, t)$ (potenziale ritardato). Di conseguenza, avremo (v. appendice III):

$$(7)\qquad \boldsymbol{A}(\boldsymbol{x}, t) = \frac{e}{2c}\,\mathrm{Tr}\,\{\dot{\boldsymbol{z}}\,|\,\boldsymbol{x} - \boldsymbol{z}\,|^{-1} + \text{con. herm.} - \frac{2}{c}\,\ddot{\boldsymbol{z}} + \ldots\} =$$

$$= \boldsymbol{A}_0(\boldsymbol{x}, t) - \frac{2}{3}\frac{e}{c^2}\,\ddot{\boldsymbol{z}} + \ldots;$$

ossia:

$$\boldsymbol{A}_1(\boldsymbol{x}, t) = -\frac{2}{3}\frac{e}{c^2}\,\ddot{\boldsymbol{z}} + \ldots;$$

sostituendo nella seconda delle (6) avremo:

$$(8)\qquad m = \ddot{\boldsymbol{z}}\,\frac{2}{3}\frac{e^2}{c^3}\,\dddot{\boldsymbol{z}} + \ldots + e\boldsymbol{E}_{\text{est}}(\boldsymbol{z}, t) + \frac{e}{2c}\,\{\boldsymbol{z}\wedge\boldsymbol{B}_{\text{est}}(\boldsymbol{z}, t) + \text{con. herm.}\}\ .$$

Ora, è ben noto dell'elettrodinamica *classica* [4] che i termini più elevati dello sviluppo del potenziale (i corrispondenti classici dei termini indicati in (7) coi puntini) dipendono dal raggio vettore $\boldsymbol{x} - \boldsymbol{z}$, che va da $\boldsymbol{z}$, posizione della particella, al punto $\boldsymbol{x}$ del campo, in maniera tale che, se nel calcolo della forza esercitata dalla carica su se stessa, prima di fare il limite $\boldsymbol{x} \to \boldsymbol{z}$, si media su tutte le direzioni, essi danno un contributo *nullo*.

[4] V. per es. L. Landau and E. Lifshitz: *The Classical Theory of Fields* (Cambridge, Mass., 1951), p. 221.

Una proprietà analoga vale, come è chiaro dal nostro procedimento, anche nella teoria *quantistica*; quindi la (8) si può scrivere semplicemente:

$$(9) \qquad m\ddot{\boldsymbol{z}} = \frac{2}{3}\frac{e^2}{c^3}\dddot{\boldsymbol{z}} + e\boldsymbol{E}_{\text{est}}(\boldsymbol{z}, t) + \frac{e}{2c}\{\dot{\boldsymbol{z}} \wedge \boldsymbol{B}_{\text{est}}(\boldsymbol{z}, t) + \text{con. herm.}\} ;$$

ossia: *l'operatore* $\boldsymbol{z}$, *posizione della particella, soddisfa alla equazione* (*non relativistica*) *di Dirac-Lorentz.*

Prendendo nella (9) i valori di aspettazione, se

$$\boldsymbol{E}_{\text{est}}(\boldsymbol{z}, t) = f(t)\boldsymbol{z}; \qquad \boldsymbol{B}_{\text{est}}(\boldsymbol{z}, t) = \boldsymbol{\varphi}(t);$$

(in particolare: per una particella libera, per una particella sottoposta a campi uniformi, per una particella sottoposta a una forza di richiamo) si ha che il baricentro del pacchetto di probabilità si muove secondo le leggi classiche. *In questi casi la nota difficoltà classica delle « runaway solutions » si ripresenta evidentemente immutata nella teoria quantistica.*

3. – Vogliamo infine discutere sommariamente la questione di un'eventuale estensione relativistica delle (6) e della (9).

Osserviamo che, volendo tentare una generalizzazione covariante del metodo precedentemente seguito, dovremmo procurarci un hamiltoniano invariante, il quale consenta inoltre una descrizione di Heisenberg avente come parametro « di evoluzione » un qualcosa di analogo al tempo proprio della particella. A prima vista si potrebbe ritenere lecito utilizzare pel nostro scopo un « hamiltoniano » $\mathcal{G}_{m_0}$ suggerito dalla teoria di Dirac-Fock-Podolsky [5]:

$$\mathcal{G}_{m_0} = c\gamma_\mu\left\{p^\mu - \frac{e}{c}\mathcal{A}^\mu(z) - \frac{e}{c}\mathcal{A}^\mu_{\text{est}}(z)\right\} - m_0c^2; \qquad (\mu = 0, \ldots 3)$$

ove $z \equiv (\boldsymbol{z}, z_0)$ e γ_μ e $\mathcal{A}_\mu$ soddisfano alle:

$$\gamma_\mu\gamma_\nu + \gamma_\nu\gamma_\mu = 2g_{\mu\nu} ;$$

$$[\mathcal{A}_\mu(x), \mathcal{A}_\nu(x')] = cg_{\mu\nu}D(x - x'); \qquad (x \equiv (\boldsymbol{x}, x_0))$$

$$(g_{\mu\nu} = 0, \ \mu \neq \nu; \qquad g_{00} = -g_{11} = -g_{22} = -g_{33} = 1) .$$

[5] V. per es. P. A. M. Dirac: *The Principles of Quantum Mechanics,* Second Edition (Oxford, 1935), p. 286 e segg.

La versione successiva data da Dirac (v. per es. *The Principles of Quantum Mechanics*, Third Edition (Oxford, 1947), p. 289 e segg.) della « many-time theory » — versione in cui figura la massa sperimentale e nella quale si fa uso essenziale del « λ-limiting process » — costituisce, come ognuno sa, una teoria insoddisfacente.

Ma è immediato rendersi conto che $\mathcal{G}_{m_0}$ *non* è un operatore hermitiano e pertanto non può essere assunto come hamiltoniano covariante dell'elettrodinamica di una particella.

Ed inoltre: una scomposizione covariante di $\mathcal{A}_\mu$, *fisicamente analoga alla* (2), non può condurre ad una espressione del tipo (5), e quindi ad una rinormalizzazione della massa, perchè la quantità di moto elettromagnetica della particella non è un quadrivettore.

In conclusione, sembra giustificato affermare che *le* (6) *e la* (9) *rappresentano il punto più avanzato al quale giunge l'analogia fra l'elettrodinamica quantistica e l'elettrodinamica classica della descrizione corpuscolare.*

Ringrazio vivamente il prof. G. Morpurgo per un'utile discussione.

Appendice I.

Dimostrazione della (5).

Prendiamo una rappresentazione in cui $\boldsymbol{z}(t)$ sia diagonale. Dalla (4) avremo:

$$\langle \boldsymbol{z}' | \boldsymbol{A}_0(\boldsymbol{x}, t) | \boldsymbol{z}'' \rangle = \frac{e}{4c} \{ \langle \boldsymbol{z}' | \dot{\boldsymbol{z}} | \boldsymbol{x} - \boldsymbol{z}'' |^{-1} | \boldsymbol{z}'' \rangle + \langle \boldsymbol{z}' | [\dot{\boldsymbol{z}} \cdot (\boldsymbol{x} - \boldsymbol{z}'')] | \boldsymbol{x} - \boldsymbol{z}'' |^{-3} (\boldsymbol{x} - \boldsymbol{z}'') | \boldsymbol{z}'' \rangle +$$

$$+ \langle \boldsymbol{z}' | \boldsymbol{x} - \boldsymbol{z}' |^{-1} \dot{\boldsymbol{z}} | \boldsymbol{z}'' \rangle + \langle \boldsymbol{z}' | (\boldsymbol{x} - \boldsymbol{z}') | \boldsymbol{x} - \boldsymbol{z}' |^{-3} [(\boldsymbol{x} - \boldsymbol{z}') \cdot \dot{\boldsymbol{z}}] | \boldsymbol{z}'' \rangle \} ;$$

e quindi:

$$\langle ' | \boldsymbol{A}_0(\boldsymbol{z}, t) | '' \rangle =$$

$$= \frac{e}{2c} \lim_{x \to z'} \{ \langle ' | \dot{\boldsymbol{z}} | '' \rangle | \boldsymbol{x} - \boldsymbol{z}' |^{-1} + [\langle ' | \dot{\boldsymbol{z}} | '' \rangle \cdot (\boldsymbol{x} - \boldsymbol{z}')] | \boldsymbol{x} - \boldsymbol{z}' |^{-3} (\boldsymbol{x} - \boldsymbol{z}') \} .$$

Se, prima di passare al limite, *mediamo su tutte le direzioni* (come è fisicamente ragionevole e corrispondentemente a quanto si suole fare nel caso classico), otterremo:

$$\langle ' | \boldsymbol{A}_0(\boldsymbol{z}, t) | '' \rangle = \frac{e}{2c} \lim_{x \to z'} \frac{4}{3} \langle ' | \dot{\boldsymbol{z}} | '' \rangle | \boldsymbol{x} - \boldsymbol{z}' |^{-1} ;$$

da cui subito la (5).

Appendice II.

Per la dimostrazione delle (6).

Calcoliamo, servendoci della (4), $-\frac{e}{c}\frac{\partial \boldsymbol{A}_0(\boldsymbol{x},t)}{\partial t}$ e $\nabla \wedge \boldsymbol{A}_0(\boldsymbol{x},t)$.

Avremo:

$$-\frac{e}{c}\frac{\partial \boldsymbol{A}_0(\boldsymbol{x},t)}{\partial t} = -\frac{e^2}{2c^2}\frac{\partial}{\partial t}\,\mathrm{Tr}\,\{\dot{\boldsymbol{z}}\,|\boldsymbol{x}-\boldsymbol{z}|^{-1} + \text{con. herm.}\} =$$

$$= -\frac{e^2}{4c^2}\{\ddot{\boldsymbol{z}}\,|\boldsymbol{x}-\boldsymbol{z}|^{-1} + [\ddot{\boldsymbol{z}}\cdot(\boldsymbol{x}-\boldsymbol{z})]\,|\boldsymbol{x}-\boldsymbol{z}|^{-3}(\boldsymbol{x}-\boldsymbol{z}) + \text{con. herm.}\} -$$

$$-\frac{e^2}{4c^2}\{-\dot{z}^2\,|\boldsymbol{x}-\boldsymbol{z}|^{-3}(\boldsymbol{x}-\boldsymbol{z}) + [\dot{\boldsymbol{z}}\cdot(\boldsymbol{x}-\boldsymbol{z})]\,\frac{3}{2}\,[\,|\boldsymbol{x}-\boldsymbol{z}|^{-5}(\boldsymbol{x}-\boldsymbol{z})\cdot\dot{\boldsymbol{z}} -$$

$$+ \text{con. herm.}]\,(\boldsymbol{x}-\boldsymbol{z}) + \tfrac{1}{2}\dot{\boldsymbol{z}}[\,|\boldsymbol{x}-\boldsymbol{z}|^{-3}(\boldsymbol{x}-\boldsymbol{z})\cdot\dot{\boldsymbol{z}} +$$

$$+ \text{con. herm.}] - [\dot{\boldsymbol{z}}\cdot(\boldsymbol{x}-\boldsymbol{z})]\,|\boldsymbol{x}-\boldsymbol{z}|^{-3}\dot{\boldsymbol{z}} + \text{con. herm.}\}\,.$$

Presi gli elementi di matrice e mediato su tutte le direzioni, la seconda parentesi a graffa fornisce un contributo nullo, mentre dalla prima consegue (cfr. app. I):

$$-\frac{e}{c}\frac{\partial \boldsymbol{A}_0(\boldsymbol{z},t)}{\partial t} = -\mu\ddot{\boldsymbol{z}}\,.$$

Il campo magnetico quasi statico è d'altra parte dato da:

$$\nabla\wedge(\boldsymbol{A}_0\,\boldsymbol{x},t) = \frac{e}{2c}\{\nabla\wedge[\dot{\boldsymbol{z}}\,|\boldsymbol{x}-\boldsymbol{z}|^{-1}] + \text{con. herm.}\} =$$

$$= \frac{e}{2c}\{\dot{\boldsymbol{z}}\wedge(\boldsymbol{x}-\boldsymbol{z})\,|\boldsymbol{x}-\boldsymbol{z}|^{-3} + \text{con. herm.}\}\,,$$

la quale espressione, presi gli elementi di matrice e mediato su tutte le direzioni, dà zero.

Appendice III.

Dimostrazione della (7).

La soluzione ritardata della prima delle (1) è:

$$\boldsymbol{A}(\boldsymbol{x},t) = \frac{e}{2c}\,\mathrm{Tr}\int\frac{\dot{\boldsymbol{z}}(T)\delta(\boldsymbol{x}'-\boldsymbol{z}(T)) + \delta(\boldsymbol{x}'-\boldsymbol{z}(T))\dot{\boldsymbol{z}}(T)}{|\boldsymbol{x}-\boldsymbol{x}'|}\,\mathrm{d}_3\boldsymbol{x}'$$

ove $T = t - \frac{|\boldsymbol{x} - \boldsymbol{x}'|}{c}$.

Sviluppando al solito modo, avremo:

$$\boldsymbol{A}(\boldsymbol{x}, t) = \frac{e}{2c} \operatorname{Tr} \left\{ \int \frac{\dot{\boldsymbol{z}}(t)\delta(\boldsymbol{x}' - \boldsymbol{z}(t)) + \text{con. herm.}}{|\boldsymbol{x} - \boldsymbol{x}'|} \, \mathrm{d}_3\boldsymbol{x}' - \right.$$

$$- \frac{1}{c} \frac{\partial}{\partial t} \int [\dot{\boldsymbol{z}}(t)\delta(\boldsymbol{x}' - \boldsymbol{z}(t)) + \text{con. herm.}] \, \mathrm{d}_3\boldsymbol{x}' + \ldots +$$

$$\left. + \frac{(-1)^n}{n!\, c^n} \frac{\partial^n}{\partial t^n} \int |\boldsymbol{x} - \boldsymbol{x}'|^{n-1} [\dot{\boldsymbol{z}}(t)\delta(\boldsymbol{x}' - \boldsymbol{z}(t)) + \text{con. herm.}] \, \mathrm{d}_3\boldsymbol{x}' + \ldots \right\}.$$

Detto $|\boldsymbol{z}'\rangle \equiv |'\rangle$ l'autovettore di $\boldsymbol{z}(t)$ appartenente all'autovalore $\boldsymbol{z}'$, sarà:

$$\int |\boldsymbol{x} - \boldsymbol{x}'|^{n-1} \dot{\boldsymbol{z}}(t)\delta(\boldsymbol{x}' - \boldsymbol{z}(t)) \, |'\rangle \, \mathrm{d}_3\boldsymbol{x}' =$$

$$= \int |\boldsymbol{x} - \boldsymbol{x}'|^{n-1} \dot{\boldsymbol{z}}(t)\delta(\boldsymbol{x}' - \boldsymbol{z}') \, |'\rangle \, \mathrm{d}_3\boldsymbol{x}' = |\boldsymbol{x} - \boldsymbol{z}'|^{n-1} \dot{\boldsymbol{z}}(t) \, |'\rangle = \dot{\boldsymbol{z}}(t) \, |\boldsymbol{x} - \boldsymbol{z}(t)|^{n-1} \, |'\rangle ;$$

pertanto:

$$\int |\boldsymbol{x} - \boldsymbol{x}'|^{n-1} \dot{\boldsymbol{z}}(t)\delta(\boldsymbol{x}' - \boldsymbol{z}(t)) \, \mathrm{d}_3\boldsymbol{x}' = \dot{\boldsymbol{z}}(t) \, |\boldsymbol{x} - \boldsymbol{z}(t)|^{n-1} ;$$

e analogamente:

$$\int |\boldsymbol{x} - \boldsymbol{x}'|^{n-1} \delta(\boldsymbol{x}' - \boldsymbol{z}(t)) \dot{\boldsymbol{z}}(t) \, \mathrm{d}_3\boldsymbol{x}' = |\boldsymbol{x} - \boldsymbol{z}(t)|^{n-1} \dot{\boldsymbol{z}}(t) ;$$

da cui subito la (7).

SUMMARY

It is shown that for a non-relativistic point-electron the position operator of the particle satisfies an equation that is formally analogous to the classical Dirac-Lorentz equation.

On the $K_{\mu 3}$- and $K_{\beta 3}$-Decay Schemes.

G. Costa and N. Dallaporta

Istituto di Fisica dell'Università - Padova
Istituto Nazionale di Fisica Nucleare - Sezione di Padova

(ricevuto il 7 Luglio 1955)

Summary. — In order to explain the three body decays of K-particles according to the reactions: $K_{\mu 3} \to \mu + \nu + \pi^0$, $K_{\beta 3} \to \beta + \nu + \pi^0$, a detailed decay scheme is proposed which seems to be the simplest possibility for obtaining for both these decays a lifetime of the same order of magnitude as the χ-decay lifetime. This scheme is based on the assumption of both the strong Gell-Mann-Pais interaction between K-particles and hyperons, and the possibility for hyperons to suffer μ- and β-decays regulated by the weak universal Fermi interaction constant.

Recent experimental work on heavy unstable mesons which decay at rest either in the metal plates of cloud chambers [1] or in big stacks of emulsion plates [2] has shown that the bulk of the so-called K-particles is essentially composed of a mixture of two well defined types of two-body decays, which disintegrate according to the schemes:

$$\chi \to \pi^{\pm} + \pi^0 + 212 \text{ MeV} \tag{1}$$

$$K_{\mu 2} \to \mu + \nu + 391 \text{ MeV} . \tag{2}$$

This important result shows that the so-called $K_{\mu 3}$ type of decay

$$K_{\mu 3} \to \mu + ? + ? \tag{3}$$

---

[1] H. S. Bridge, H. DeStaebler, B. Rossi and V. B. Sreekantan: *Nuovo Cimento*, **1**, 874 (1955); R. Armenteros, B. Gregory, A. Hendel, A. Lagarrigue, L. Leprince-Ringuet, F. Muller et C. Peyrou: *Nuovo Cimento*, **1**, 915 (1955).

[2] Report on the work of the Bristol-Dublin-Milano-Padova collaboration: Pisa Conference, to be published on *Suppl. Nuovo Cimento*.

(a μ-meson secondary plus two neutral particles) of which some very well analyzed examples [3] have been known for some time, and the more recently discovered $K_{\beta 3}$ decay [4]

$$K_{\beta 3} \to \beta + ? + ? \tag{4}$$

(one electron secondary plus two neutral particles) are relatively rare modes of decay, and that, according to some preliminary estimate, it seems very probable that their frequency of occurrence does not exceed $\sim 20\,\%$ of all the K's.

At present we have no experimental indication of what the two neutral decay products are. A first assumption was made by different authors [5] that both particles are neutrinos, so that both $K_{\mu 3}$ and $K_{\beta 3}$ should be fermions. Assuming the Fermi interaction constant for the decay reactions, one obtains in both cases very reasonable values for the mean lives. Moreover, if these two kinds of K's were fermions, and therefore interacting weakly with nucleons, we would expect that they would decay even when negative and bound in a Bohr orbit.

More recently, a second possible hypothesis has been made for the neutral decay products of $K_{\mu 3}$ [6]. If we assume the scheme:

$$K_{\mu 3} \to \mu + \nu + \pi^0 \tag{5}$$

this could be considered as an alternative mode of decay of the same particle that decays according to the reaction (1), the charged pion being converted virtually into a μ-neutrino pair. In this way, the $K_{\mu 3}$ could be also a boson, and we could be led to different decay schemes for a single particle. It is this second possibility that we would like to discuss here in some detail.

At first sight, one feels that there are very strong objections to this possibility, which seem to rule it out immediately. In fact, from a purely phenomenological point of view, whatever the true decay pattern of scheme (1) may be, we just assume that the $K_{\mu 3}$ decay is obtained as a second order process through the χ-decay as an intermediate state:

$$K_{\mu 3} \to \pi + \pi^0 \to \mu + \nu + \pi^0 .$$

---

[3] M. G. K. MENON and C. O'CEALLAIGH: *Proc. Roy. Soc.*, **221**, 292 (1954); Report of the Committee on K-particles: *Suppl. Nuovo Cimento*, **12**, 433 (1954).

[4] M. W. FRIEDLANDER, D. KEEFE and M. G. K. MENON: *Phil. Mag.*, **45**, 1043 (1954).

[5] A. M. L. MESSIAH: *Rochester report*, NYO 3036 (1951); L. MICHEL and R. STORA: *Compt. Rend.*, **234**, 1257 (1952); J. P. DAVIDSON: *Phys. Rev.*, **91**, 1020 (1953); N. DALLAPORTA: *Nuovo Cimento*, **11**, 82 (1954).

[6] B. ROSSI's *Report at the 5-th Rochester Conference* (1955).

We obtain, very roughly, for the order of magnitude of the ratio of the two decay probabilities:

$$\frac{w_{K_{\mu 3}}}{w_\chi} = \frac{1}{288\pi^6}\,\frac{g^2}{4\pi\hbar c}\,\frac{G^2M^4c^2}{\hbar^6}\,\frac{w_\pi^2}{p_\pi^2c^2}\,\frac{v_1+v_2}{c}\,f(\eta) \approx 10^{-14},$$

which would make the $K_{\mu 3}$ process absolutely undetectable. In this formula G is the universal Fermi interaction constant $= 2\cdot 10^{-49}$ erg·cm^3 and g the interaction constant between pions and nucleons (we take $(g^2/4\pi\hbar c) \sim 0.25$); M is the mass of the nucleon; p_π and w_π are the momentum and the total energy of the two final pions of the χ; v_1 and v_2 their velocities; and $f(\eta)$ (with $\eta = p_\pi/\mu_\pi c$) a numerical factor depending on the density of the final states, which it is not necessary to specify here.

Moreover, the proposed explanation, even if it had turned out to be acceptable for the $K_{\mu 3}$, could not be assumed for the $K_{\beta 3}$. We know in fact that the decay of a pion into an electron is highly forbidden, so that the scheme corresponding to (5)

$$K_{\beta 3} \to \beta + \nu + \pi^0 \tag{6}$$

should be many orders of magnitude less probable than (5), and therefore outside of the possibilities of this explanation.

Faced with this negative evidence, and before discarding the proposed possibilities, let us see if some deeper insight of the χ-decay process may alter our conclusions.

We will therefore assume, as is usually done, that bosons interact through virtual fermion pairs. We may do this: *a*) either by assuming that the meson transforms virtually into a nucleon and antinucleon pair with a phenomenological interaction constant G_K adjusted so as the give the probable value of the mean life, while the nucleons convert into pions through the normal strong interaction processes; *b*) or, according to the specific assumption of the Gell-Mann Pais hypothesis, by supposing that the χ transforms into a virtual hyperon plus antinucleon, or the reverse

$$\chi \to Y + \overline{N} \quad \text{or} \quad \chi \to \overline{Y} + N \tag{7}$$

with strong interaction constant, g_K while this pair emits one pion by normal nuclear interaction and converts into the other pion through the process

$$Y + \overline{N} \to N + \overline{N} \to \pi$$

which according to its first step is regulated by the weak interaction constant G (7).

(7) N. DALLAPORTA: *Nuovo Cimento*, **1**, 962 (1955).

We then obtain the following decay schemes, corresponding to cases *a*) and *b*):

a) 

$$\chi \to N + \bar{N} \to N + \bar{N} + \pi \to \pi + \pi$$

b) 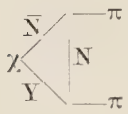

$$\chi \to Y + \bar{N} \to N + \bar{N} + \pi \to \pi + \pi$$

from which the corresponding $K_{\mu 3}$ decay schemes are obtained just by substitution in both cases of the strong interaction

$$N + \bar{N} \to \pi$$

by the weak Fermi interaction

$$N - \bar{N} \to \mu + \nu$$

a) 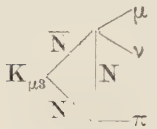

$$K_{\mu 3} \to N + \bar{N} \to N + \bar{N} + \pi \to \mu + \nu + \pi$$

b) 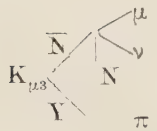

$$K_{\mu 3} \to Y + \bar{N} \to N + \bar{N} + \pi \to \mu + \nu + \pi \,.$$

In both cases, the ratio of the probabilities of transition is:

$$\frac{w_{K_{\mu 3}}}{w_\chi} = \frac{1}{32\pi^3} \frac{G^2 M^4 c^2}{\hbar^6} \left(\frac{g^2}{4\pi\hbar c}\right)^{-1} \frac{\mu_\pi^4}{M^4} \frac{w_\pi^2}{p_\pi^2 c^2} \cdot$$

$$\cdot \frac{v_1 + v_2}{c} \int_0^{\eta_{\max}} \left[\frac{1}{4}\eta^4 - \left(\frac{Q}{\mu_\pi c^2} + \frac{1}{3}\right)\eta^2 + \frac{Q^2}{\mu_\pi^2 c^4}\right] \frac{\eta^2}{\sqrt{1+\eta^2}}\, d\eta \approx 10^{-13} \,.$$

The numerical statistical factor is given here by the integral, where Q is the Q-value of the $K_{\mu 3}$ reaction; the integration is made over all the values of $\eta = p_\pi/\mu_\pi c$ allowed by energy conservation.

It is apparent that also in these cases, the probability of the $K_{\mu 3}$ decay

is negligible. A quite similar result should have been obtained for the $K_{\beta 3}$ decay by assuming the interaction

$$N + \bar{N} \rightarrow \beta + \nu .$$

There is however another possibility in case *b*) which does not exist in case *a*). Let us assume that the hyperon, being a fermion, may decay according to the schemes

$$Y \rightarrow N + \mu + \nu \tag{8}$$

and also

$$Y \rightarrow N + \beta + \nu \tag{9}$$

both interactions being regulated by the general Fermi interaction.

We find immediately for the order of magnitude of the transition probabilities of these decays:

$$w_{\substack{Y_\mu \\ Y_\beta}} = \frac{1}{16\pi^3}\,\frac{1}{\hbar}\,\frac{G^2 M^4 c^2}{\hbar^6}\,Mc^2 \int_0^{\eta_{\max}} \left[\frac{1}{4}\,\eta^4 - \left(\frac{Q}{Mc^2} + \frac{1}{3}\right)\eta^2 + \frac{Q^2}{M^2 c^4}\right] \eta^2\,\mathrm{d}\eta \quad \text{with} \quad \eta = \frac{p_N}{Mc} ,$$

which compared to the normal decay of the Λ^0 (v_1 and v_2 are here the velocities of the two decay products of the Λ^0) give:

$$\frac{w_{\substack{Y_\mu \\ Y_\beta}}}{w_{\Lambda^0}} = \frac{\pi}{0.2}\left(\frac{g^2}{4\pi\hbar c}\right)^{-1} \frac{Mc^2}{p_\pi c}\,\frac{w_\pi}{p_\pi c}\,\frac{v_1 + v_2}{c} \int_0^{\eta_{\max}} \left[\frac{1}{4}\,\eta^4 - \left(\frac{Q}{Mc^2} + \frac{1}{3}\right)\eta^2 + \frac{Q^2}{M^2 c^4}\right] \eta^2\,\mathrm{d}\eta ,$$

$$\frac{w_{Y_\mu}}{w_{\Lambda^0}} = 0.49 \cdot 10^{-3} , \qquad \frac{w_{Y_\beta}}{w_{\Lambda^0}} = 2.5 \cdot 10^{-2} .$$

So the mean life of these postulated alternative modes of decays of the Λ should be, as order of magnitude, sufficiently long to explain why no sure case of this kind has been observed up until now in cloud chambers.

With these assumptions we may now try to explain both $K_{\mu 3}$ and $K_{\beta 3}$ decays according to the schemes:

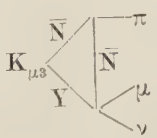

$$K_{\mu 3} \rightarrow Y + \bar{N} \rightarrow Y + \bar{N} + \pi \rightarrow \mu + \nu + \pi$$

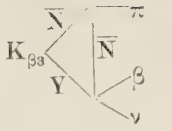

$$\mathrm{K}_{\beta 3} \to \mathrm{Y} + \overline{\mathrm{N}} \to \mathrm{Y} + \overline{\mathrm{N}} + \pi \to \beta + \nu + \pi \,.$$

We get in this way for the transition probabilities

$$w_{\substack{\mathrm{K}_{\mu 3} \\ \mathrm{K}_{\beta 3}}} = \frac{0.044}{128\pi^5} \frac{1}{\hbar} \frac{g_{\mathrm{K}}^2}{4\pi\hbar c} \frac{g^2}{4\pi\hbar c} \frac{G^2 M^4 c^2}{\hbar^6} \frac{(\mu_\pi c^2)^4}{M^2 c^4 \cdot \mu_{\mathrm{K}} c^2} \int_0^{\eta_{\max}} \left| \frac{1}{4}\eta^4 - \left(\frac{Q}{\mu_\pi c^2} + \frac{1}{3} \right) \eta^2 + \frac{Q^2}{\mu_\pi^2 c^4} \right| \mathrm{d}\eta \,.$$

$$\eta = \frac{p_\pi}{\mu_\pi c} \,,$$

(where μ_{K} is the mass of the K) and for their ratios to the decay probability of the χ:

$$\frac{w_\chi}{w_{\substack{\mathrm{K}_{\mu 3} \\ \mathrm{K}_{\beta 3}}}} = \frac{0.1}{\pi} \frac{g^2}{4\pi\hbar c} \frac{p_\pi^2 c^2}{w_\pi^2} \frac{c}{v_1 + v_2} \left(\frac{M}{\mu_\pi} \right)^4 \left\{ \int_0^{\eta_{\max}} \left| \frac{1}{4}\eta^4 - \left(\frac{Q}{\mu_\pi c^2} + \frac{1}{3} \right) \eta^2 + \frac{Q^2}{\mu_\pi^2 c^4} \right| \mathrm{d}\eta \right\}^{-1} ,$$

$$\frac{w_\chi}{w_{\mathrm{K}_{\mu 3}}} = 2.7 \,, \qquad \frac{w_\chi}{w_{\mathrm{K}_{\beta 3}}} = 1.05 \,.$$

As far as present evidence is concerned, these figures, as order of magnitude, are in good agreement with data. Moreover, the same kind of explanation is obtained for both $\mathrm{K}_{\mu 3}$ and $\mathrm{K}_{\beta 3}$, which appear as alternative modes of decay of the χ-meson. We should furthermore point out that the same kind of alternative processes can of course be possible also for the neutral counterpart of the χ (the θ^0) and that there is some evidence that in cloud chambers some rare events have been found which could correspond to the decay [8]

$$\theta^0 \to \pi + \mu + \nu \,.$$

Much more experimental material and the direct evidence of a π^0 among the neutral decay products is naturally needed before any conclusion can be reached concerning the real modes of decay of $\mathrm{K}_{\mu 3}$ and $\mathrm{K}_{\beta 3}$. But if experimental data should confirm the proposed decays (5) and (6), (it would be also necessary to observe decays (8) and (9)) this could be considered, in the light of

---

[8] R. W. THOMPSON: *Progr. in Cosmic Ray Phys. III - Hyperons and heavy mesons: the uncharged particles.* We are greatly indebted to Prof. THOMPSON for having let us read his report before publication.

present considerations as an indirect test of both the basic hypothesis (7) of the strong interaction of the Gell-Mann Pais theory and of the generalization of the Fermi interaction to hyperons.

In the spirit of the preceding considerations one might feel inclined to interpret also the $K_{\mu 2}$ decay with the scheme:

$$K_{\mu 2} \rightarrow Y + \bar{N} \rightarrow \mu + \nu .$$

With the same interaction constants as before one obtains:

$$w_{K_{\mu 2}} = \frac{(0.267)^2}{8\pi^4} \frac{1}{\hbar} \frac{g_K^2}{4\pi\hbar c} \frac{G^2 M^4 c^2}{\hbar^6} \frac{p_\mu^2 c^2}{\mu_K c^2} \frac{c}{r_1 + r_2} .$$

and for the ratio of this probability of decay to the χ-decay probability:

$$\frac{w_{K_{\mu 2}}}{w_\chi} = 2.8 \cdot 10^3 .$$

If $K_{\mu 2}$ and χ were also alternate modes of decay of the same particle, their relative frequency of production according to the present scheme would be much higher than has in fact been observed, the actual experimental data indicating that these decays occur in a frequency ratio of about 2 : 1 ([2]). But, of course, the present calculation is much too rough to allow to draw any definite conclusion about this discrepancy.

RIASSUNTO

Per potere spiegare i decadimenti in tre corpi delle particelle K secondo le reazioni: $K_{\mu 3} \rightarrow \mu + \nu + \pi^0$, $K_{\beta 3} \rightarrow \beta + \nu + \pi^0$ viene proposto uno schema dettagliato di decadimento che sembra essere il modo più semplice onde ottenere per ambedue questi decadimenti una vita media dello stesso ordine di grandezza di quella del decadimento χ. Lo schema proposto assume l'interazione forte di Gell-Mann-Pais tra particelle K ed iperoni, nonchè l'ipotesi che gli iperoni siano soggetti sia al decadimento μ che al decadimento β con costante di interazione pari alla costante universale di Fermi.

Velocità di propagazione e coefficiente di assorbimento degli ultrasuoni nei liquidi mesomorfi (*).

I. Gabrielli (+) e L. Verdini (×)

(+) *Istituto di Fisica dell'Università - Trieste*
(×) *Istituto Nazionale di Ultracustica «O. M. Corbino» - Roma*

(ricevuto l'8 Luglio 1955)

Riassunto. - - Si sono determinati la velocità di propagazione ed il coefficiente di assorbimento degli ultrasuoni, a varie temperature, nel p-azossianisolo e nel benzoato di colesterina, che presentano nella fase di liquidi mesomorfi eccezionali proprietà ottiche e strutturali, valendosi di un metodo di misura fondato sull'uso di treni d'onde. Si sono altresì eseguite misure di densità, che consentono il calcolo del coefficiente di compressibilità adiabatica e della velocità sonora molecolare. Le curve che dànno, in funzione della temperatura, la velocità, il coefficiente di compressibilità, il coefficiente di assorbimento e la velocità sonora molecolare relativi al p-azossi-anisolo, presentano anomalie che ci si propone di interpretare: particolarmente interessanti i massimi della compressibilità e dell'assorbimento alla temperatura di transizione da liquido mesomorfo a liquido isotropo. Le analoghe misure eseguite nel benzoato di colesterina non presentano particolarità notevoli. Viene discussa tale differenza di comportamento.

1. – Introduzione.

Al fine di estendere le conoscenze che si hanno sulla struttura e sulle interazioni molecolari dei liquidi, si è ritenuto utile studiare l'andamento della velocità di propagazione e del coefficiente di assorbimento degli ultrasuoni, in funzione della temperatura, in alcuni composti che, in un opportuno inter-

(*) I risultati sperimentali di questa ricerca, fanno parte della tesi di laurea del dott. L. Verdini, discussa all'Università di Trieste il 19 luglio 1954; essi furono successivamente presentati al XL Congresso Nazionale della Società Italiana di Fisica (Parma, 3-7 Settembre 1954).

vallo della stessa, presentano una fase mesomorfa (*), e precisamente nel p-azossi-anisolo (che appartiene al tipo nematico) e nel benzoato di colesterina (che appartiene al tipo colesterico).

Questa ricerca è stata suggerita dalle eccezionali proprietà strutturali ed ottiche che tali sostanze presentano nella loro fase liquido-cristallina, e precisamente:

a) particolare struttura a fibre (nematici) od a piani (colesterici) ([1]);

b) presenza di lunghe catene molecolari ([2]);

c) particolari proprietà ottiche e colorazione superficiale ([3,4]);

d) torbidità analoga all'opalescenza al punto critico ed a quella di certe mescolanze binarie ([5-7]);

e) anomalie di viscosità ([8]);

f) possibilità di orientare le molecole fibrose di tipo nematico con un forte campo magnetico od elettrico ([2,9]).

2. – Metodo di misura.

Il metodo di misura impiegato per la determinazione della velocità di propagazione e del coefficiente di assorbimento degli ultrasuoni, è fondato sull'uso di treni d'onde.

Le misure di velocità sono state eseguite valendosi di una tecnica già illustrata in un'altra nota ([10]) e che si è dimostrata particolarmente utile in questa

(*) La fase « liquido-cristallina » o di « liquido-mesomorfo » è compresa fra due temperature dette usualmente: *punto di transizione* quella che segna il passaggio da solido a liquido mesomorfo e *punto di fusione* quello in cui il liquido diventa isotropo. Tale denominazione è basata sulla convenzione di riguardare come solida la fase anisotropa, invalsa per alcuni aspetti caratteristici della stessa, fra cui il fatto che la curva tensione di vapore-temperatura di tale fase, assieme a quella della fase solida, ricordano le corrispondenti curve di quei solidi che presentano polimorfismo (si confronti per esempio J. E. Ricci: *The Phase Rule* (New York, 1951).

Altre considerazioni invece, tra cui il fatto che la scomparsa dello stato solido è accompagnata da notevole assorbimento di calore latente, porterebbero a considerare come una fusione la transizione solido-liquido mesomorfo.

([1]) M. G. Friedel: *Ann. Phys.*, **18**, 273 (1922).
([2]) W. Kast: *Phys. Zeits.*, **38**, 627 (1937).
([3]) J. Lehmann: *Ann. Phys.*, **2**, 649 (1900).
([4]) J. Lehmann: *Phys. Chem.*, **102**, 91 (1922).
([5]) R. Riwlin: *Arch. Néerl. Sci.*, **7**, 95 (1923).
([6]) P. Chatelain: *Acta Crystall.*, **1**, 315 (1948).
([7]) P. Chatelain: *Acta Crystall.*, **4**, 453 (1951).
([8]) E. Bose: *Phys. Zeits.*, **10**, 32 (1909).
([9]) G. Föex: *Trans. Farad. Soc.*, **29**, 958 (1933).
([10]) I. Gabrielli e L. Verdini: *Ric. Scient.*, **25**, 1125 (1955).

ricerca. La precisione raggiunta nelle misure di velocità supera l'1 ‰, tenuto conto degli errori derivanti dalle fluttuazioni della temperatura.

Il metodo che si è seguito per la determinazione del coefficiente di assorbimento, anche se non permette di eseguire delle misure assolute di grande precisione, ha tuttavia il pregio di essere particolarmente semplice e di dare, al variare della temperatura, le differenze del coefficiente di assorbimento con l'errore che si ha usualmente nelle misure di questa grandezza.

Il coefficiente di assorbimento è stato misurato, in base all'ampiezza della prima eco alle varie temperature, mantenendo costante la distanza quarzo-riflettore.

Dette A_1 ed A_2 le ampiezze dell'eco a due temperature diverse, α_1 ed α_2 i corrispondenti coefficienti di assorbimento e d il doppio della distanza quarzo-riflettore, si ha

$$\alpha_2 - \alpha_1 = \frac{1}{d} \ln \frac{A_1}{A_2}, \tag{1}$$

dalla quale è possibile ricavare il coefficiente di assorbimento, alle varie temperature, a meno di una costante additiva. Il valore α_1, preso come riferimento, è stato ricavato, con un'approssimazione del 15 %, in base all'attenuazione che l'eco subisce nelle successive riflessioni, cioè in base all'ampiezza degli echi successivi.

Il notevole errore di cui è affetto α_1, sposta di un valore costante tutta la curva dell'assorbimento, mentre l'andamento della stessa resta determinato con una precisione superiore ed indipendente da tale errore.

Si sono altresì eseguite misure della densità, in funzione della temperatura, con una bilancia di Mohr-Westphal, che hanno permesso di calcolare il coefficiente di compressibilità adiabatica e la velocità sonora molecolare, definita da M. R. Rao [11], come:

$$\mathcal{R} = v^{\frac{1}{3}} V = v^{\frac{1}{3}} \frac{M}{\varrho}, \tag{2}$$

in cui v è la velocità degli ultrasuoni, V il volume molecolare, ϱ la densità ed M il peso molecolare.

La precisione raggiunta nelle misure di densità è dell'ordine dell'1 ‰.

Le misure di tutte le grandezze considerate sono state eseguite a temperatura decrescente, salvo specifica precisazione.

[11] M. R. Rao: *Ind. Journ. Phys.*, **14**, 109 (1940).

3. – Risultati sperimentali nel p-azossi-anisolo.

Nella tabella I si sono riportate le temperature di transizione da solido a liquido mesomorfo e da liquido mesomorfo a liquido isotropo del p-azossi-anisolo, determinate da vari Autori.

Dall'esame dei nostri dati sperimentali ci sembra di poter assumere per le due temperature di transizione, i seguenti valori:

passaggio da solido a liquido mesomorfo . . . . . $T_1 = 116$ °C
» » liquido mesomorfo a liquido isotropo . . . . . $T_2 = 134$ °C

Essi sono in buon accordo con i dati della tabella I.

TABELLA I. – *Temperature di transizione del p-azossi-anisolo.*

T_1 (°C)	T_2 (°C)	Autore
117.3	135.9	INT. CRIT. TABLES [13]
116	135	GLASSTONE [14]
116	133	FÖEX [9]
116	133	FRIEDEL [1]

T_1 = Temperatura di transizione da solido a liquido mesomorfo.
T_2 = Temperatura di transizione da liquido mesomorfo a liquido isotropo.

Nella tabella II sono raccolti i più significativi tra i dati sperimentali, da noi ricavati usando treni d'onde della frequenza di 1.95 MHz. Le misure sono state eseguite sia a temperatura crescente che a temperatura decrescente, in un intervallo che comprende tutta la fase liquido-cristallina del p-azossi-anisolo ed una quindicina di gradi dello stato di liquido isotropo (*). I valori

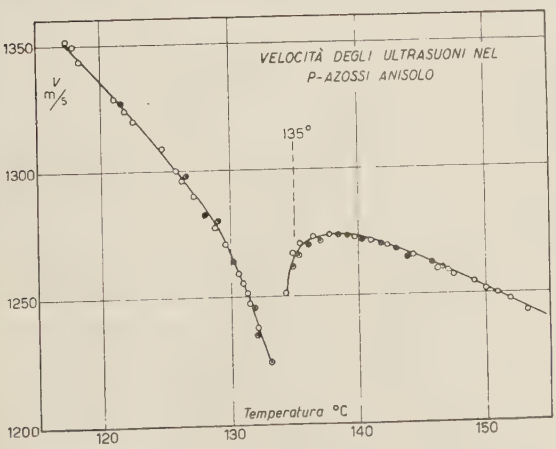

Fig. 1. – Velocità di propagazione degli ultrasuoni nel p-azossi-anisolo in funzione della temperatura (f = = 1.95 MHz): ○ punti determinati a temperatura decrescente; ◉ punti determinati a temperatura crescente; ● punti coincidenti nelle due serie di misure.

(*) Il p-azossi-anisolo adoperato in questa ricerca è stato fornito dalla « British Drug House » di Londra.

TABELLA II. – *Risultati sperimentali relativi al p-azossi-anisolo.*

T °C	v m s^{-1}	ϱ g cm^{-3}	β 10^{12} cm^2 dine^{-1}	$\mathcal{R}$ $10^{-\frac{2}{3}}$ cm$^{\frac{10}{3}}$ s$^{-\frac{1}{3}}$	$\varkappa$ cm^{-1}	$\varkappa/f^2$ 10^{17} cm^{-1} s^2
115.6	—	—	—	—	0.374	9 850
116	—	1.178	—	—	0.251	6 620
117	—	—	—	—	0.167	4 400
118	1 347.5	1.176	46.83	2 425.6	0.153	4 030
118.3	1 345.5	—	—	—	0.149	3 920
119	1 341.0	—	—	—	0.153	4 030
120	1 335.5	—	—	—	0.157	4 130
122	1 324.5	1.172	48.64	2 419.5	0.166	4 370
124	1 312.5	—	—	—	0.171	4 500
126	1 300.0	1.168	50.66	2 413.5	0.192	5 050
128	1 282.4	—	—	—	0.219	5 770
130	1 265.5	1.164	53.65	2 399	0.265	7 000
131	1 254.5	1.163	54.64	2 395	—	—
132	1 240.0	1.162	56.11	2 388	0.369	9 700
133	1 224.5	1.1615	57.42	2 344	0.463	12 200
134.5	1 249.5	1.1585	55.29	2 401	—	—
135	1 263.0	1.156	54.23	2 413	—	—
135.8	1 269.5	—	—	—	0.495	13 000
136	1 270.5	1.153	53.71	2 426	0.316	8 330
137	1 272.5	—	—	—	0.200	5 270
138	1 273.0	1.151	53.63	2 432	0.160	4 200
140	1 271.5	1.150	53.78	2 433	0.142	3 720
142	1 269.0	1.1485	54.09	2 435.5	0.134	3 530
144	1 265.0	1.147	54.54	2 434	0.132	3 480
146	1 261.0	1.1455	54.92	—	—	—
150	1 252.0	1.1425	55.86	2 438	—	—

del coefficiente di assorbimento relativi a temperature inferiori a 116 °C si riferiscono al liquido mesomorfo lievemente « sopraffuso ».

La fig. 1 rappresenta la velocità di propagazione degli ultrasuoni in funzione della temperatura; i punti segnati con un cerchietto bianco si riferiscono a misure eseguite a temperatura decrescente, mentre quelli segnati con un cerchietto con punto al centro si riferiscono a misure ese-

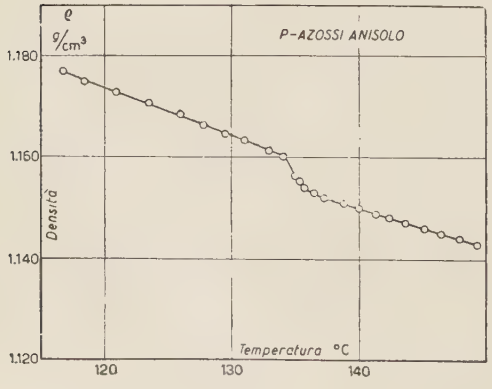

Fig. 2. – Densità del p-azossi-anisolo in funzione della temperatura.

guite a temperatura crescente; i cerchietti neri indicano i punti coincidenti nelle due serie di misure.

Dato il particolare andamento della curva, ci sembra utile mettere in evidenza le seguenti temperature:

118 °C 134 °C

138 °C 144 °C

che separano il grafico in intervalli che presentano caratteristiche diverse.

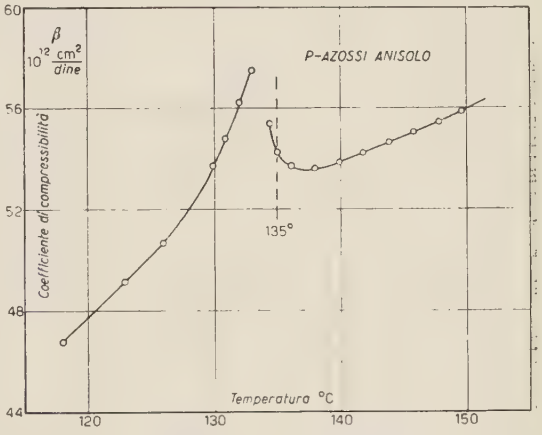

Fig. 3. – Coefficiente di compressibilità adiabatica del p-azossi-anisolo.

Nel primo tratto rettilineo della curva (118 ÷ 125 °C) il coefficiente di temperatura della velocità vale — 4.5 ms^{-1} $°C^{-1}$, mentre nel tratto rettilineo che si ha oltre i 144 °C esso è molto diverso ed ha un valore di — 2.1 ms^{-1} $°C^{-1}$. Si notino il minimo pronunciato al punto di transizione T_2 ed il successivo massimo (138 °C).

Nelle figg. 2 e 3 sono riportati rispettivamente la densità ed il coefficiente di compressibilità adiabatica del p-azossi-anisolo, in funzione della temperatura. L'andamento del coefficiente di compressibilità, piuttosto irregolare, rispecchia quello della velocità di propagazione degli ultrasuoni, mentre la curva della densità, lineare sia nella fase anisotropa che in quella isotropa anche se con pendenza diversa, presenta una più rapida diminuzione nell'immediato intorno del punto di transizione T_2.

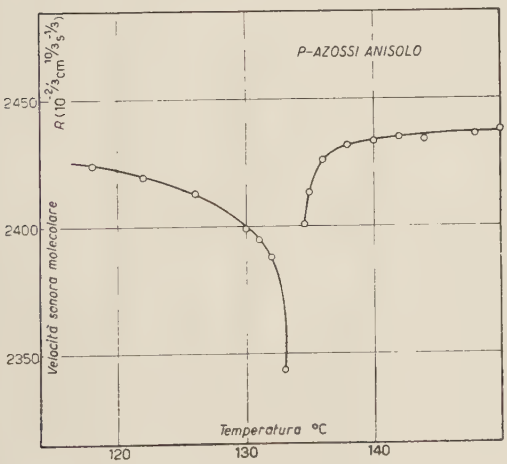

Fig. 4. – Velocità sonora molecolare $\mathcal{R} = v^{\frac{1}{3}} \cdot M/\varrho$ nel p-azossi-anisolo.

La velocità sonora molecolare, in funzione della temperatura, è presentata nel diagramma di fig. 4.

Anche il coefficiente di assorbimento, in funzione della temperatura, mostra notevoli particolarità (fig. 5). Innanzi tutto si nota un massimo assai accentuato in corrispondenza al punto di transizione T_2: infatti a questa temperatura

l'assorbimento delle onde ultrasonore diviene tanto elevato che l'eco non è più visibile sullo schermo del sincroscopio. È interessante notare che anche questa curva, come le altre, si può suddividere in intervalli limitati dalle stesse temperature messe precedentemente in evidenza.

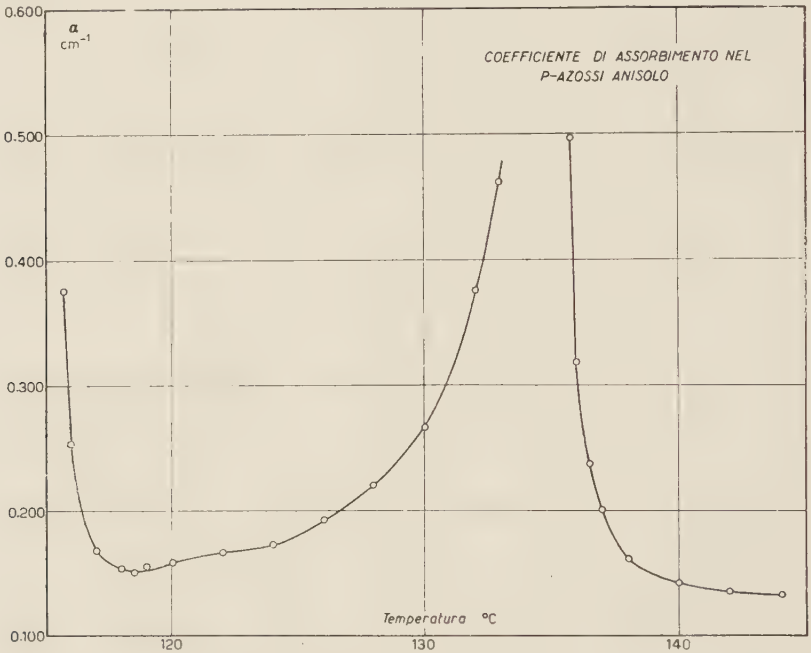

Fig. 5. – Coefficiente di assorbimento degli ultrasuoni nel p-azossi-anisolo, in funzione della temperatura (f = 1.95 MHz).

4. – Risultati sperimentali nel benzoato di colesterina.

La tabella III presenta le due temperature di transizione del benzoato di colesterina che si possono trovare nella letteratura, mentre nella tabella IV sono raccolti i nostri dati sperimentali (*). Anche in queste misure di velocità e di assorbimento degli ultrasuoni, la frequenza dei treni d'onde usati era di 1.95 MHz.

Il diagramma di fig. 6 rappresenta l'andamento della velocità di propagazione degli ultrasuoni ed il coefficiente di compressibilità adiabatica, in un intervallo di temperatura che va da 170 °C fino a 200 °C e che comprende pertanto solo una piccola parte della fase liquido-cristallina, in quanto, per tem-

(*) Il benzoato di colesterina è stato gentilmente preparato presso l'Istituto di Chimica dell'Università di Trieste.

perature inferiori, l'assorbimento delle onde ultrasonore è così intenso da impedire le misure sia della velocità che dell'assorbimento.

TABELLA III. – *Temperature di transizione del benzoato di colesterina.*

T_1 (°C)	T_2 (°C)	Autore
145.5	178.5	LEHMANN [3,4]
145	178	FRIEDEL [1]
146	179.5	GLASSTONE [14]

T_1 = Temperatura di transizione da solido a liquido mesomorfo.
T_2 = Temperatura di transizione da liquido mesomorfo a liquido isotropo.

TABELLA IV. – *Risultati sperimentali relativi al benzoato di colesterina.*

T °C	v m s^{-1}	ϱ g cm^{-3}	β 10^{12} cm^2 dine^{-1}	$\mathcal{R}$ $10^{-\frac{2}{3}}$ cm$^{\frac{10}{3}}$ s$^{-\frac{1}{3}}$	α cm^{-1}	α/f^2 10^{17} cm^{-1} s^2
170.3	1 122.5	0.9556	83.06	5 337.2	—	—
171	1 121.5	0.9545	83.29	5 341.8	0.302	8 000
172	1 120.4	0.9541	83.49	5 341.9	0.255	6 700
172.5	1 119.8	0.9539	83.61	—	—	—
173	1 119.2	0.9537	83.71	5 342.2	—	—
173.5	1 118.7	0.9535	83.80	—	—	—
174	1 118.3	0.9532	83.88	5 343.9	0.187	4 930
174.5	1 117.8	—	—	—	—	
175	1 117.1	0.9525	84.13	5 345.8	—	
176	1 115.0	0.9518	84.51	5 346.7	0.152	4 000
177	1 113.0	0.9512	84.87	—	—	—
178	1 111.5	0.9506	85.15	5 347.7	0.125	3 300
179	1 108.1	0.9500	85.73	5 347.2	—	—
180	1 106.0	0.9494	86.11	5 345.7	0.105	2 760
181	1 104.2	0.9490	86.45	—	—	—
182	1 102.0	0.9484	86.83	—	0.090	2 360
184	1 098.0	0.9474	87.55	5 344.0	0.077	2 000
188	1 089.1	0.9455	89.18	5 339.7	—	—
190	1 085.0	—	—	—	0.065	1 700
192	1 080.2	0.9438	90.84	5 334.8	—	—
196	1 070.9	0.9425	92.51	5 327.0	—	
200	1 062.2	0.9413	94.15	5 319.0	0.054	1 420

È interessante notare che, in corrispondenza al punto di transizione T_2, non si nota alcuna particolarità nell'andamento delle due curve, mentre risulta

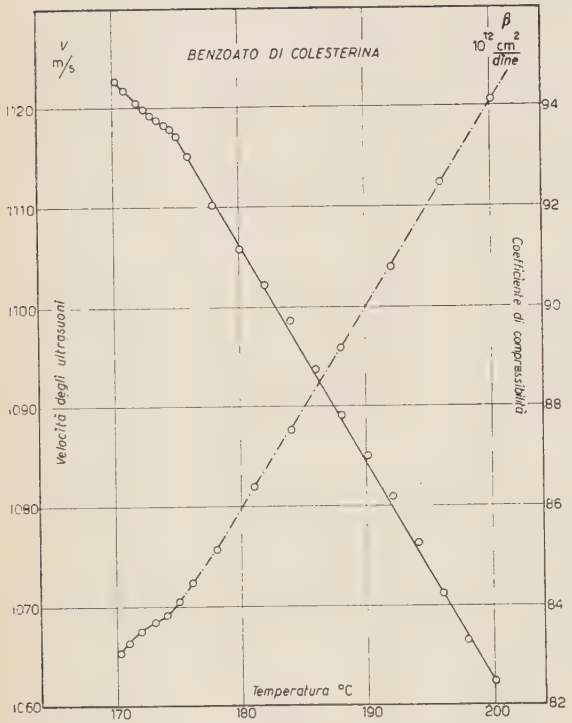

Fig. 6. – Velocità di propagazione (—) e coefficiente di compressibilità adiabatica (–·–) del benzoato di colesterina.

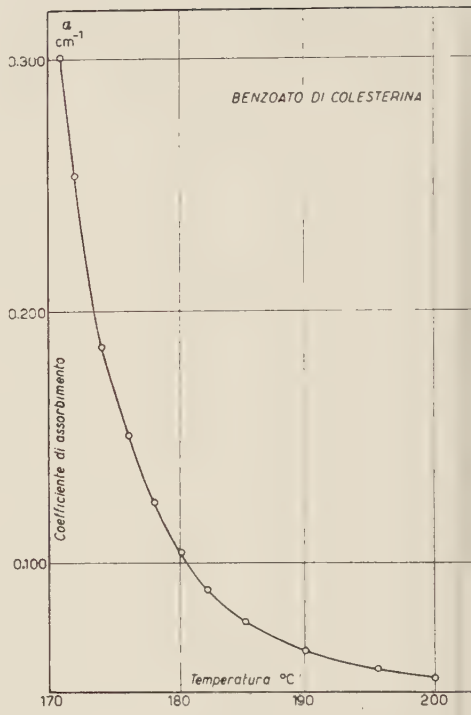

Fig. 7. – Coefficiente di assorbimento degli ultrasuoni nel benzoato di colesterina (f = 1.95 MHz).

evidente un cambiamento del coefficiente di temperatura per valori della temperatura inferiori ai 175 °C, cioè nell'intervallo in cui si hanno i particolari fenomeni di colorazione superficiale. Nel tratto rettilineo corrispondente a temperature superiori ai 175 °C, il coefficiente di temperatura della velocità vale — 2.2 ms^{-1} $°C^{-1}$.

Anche nel diagramma di fig. 7, che rappresenta il coefficiente di assorbimento

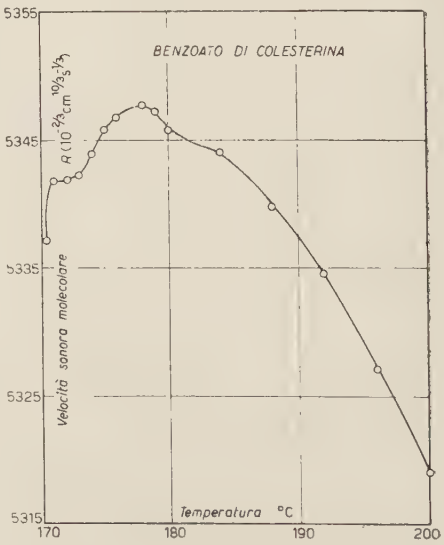

Fig. 8. – Velocità sonora molecolare $\mathcal{R} = v^{\frac{1}{3}} \cdot M/\varrho$ nel benzoato di colesterina in funzione della temperatura.

in funzione della temperatura, non si nota nulla di particolare in corrispondenza al punto di transizione.

L'unica delle grandezze considerate che mostra un andamento particolare alla transizione liquido mesomorfo-liquido isotropo (178 °C) è la velocità sonora molecolare, che presenta un massimo a tale temperatura (fig. 8), ed un andamento costante tra 171 °C e 174 °C, intervallo in cui, come si è detto, si possono notare i fenomeni ottici messi in evidenza da J. LEHMANN ([3,4]).

5. – Discussione dei risultati sperimentali.

Le notevoli differenze di comportamento in campo ultrasonoro, presentate dai due composti, potrebbero caratterizzare i due tipi di liquidi mesomorfi cui essi appartengono e cioè il nematico ed il colesterico.

D'altra parte osserviamo che i due composti considerati, mantenuti a contatto con l'aria, possono subire dei processi di ossidazione alla temperatura in cui presentano la fase isotropa, essendo tale fenomeno più intenso nel benzoato di colesterina, che diviene isotropo ad una temperatura maggiore. Può quindi sorgere il dubbio che l'assenza dei massimi per la compressibilità e per l'assorbimento nel benzoato di colesterina si possa giustificare pensando che i prodotti dell'ossidazione siano capaci di diminuire la variazione dell'energia di coesione e di bloccare i processi di rilassamento, eventualmente presenti al secondo punto di transizione.

Si è verificato tuttavia che, anche portando rapidamente il benzoato di colesterina non ossidato alla temperatura di transizione T_2, non si verifica ugualmente un minimo della velocità ed un massimo dell'assorbimento, per cui il comportamento di un campione nel quale l'ossidazione, pure inevitabile, è mantenuta in limiti ridotti, è qualitativamente eguale a quello riportato nelle figg. 6 e 7. Si è inoltre constatato che la torbidità e la colorazione superficiale del benzoato di colesterina sussistono, nell'opportuno intervallo di temperatura, indipendentemente da eventuali processi di ossidazione dei campioni in esame.

a) *p-azossi-anisolo.* Nel p-azossi-anisolo la transizione da liquido mesomorfo a liquido ordinario influisce sensibilmente sui valori delle costanti elastiche e viscose.

Il composto diventa liquido, ma in fase mesomorfa, a 116 °C e la rapida diminuzione dell'assorbimento all'aumentare della temperatura, unita alla regolare variazione della velocità di propagazione degli ultrasuoni, rivelano che questa transizione avviene come un cambiamento di stato ben definito, analogamente a quanto si ha nella normale fusione delle sostanze cristalline.

Nel liquido mesomorfo, mescolati ad una « madrefase », esisterebbero degli

aggregati molecolari che vengono chiamati « Schwärme » da E. Bose [12], « domains» da R. Riwlin [5], « long-range groups » da N. A. Tolstoi [15], oppure seguendo la recente denominazione di alcuni Autori, « clusters » [16].

Nel seguito, tali aggregazioni molecolari verranno indicate nel testo indifferentemente col nome di « *sciami* » o di « *macrogruppi* ».

Quando la temperatura si avvicina alla transizione liquido mesomorfo-liquido isotropo, i macrogruppi diventano molto instabili e presentano una grande tendenza a spezzarsi. Un lieve aumento della temperatura ne determina infatti la totale sparizione, mentre nel liquido rimangono ancora presenti agglomerati di entità molto minori, che N. A. Tolstoi [15] chiama « *near-range groups* »: questi, riunendosi in un certo numero e orientandosi secondo una direzione privilegiata (asse dello sciame) costituirebbero i macrogruppi presenti nella fase mesomorfa.

In tale situazione, le onde ultrasonore hanno la possibilità di cedere ai macrogruppi l'energia necessaria alla loro distruzione. Gli sciami quindi sono facilmente frantumati durante la fase di rarefazione dell'onda sonora, mentre la loro riformazione, determinata dal fatto che la temperatura del liquido non è ancora sufficiente ad evitarla, può aver luogo con ritardo rispetto alla successiva compressione, od addirittura portare a configurazioni strutturali diverse, dando così origine a fenomeni irreversibili.

La rapida diminuzione della densità al crescere della temperatura nell'intorno del punto di transizione T_2, indica chiaramente che la frantumazione dei macrogruppi comporta un aumento del volume occupato dal liquido e quindi variazioni dell'energia di coesione che si ripercuotono sull'andamento della compressibilità.

La velocità sonora molecolare sembra perdere, nella fase nematica di questo liquido, il suo significato di indice delle associazioni molecolari: infatti in tale intervallo essa indicherebbe un aumento graduale dell'associazione con la temperatura. Una tale anomalia si può spiegare col fatto che i macrogruppi, i quali sostituiscono, agli effetti della propagazione dell'onda ultrasonora, le molecole associate dei liquidi ordinari, hanno dimensioni ben superiori a quelle delle normali associazioni presenti nello stato liquido ordinario.

La totale sparizione dei macrogruppi, per un lieve aumento della temperatura al disopra del punto di transizione T_2, è confermata dalla rapida diminuzione dell'assorbimento e della compressibilità in tale intervallo.

La dissimetria nell'intorno del massimo che queste due grandezze presentano, rivela appunto un graduale raggiungimento delle condizioni di insta-

---

[12] E. Bose: *Phys. Zeits.*, **10**, 230 (1909).
[13] Int. Crit. Tables, **4**, p. 10.
[14] S. Glasstone: *Physical Chemistry* (London, 1951).
[15] N. A. Tolstoi: *Journ. Exp. Theor. Phys.*, **17**, 724 (1947).
[16] D. Sette: *Journ. Chem. Phys.*, **21**, 558 (1953).

bilità (stato di pre-transizione) quando la temperatura aumenta verso il punto di transizione, ed un rapido stabilirsi di una condizione di omogeneità al disopra di questo.

Se consideriamo altri liquidi, in cui, per cause diverse, si producono fluttuazioni eterofasi, notiamo che quest'ultime sono sempre accompagnate da un forte massimo del coefficiente di assorbimento (mescolanze di liquidi con lacune di miscibilità per valori della temperatura prossimi al punto critico di soluzione, come nei sistemi binari anilina-n-esano, trietilamina-acqua [17], anilina-cicloesano e acqua-fenolo [18]).

Oltre al massimo di assorbimento, si riscontra un sensibile minimo della velocità di propagazione degli ultrasuoni anche in quei casi in cui gli scostamenti locali della densità dal valor medio sono particolarmente forti, come nei liquidi al punto critico, nei quali le variazioni di densità sono dovute a bolle di vapore o di gas (esafluoruro di zolfo [19], anidride carbonica liquida [20], xenon liquido [21]).

In questi ultimi casi, come pure nel p-azossi-anisolo, la presenza in seno al liquido di nuclei di un secondo componente (sia esso un gas, od un liquido non miscibile, od una seconda fase di densità diversa) comporta un massimo della compressibilità e dell'assorbimento, legati rispettivamente ad una forte variazione dell'energia di coesione ed a fenomeni di rilassamento. Pertanto questo comportamento caratteristico sembra manifestarsi indipendentemente dal particolare tipo di aggregazione molecolare interessato alla propagazione delle onde elastiche. Esso può essere spiegato attribuendolo ad un effetto di rilassamento configurazionale, dovuto alla instabilità caratteristica di una sostanza che si presenta in due fasi intimamente mescolate fra loro e tendente ad assorbire dal campo ultrasonoro quella energia che permette l'evoluzione del sistema verso lo stato proprio delle temperature superiori al punto critico od al punto di transizione. Gli ultrasuoni, propagandosi in un mezzo che si trova in tali condizioni, producono delle particolari variazioni strutturali periodiche, ma sfasate rispetto al campo ultrasonoro, che implicano una dissipazione di energia.

Un analogo comportamento della velocità e dell'assorbimento è pure presentato dall'elio liquido al punto λ (2.19 °K), cioè quando, per variazioni della temperatura, esso passa dallo stato I allo stato II o viceversa [22-24].

[17] A. G. Chyanoweth and W. G. Schneider: *Journ. Chem. Phys.*, **19**, 1566 (1951).
[18] S. Petralia: *Rend. Acc. Lincei*, **12**, 674 (1952).
[19] W. G. Schneider: *Can. Journ. Chem.*, **29**, 243 (1951).
[20] H. Tielsch und, H. Tannenberger: *Zeits. f. Phys.*, **137**, 256 (1954).
[21] A. G. Chyanoweth and W. G. Schneider: *Journ. Chem. Phys.*, **20**, 1777 (1952).
[22] J. C. Findlay, A. Pitt and H. Grayson Smith: *Phys. Rev.*, **54**, 506 (1938).
[23] J. R. Pellam and C. F. Squire: *Phys. Rev.*, **72**, 1245 (1947).
[24] U. R. Atkins and C. E. Chase: *Colloq. Ultras. Trill.* (Bruxelles, 1951), p. 270.

Normalmente in questi fenomeni si esclude l'effetto della diffusione delle onde ultrasonore causata dalle disomogeneità presenti, e ciò si può fare anche nel caso del liquido nematico considerato, tenendo conto che, mentre la lunghezza d'onda degli ultrasuoni impiegati in questa ricerca era dell'ordine di mezzo millimetro, le dimensioni dei gruppi molecolari si aggirerebbero intorno ai $2 \div 3$ decimi di micron, secondo le valutazioni di H. TROPPER (in base ai moti browniani) ([25]), di P. CHATELAIN (da misure sulla luce diffusa) ([6,26]), e di W. KAST (dalle costanti elettromagnetiche) ([27]).

Un calcolo del contributo portato al coefficiente di assorbimento dalla diffusione degli ultrasuoni su disomogeneità di tali dimensioni presenti nel liquido, si può fare seguendo le considerazioni di L. LIEBERMANN ([28]). Ma, pur estrapolando a 1200 ms^{-1} il valore minimo della velocità nel diagramma di fig. 1, ed attribuendo alla differenza di velocità tra la fase omogenea e la fase a macrogruppi un valore del 6%, l'assorbimento per diffusione risulta appena dell'ordine di 10^{-3} cm^{-1}.

La presenza di « *microgruppi* », cioè di associazioni molecolari di tipo ordinario, e la loro diminuzione all'aumentare della temperatura, sono rivelate nell'intervallo tra i 138 °C e i 144 °C, sia dal massimo della velocità di propagazione, sia dal crescente valore della velocità sonora molecolare, che qui sembra riprendere il suo significato di indicatrice del grado di associazione. Inoltre, l'ulteriore diminuzione del coefficiente di assorbimento, rivela anche qui fenomeni di rilassamento legati alla perturbazione da parte delle onde ultrasonore di equilibri tra forme strutturali di diversa densità, ma analoghi a quelli che si riscontrano nel campo delle associazioni molecolari di tipo comune ([29]).

Oltre i 144 °C i fenomeni di associazione sembrano divenire trascurabili: il comportamento lineare della velocità di propagazione ed i valori pressocchè costanti della velocità sonora molecolare e del coefficiente di assorbimento, in funzione della temperatura, indicano che siamo in presenza di un liquido isotropo e privo di associazioni. A questa temperatura spariscono anche le particolari proprietà ottiche riscontrate da J. LEHMANN ([3,4]).

b) *Benzoato di colesterina.* A differenza di quanto si è riscontrato nel p-azossi-anisolo, i risultati trovati per il benzoato di colesterina non indicano nessuna variazione strutturale importante alla transizione liquido mesomorfo-liquido isotropo. Il passaggio tra le due fasi sembra essere un fenomeno che interviene senza dar luogo a brusche variazioni dell'entità degli agglomerati

([25]) H. TROPPER: *Ann. der Phys.*, **30**, 371, (1937).
([26]) P. CHATELAIN: *Compt. Rend.*, **224**, 130 (1947).
([27]) W. KAST: *Zeits. für Elektrochem.*, **45**, 184 (1939).
([28]) L. LIEBERMANN: *Journ. Acoust. Soc. Am.*, **23**, 563 (1951).
([29]) D. SETTE: *Ric. Scient.*, **25**, 576 (1955).

molecolari, che, come si è detto, comportano fluttuazioni di densità e che influenzano la compressibilità e l'assorbimento degli ultrasuoni.

La sparizione della torbidità alla luce del liquido colesterico, può essere spiegata ammettendo che, al crescere della temperatura, le dimensioni delle grosse associazioni molecolari diminuiscano gradualmente al disotto della lunghezza d'onda delle radiazioni visibili, per cui ad un certo punto non si ha più diffusione della luce. I fenomeni di colorazione violetta che compaiono in prossimità della temperatura di transizione T_2, confermerebbero che, al limite tra la fase di liquido torbido e quella di liquido trasparente, sono prevalenti degli aggregati molecolari capaci di diffondere solamente le radiazioni di lunghezza d'onda minore. Questa variazione delle dimensioni dei macrogruppi, che avviene in modo graduale su tutto un intervallo di temperatura e non ad una temperatura ben definita, come nel caso del p-azossi-anisolo, resta confermata anche dall'andamento delle curve della velocità di propagazione e del coefficiente di assorbimento degli ultrasuoni.

Un cambiamento strutturale, che non comporta l'insorgere di sensibili disomogeneità, potrebbe essere rappresentato dal gomito delle curve di velocità, compressibilità e densità a 175 °C. L'accenno ad un flesso che si riscontra fra i 172 °C e i 175 °C, si trova al limite degli errori sperimentali. Tale comportamento, del resto, ricorda il flesso che la curva della velocità di propagazione degli ultrasuoni nello zolfo fuso presenta nella regione di transizione (160 ÷ 220 °C) ([30]).

Il coefficiente di assorbimento, che mantiene valori elevati dalla fusione (145 °C) fino a 170 °C e che poi diminuisce come nelle sostanze pseudosolide ([31]) e nella gomma ([32]), fa pensare a fenomeni di rilassamento di tipo strutturale, i cui effetti si risentono non solo durante tutta la fase mesomorfa, ma anche nel liquido trasparente. Questo è in accordo con le precedenti ipotesi.

L'unica grandezza che al punto di transizione T_2 mostra una particolarità, è la velocità sonora molecolare, che ivi presenta un massimo. Nel significato valido per i liquidi ordinari, questo corrisponderebbe ad un minimo di associazione e, mentre per il comportamento fino a 178 °C si accorda con le ipotesi precedenti, appare inspiegabile come al punto di transizione T_2, supposto determinato essenzialmente dalla relazione tra le dimensioni degli agglomerati molecolari e la lunghezza d'onda della luce, la curva presenti un'inversione della pendenza. Per temperature superiori si avrebbe poi un'insolita indicazione di aumento della associazione: forse anche in questo caso, come già si è accennato per il liquido nematico, l'entità delle associazioni molecolari rende inapplicabile la teoria di Rao ([11]).

([30]) O. J. Kleppa: *Journ. Chem. Phys.*, **18**, 1303 (1950).
([31]) P. G. Bordoni and M. Nuovo: *Colloquium Ultras. Trill.* (Bruxelles, 1951), p. 164.
([32]) I. Gabrielli e G. Iernetti: *Nuovo Cimento*, **1**, 403 (1955).

Notiamo che la variazione relativa della velocità sonora molecolare non supera il 6 ‰ su un intervallo di 25 °C, ed è quindi inferiore, per esempio, a quella dell'alcool metilico od etilico. Per il p-azossi-anisolo, tale variazione relativa è invece del 4 % in meno di 20 °C e quindi doppia di quella, pur elevata, dell'acqua ([33]). Anche da questo confronto, aggiunto al fatto che alla transizione il liquido nematico presenta un minimo mentre quello colesterico presenta un massimo per la velocità sonora molecolare, rimane confermata la differenza delle proprietà dei due liquidi mesomorfi.

6. – Conclusioni.

Per il benzoato di colesterina (liquido mesomorfo di tipo colesterico) l'indagine ultrasonora rivela solamente una leggera variazione del coefficiente di temperatura della compressibilità a 175 °C, cioè ad una temperatura lievemente inferiore a quella comunemente indicata come temperatura di transizione (178 ÷ 179 °C).

Nel p-azossi-anisolo (liquido mesomorfo di tipo nematico) il punto di transizione liquido anisotropo-liquido isotropo è invece caratterizzato da particolarità notevoli nella compressibilità e nell'assorbimento degli ultrasuoni.

Per spiegare tali diversità di comportamento si è affacciata l'ipotesi che nel caso del liquido nematico la transizione a liquido ordinario intervenga bruscamente ad una temperatura ben definita e caratterizzata da fluttuazioni eterofasi, particolarmente sensibili al campo ultrasonoro, in quanto determinano fenomeni di rilassamento configurazionale.

Nel caso del liquido colesterico, lo sfaldamento delle grosse associazioni molecolari sarebbe invece graduale, al disopra e al disotto del punto in cui sparisce la torbidità alla luce, senza che nel liquido si manifesti una condizione di equilibrio instabile, notevolmente perturbato dal campo ultrasonoro.

Per chiarire tali punti, sarà necessario estendere queste misure su altri liquidi mesomorfi.

Saranno pure necessarie misure a diverse frequenze, per verificare se le differenze di comportamento presentate dai due liquidi nel campo ultrasonoro non siano dovute alla particolare frequenza usata. Infatti si può pensare che questa esalti tali differenze, interessando solo in un liquido quei particolari meccanismi di rilassamento che nell'altro potrebbero corrispondere ad una frequenza differente.

Ci proponiamo infine di eseguire delle misure di velocità e di assorbimento degli ultrasuoni nei liquidi mesomorfi sottoposti all'azione orientatrice di un campo elettrico o magnetico.

([33]) A. Weissler: *Journ. Chem. Phys.*, **15**, 210 (1947).

* * *

Ringraziamo il prof. D. SETTE per le utili discussioni avute sull'argomento ed il dott. C. VILLI per averci suggerito di verificare in campo ultrasonoro l'eccezionale comportamento dei liquidi mesomorfi, rilevato finora prevalentemente con metodi ottici.

NOTA. – Mentre questo lavoro era in corso di pubblicazione, abbiamo avuto notizia che una analoga ricerca è stata compiuta da W. A. HOYER e A. W. NOLLE e presentata ad Austin (Texas) al 48° Congresso della American Acoustical Society, nel Novembre 1954. Un riassunto di questo lavoro si può trovare a pag. 15 del Programma di tale Congresso, oppure sulla rivista *Journ. Acoust. Soc. Amer.*, **27**, 204 (1955).

SUMMARY

The velocity of propagation and the absorption coefficient of ultrasound in para-azoxyanisole and in cholesterol-benzoate have been measured as a function of temperature, by means of a pulsed wave method. These substances present a mesomorphic phase with special optical and structural characters. From density measurements the adiabatic compressibility and the molecular sound velocity have been calculated. The para-azoxyanisole shows a peculiar temperature dependance of ultrasound velocity, absorption and molecular sound velocity. The maxima of compressibility and of absorption coefficient at the transition temperature from mesomorphic to isotropic liquid phase are particularly noticeable. No remarkable unusual behavior for cholesterol-benzoate has been found. The differences between the two liquid crystals (nematic and cholesteric) in ultrasonic field are briefly discussed.

An Unstable Fragment Produced on the Nuclear Capture of a Hyperon.

M. Ceccarelli (*), N. Dallaporta, M. Grilli, M. Merlin, G. Salandin, B. Sechi

Istituto di Fisica dell'Università - Padova
Istituto Nazionale di Fisica Nucleare - Sezione di Padova

M. Ladu (+)

Istituto di Fisica dell'Università - Milano
Istituto Nazionale di Fisica Nucleare - Sezione di Milano

(ricevuto il 9 Luglio 1955)

Summary. — An event is described which consists in a slow singly charged particle of superprotonic mass, coming to rest in the emulsion and giving rise to an excited fragment and no other visible secondary; after a range of 46 μm, the fragment disintegrates into a proton of 110 MeV and a singly charged particle with a range of 300 μm, which may be either a proton or a deuteron. The event is consistent with the assumption that a negative hyperon captured by a nucleus interacts according to reaction: $\Sigma^- + P \to \Lambda^0 + N$, the Λ^0 remaining bound into an unstable nuclear fragment. All other hyperon capture events known up to now are discussed in order to see if they could be interpreted as being due to the same reaction.

1. – During the scanning of the plates of the *G*-stack, flown in Northern Italy in October 1954, an event has been observed, which may be interpreted as a capture of a negative hyperon giving rise to an excited fragment. A slow singly charged particle, *A* (Fig. 1) is emitted from a 23+0p star and comes to rest in the emulsion after 2.75 mm at point *P*, where it gives rise to

(*) At present at the Max Planck-Institut für Physik - Göttingen.
(+) On leave from the Istituto di Fisica dell'Università - Cagliari.

Fig. 1. *Observer*: G. Gesuato

a single heavily ionising track (B) and no other visible secondary, apart from a small blob of 1.5 μm (recoil, chance grain or slow electron).

Track B which has a dip of 50° stops after a path of 46 ± 2 μm and from its stopping point two ionizing tracks emerge, one of which (C) has in 17 plates a total range of 37 ± 1 mm (*) and the other (D) a range of $300 \pm \pm 10$ μm (1). Both of these particles are singly charged. Ionization-range measurements indicate that track C is a proton of energy 110 ± 4 MeV and track D either a 7 ± 0.25 MeV proton or a 9.2 ± 0.3 MeV deuteron. The errors on the energy quoted include the errors on range and a further 2 % uncertainty on the stopping power of the emulsion.

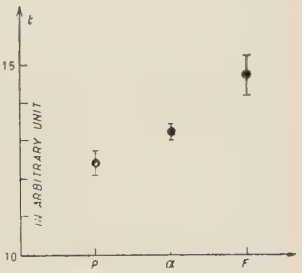

Fig. 2.

The mass of the primary particle A as measured by constant sagitta is 4000 ± 1500 m_e and by gap counting is 2000 ± 400 m_e. The apparent difference in the two estimates of the mass, obtained by different methods, although not statistically significant, may possibly result if the particle does not, in fact, come to rest at point P. To test this, we have studied the scattering of the particle on the last 50 μm of its range, and compared it with the scattering of protons on the last 400 μm of their range; the results are consistent with the assumption that track A comes to rest at point P. From the preceding evidence, we can conclude that particle A is likely to be an hyperon.

In order to obtain some indication on the nature of the fragment (track B), its mean thickness was measured (1) and compared with the last 46 μm of the track of eleven α-particles of the same dip and at the same depth in the plate. The results obtained are summarised in Fig. 2. The main difficulty in assessing the value of the information given by this as yet rudimentary method lies in our ignorance of the nature and extent of the fluctuations. The errors quoted in Fig. 2 are the mean square deviations $\sqrt{\Sigma(x^2-\bar{x}^2)/n(n-1)}$:

a) of the 70 individual measurements t_F around the mean $\bar{t}_F$ of the fragment,

b) of the mean thicknesses $\bar{t}_{\alpha i}$ of each of the eleven α-tracks around their mean $\bar{t}_\alpha$ (**),

(*) Including straggling and other sources of errors.

(1) A. Bonetti, C. Dilworth, M. Ladu and G. Occhialini: *Rend. Acc. Linc.*, **17**, 311 (1954).

(**) The distribution of the t values of a single track is not Gaussian, but has a tail towards high t values. In our particular case the mean square deviation of the measurements on the fragment was found to be equal to the dispersion $\sqrt{\Sigma(x^2 - \bar{x}^2)/n}$ on the eleven α-particle means.

c) of the mean thickness $\bar{t}_{pi}$ of 5 protons around their mean.

We see that the mean thickness of the track B lies at a bare two standard deviations above the mean of the α's, and at three standard deviations above that of the protons.

So it is probable that the charge is greater than 1; it is possible that the fragment is an isotope of charge 2.

With a charge $Z > 2$ for the fragment it is not possible to draw any definite conclusion as to the reaction which takes place in its delayed disintegration. However, the total energy release is compatible with that to be expected from the disintegration of a fragment containing a bound Λ^0.

We can speculate on the possible reactions if the fragment has charge two, a value which is not completely excluded by our measurements.

Two of the possibilities are:

$$(1) \qquad {}^3\mathrm{He} = \mathrm{p} + \mathrm{p} + \mathrm{n} + Q_1$$

$$(2) \qquad {}^4\mathrm{He} = \mathrm{p} + \mathrm{d} + \mathrm{n} + Q_2 \,.$$

If we assume that particle D is a proton (scheme 1) we obtain from the momentum balance a Q-value $Q_1 = 182.4 \pm 7.7$ MeV; assuming D to be a deuteron (scheme 2) we obtain $Q_2 = 162.4 \pm 7.4$ MeV. Both these values are in fair agreement with the Q-value one should expect for a bound Λ^0.

For the $\Delta = B_N - B_{\Lambda^0}$ ([2]) we obtain $\Delta({}^3\mathrm{He}) = 14.1 \pm 7.7$ MeV and $\Delta({}^4\mathrm{He}) = 12.4 \pm 7.4$ MeV. If we assume for the binding energy of the neutron in the ^{3}He the maximum value corresponding to the total binding energy of the nucleus $B_N = 7.6$ MeV, and in case of ^{4}He the well known value $B_N = 20.5$ MeV, we get for the binding energy of the Λ^0:

$$B_{\Lambda^0}({}^3\mathrm{He}) \leqslant -6.5 \pm 7.7 \text{ MeV}\,, \qquad B_{\Lambda^0}({}^4\mathrm{He}) = 8.1 \pm 7.4 \text{ MeV}\,.$$

From these values it is not possible to exclude either scheme (1) or scheme (2).

From all the preceding discussion we can conclude that for $Z \geqslant 2$ particle B can be interpreted as an unstable fragment containing a bound Λ^0.

No other unstable particle was found among the prongs of the parent star of the hyperon, although twenty of them were seen to end in the stack, and the other three were followed for more than 4 cm untill they left the stack.

2. – We may now discuss the reaction that could be responsible for the event under discussion. The observation indicates that a negative hyperon captured in the Bohr orbit of a nucleus of the emulsion reacts with it and gives

([2]) M. GRILLI and R. LEVI SETTI: *Suppl. Nuovo Cimento*, **12**, 466 (1954). R. LEVI SETTI: Unpublished Report on Unstable Fragments.

rise to a Λ^0 particle which remains bound in a fragment. According to the Gell-Mann-Pais selection rules [3], from a hyperon such as the Σ^- reacting with a proton, a Λ^0 particle can be produced, either with a neutron, as may happen in the most simple way through the reaction:

$$\Sigma^- + \mathrm{P} \to \Lambda^0 + \mathrm{N} + Q \qquad Q \sim 70 \text{ MeV} \tag{3}$$

or, if we postulate the existence of a Σ^0 state that has not yet been observed, also with a γ-ray, through the reactions:

$$\Sigma^- + \mathrm{P} \to \Sigma^0 + \mathrm{N}, \qquad \Sigma^0 \to \Lambda^0 + \gamma + Q \qquad Q \sim 70 \text{ MeV}. \tag{4}$$

Although reaction scheme (4) is much less probable, it has been considered because it would offer one of the less indirect ways to test the existence of the Σ^0 state.

We easily see that our event may in fact be interpreted according to one of these possibilities. We have first of all to assume that the created Λ^0 remains bound in a fragment. Then, as in both cases the remaining reaction products are also neutral, they can easily escape observation, unless, as may happen in the case of the neutrons, they excite the residual nucleus and cause its subsequent evaporation. But also in this case, for such small energies, the probability that no ionizing prong will come out from the excited nucleus is rather high.

The possible values for the momentum of the fragment can be calculated according to the possible different values of its charge. In any case, this value is high enough as to make reaction (3) appear much more probable than reaction (4) also from this viewpoint. In fact, in this second case, the Λ^0 is produced with very low energy and the γ-ray has a great probability of escaping without interacting, so that it does not appear very likely that in such a reaction, a fragment with a high momentum could be produced.

From the preceding discussion we may conclude that evidence, although very far from being complete, is not in contradiction with the proposed assumptions, but favours reaction (3) as compared with reaction (4), in agreement with what should also be expected on probability grounds.

3. – Up until now, 11 other cases of nuclear capture of a negative hyperon with subsequent disintegration of the nucleus have been observed, five of which are quoted by JOHNSTON and O'CEALLAIGH [4] while the others

---

[3] M. GELL-MANN and A. PAIS: *Proc. of the Glasgow Conference* (Pergamon Press, 1954), p. 342.

[4] R. H. JOHNSTON and C. O'CEALLAIGH: *Nuovo Cimento*, **1**, 468 (1955).

have been comunicated at the Pisa Conference [5]; in all cases a rather small energy disintegration star is observed, and only in one case a visible π-meson is emitted. Owing to these general features, it may be therefore tempting to try to interpret all the hyperon captures as due to reactions of type (3) or (4). This would, on one hand, explain why generally in those events so little of the total energy available goes into excitation. On the other hand, according to the Gell-Mann Pais theory, only strong reactions such as (3) and (4) can happen between a Σ^- hyperon at rest and a nucleon; we should then expect that other weak interactions as simple transformations of the hyperon into a nucleon with or without emission of a pion, could not compete with them: so that the transformation into a Λ_0 of the Σ^- should occur in practically all cases.

The general features of this kind of events should then be the following:

According to reaction (3), the Λ^0 has about 35 MeV, as the total amount of 70 MeV is about half shared between neutron and Λ^0, so it can escape from the nucleus or may loose its energy in some scattering process with a nucleon. According instead to the much less frequent reaction (4), the γ-ray will take about all of the energy and the Λ^0 is directly produced with a very small energy.

Two different possibilities should then occur:

a) if the Λ^0 has conserved energy enough as it may happen in the first production process, it will escape from the nucleus, so that the disintegration star will be very small, as being due only to the recoil nucleons of the scattering process suffered by the neutron and the Λ^0 before escaping;

b) in the case where the Λ^0 has not energy enough to escape directly from the nucleus, either because it has lost its energy by scattering inside the nucleus or has been produced through reaction (2), it can either be emitted bound in an excited fragment or remain trapped in the original nucleus, where it will suffer « non-mesonic » or less probably from what we know at present, « mesonic decay »; the aspect of the star will then correspond to what is to be expected in each of these well known cases.

All 12 cases of hyperon capture known up until now are listed in the following Table I. The last one (Pd_2) is the event discussed in this paper. It is seen that 5 (Du_1, Du_2, Ro_1, Ge-Mi_1, Ge-Mi_2) of them are just small stars with a total energy of ionizing prongs less than 70 MeV, so that they can correspond to the case in which the Λ^0 escapes from the nucleus. Three other cases (Br_1 [6], $Gö_1$. Ber_1 [5]) have an energy greater than 100 MeV, and could cor-

[5] *Pisa Conference* (June 1955).

[6] M. FRIEDLANDER: *Phil. Mag.*, **45**, 418 (1954).

TABLE I.

Event	Primary Mass	Secondaries		
		Range μm	Nature	Total visible Energy MeV
Du_1	2170 ± 500	2000	p?	$\sim$ 20
		4	p?	
Du_2	2760 ± 500 $(\alpha - R)$	430	p?	$\sim$ 20
		343	p?	
		52	p?	
		15	p?	
		5	?	
	2400 ± 250 $(I - R)$	4	?	
Pd_1	2000 ± 300	short		$\sim$ 63 $\pm$ 5
		short		
		> 11000	p	
Br_1	2680 ± 350 $(\alpha - R)$ 2200 ± 350 $(I - R)$	> 13200	p	100 $\pm$ 15
Br_2	—	14900	π	29 } 30
		14	p	1 }
$Gö_1$			p	140
			p	
Ro_1	2380 ± 380 $(\alpha - R)$ 2410 ± 250 $(I - R)$	1240	p	16
Bo_1	2100^{+310}_{-210}	1733	$D - T$	$\sim$ 25 } 117
			$(e^+e^-) = \gamma$	92.2 $\pm$ 10.5 }
Be_1	2010^{+600}_{-400}		p?	109
			p?	
			p?	
			p?	
			p?	
			p?	
			p?	
$GeMi_1$	3000 ± 1600	262	p?	5
		4	p?	
$GeMi_2$	1500 ± 900	2500	p?	
		300	p?	
		132	p?	
		30	p?	35
Pd_2	4000 ± 1500 $(\alpha - R)$ 2000 ± 400 $(I - R)$	46	Fr	

respond to a non mesonic decay of the Λ^0 inside the nucleus; the Padua case (7), with a single proton of 60 MeV as ionizing prong could be ascribed either to the first or to the second of the preceding types, while the case Br_2 (8) could perhaps represent the mesonic decay of the bound Λ^0. Finally the case of Bol_3 is certainly the most peculiar, as an energetic γ-ray is observed to emerge from it; it might be explained according to the present ideas, either by assuming that the bound Λ^0, instead of the known ordinary way, decays into a neutron and a π^0, which is revealed by one of its decay photons, or, by assuming that the γ-ray is the decay product of a Σ^0 which should be obtained through reaction (4). The experimental value observed for the energy of the electron pair 92 ± 10 MeV is in approximate agreement with what should be expected for the energy of the photon in both of these cases.

When dealing with the capture of negative hyperons, we must of course keep in mind that we have also to expect to find captures of the Ξ^--particle. According to the Gell-Mann Pais selection rules, the only allowed reaction in this case should be

$$\Xi^- + \mathrm{P} \to \Lambda^0 + \Lambda^0 + Q\,, \qquad\qquad Q \sim 25 \text{ MeV}.$$

Such events which should be characterized by the presence of 2 Λ_0 should, according to the preceding discussion, present about the same qualitative features as the Σ^- capture events, and could be distinguished from these only in exceptional cases (as an example mesonic decay of both Λ^0 trapped in the nucleus, or non mesonic decay of both with great part of the energy going into ionizing prongs).

We can tentatively conclude that present experimental evidence on Σ^- captures is not in contradiction with the present hypothesis, although some of the cases observed among the very poor sample of events as yet available can be explained only through reactions that should not be expected to occur very frequently (*).

(7) M. Baldo, G. Belliboni, M. Ceccarelli and B. Vitale: *Suppl. Nuovo Cimento*, **12**, 289 (1954).

(8) M. W. Friedlander, D. Keefe and M. G. K. Menon: *Nuovo Cimento*, **1**, 482 (1955).

(*) *Note added in proof:* - After the present work has been submitted for publication, a paper by M. W. Friedlander *et al.* with similar discussions and conclusions about hyperon captures has appeared in the July issue of the *Nuovo Cimento* **2**, 135 (1955).

RIASSUNTO

Viene descritto un evento consistente in una particella lenta di carica unitaria e di massa superprotonica che si ferma in emulsione e dà luogo ad un frammento eccitato senza altri secondari visibili: tale frammento dopo un range di 46 μm, si disintegra dando luogo ad un protone di 110 MeV ed una traccia di carica unitaria con range di 300 μm che potrebbe essere tanto un protone come un deutone. L'evento si può interpretare come un iperone negativo che catturato da un nucleo dell'emulsione interagisce secondo la reazione: $\Sigma^- + P \rightarrow \Lambda^0 + N$, il Λ^0 prodotto rimanendo rinchiuso in un frammento instabile. Tutti gli altri eventi interpretati come catture di iperoni noti fino ad oggi vengono discussi per vedere se possono pure essere spiegati in base alla reazione precedente.

IL NUOVO CIMENTO Vol. II, N. 3 1° Settembre 1955

Observations on Unstable Fragments.

C. Castagnoli, G. Cortini and C. Franzinetti

Istituto di Fisica dell'Università - Roma
Istituto Nazionale di Fisica Nucleare - Sezione di Roma

(ricevuto il 14 Luglio 1955)

Summary. — Six events interpreted as disintegrations of hyperfragments are described. Five of these are associated with releases of energy which are consistent with the values measured by other authors and all could be interpreted as system of nucleons containing a Λ^0. One (event 6) can only be interpreted assuming that the bound hyperon is a Ξ^- or a more massive particle. This hyperfragment is emitted from a star from which a K-particle is also emitted. The hypothesis of a bound Ξ^- is briefly discussed together with possible disintegration schemes and the Q values relative to them.

1. – Introduction.

From the examination of $\sim 24\,000$ stars produced by cosmic rays in stripped G5 emulsions (1), we have found 6 events which can be interpreted as being due to the spontaneous decay of unstable heavy fragments of the same type as those observed first by Danysz and Pniewski (2).

In the following pages we shall give a description of these events and the results of the individual measurements. These data have been summarized in the table at the end. In the most favorable cases we have also attempted an interpretation of the observed event, but the interpretation was, unfortunately, unambiguous in only one case. In all the others a large variety of possible decay schemes had to be considered as the charge and the mass of

(1) The emulsions were exposed during the Sardinian Expedition 1953 at an altitude of about 25000 km for 7 hrs.

(2) M. Danysz and J. Pniewski: *Phil. Mag.*, **44**, 348 (1953).

the particles involved in the disintegration were known only within the rather wide limits of the experimental errors. Many of these schemes were found to be consistent with the observations although a large number of them seemed very unlikely according to our criterion of selection which we shall discuss later.

2. – Experimental Procedure.

In a nuclear emulsion events due to hyperfragments [3] appear as « double stars », i.e. two stars associated by an interconnecting track. We have selected only those events in which the nature of the interconnecting track, interpreted as an hyperfragment, could be established. All the cases in which the interpretation of the event in terms of other unstable particles was possible have been rejected.

This selection most probably introduces a systematic bias into the Z-distribution of the events. Highly charged hyperfragments have presumably shorter residual ranges than those of lower charge. The events due to short interconnecting tracks are the most difficult to interpret because in their identification one relies entirely on the measurements of charge, mass, energy and momentum of the particles of the secondary star. In many instances, one can not be sure that the event is due to a hyperfragment rather than a π^- or a K^--meson. Because of this, we have disregarded most of the « short » hyperfragments, and in doing so we believe that we have rejected preferably events due to highly charged hyperfragments.

As pointed out in the introduction, the identification of the « decay scheme » was not easy and rarely unambiguous. Only in one case could we establish the nature of all the ionizing particles involved and measure all the parameters of the decay process. In most cases, however, both the charge and mass of the particles involved could be established within ± 1 unit both of charge and mass.

Of the large variety of schemes which were acceptable on the basis of these measurements and also on that of conservation of momentum and energy, some were obviously unlikely as for example one starting from a fragment containing twice as many protons as neutrons (unless of very small Z). In the present work it has been assumed that the unstable fragment was either one of the known isotopes, irrespective of their lifetime for radioactive decay or

---

(3) We shall follow here a suggestion of M. GOLDHABER, calling hyperfragment an unstable nuclear fragment containing particles different from nucleons.

an isotope which could be obtained from the previous ones by varying Z by ± 1 and/or M by ± 1 (4).

In most cases it was not possible to establish by direct measurements the mass of the particles which produced the various tracks, but we were forced by other considerations to attribute to them different masses. In these cases the highest mass has been associated with the shortest track.

3. – Description of the Events.

3·1. *Mesonic decays.*

Event No. 1 (Fig. 1). The parent star is a 6+3n star. The average energy of stars of this size is ~ 3000 MeV. One of the six heavily ionizing tracks is brought to rest after a range of 5800 μm. Applying the gap-range method and the scattering-range method one obtains for the mass of this particle

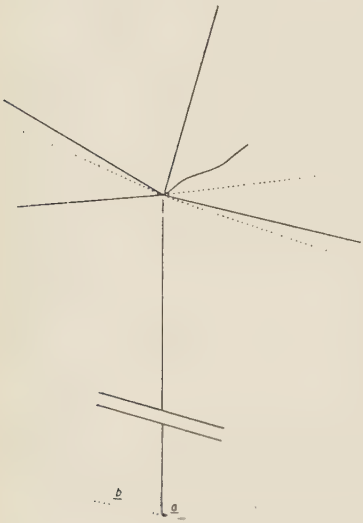

Fig. 1.

$m = 4.6 \pm 0.8\ M_p$ (gap method)

$m = 3.0 \pm 0.8\ M_p$ (scattering method)

M_p being the protonic mass. Its charge, as measured from δ-ray counting, is almost certainly not bigger than e. This leads us to assume that we are observing the track due to an excited ^3H or ^4H nucleus (5).

At the end of its range it disintegrates into two charged particles (a and b; see Fig. 1) going in opposite directions. One of these is highly ionizing and stops after 10.3 μm. The other escapes from the emulsions after a range of 6 mm. From ionization and scattering measurements averaged over all the 6 mm, we get

$$g/g_0 \quad 1.64 \pm 0.09\,, \qquad p\beta = 68 \pm 7 \text{ MeV/c}\,.$$

(4) This is intended to take into account the fact that a hyperfragment, intended as a fragment containing a bound hyperon, might contain a number of particles and charges different from any known nucleus, owing to the nature of the hyperon.

(5) ^3H-events have already been observed first by A. Bonetti, R. Levi Setti, M. Panetti, L. Scarsi and G. Tomasini: *Nuovo Cimento*, **11**, 210 (1954).

^4H-events have been suggested by Dalitz (private communication) and recently observed by J. H. Davies *et al.*: In the press.

It is reasonable to assume that this is a π-meson having an energy of 38.8 ± 4.5 MeV.

The two possible disintegration schemes are accordingly

(1) $$^3\mathrm{H}^* \to {}^3\mathrm{He} + \pi^- + Q_1$$

(2) $$^4\mathrm{H}^* \to {}^4\mathrm{He} + \pi^- + Q_2 \,.$$

The energy of the recoiling nucleus can be deduced either from momentum conservation or from its range. We get, in either case

	E (^{3}He)	E (^{4}He)
from momentum cons.	2.2 ± 0.3 MeV	1.62 ± 0.2 MeV
» range measur.	2.9 ± 0.7 MeV	3.2 ± 0.8 MeV

The two estimates are consistent for ^{3}He but hardly for ^{4}He. We shall assume then that the scheme (1) is correct. We obtain then, for the Q of the disintegration

$$Q = Q_1 = 41.2 \pm 4.7 \text{ MeV}$$

and for the quantity Δ defined by the equation ([6])

$$\Delta = m_{^3\mathrm{He}} + m_{\pi^-} + Q - m_{^3\mathrm{H}} - (m_{\Lambda^0} - m_n)$$

the value

$$\Delta = 4.4 \pm 4.7 \text{ MeV},$$

which gives for the binding energy of the Λ^0 the value $B_{\Lambda^0} \sim 1.7 \pm 4.5$ MeV. The time of flight (moderation time) is

$$\tau = 1.26 \cdot 10^{-10} \text{ s} \,.$$

Event No. 2 (Fig. 2.). The parent star is of type 4 + 10p. The energy associated with it can be estimated in two different ways: either from the total number of branches using the empirical formula of BROWN *et al.* (see further on, footnote ([12])) or from the angular distribution of shower prongs using the method suggested by CASTAGNOLI *et al.* ([7]).

With the first method one gets $E \sim 11$ GeV while with the second $E \sim$

([6]) See A. BONETTI, R. LEVI SETTI, M. PANETTI, L. SCARSI and G. TOMASINI: *Nuovo Cimento*, **11**, 330 (1954).

([7]) C. CASTAGNOLI, G. CORTINI, C. FRANZINETTI, A. MANFREDINI and D. MORENO: *Nuovo Cimento*, **10**, 1539 (1953).

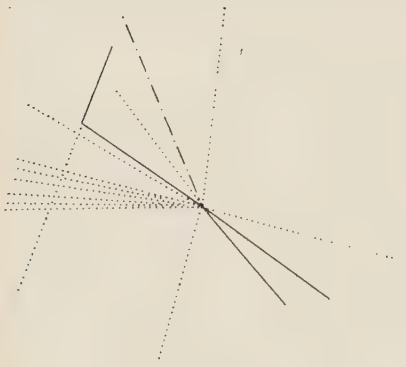

Fig. 2.

~ 70 GeV. The two values are to be considered as a lower and upper limit respectively.

One of the heavily ionizing particles coming out of this star stops after 281 μm and then decays emitting at least two ionizing particles. The three tracks are not co-planar which shows that one or more neutral particles are also emitted.

The interconnecting particle has a charge $Z = 2$ or 3 as measured from the δ-ray density and the taper-length. Taking $Z = 2$ or 3 alternatively, one can measure the limits within which its mass lies. This has been done using the constant sagitta method and we get

$$1.8 \leqslant m_f \leqslant 7.2 \ \mathrm{m_p} .$$

One of the decay products is brought to rest in the emulsion after 283 μm. Despite its short range, scattering measurements have been made and they suggest that it is a proton of 6.6 MeV.

The other particle escapes from the emulsion after 1.35 mm. Grain counting and scattering measurements give

$$g/g_0 = 2.3 \pm 0.1 , \qquad p\beta = 62 \pm 14 \ \mathrm{MeV/c} .$$

Most probably it is a π-meson of 37.5 ± 5 MeV.

The interpretation of this event, from the available data, is not unambiguous. The geometry of the two secondary tracks indicates that a momentum of 50 ± 2.4 MeV/c is carried away by invisible particles. These may be either neutral particles or a residual nucleus, or both. The first hypothesis is ruled out on the basis of charge conservation. The second one requires that the residual nucleus be heavy enough to have such a short range as to be undetectable; this seems to be plausible since even a fragment as light as ^{3}He would have a range of 0.7 μm in this case.

We shall assume that the disintegration of the hyperfragment is due to a bound Λ^0. In the following table we give the values of the Q's, of the binding energies B_{Λ^0} and of the moderation time of the hyperfragment obtained according to the different possible schemes.

Other schemes, involving heavier isotopes, can also be considered and they appear equally possible. Events of type (1) and (3) have been considered

already by CRUSSARD and MORELLET (8) and by HILL *et al.* (9).

TABLE I.

Scheme	Q (MeV)	B_{Λ^0} (MeV)	τ_z (s) (10)	τ_1 (s)
1) $^4He \rightarrow {}^3He + p + \pi^- + Q$	44.3 ± 5	5.4 ± 5	$4.4 \cdot 10^{-11}$	$1.6 \cdot 10^{-11}$
2) $^5He \rightarrow {}^4He + p + \pi^- + Q$	44.4 ± 5	3.6 ± 5	$4.5 \cdot 10^{-11}$	$1.75 \cdot 10^{-11}$
3) $^7Li \rightarrow {}^6Li + p + \pi^- + Q$	44.1 ± 5	6.6 ± 5	$9.1 \cdot 10^{-11}$	$1.9 \cdot 10^{-11}$

3·2. *Non-mesonic decay.*

Event No. 3 (Fig. 3). The parent star is of type 8+0n. One of the heavily ionizing tracks 187.5 μm long, is associated with a small star at the end of its range, having three prongs respectively 17.1 μm, 12.1 μm and 170 μm long. The particle responsible for the interconnecting track is too slow to allow the interpretation of the secondary star as due to a collision of a fragment with a nucleus of the emulsion. In fact the « tapering » of the track, typical of heavy particles approching the end of their range is clearly visible in the last 12 μm near the secondary star. The measurement of the δ-ray density suggests that it is a fragment of charge $Z = 4 \pm 1$ which disintegrates when at rest or almost at rest.

Fig. 3.

The interpretation of the event is, in this case very difficult as none of the decay products could be identified. If it is to be considered a non-mesonic decay, the visible energy is too small. In fact it is most probably smaller than 15 MeV. If the difference is to be filled by neutrons one would require at least two (and probably more) neutrons to carry away ~ 160 MeV. This seems unlikely.

One could assume that a π^0 is emitted. If the instability of the hyperfragments was due to a Λ^0 and a π^0 was emitted which escaped without losing

(8) J. CRUSSARD et D. MORELLET: *Compt. Rend.*, **236**, 64 (1953).

(9) R. HILL, E. SALANT, M. WIGDOFF, L. S. OSBORNE, A. PEVSNER, D. M. RITSON, J. CRUSSARD and W. D. WALKER: *Bull. Am. Phys. Soc.*, **29**, 60 (1954).

(10) The value of the moderation time could be calculated exactly if the charge of the fragment remained the same until it reaches the end of its range. It is well known that this does not happen because, by capture and loss processes the charge of the fragment may vary considerably. The values given in the fourth column (τ_z) have been calculated as if the Z was constant and therefore they represent only upper limits. The values given in the fifth column (τ_1) have been calculated assuming $Z = 1$. The true moderation time lies in between.

momentum, then the momentum of the recoiling fragment could not exceed 95.6 MeV/c. In our case $P \gtrsim 200$ MeV/c.

If the fragment was «almost at rest» but not exactly, things could be put right. For instance a Be nucleus of 200 MeV/c would have a residual range of less than 2 μm (assuming $Z = 4$).

One could remark that the probability of a decay in flight in the last few microns (say 10 μm) of range is small. In fact, if the life time of such a fragment is comparable with that of the Λ^0, this probability certainly lies between 1 and 6 percent, according to its charge. On the other hand, the chance that the fragment decays at rest and that the resultant visible momentum should lie just along or very close to the direction of motion of the fragment (as it appears to be in this case: $P_\perp \sim 0.1 P_\parallel$) [11] is also small. In our case it is less than 1 percent.

If the hyperfragment is a Beryllium nucleus, its moderation time lies between the limits:

$$\tau_z = 1.1 \cdot 10^{-10} \text{ s} \qquad \tau_1 = 1.5 \cdot 10^{-11} \text{ s} .$$

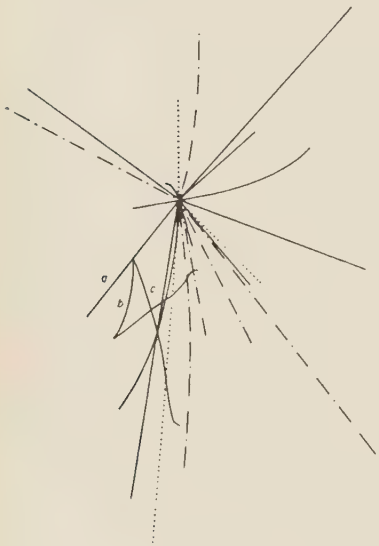

Fig. 4.

Event No. 4 (Fig. 4). The parent star is of type 18+3n. The unstable fragment produces a track 83.5 μm long. The density of δ-rays is consistent with a charge $Z = 6 \pm 2$. The shortness of this track does not allow one to decide whether the fragment was at rest or not when it disintegrated, but no «thinning down» was detectable near the end of its visible track.

The secondary star has three branches, the lengths of which are 81.4 μm, 355 μm and 157 μm respectively. The first has most probably charge $Z=2$; the second 2 or 1; the remaining one has charge 1 and is probably a proton.

If we assume that track *a* is due to an α-particle and the other two are due to protons, the total visible momentum parallel to the direction of motion of the fragment $P_\parallel$ is 274 MeV/c and the transverse momentum $P_\perp = 350$ MeV/c. The total momentum is then $P \simeq 450$ MeV/c and the energy $\simeq 25$ MeV.

---

[11] $P_\parallel$ indicates the component of the momentum parallel to the direction of motion of the hyperfragment determined at the point of decay; $P_\perp$ the component on the plane perpendicular to the direction of motion.

One or two neutrons could easily balance the « visible » momentum but then almost all the energy would be carried away by neutrons. As mentioned in the previous case, this does not seem likely. The ejection of a π^0 is ruled out as a π^0 having the required momentum would have an energy of ~ 400 MeV. Equally impossible on the same ground appears the ejection of a π^0 and one or more neutrons.

The difficulty could be removed without invoking the existence of heavier particles, if one assumed that the unstable fragment was not at rest when it disintegrated and is therefore responsible for a large part of $P_{\parallel}$. If this is true, the momentum to be accounted for is chiefly $P_{\perp}$. The observations are consistent with the following scheme:

$$^{9,10,11}\mathrm{B}^* \rightarrow {}^4\mathrm{He} + {}^3\mathrm{He} + {}^{1,2,3}\mathrm{H} + \mathrm{n} + Q,$$

where $Q \sim 170 \pm 20$ MeV. This value is to be taken as nothing more than an indication of an order of magnitude since it has been deduced assuming that $P_{\parallel} = 0$ in the system of the moving fragment.

The time of flight, considering all the possible alternatives and taking into account the variation of charge during the motion, should be within limits

$$0.9 \cdot 10^{-11} \quad \text{and} \quad 7.6 \cdot 10^{-11} \text{ s}.$$

Event No. 5 (Fig. 5). The parent star is of type 5+9p. The unstable fragment comes out of the star making an angle of 41° with respect to the direction of the primary proton. It stops after a range of 185 μm. From the measurement of the « taper length » and of the δ-ray density one can attribute a charge $Z = 4 \pm 1$ to it.

Fig. 5.

The secondary star is formed by three tracks respectively 3800 μm, 4360 μm and 10 μm long. Using the constant sagitta method we have obtained the following values for the masses of the particle producing the first two tracks:

$$M_a = 2100 \div 500 \ \mathrm{m_e}; \qquad M_b = 1870 \div 650 \ \mathrm{m_e}.$$

We have therefore assumed that they are protons. Their energies are then

$$E_a = 30.2 \text{ MeV}; \qquad E_b = 32.8 \text{ MeV}.$$

Owing to the large values of these energies, a π^0-decay of the fragment is ruled out, unless the unstable fragment is to be assumed bound to a very massive hyperon. Since the fragment was at rest when it exploded one is

led to assume that at least one neutron is emitted in order to balance the momentum. The simplest scheme is

$$^{7}\mathrm{Be}^{*} \rightarrow {}^{4}\mathrm{He} + {}^{1}\mathrm{H} + {}^{1}\mathrm{H} + \mathrm{n} + (166 \pm 10)\ \mathrm{MeV}\,.$$

The neutron should balance a missing momentum of 442 MeV/c, so carrying away ~ 100 MeV. If one expects the total release of energy to be 176 MeV one finds that the binding energy of the Λ^{0} in the ^{7}Be*-fragment is very close to that of a nucleon in the same nucleus. The quantity Δ, as defined at the beginning of this paragraph is

$$\Delta = 0 \pm 15\ \mathrm{MeV}\,.$$

Event	Parent star	Range (μm)	Angle with respect to the primary	Z	Moderation time (10^{-11} s)	Charged disintegration produc and their energy (MeV)		
Ro_1	$6+3n$	5800	—	1	12.6	^{3}He 2.55±0.8	π 38.8±4.7	
Ro_2	$4+10p$	281	15° (**)	2-3	4.4 — 1.6 4.6 — 1.7 9.1 — 1.9	^{1}H (6.6±0.2)	π (37.7±5.0)	^{3}He (* (0.44±0.0 ^{4}He (* (0.30±0.0 ^{6}Li (*) (0.2±0.02
Ro_3	$8+0n$	187.5	—	4±1	1.1 — 0.15	^{4}He (ass) (3.58)	^{3}H (ass) (1.51)	^{1}H (ass (6.5)
Ro_4	$18+3n$	83.5	—	6±2	7.6 — 0.9	^{4}He (ass) (12.6)	^{3}He (ass) (27.3)	^{1}H (ass) (7.2) ^{2}H (ass (6.2) ^{3}H (ass (4.7)
Ro_5	$5+9p$	185	41°	4±1	10 — 1.4	^{4}He (ass) (3.20)	^{1}H (30.2±6.3)	^{1}H (32.8±0
Ro_6	$26+9n$	1240	—	4±1	44 — 6	^{4}He (ass) (144) ^{3}He (ass) (127)	^{1}H (ass) 9.7 ^{3}He (ass) 21.8	^{1}H (ass 2.0

(*) As obtained from momentum conservation.
(**) The origin of the angular coordinate is adjusted so that 0° is the forward direction.

For the moderation time we get

$$0.8 \cdot 10^{-11} \leqslant \tau \leqslant 10^{-10} \text{ s} .$$

3·3. *Hyperfragment associated with an anomalous value of Q.*

Event No. 6 (Fig. 6). The parent star is of type 26+9n. From it, two particles have been emitted, which have produced tracks having the following characteristics:

eV)	Probable disintegration schemes	B (MeV)	Remarks
±5	$^3H \rightarrow {}^3He + \pi^- + Q$	1.7±5	
±5	$^4He \rightarrow {}^3He + {}^1H + \pi^- + Q$	5.4±5	
	$^5He \rightarrow {}^4He + {}^1H + \pi^- + Q$	3.6±5	
	$^7Li \rightarrow {}^6Li + {}^1H + \pi^- + Q$	6.6±5	
	$^9Be \rightarrow {}^4He + {}^3H + {}^1H + \pi^0 + n + Q$	—	
-180	$^9B \rightarrow {}^4He + {}^3He + {}^1H + n + Q$	—	Probable decay in flight
	$^{10}B \rightarrow {}^4He + {}^3He + {}^2H + n + Q$	—	
	$^{11}B \rightarrow {}^4He + {}^3He + {}^3H + n + Q$	—	
±10	$^7Be \rightarrow {}^4He + {}^1H + {}^1H + n + Q$	5.5±16	
500	$^{10}B \rightarrow {}^4He + {}^3He + {}^1H + 2n + Q$	—	For other possible schemes considered $Q \geqslant 340$ MeV The hyperfragment is emitted together with a K-meson

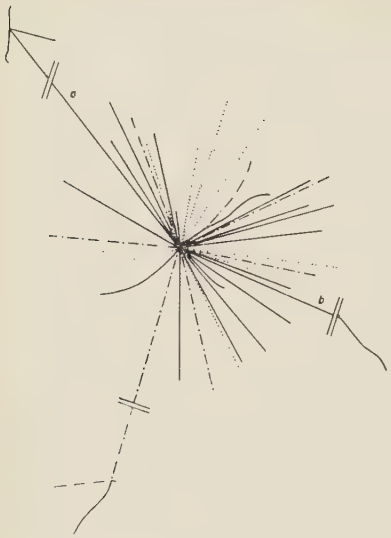

Fig. 6.

Track *a*). This track is 1.240 μm long and no gap is visible. From δ-ray counting and thin-down length we deduce a value of $Z = 4 \pm 1$. The value $Z = 3$ is difficult to accept as the secondary star is formed by 3 branches one of which is certainly due to a charge $\geqslant 2e$.

The mass of track *a*, as obtained from scattering measurements (constant sagitta method), is 9 ± 1 proton masses.

Two of the branches of the secondary stars are 239 μm and 40 μm long and if they are taken to be protons their energy would be 9.7 and 2 MeV respectively. The third track is 5120 μm long. The average density of δ-rays is $(1.7 \pm 0.2)/100$ μm which indicates a charge $Z = 2$. The mass can not be deduced from scattering and gap measurements because the track is too steep.

If it is to be assumed to be a ^{4}He its energy would be 144 MeV; if a ^{3}He, 127 MeV.

In order to interpret this event as due to a decaying hyperfragment one has to balance the visible momentum by assuming that either some neutrons or a very massive fragment are emitted in a convenient direction. The latter hypothesis does not seem acceptable: in fact, considering that the charge of the hyperfragment cannot be much higher than $5e$, a fragment capable of balancing the missing momentum could not have escaped detection.

We would like to point out that all the tracks of the secondary star form an angle of less than 90° with respect to the interconnecting track. Therefore, if one assumes that the particles of the secondary star are heavier than protons the missing momentum can only increase. Nor would it help to assume that the hyperfragment decayed when in flight as $P_{\|}$ points to the opposite direction with respect to the direction of motion of the hyperfragment itself.

Under these circumstances we have found it impossible to think of a disintegration scheme which would lead to a release of energy smaller than 340 MeV. This minimum value has been obtained from the scheme

$$^7\mathrm{Be}^* \rightarrow {}^3\mathrm{He} + {}^1\mathrm{H} + {}^1\mathrm{H} + k\mathrm{n} + Q\,.$$

The visible momentum totals 830 MeV/c. Assuming that two neutrons are emitted ($k = 2$), which come out as one unique particle of mass $2m_p$, to com-

pensate the observed momentum the total kinetic energy released would be 310 MeV; and to this one must add the binding energy ~ 30 MeV. Values of $k > 2$ seem unlikely and in any case it would be difficult to assume that all the neutrons are emitted in the same direction.

If one assumes for the mass the value obtained from direct measurements the following decay scheme seems probable

$$^{10}\mathrm{B}^{*} \rightarrow {}^{4}\mathrm{He} + {}^{3}\mathrm{He} + {}^{1}\mathrm{H} + 2\mathrm{n} + Q$$

with $Q \sim 500$ MeV.

Track *b*). This track, which is 2.120 μm long, is due to a particle which is brought to rest in the emulsion and decays into a light particle having a minimum grain density. Its mass, as measured from the scattering of the track is

$$M = 1.290 \pm 350 \ \mathrm{m_e}$$

and its charge is certainly 1. It is reasonable to assume that it is a K-particle.

4. – Discussion of the Results.

In Fig. 7 the frequency of occurrence of hyperfragments is plotted as a function of the energy of the parent star. The graph includes all published data available to us. The distribution is compared with that relative to hyperons.

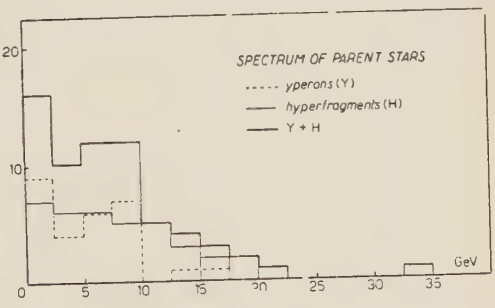

Fig. 7.

The energy of each star has been estimated using the formula

$$E_{\mathrm{MeV}} = 37 N_h + 4 N_h^2 + 10^3 N_s ,$$

where N_s is the number of shower particles and N_h the number of « gray » and « black » tracks. The first two terms are identical with the formula given by BROWN *et al.* [12] and the third takes into account the energy associated with the fast mesons.

As mentioned before, the 6 hyperfragments described here have been found

---

[12] R. BROWN, U. CAMERINI, P. FOWLER, H. HEITLER, D. KING and C. F. POWELL: *Phil. Mag.*, **40**, 862 (1949).

amongst ~ 24000 stars. If the observations were not affected by any experimental bias one could take the value $(6/2400) = 2.5 \cdot 10^{-4}$ as the frequency of occurrence of these events. Unfortunately the experimental method is biased and the value given here gives only the order of magnitude of the real frequency. It might be interesting to compare it with the value $8 \cdot 10^{-4}$ found by FRY *et al.* [13] and with the value $2 \cdot 10^{-3}$ predicted on theoretical grounds by JASTROW [14]. Fig. 8 shows the distributions in energy of stars associated with the emission of K- and τ-mesons, hyperons and hyperfragments and of all stars normalized to give the same number for an energy of 1 GeV. The slopes of the distributions are noticeably different: stars from which heavy particles are emitted have a much higher mean energy than ordinary stars. In addition, Y-H stars (i.e. stars emitting hyperons or hyperfragments) seem to be somewhat more energetic than K-stars. This statement is to be taken as provisional as the difference relies only on the normalization point which is affected by a large statistical error.

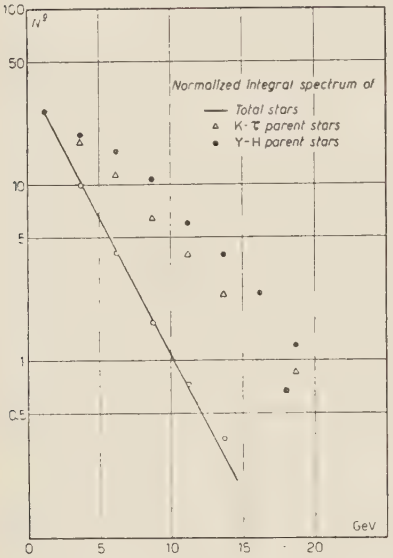

Fig. 8.

4·1. *Charge distribution of hyperfragments.* – In Fig. 9 we give the charge distribution of the hyperfragments. The shaded parts indicate the hyperfragments undergoing (charged) mesonic decay.

For $Z \geqslant 3$ the distribution is very similar to that of the ordinary fragments.

For low Z the hyperfragments are comparatively much less frequent than the fragments. Here again we would like to point out that the true distribution may have been deformed by an experimental bias. Consider for instance the decay of a hyperdeuteron. This particle would probably disintegrate according to one of the following schemes

$$
\begin{aligned}
{}^2\mathrm{H}^* &\to {}^1\mathrm{H} + {}^1\mathrm{H} + \pi^- - Q \\
{}^2\mathrm{H}^* &\to {}^1\mathrm{H} + \mathrm{n} + \pi^0 + Q \\
{}^2\mathrm{H}^* &\to {}^1\mathrm{H} + \mathrm{n} + Q \\
{}^2\mathrm{H}^* &\to {}^2\mathrm{H} + \pi^0 + Q .
\end{aligned}
$$

[13] W. F. FRY, J. SCHNEPS and M. S. SWAMI: *Disintegration of hyperfragments.* In press.

[14] A. B. JASTROW: *Phys. Rev.*, **97**, 179 (1955).

Events of this type, especially when in flight, are easily confused with ordinary disintegrations which are very frequent in emulsions exposed to cosmic rays, unless precise measurements are made. For $Z = 2$ the experimental bias should be much smaller than for $Z = 1$. If so Fig. 9 indicates that, at least for $Z = 2$, the relative frequency of hyperframgents is smaller than that of fragments.

The above graph also clearly indicates that mesonic decays are rarely associated with hyperfragments of $Z \geqslant 4$. This is in agreement with theory ([15]).

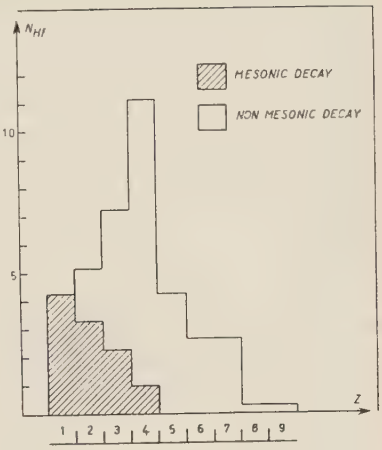

Fig. 9.

4·2. *Associated production of hyperfragments and* K*-mesons.* – The association of the production of charged hyperons and K-mesons has been observed by several research workers. To our knowledge, only one case of associated production of hyperfragments and K-mesons has been observed ([16]). In the present work one more example has been reported, which can be interpreted in this way.

It might be worth remarking that the « associated K's » described here as well as the others found in other laboratories both in association with hyperfragments or hyperons are all decaying at rest.

4·3. *Modes of decay of hyperfragments.* – Hyperfragments have been interpreted as a bound system formed by nucleons and other particles. If the other particle is assumed to be a hyperon, then according to the particular hyperon which is considered, the « visible » energy can vary within different limits. All but one of the cases reported here are consistent with the assumption that the bound hyperon is a Λ^0. One (event 6) is not and it could fit the hypothesis that a Ξ^- is bound and that all its available energy is released in the disintegration without the emission of any meson or hyperon. This process would supply 380 MeV which is above the « minimum » estimated in the previous paragraph. On the other hand such a low value has been obtained assuming that two neutrons are emitted as one particle twice as heavy. If a less restrictive hypothesis is made, the estimated energy goes up and for the scheme

([15]) W. Cheston and H. Primakoff: *Phys. Rev.*, **92**, 1537 (1953).

([16]) A. Debenedetti, C. M. Garelli, L. Tallone and M. Vigone: *Nuovo Cimento*, **14**, 466 (1954).

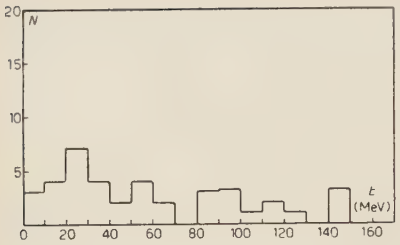

Fig. 10.

indicated at pag. 560 one gets a Q-value of the order of ~ 500 MeV. This would require an even more massive hyperon.

Events involving very massive hyperons in the disintegrations of hyperfragments have been observed before [see FRY *et al.* ([13])]. In fig. 10 the distribution in energy is given of the protons emitted in the disintegration of hyperfragments. The data have been collected from all the papers published on this subject and available to us.

* * *

We wish to thank Prof. A. MANFREDINI for her continuous interest and helpful advice; and Mr. SGARBI for his assistance in the numerical calculations.

RIASSUNTO

Si descrivono sei eventi interpretati come disintegrazioni di iperframmenti. Cinque di questi sono associati ad energie che sono in accordo con i valori misurati da altri autori e possono essere interpretati come sistemi associati a un Λ^0. Un evento (evento 6) può essere interpretato solo ammettendo che l'iperone legato sia uno Ξ^- o un iperone ancora più pesante. Questo iperframmento è emesso da una stella che emette anche un mesone K. L'ipotesi di uno Ξ^- legato è discussa brevemente insieme con i possibili schemi di disintegrazione e i valori delle Q relativi ad essi.

K-Meson and Hyperon Events.

C. Castagnoli, G. Cortini and A. Manfredini

Istituto di Fisica dell'Università - Roma
Istituto Nazionale di Fisica Nucleare - Sezione di Roma

(ricevuto il 14 Luglio 1955)

Summary. — 21 K-meson and 5 hyperon events observed in the Rome laboratory after the Padua Congress are described. Detailed discussion is given of the probable interaction of a negative hyperon at rest and of the decay in flight of a hyperon (Y-Ro$_7$) which shows a Q-value of 71 ± 5 MeV and is interpreted as due to a Ξ-particle.

1. – Introduction.

1. – In the present paper the results obtained in this laboratory on K-mesons and hyperons during the systematic investigation of heavy unstable particles in photographic emulsions are reported. This research has been performed after the Padua Congress (1954).

The events were observed in emulsion stacks ns. 21 and 29 exposed in flights ns. 15 and 20 of the Sardinia expedition 1953 [1]. All the events were observed during systematic scanning, except those which were found following the tracks of the parents stars. As a matter of fact we want to point out that all the parent stars were carefully examined in order to get some information on associated production.

The emulsion volume actually explored is about 70 cm^3. Scattering measurements were performed with special Koritska microscopes. As to the method of the constant sagitta the schemes used are those suggested by Dilworth *et al.* [2].

(1) J. Davies and C. Franzinetti: *Suppl. Nuovo Cimento*, **12**, 480 (1954).

(2) C. C. Dilworth, S. J. Goldsack and L. Hirschberg: *Nuovo Cimento*, **11**, 119 (1954).

The gap measurements were carried out with a special method improved in this laboratory, which has been described in other papers ([3,4]).

The range-energy curves used are those calculated by us and suggested to the Bureau of Standards of CERN ([5]).

The ionization-range and scattering-range measurements were always in good agreement.

2. – K-mesons.

Details of 21 K-mesons observed are shown in Table I. Only in five cases was it possible to perform a careful measurement of the $p\beta$ of the secondary particles. However, these measurements do not allow an exact identification of the decay particles. The events K-Ro_{11} and K-Ro_{19} are compatible with the decay scheme

$$K_{\mu 2} \rightarrow \mu + \nu + Q \qquad Q = 390 \pm 9 \text{ MeV} \quad (1)$$

([6]),

while the events K-Ro_{14} and K-Ro_{20} are compatible with the decay scheme

$$K_{\pi 2} \rightarrow \pi + \pi^0 + Q \qquad Q = 219 \pm 6 \text{ MeV} \quad (2)$$

([6]).

Mass measurements by the constant sagitta method were performed on all the primaries. All the results are in agreement with a single mass value. The weighted mean is

$$m_{\text{scatt}} = 970 \pm 40 \ m_e .$$

The measurement of the mass by the ionization at the end of the range can be made successfully only for very flat tracks. In fact our extensive calibration work ([4]) shows that the mass extimate is reliable only for tracks (at the end of their range) having an angle of dip φ less than $10^0 \div 12^0$. The actual measurement was performed for 9 primary tracks having $\varphi < 25^0$ (see Table I). However, the most reliable mean value of the mass is obtained if we consider only the 4 primary tracks of Table I for which $\varphi < 12^0$ (K $Ro_{6,10,11}$ and $_{14}$). So doing we get

$$m_{\text{ion}} = 966 \pm 35 \ m_e .$$

([3]) C. CASTAGNOLI, G. CORTINI and A. MANFREDINI: *Nuovo Cimento* **2**, 301 (1955).

([4]) G. BARONI and C. CASTAGNOLI: *Suppl. Nuovo Cimento*, **12**, 364 (1954).

([5]) G. BARONI, C. CASTAGNOLI, G. CORTINI, C. FRANZINETTI and A. MANFREDINI: CERN BS. 9.

([6]) J. DAVIES *et al.*: *Preprint on Bristol, Dublin, Genova, Milano, Padova results.* H. S. BRIDGE, H. DE STAEBLER jr., B. ROSSI and B. V. SREEKANTAN: *Nuovo Cimento*, **1**, 874 (1955).

TABLE I.

PRIMARY					SECONDARY			
-part-icle	Parent star	Range (mm)	Masse in m_e $\langle\theta\rangle - R$	Masse in m_e Gaps	length (mm)	g/g_0	$p\beta$ (MeV/c)	Observations
-Ro_5	11+3 n	25.8	1060±260	—	4.0	.92±.04	—	$M_k = 850\pm70$ from g/g_0 versus R
-Ro_6	4+3 n	4.47	1320±250	950±60	4.0	1.00±.04	—	
-Ro_7	20+9 p	2.22	430	—	—	1	—	Primary very steep associated with hyperon Ro_3
-Ro_8	1+1 p	0.65	1240±430		-	-		
-Ro_9	—	36.6	1020±180	—	—	1.2	—	$M_k = 1090\pm30$ from g/g_0 versus R
-Ro_{10}	3+2 n	37	1060±150	940±70	4.7	—	—	
-Ro_{11}	8+5 n	31	1130±160	1090±100	36.0	1.05±.04	210±14	
-Ro_{12}	15+10 n	38	725±120	980±90 *	20.0	.96±.07	—	
-Ro_{13}	35+8 p	4.5	1170±280	1400±400*	—	1.17±.08	120±24	
-Ro_{14}	—	47	810±120	1260±300	38.8	.97±.08	180±10	
-Ro_{15}	26+9 n	2.12	1200±350	—	—	—	—	Associated with hyperfragment Ro_6
-Ro_{16}	1+0 n	7.75	960±270	—	-	—	-	
-Ro_{17}	15+6 n	23	850±130	1130±200*	—	.95±.10	—	
-Ro_{18}	7+6 p	9.8	980±270	990±100*	15.7	1.18±.10	—	
-Ro_{19}	36+16 p	20	1035±270	—	57.8	.95±.04	200±10	
-Ro_{20}	20+14 α	22	1040±250	980±100*	40.0	1.07±.07	185±12	
-Ro_{21}	4+3 p	0.83	1280±450	—	—	1.00±.04	—	
-Ro_{22}	5+0 p	7.05	895±155	—	—	—	--	
-Ro_{23}	5+4 n	37.2	810±130	—	16.1	1.07±.07	—	
-Ro_{24}	—	15.6	820±115	--	—	—	—	
-Ro_{25}	26+13 p	9.2	925±125	—	4	—	--	

(*) The dip of this track is $> 12°$.

Taking into account also the K-mesons previously reported [7], we get, from constant sagitta measurements

$$m_{scatt} = 960 \pm 36\ m_e\,,$$

and from gap measurements (2 more «flat» K-meson tracks: K-Ro_3 and Ro_4):

$$m_{gap} = 965 \pm 25\ m_e\,.$$

[7] E. AMALDI, G. CORTINI and A. MANFREDINI: *Suppl. Nuovo Cimento*, **12**, 210 (1954).

The errors quoted are standard deviations obtained by the conventional methods.

No interaction of K-mesons at rest (σK) has been identified with certainty, while the research of K-mesons interaction in flight is still in progress.

3. – Hyperons.

Details of five hyperons observed are reported in Table II. The first of them (Y-Ro$_3$) has already been communicated ([8]) and we will not discuss it here.

PRIMARY

Event	Range (mm)	MASS				Parent star	β-decay
		$\langle\theta\rangle - R$	Ion. $- R$	Ion. $- \langle\theta\rangle$	Gap Length		
Y-Ro$_3$	1.25	$2\,800^{+1500}_{-900}$			2670 ± 500	20.9 p	at rest
Y-Ro$_4$	1.53	$2\,720^{+1100}_{-700}$			$2\,400 \pm 500$	33.13 n	»
Y-Ro$_5$	2.41	—	—	$1\,980 \pm 280$	—	22.5 n	0.304 ± 0.010
Y-Ro$_7$	6.30			$2\,640 + 300$ (*)	$2\,390 \pm 460$ (*)	16.14p	$0.278 \pm .007$
Y-Ro$_6$	18.33	$2\,380 \pm 380$	$2\,410 \pm 250$	—	$2\,700 \pm 200$	9,7 n	at rest (?)

(*) See text.

3·1. *Decay at rest.* – The particle Y-Ro$_4$ decays at rest. The secondary track shows a grain density $g = (1.32 \pm 0.03) g_0$ and the scattering measurement gives $p\beta = 132 \pm 6$ MeV/c. By means of our calibration curves, we can identify the secondary particle as a π-meson, having a kinetic energy of 86 ± 10 MeV. Interpreting this event according to the scheme

$$\Sigma^{\mp} \to \mathrm{n} + \pi^{\mp} + Q \tag{3}$$

we get $Q = 103 \pm 10$ MeV, in agreement with the accepted value for reaction (3): $Q = 109 \pm 1$ MeV ([9]).

([8]) C. CASTAGNOLI, G. CORTINI and A. MANFREDINI: *Nuovo Cimento*, **12**, 464 (1954).

([9]) M. W. FRIEDLANDER, D. KEEFE and M. G. K. MENON: *Nuovo Cimento*, **1**, 482 (1955).

3·2. *Decays in flight.* – Events Y-Ro$_5$ and Y-Ro$_7$ can be certainly interpreted as hyperons decaying in flight, and in both cases the decay particle can be identified as an L meson from ionization and p measurements.

Event Y-Ro$_5$ can be interpreted according to the scheme (3) and it does not disagree with the known Q value (see Table II).

The Y-Ro$_7$ is a case of « cascade » decay in flight of a hyperon: as far as we know, it is the third case identified in photographic emulsions and therefore we think it worthwhile to discuss it with some detail.

A particle comes out from a star (16, 14, p) giving a gray track, having a mean angle of dip of $\sim 15°$, which disappears after a path 6.30 mm long.

SECONDARY

nge m)	g/g_0	$p\beta$ (MeV/c)	T (MeV)	Mass	Q (MeV)
±0.037	black	—	19.0±0.25	proton	117±1.3
28	1.32±0.03	132±6	86±10	L-meson	103±10 (*)
3.7	0.85±0.05	234±32	—	L-meson	130±40
5.25	1.36±.06 (*)	~ 70	—	L-meson	71±5
1.24	—	—	16.0	proton	—

(*) See text.

From the final point of the gray track, a near minimum track originates, making an angle $\theta = 63.4° \pm 1.0°$, with its line of flight. The angle was measured and the correction for distortion ($\sim 1°$) was calculated in the conventional way.

The measurement of ionization on the primary track has been made by means of the variable r, that is the total gap length per cell (of 200 μ). The value of r changes appreciably along the track. Five indipendent measurements on different sections of the track were made. Each of them by means of our calibration curves [3] gave a value of $r - R/M$. In this way, it was possible to construct a diagram (Fig. 1) plotting the measured values of r against the *visible* residual range X. Obviously, if R_0 is the (unknown) residual range at the point of decay, one has:

$$X = R - R_0 = M_r - R_0 : \qquad r = \frac{X}{M} + \frac{R_0}{M} .$$

The straight line in Fig. 1 was fitted to the experimental points by the least square method; the slope and the addittive constant of it give at once:

$$(4) \qquad M_Y = 2390 \pm 460\ m_e\ ; \qquad \frac{R_0}{M_Y} = 5760 \pm 460\ \mu m/m_p\ .$$

The last value corresponds to a final velocity (at the point of decay):

$$(5) \qquad \beta_Y = 0.278 \pm 0.007\ .$$

This value has been checked by the conventional grain counting method, which gives excellent agreement.

The scattering was also measured. Since the statistical error in the $p\beta$ determination is of same order of the variation of $p\beta$ about its mean value, as calculated by the above data, we can reasonably neglect this variation, and take the value of β in the middle point of the track as it can be deduced by the described procedure. By the straight line of Fig. 1 we deduce $\bar{r} = 8200\ \mu m/m_p$, which for a proton mass would give $p\beta = 90.3 \pm 2.7$ MeV/c. As the measured value is

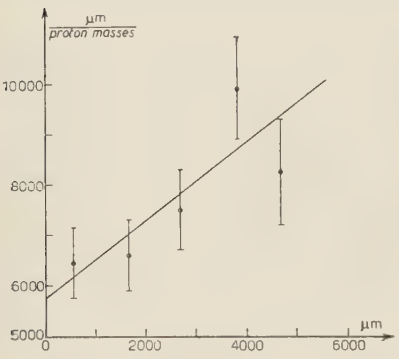

Fig. 1.

$$p\beta = 130 \pm 14\ \text{MeV/c}\ ,$$

we deduce

$$(4') \qquad M_Y = 2640 \pm 300\ m_e\ .$$

The two values of the mass (4) (4′) are not statistically independent, so that we cannot combine them by a weighted mean. A more complex method ought to be employed in order to obtain the best value of M_Y. However we can be satisfied with the observation that the two values are in good agreement within the statistical errors and that if one recalculates R_0/M_Y from the data of Fig. 1 using the M_Y value (4′) one gets 5740 microns/proton masses, in complete agreement with value (4). In other words, the value of R_0/M_Y (*not* of R_0!) is rather insensitive to the value of M_Y.

Measurements on the secondary track give the following results:

scattering:	$p\beta \sim 70$ MeV/c	
grain density:	$g/g_0 = 1.36 \pm 0.06$	(that is $\beta_L = 0.76$)
mean gap length:	$\bar{w} = 2.40 \pm 0.07$	that is

$$(6) \qquad \beta_L = 0.756 \pm 0.013\ .$$

The error in the scattering measurement is large, due to distortion. Again the 2 ionization measurements agree very well with each other; both of them were accurately checked by calibration measurements on plateau tracks of the same angle of dip ($\sim 40^\circ$).

In conclusion the primary and secondary particles are certainly a hyperon and an L-meson. If we want to interpret the event in terms of known processes we must choose among the Σ-decay (eq. (3)) and the « cascade » Ξ-decay:

$$\Xi \to \Lambda^0 + \pi + Q \,. \tag{7}$$

The best choise is easily made by calculating the corresponding Q-values. From the θ, β_Y and β_L values quoted above (eqs. (5) and (6)) and with the assumption that the neutral secondary is a neutron, one gets $Q_{(\text{eq. 3})} = 73 \pm 5.0$ MeV. The discrepancy with the known value is large enough to rule out completely the decay scheme (3). On the contrary, taking for the neutral secondary the Λ^0 mass, one gets

$$Q_{(\text{eq. 7})} = 71 \pm 5.0 \text{ MeV} \,. \qquad \text{(Event Y-Ro}_7\text{)}.$$

The error quoted is the standard deviation calculated on a purely statistical basis and taking into account the errors of the calibration measurements. It arises almost completely from the value (6) of β_L, since the kinematics of the event is such that the Q-value is almost insensitive to small changes in β_Y.

Up to now—to our knowledge—9 events have been attributed to the decay scheme (7). In the 7 cases observed in Wilson chambers [10-15] the π was always negative.

The two cases in photographic emulsion (events Br_2 and Br_3) were recently interpreted as Ξ-decays [9,16], in the light of the present cloud-chamber evidence. At the Padua Conference they had been considered as 2 of the only 3 events showing definite disagreement from the known Q-value of the

---

[10] R. Armenteros, K. H. Barker, C. C. Butler, A. Cachon and C. York: *Phil. Mag.*, **43**, 597 (1952).

[11] E. W. Cowan, C. D. Anderson, R. B. Leighton and V. W. J. Van Lind: *Phys. Rev.*, **92**, 1089 (1953).

[12] E. W. Cowan: *Phys. Rev.*, **94**, 161 (1954).

[13] W. B. Fretter and E. W. Friesen: *Phys. Rev.*, **96**, 853 (1954).

[14] R. Armenteros, B. Gregory, A. Lagarrigue, L. Leprince-Ringuet, F. Muller and Ch. Peyrou: *Suppl. Nuovo Cimento*, **12**, 327 (1954).

[15] H. W. Arnold: Thesis, 1955.

[16] C. Dahanayake, P. E. Francois, Y. Fujimoto, P. Iredale, C. J. Waddington and M. Yasin: *Nuovo Cimento*, **1**, 888 (1955).

Σ-decay ([17]). The third event was the It_1 event ([18]), having $Q = 72 \pm 20$ MeV. If we include it in our considerations, the summary of all the known possible Ξ events is that shown in Table III. It is seen that the Q-values from Wilson chambers and photographic emulsions show good agreement. Besides, as we have seen, by this interpretation all the « anomalous » Q-values presented at the Padua Conference disappear. These two circumstances seem to make very reasonable indeed the assumption that the 4 photographic emulsion events are due to the same particle which (suffering a two-body decay) gives the « hyperon cascade » in the cloud chamber, although the secondary Λ^0 decay has never been found in the nuclear plate events.

TABLE III.

Instrument	Cloud Chamber					Photographic emulsion			
Author	COWAN	FRETTER *et al.*	ARMENTEROS *et al.*	ARNOLD	COWAN *et al.*	FRIEDLANDER *et al.*	DAHANAYAKE *et al.*	BARRETT	Present work
Reference and event	([12])	([13])	([10])	([15])	([11])	([9]) Br_3	([16]) Br_2	([18]) It_1	Ro_7
Q (MeV)	67 ± 12	66 ± 6	$< 60^{-15}$	63 ± 9	60 ± 15	59 ± 11	63 ± 27	72 ± 20	71 ± 5

Under this assumption, the best values of the Q in eq. (4) and of the Ξ-mass can be calculated from the weighted mean of the Q's in Table III. The results are

$$Q = 67.2 \pm 3.1 \text{ MeV} \qquad \text{(weighted mean)},$$

$$M = 2586 \pm 6.5 \ m_e .$$

3·3. – Event Y-Ro_6 consists of a proton track 1.24 mm long coming out from the end point P of a track 18.3 mm long, which is associated with a star (9, 7, n) and shows all the features of a proton or a hyperon track at the end of its range. A small blob is present at the point P. The mass of the primary particle has been measured by 3 different methods, with the following results:

constant sagitta scattering	$M = 2380 \pm 380 \ m_e$
grain density near the star	$2410 \pm 250 \ m_e$
gap length all along the track . . .	$2700 \pm 200 \ m_e$

([17]) P. ASTBURY *et al.*: *Suppl. Nuovo Cimento*, **12**, 448 (1954).
([18]) P. H. BARRETT: *Phys. Rev.*, **94**, 1328 (1954).

All the measurements on the secondary track are consistent with a proton coming to rest inside the emulsion.

Now, the event can be interpreted in term of known processes as follows:

a) Negative hyperon coming to rest and giving rise to a star consisting of a blob and one single proton track.

b) Decay of a Y-particle according to the scheme (3). In this case, the decay must take place in flight, as the range of the proton is definitely different from the expected one (1.67 mm) ([8]).

Moreover, the blob at point P must be due either to an accidental coincidence, or to a sudden change of the line of flight of the primary particle immediately before the decay. If this is the case, the angle θ between the two tracks ($\sim 90°$), is subject to a large uncertainty. In any case, the possibility *b*) cannot be ruled out by measuring the possible residual range of the primary particle by any known method ([19]). In fact, even for $\theta = 90°$, the residual range necessary to reduce the range from 1.67 mm to 1.24 mm would be only 65 μm. However, due to the existence of the blob, and to the results of mass measurements, we feel that the interpretation of event Y-Ro_6 as a negative hyperon (possibly a Ξ^--particle) interacting at rest is rather more probable.

In our laboratory another event, which can be interpreted as an interaction at rest of a hyperon, was found: but the geometry of this event is poor and therefore the measurements performed as in the previous case are less significant. The assumption of a simple scattering of a proton track, though improbable, cannot be excluded. In other two cases a particle at rest associated with a small blob was observed. The mass seems to be greater than the proton mass. Since in these cases the interpretation of the event is based exclusively on mass measurements, one must be very careful about it. Further very accurate measurements are still in progress.

([19]) G. Baroni, G. Cortini and A. Manfredini: *Nuovo Cimento*, **1**, 473 (1955).

RIASSUNTO

Si descrivono 21 mesoni K e 5 iperoni osservati nel laboratorio di Roma dopo il Congresso di Padova (1954). In particolare viene discussa la probabile interazione di un iperone negativo alla fine del suo percorso e il decadimento in volo di un iperone con un $Q = 71 \pm 5$ MeV che viene interpretato come dovuto ad una particella Ξ.

IL NUOVO CIMENTO Vol. II, N. 3 1° Settembre 1955

Self-Diffusion in Liquid Indium and Tin.

G. Careri and A. Paoletti

Istituto di Fisica dell'Università - Roma

(ricevuto il 16 Luglio 1955)

Summary. — Self-diffusion measurements have been made on liquid indium and tin over a wide range of temperatures, and a small but systematic deviation from the ordinary Arrhenius equation has been detected. After the customary discussion of the Stokes-Einstein and Eyring equations, new expressions are worked out in the quasi crystalline picture of the liquid state following the solid state treatment of the diffusion processes. It is then shown how the deviations from the Arrhenius equation are accounted for by a direct interchange mechanism of nearest neighbours, due to a ring movement of two atoms.

1. – Introduction.

Our present knowledge of the liquid state is still so poor, that a sound reference to the crystalline state can be useful to obtain a picture of it. Metals are fairly simple molecular systems and have been extensively studied in the solid state; much has yet to be learnt, however, of their properties in the liquid state.

The transport properties, such as viscosity and diffusion, show such a large change at the melting point as to awake interest. Furthermore self-diffusion deals with the system in a state so close to that of equilibrium and can be so satisfactorily described in the solid state in terms of microscopic quantities, as to raise the hope that self-diffusion measurements in the liquid metal can provide valuable information from the direct comparison of properties in the two states.

The self-diffusion coefficient in liquid tin and indium has therefore been measured in this laboratory over a wide temperature range. Details of the experimental method and first results for indium in a small temperature

range have already been published (1) (latter referred to as I) and some results on tin very briefly announced (2). The object of this paper is to give a full account of the indium and tin experimental data, and to use them to discuss the atom movements and the picture of the liquid which therefrom arises.

2. – Experimental Technique and Results.

The experimental technique has already been described in I and will not be referred to here. The schematic arrangement is shown in Fig. 1, and the main operation consists in allowing the two half rods of active and inert metal to follow a thermal cycle, during which diffusion takes place. The solidified rod is then cut into small segments, and from the penetration curve of the active component the diffusion coefficient is evaluated.

After our first measurements described in I, we found that a small temperature gradient, as 0.1 °C cm^{-1}, was enough to cause turbolence when the lower part of the capillary was warmer than the upper part. Therefore a small positive temperature gradient from the top to the bottom was always maintained during the runs (3).

It was also realized that the finite length of the capillary could play a more disturbing role than was expected. Actually in order to reach a good accuracy one has to choose the diffusion time long enough to have a non steep penetration curve, but then the reflection at the capillary end can become appreciable. For instance in Fig. 2*a* and 2*b* is shown a good ordinary penetration curve, and in Fig. 3 a typical example of reflection at one end. As a matter of fact the penetration curve of Fig. 3 gave too high a diffusion coefficient and was discarded.

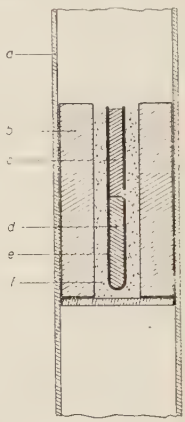

Fig. 1. Schematic view of the diffusion cell. Three Chromel-Alumel thermocouples were placed at different heights near the capillary, but are omitted in this scheme. *a*) Vacuum pipe of stainless steel. *b*) Copper tube *c*) Radiactive rod. *d*) Inactive rod. *e*) Porcelain capillary. *f*) Quarz sand. The capillary inner diameter was ranging from 1 to 2 mm, and the lenght was about 160 mm.

(1) G. Careri, A. Paoletti and F. Salvetti: *Nuovo Cimento*, **11**, 399 (1954).

(2) G. Careri and A. Paoletti: *Suppl. Nuovo Cimento*, **1**, 161 (1955); *Nuovo Cimento*, **1**, 517 (1955).

(3) This is in agreement with a recent paper by G. I. Taylor: *Proc. Phys. Soc.*, **67**, 557 (1954).

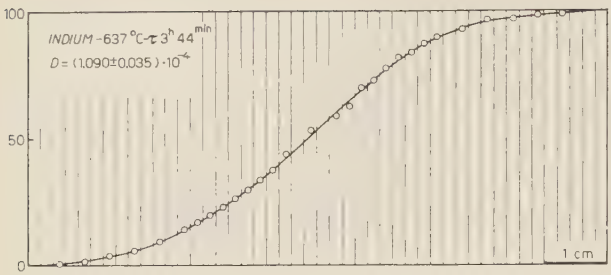

Fig. 2*a*. – A typical good penetration curve for Indium, for which diffusion affected only the central part of the rod. The ordinates represent the activity and the abscissae the position of the center of the section of rod.

For the above reason the indium runs no. 9, 12, 11 of I have been now discarded, and no. 8, 23 have been retained. The new activation energy gave rise to a little difference in the average temperature of the thermal cycle, and a revised calculation of the D values gave new figures, still within the experimental error. These new values together with the new results are given in Table I. One may note that the standard error assumed in the single runs may be too large, as shown from the good reproducibility of the results. The materials used were the same in both the new and the old runs.

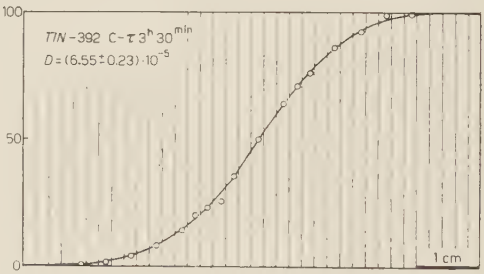

Fig. 2*b*. – A typical penetration curve for Tin.

The same procedure was applied to detect the activity of tin (4) sections. ^{113}Sn was employed as tracer (5), which decays in ^{113}In with a half-life $T_1 = 112$ d emitting a β_1^+ of 0.05 MeV and a γ_1 of about 0.09 MeV, and further decays in ^{113}In with $T_2 = 1.73$ h and $\gamma_2 = 0.39$ MeV. Since ordinary mica counters were used, with a wall thickness of $2 \div 3$ mg/cm^2, it was the second disintegration that we detected, and not the first one. However, since the samples were left for at least one day after the diffusion experiment before being counted, we were sure to follow the diffusion of the tin atoms and not of the indium ones. The results are shown in Table II.

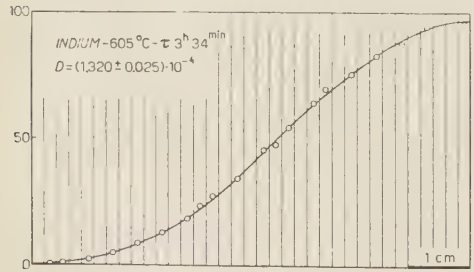

Fig. 3. – An Indium penetration curve reflected at the active end.

(4) *Spectroscopically pure tin has been employed.* Manufactured by Johnson, Matthey & Co.

(5) Obtained by the Atomic Energy Res. Establishment, Harwell, England.

In Fig. 4 all the above results are shown in typical log D versus $1/T$ plot. The systematic deviation from a straight line, namely the simple Arrhenius law

$$D = D_0 \exp [- H_0/RT] \tag{1}$$

is evident.

TABLE I. – *Indium Self-Diffusion coefficients.*

Run	T °C	$10^3\ 1/T$ °K	Duration	$D \cdot 10^5$ cm^2 s^{-1}
8	254.9	1.894	9^h 20^{min}	4.84 ± 0.27
23	285.6	1.790	8^h 00^{min}	5.45 ± 0.16
34*a*	451.6	1.380	3^h 20^{min}	8.64 ± 0.14
34*b*	451.6	1.380	3^h 20^{min}	8.61 ± 0.21
35	635.0	1.101	7^h 40^{min}	10.8 ± 0.35
38	492	1.32	2^h 19^{min}	9.32 ± 0.20

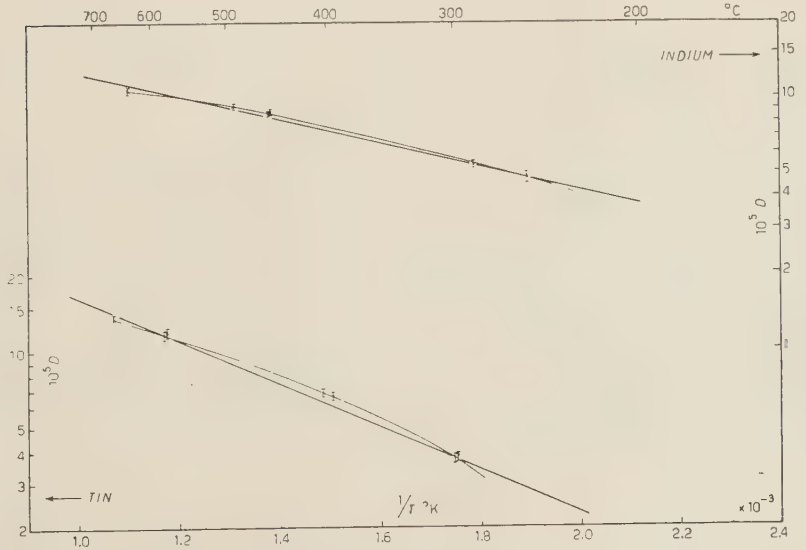

Fig. 4. – The self diffusion coefficient of liquid Indium and Tin plotted versus $1/T$. The straight line is the eq. (1).

If however one wants to fit the experimental data by eq. (1), one gets by the least square method D_0 and H_0 values which are given in Table III.

TABLE II. – *Tin self-diffusion coefficents.*

Run	T °C	$10^3\ 1/T$ °K	Duration	$D \cdot 10^5$ cm^2 s^{-1}
2	400.0	1.485	$7^h\ 00^{min}$	6.80 ± 0.20
4*a*	299.0	1.748	$9^h\ 10^{min}$	3.74 ± 0.10
4*b*	299.0	1.748	$9^h\ 10^{min}$	3.63 ± 0.10
8*a*	581.0	1.171	$4^h\ 40^{min}$	11.6 ± 0.33
8*b*	581.0	1.171	$4^h\ 40^{min}$	11.7 ± 0.40
22	662.0	1.070	$2^h\ 53^{min}$	13.5 ± 0.64
38	392.3	1.503	$3^h\ 30^{min}$	6.55 ± 0.24

TABLE III. – *The Arrhenius constants.*

	D_0 cm^2/s	H_0 cal/mole
Indium	$4.25 \cdot 10^{-4}$	2 200
Tin	$13.90 \cdot 10^{-4}$	4 000

3. – The Customary Discussion.

The present status of the theory of liquids does not provide a satisfactory description of the diffusion processes; the work of KIRKWOOD and of BORN and GREEN do not give explicit expressions for the diffusion coefficient to be applied practically. The only expressions for D so far available are the well known Eyring and Stokes-Einstein equations.

The Eyring expression has been derived postulating a liquid as a mixture of atoms and vacancies. The viscosity and diffusion coefficients are then expressed in terms of the activated state properties, which are difficult to evaluate, but can be combined to get

$$D = \frac{kT}{2r\eta}, \tag{2}$$

where η is the viscosity coefficient and r a length close to the atomic radius.

The failure of this expression to deescrib self diffusion in liquid metals is known from the work of HOFFMANN (6) in liquid mercury.

Also in our case if one attempts to calculate r from (2), one gets values too large and also dependent on the temperature. In Table IV the radii thus calculated are compared with the Pauling radii and with that calculated by the Stokes-Einstein relation

$$D = \frac{kT}{6\pi r \eta} . \tag{2'}$$

It is well known that this equation cannot be applied to a sphere of atomic size; however, following the work of KIRKWOOD it is gratifying to see that it holds to a moderate extent.

TABLE IV.

	Metallic radii (PAULING)	Radii calculated (*)		
		T °K	EYRING	EINSTEIN
Indium	1.62 Å	429	8.06 Å	0.91 Å
		1000	19.20 Å	2.04 Å
Tin	1.40 Å	505	14.00 Å	1.48 Å
		1000	8.20 Å	0.87 Å

(*) The viscosity values have been taken for Tin from SAUERWALD: *Zf. Allg. Anorg. Chem.*, **157**, 117 (1926) and for indium from Da Andrade, Private Communication.

4. – Quasi-Crystalline Treatment.

With the aim of getting a rough picture of the diffusion processes in liquid metals, we shall now try to apply the customary description of diffusion, widely used in the solid state physics, to a quasi cristalline liquid.

We make a brief reminder here that diffusion in a crystal can be described as a random walk processes (7), and denoting by a the lattice distance, τ the mean time of stay between jumps and γ a geometrical factor, one can derive

$$D = \gamma a^2/\tau . \tag{3}$$

(6) R. R. HOFFMANN: *Journ. Chem. Phys.*, **20**, 1567 (1952).
(7) C. ZENER: *Imperfections in nearly perfect crystals* (New York, 1952), p. 289.

The quantity τ can be derived by application of the activated state method, but we prefer here to follow a direct kinetic method ([8]). For the processes which will interest us, we can write

$$\frac{1}{\tau} = \nu P \,, \tag{4}$$

P being the probability of the process, and ν the Debye frequency, mainly the number of times per second the atom strikes the potential barrier.

Of the basic mechanism leading to diffusion in a solid, only the vacancies and the direct interchange mechanism can operate in a metallic liquid thought as quasi crystal and therefore will next be subjected to analysis.

If diffusion goes via vacancies, denoting by E_m the energy required for motion of an atom into an adjacent imperfection, by E_v the energy to create the imperfection using the Boltzmann statistics one has obviously

$$P = P_m P_v = \exp\left[-(E_m + E_v)/kT\right] . \tag{5}$$

The energies E_m and E_v must be considered as sligthly dependent on the temperature. In a face centered cubic crystal, denoting now by δ the interatomic distance, eqs. (3), (4) and (5) give

$$D = D_0 \exp\left[-H/RT\right] \tag{6}$$

$$E_m + E_v = H/N(1 - \eta T) \tag{6'}$$

$$D_0 = 2\delta^2 \nu \exp\left[\eta H/R\right] . \tag{6''}$$

As well known a possible diffusion mechanism is also the interchange of neighbours by a ring displacement. But due to the thermal agitation, rings with large n have a small probability. Therefore we shall limit ourselves in the following to considering only rings of two atoms, namely direct interchange of one atom with one neighbour.

If the diffusion goes via direct interchange of neighbours by a ring of 2 atoms ([9]), one can write P as the product of a steric factor $(1/6)^2$ to take into account that the two atoms have to mouve in right phase, times the probability P_E the system to have an energy $\geq$ the peak of the potential barrier, times a factor of 4 since we have two rings which rotate in two directions. Therefore

$$P = 4(1/6)^2 P_E \,. \tag{7}$$

([8]) D. LAZARUS: *Phys. Rev.*, **93**, 973 (1954).
([9]) R. M. BARRER: *Trans. Farad. Soc.*, **37**, 590 (1941).

The quantity P_E can be easily obtained [10] for a system of n harmonic oscillators classically excited, or more generally by n freedom degrees contributing each by two square terms to the energy of the classicals system, and is

$$P_E = \exp[-E/RT] \sum_0^{n-1} \frac{1}{n!} (E/RT)^n . \tag{8}$$

The analogue of eq. (8) for two quantized oscillators has been derived in Appendix I; using (23) and (3), (4) and (7) one gets

$$D = D_1 \{\exp[-\vartheta/T] + (1 - \exp[-\vartheta/T])(1 - \varepsilon T) H/R\vartheta\} \exp[-H/RT] , \tag{9}$$

$$E = \frac{H}{N}(1 - \varepsilon T) , \tag{10}$$

$$D_1 = 8 \left(\frac{1}{6}\right)^2 \delta^2 \nu \exp[\varepsilon H/R] , \tag{11}$$

$$\vartheta = \frac{\nu h}{k} . \tag{12}$$

The eq. (11) stands for a f.c.c. structure; for a b.c.c. structure, the factor 8 must be replaced by 16/3.

So far for the perfect crystal diffusion. Now in order to apply the above treatment to a quasi crystal, we have to make some small changes. We first notice that eq. (3) has been derived with the assumption that P is so small that the occurrence of simultaneous diffusion processes for close neighbours can be neglected. But in a liquid the diffusion coefficient is known to be much larger than in a solid, therefore one is in considerable doubt whether to apply this assumption. However a numerical inspection of eqs. (3) and (4) for our experiments, gives P values reaching at the most a few units times 10^{-2}, which seems to be small enough to let the simultaneous occurrence of diffusion processes for close neighbours to be nearly neglected. We therefore believe eq. (3) to be fairly good for a quasi crystal, but we shall correct the jumping probability P by a factor $(1 - 3P)^2$ to take into account the fact that both the neighbours in question may be engaged in a similar exchange process with other neighbours. The factor 3 arises from the fact that of the 12 or 8 neighbours of the f.c.c. or b.c.c. crystals, only about 3 can combine their velocity components to form a ring of two.

In the case of diffusion via vacancies the probability P should be corrected

[10] R. H. Fowler and E. A. Guggenheim: *Statistical Thermodynamics* (Cambridge, 1939), p. 495.

by a factor $(1 - NP_v)(1 - NP_m)$ where N is the number of close neighbours, to take into account the fact that the vacancies may be filled by the other surrounding atoms during the mouvement of the atom in question, and that more vacancies can crowd around the same atom. Of course one may modify eq. (3) in this simple way only if the above factors remain small corrections.

Further in solid state physics the temperature dependence of ν and δ are neglected since the exponential plays the dominant role, but in the case of liquids the activation heat H is much smaller, and these dependences must be considered. The interatomic distance will change with the temperature by the ordinary expansion law

$$\delta = \delta_0(1 + \alpha T) , \tag{13}$$

where α is the thermal expansion coefficient. It is more difficult to express the change of ν, which is due to the variation of intermolecular forces with the interatomic distances, namely the specific volume V, with the temperature. In a crystal one can use the well known Gruneisen approximation and write

$$\nu = \frac{\text{cost}}{V^\gamma} , \tag{14}$$

where γ is about 2. Some calculations performed by RICE [11] on a system of argon atoms, show that one has nearly the same variation of ν with the intermolecular distance, in the most extreme cases of a face centered cubic arrangement and of a linear chain of oscillators. One can therefore use the Gruneisen approximation also for a liquid, though as a blurred copy of a crystal. We shall therefore write in the above (7) and (11)

$$\delta_0^2 \nu = \delta^2 \nu_0 / (1 + \alpha T)^{3\gamma - 2} . \tag{15}$$

Before concluding this section, a few words should be added about the quantities ε and η. Without going here into a detailed discussion of these quantities in the solid state problems, we note that in the liquid state H will be found so small that the inaccuracy of the quantity $\exp[\varepsilon H]$ will not be too serious. One has in general

$$-\frac{H}{N}\varepsilon = \partial E/\partial T = (\partial E/\partial r)(\partial r/\partial T) = r_0 \alpha (\partial E/\partial r) . \tag{16}$$

Assuming the dominant terms in $\partial E_m/\partial r$ to arise from the closed shell re-

[11] O. K. RICE: *Phase transformations in Solids* (New York, 1941), p. 229.

pulsion energy, we write as usual this repulsion energy

$$E = \frac{c}{r^n}, \tag{17}$$

where n is about 12, and get simply

$$\varepsilon = \alpha n . \tag{18}$$

It is more difficult find an expression for η, due to the term $(\partial E_r/\partial r)$ and since it will not be needed for the following discussion, we only note that $\eta > \varepsilon$.

5. – Determination of the Mechanism of Diffusion.

In this section we shall try to interpretate our experimental results from the expression of the foregoing section.

a) We shall first consider the vacancies mechanism. A mere application of eq. (6), (6′), (6″) corrected by (13) shows at once very poor fitting of the experimental points, and H values of 1260 and 4000 cal/mole, for indium and tin respectively. We remember that for solid indium H was 17.900 cal/mole ([12]), and therefore conclude these energies not to be enough in the liquid to create and to move a vacancy. Furthermore, an application of eq. (3) and (4) shows that P ranges from 10^{-3} to 10^{-2}. If then all the vacancies are supposed to have been created at the melting, and P_v to be about 10^{-2} as should be expected from the increase of specific volume, one would find P_m values about 10^{-1} or higher. In this situation all close neighbours would crowd in the vacancy, and the correction $(1 - NP_m)$ would be found to be too large to maintain any value in the treatment itself. We see therefore that a mere application of the vacancy mechanism to a liquid, considered as a crystal with many more empty sites, gives rise to a nonsense. This is a different way of understanding the failure of the Eyring treatment. We may notice in this connection that the equilibrium properties also are badly described by a cell method with empty cells. The idea that diffusion can be due to local fluctuation of density cannot be discarded but the way to treat the problem should be entirely different.

b) We shall now try to interpret our data by a mechanism of direct interchange between neighbours. We start from eq. (3) and (4) and correct

([12]) H. G. Drickamer and R. E. Eckert: *Journ. Chem. Phys.*, **20**, 13 (1952).

eq. (3) for the occurrence of multiple processes, and write for a f.c.c.

$$D = \frac{\delta_0^2 \nu_0}{(1 + \alpha T)^4} 2P(1 - 3P)^2 , \tag{18}$$

and a similar expression for the b.c.c., where the factor 2 is replaced by 4/3 [13]. By equation (18) the P values have been obtained from the corresponding experimental points and can be fitted by the P_E expressions derived in the Appendix. The value of ν_0, δ_0 and α used in the computation are given in Table V in c.g.s. units.

TABLE V.

	ν_0	δ_0	α
Indium	*a*) $2.08 \cdot 10^{12}$	*b*) $3.3 \cdot 10^{-8}$	*c*) $3.8 \cdot 10^{-5}$
Tin	*a*) $3.33 \cdot 10^{12}$	*b*) $3.2 \cdot 10^{-8}$	*d*) $3.3 \cdot 10^{-5}$

a) Calculated from the Debye Temperature of the elements, as reported by EUCKEN: *Handbuch der Experimental Physik*, Vol. VIII.
b) W. HUME-ROTHERY: *Institute of Metals Monograph*, n. 1, London, 1947.
c) D. D. WILLIAMS, R. R. MILLER: *J.A.C.S.* **72**, 3821 (1950).
d) *International Critical Tables.*

We shall first approximate to the exchange by the « Two oscillators » mechanism, as shown above for the solid state case by eq. (19), and we write

$$P = 4 \left(\frac{1}{6}\right)^2 \exp\left[\varepsilon H_1/R\right] \cdot \cdot \{\exp\left[-\vartheta/T\right] + (1 - \exp\left[-\vartheta/T\right])(1 - \varepsilon T) H_1/R\vartheta\} \exp\left[-H_1/RT\right] . \tag{19}$$

At present there is no way of calculating H_1 from quantum mechanics, and so we shall treat it as a parameter. Furthermore eq. (18) for ε and the rather rough $(1/6)^2$ value for the steric factor are not reliable enough, and so it is better to fit an expression like

$$P = A_1 \{\exp\left[-\vartheta/T\right] + (1 - \exp\left[-\vartheta/T\right])(1 - \varepsilon T) H_1/R\vartheta\} \exp\left[-H_1/RT\right] , \tag{20}$$

where A and H_1 are to be considered as parameters, and any inaccuracy in ε can now be neglected. By a method of best fitting the « experimental »

[13] For the γ values of Eq. (3), see G. J. DIENES: *Phys. Rev.*, **89**, 185 (1953).

parameters A, and H_1 have been found from the experimental P data for different lattice structure and ε values, and are given in Tables VI and VII.

TABLE VI. - *Experimental H_1 values for the « Two oscillators » model in* cal/mole.

	f.c.c.		b.c.c.	
ε	$3.6 \cdot 10^{-4}$	$5 \cdot 10^{-4}$	$3.6 \cdot 10^{-4}$	$5 \cdot 10^{-4}$
Indium	3.550	3.700	4.000	4.200
Tin	5.400	5.600	5.750	5.950

The experimental D data are well fitted by equation (18) as shown by Fig. 5 and 6. Here again we remind that the indicated error of the single experimental points is too large, as the reproducibility of some points indicates.

TABLE VII. – *Experimental A values for the « Two oscillators » model in* cm^2/s.

	f.c.c.		b.c.c.	
ε	$3.6 \cdot 10^{-4}$	$5 \cdot 10^{-4}$	$3.6 \cdot 10^{-4}$	$5 \cdot 10^{-4}$
Indium	0.107	0.129	0.227	0.271
Tin	0.178	0.222	0.349	0.439

For Indium the fitting is excellent both for b.c.c. and f.c.c. structures, but for Tin, which exhibits the larger deviation from an Arrhenius equation and therefore provides a more sensitive test, the b.c.c. structure proves to be clearly the best. Further the fitting seems not to depend much from the ε

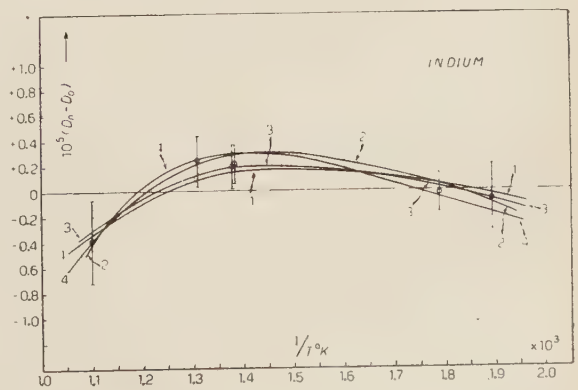

Fig. 5. – The fitting of experimental Indium points, by a direct interchange mechanism, in the « two oscillators » treatment. The difference between the D values and the ones calculated from the Arrhenius equation are plotted in the ordinates. The curves correspond to the following assumptions: 0) Arrhenius equation. 1) F.c.c. structure, ($\varepsilon = 3.6 \cdot 10^{-4}$). 2) B.c.c. structure, ($\varepsilon = 3.6 \cdot 10^{-4}$). 3) F.c.c. structure. ($\varepsilon = 5.0 \cdot 10^{-4}$). 4) B.c.c. structure, ($\varepsilon = 5.0 \cdot 10^{-4}$).

values. To get another independent test of this treatment one can attempt to calculate the A values by the above derived expression, to get

$$A = 4\left(\frac{1}{6}\right)^2 \exp\left[\varepsilon H/R\right], \tag{21}$$

where H is the experimental value, and try to compare for every ε the A calculated by (21) with the one experimentally found in Table VII. The calculated values are given in Table VIII, and a comparison with the corresponding experimental values of Table VII proves that the order of magnitude is always the right one, but also here the b.c.c. structure gives almost perfect agreement. Here again the influence of ε seems not to be serious.

TABLE VIII. – *Calculated A values for the « Two oscillators » model in* cm^2/s.

	f.c.c.		b.c.c.	
ε	$3.6 \cdot 10^{-4}$	$5 \cdot 10^{-4}$	$3.6 \cdot 10^{-4}$	$5 \cdot 10^{-4}$
Indium	0.208	0.276	0.224	0.302
Tin	0.294	0.454	0.316	0.498

To summarize, one can state that eq. (18) can describe really well our diffusion data both for Indium and Tin by a direct interchange mechanism, and seems also sensitive enough to the assumed lattice structure of these liquid metals. It is comforting to see that the X rays diffraction results [14] also indicate a coordination number close to 8 for these metals in our range of temperature so also suggesting a local structure similar to a b.c.c. lattice.

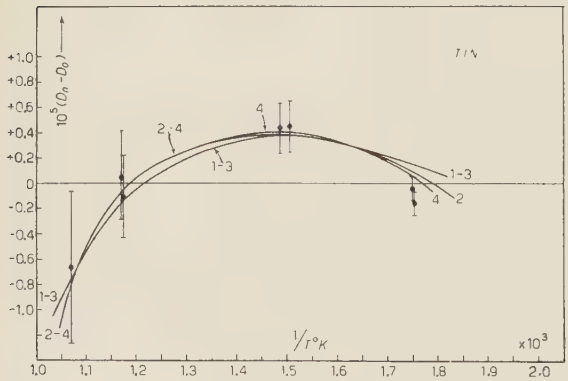

Fig. 6. – The analogous of Fig. 5, for Tin.

This description might then be said to have succeeded completely, but we are well aware of the crude assumption involved in the « Two oscillators » treatment, namely the assumption that the energies of the two oscillators are simply

[14] H. HENDUS: *Zeits. f. Naturfor.*, **2**, 505 (1947).

summed up to overcome the potential barrier. This assumption is difficult to discuss without going into details of the quantum mechanises of the many atoms movements. We shall therefore try to describe things by the opposite rough model, namely assuming the pair of rotating atoms to behave as a hindered rigid rotator. By the help of the eq. (26) derived in the Appendix we write now:

$$(22)\quad \begin{cases} P = 4\left(\frac{1}{6}\right)^2 \dfrac{z}{\int_0^z \exp[y^2]\,dy} \\ z = [2H_2(1-\varepsilon T)/RT]^{\frac{1}{2}}, \end{cases}$$

and try to fit the experimental P data, as we did before for the two oscillators model. Both for indium and tin the fitting for a f.c.c structure is extremely poor. Instead for a b.c.c. structure the fitting can be very good, as shown in Fig. 7 and 8, if a convenient ε value is chosen. The H_2 experimental values are given in table IX; it is seen that they are smaller by a factor nearly (1/2) than the H_1 values. The reason must be found in the assumed model of the rigid

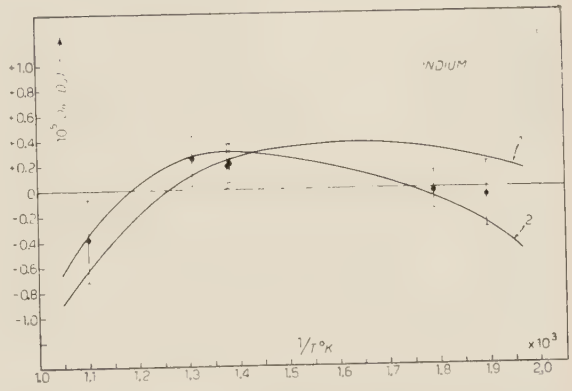

Fig. 7. The fitting of experimental Indium points by direct interchange mechanism, in the « *Rigid rotator* » treatment. The curves are: 1) B.c.c. structure, ($\varepsilon = 3.6 \cdot 10^{-4}$). 2) B.c.c. structure, ($\varepsilon = 5.0 \cdot 10^{-4}$).

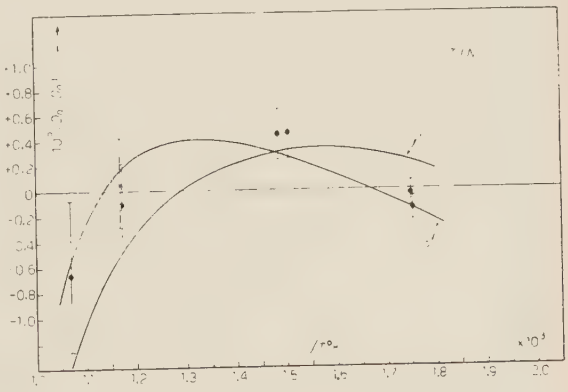

Fig. 8. – The analogous of fig. 7 for Tin.

TABLE IX. – *Experimental H_2 values for the Rigid « Rotator » model in* cal/mole.

	b.c.c.	
ε	$3.6 \cdot 10^{-4}$	$5 \cdot 10^{-4}$
Indium	2.200	2.500
Tin	3.200	3.700

rotator, which contributes classically by two square terms to the energy of the system, and therefore behaves like one single oscillator in the P_E expression.

We conclude that in spite of the roughness of the treatment, the direct interchange mechanism can describe things adequately, but too much importance must not be attached to the detailed expressions and to the values of the constants involved.

6. – Concluding Remarks.

The success of the direct exchange mechanism in describing these experiments suggests a model for the liquid state, very close to the quasi crystalline one, where couples of atoms are rotating in a random fashion. The probability of exchange is so small, or in other words there are so few rotating couples, that if the quasi crystalline structure is admitted, this is not destroyed by these ring movements. Furthermore the probability of having complete cycles is so small that the result will be a random mixing of the atoms by this ring movements. The boiling point of indium and tin are respectively 1 450 and 2 270 °C; extrapolation of the above equations gives P values nearly constant above the maximum temperatures reached in these experiments. One should therefore expect the same mechanism to hold over the full range of stability of the liquid phase for the systems in question at atmospheric pressure. We have to remember that for indium and tin the critical temperature is so extremaly high, that one deals with a kind of liquid which is always close to the solid. Approaching the critical point the number of rings should increase, but at the same time the steric hindrances will increase too and the resulting motion will probably be more brownian-like than ordered in rings. Therefore we can not assume this exchange mechanism to hold for any liquid under any condition, but on the above ground we are led to think it possible to operate also in other liquids close to the melting point, or otherwise particularly ordered systems. In this connection the most recent interpretation of FEYNMAN [15] of the Landau rotons as molecular rings, and the DE BOER and COHEN [16] application to rings of two atoms as the most important term in the rings spectrum to explain the behaviour of the superfluid state of liquid helium, are very gratifying.

[15] R. P. FEYNMANN: *Progress in low Temperature Physics, I* (Amsterdam, 1955), p. 17.

[16] J. DE BOER and E. G. COHEN: *Physica*, **21**, 79 (1955).

APPENDIX

In the following we shall give detailed expressions of P_E for some models of molecular systems.

a) *Two quantum excited Oscillators.* – Neglecting the zero point energy, the probability of having one of the two oscillators in the quantum state m and the other in n is

$$P_{n,m} = (1 - \exp[-\vartheta/T])^2 \exp[-n\vartheta/T] \exp[-m\vartheta/T] .$$

We have first to find out the number of systems for which the total energy of the two oscillators is exactly E. One has:

$$\begin{aligned}
&(1 - \exp[-\vartheta/T])^2 \cdot 1 \exp[-E/RT] \\
&(1 - \exp[-\vartheta/T])^2 \exp[-\vartheta/T] \exp[-((E/RT) - (\vartheta/T))] \\
&\quad . \quad . \quad . \quad . \quad . \quad . \quad . \quad . \quad . \quad . \quad . \quad . \quad . \\
&(1 - \exp[-\vartheta/T])^2 \exp[-E/RT] \cdot 1 .
\end{aligned}$$

Therefore if $s = E/R\vartheta$, this number is

$$s \exp[-E/RT] .$$

We have then to evaluate

$$P_E = (1 - \exp[-\vartheta/T])^2 \sum_{s_0 = E_0/R\vartheta}^{\infty} s \exp[-s\vartheta/T] .$$

The sum can be easily written, and after some manipulations one gets

$$P_E = \exp[-E/RT] \{\exp[-\vartheta/T] + (1 - \exp[-\vartheta/T])E/R\vartheta\} . \tag{23}$$

Expanding as a function of ϑ/T, one has:

$$P_E = \exp[-E/RT] \left\{ 1 + E/RT - \left(\frac{\vartheta}{T}\right)\left(1 + \frac{E}{2RT}\right) + \ldots \right\},$$

wich approaches the classical expression if $T \gg \vartheta$

$$P_E = \exp[-E/RT] \{\exp[-\vartheta/T] + (1 - \exp[-\vartheta/T]E/R\vartheta\} .$$

b) *Three or more quantum oscillators.* – The expression of P_E for a system th ree oscill ators can be derived in a similar way to the above for a system

of two. After some long and cumbersome arithmetic one gets:

$$(24) \qquad P_E = \frac{\exp[-E_0/RT]}{2}\left\{\left[\left(\frac{E_0}{R\vartheta}\right)^2 - 2\left(\frac{E_0}{R\vartheta}\right) + 1\right]\exp[-2\vartheta/T] - \right.$$

$$- \left[2\left(\frac{E_0}{R\vartheta}\right)^2 - 2\left(\frac{E_0}{R\vartheta}\right) - 1\right]\exp[-\vartheta/T] + \left(\frac{E_0}{R\vartheta}\right)^2 +$$

$$\left. + (1 - \exp[-\vartheta/T])^2\left(\frac{E_0}{R\vartheta} + \frac{\exp[-\vartheta/T]}{1 - \exp[-\vartheta/T]}\right)\right\},$$

wich can also be expanded as

$$P_E = \exp[-E/RT]\,\{1 + E/RT + \tfrac{1}{2}(E/RT)^2 - $$

$$- \vartheta/T\,[1 + \tfrac{3}{2}[E_0/RT] + \tfrac{1}{2}[E_0/RT]^2 + \ldots]\}\,,$$

and approaches the classical expression if $T \gg \vartheta$.

If the temperature is high enough, one can therefore use as an approximation the classical expression multiplied by a factor $(1 - \vartheta/T)$. This is supposed to be true also for a system of more than three oscillators.

c) *Hindered rigid rotator.* – If E is the peak of the energy barrier for rotation, the quantity P_E is exactly the sum of probabilities of the states of free rotation of the hindered rotator. Therefore:

$$P_E = \frac{1}{f(T)}\int_{J_0=(E/RT\alpha)^{1/2}}^{\infty} 2J\exp[-J^2\alpha]\,\mathrm{d}J = \frac{1}{\alpha f(T)}\exp[-J_0^2\alpha]\,,$$

where $\alpha = \vartheta/T$, being the characteristic temperature of the rotator, and $f(T)$, the partition function of the hindered rotator, this partition function can be derived classically whenever $T \gg \vartheta$. Assuming for the potential energy a cosine form of period π, the Hamiltonian will be:

$$H = \frac{1}{2I}\left(P_\vartheta^2 + \frac{P_\varphi}{\sin^2\vartheta}\right) - E\cos^2\vartheta$$

and the partition function will be:

$$f(T) = \frac{1}{a}\int_0^{\pi}\exp[(2\cos^2\vartheta - 1)]E/RT\sin\vartheta\,\mathrm{d}\vartheta = \frac{1}{a}\,\frac{\exp[-E/RT]}{(2E/RT)^{\frac{1}{2}}}\,\mathcal{J}(E/RT)\,,$$

where

$$\mathcal{J}(E/RT) = \int_0^{(2E/RT)^{1/2}}\exp[v^2]\,\mathrm{d}v$$

therefore one has

$$(26) \qquad P_E = (2E/RT)^{\frac{1}{2}}\,\mathcal{J}^{-1}(E/RT)\,.$$

d) *Hindered non rigid rotator.* – Suppose the interchange between the rotational and vibration energy to be such as to allow one to sum them simply to get the total energy E. Then the probability P_E will be the sum of the states wich becomes that of free rotation by the energy release of the vibrator, plus the state of free non rigid rotators.

Neglecting the interaction between rotation and vibration one has

$$P_E = \frac{1}{f'(T)}\left\{\sum_{n=0}^{n=E/\hbar\nu} \exp\left[-n\vartheta/T\right] \int_{E-n\hbar\nu=J_0\theta/T}^{\infty} 2J \exp\left[-J^2\theta/T\right] \mathrm{d}J + \right.$$

$$+ \sum_{n=E/\hbar\nu}^{\infty} \exp\left[-n\vartheta/T\right] \int_{0}^{\infty} 2J \exp\left[-J^2\theta/T\right] \mathrm{d}J =$$

$$\left. = \frac{1}{f'(T)} \frac{T}{\theta} \exp\left[-E/RT\right] \left\{\frac{E}{R\vartheta} + \frac{1}{1-\exp\left[-\vartheta/T\right]}\right\}\right\},$$

where $f'(T)$ is the partition function of the non rigid rotator, and θ the caracteristic temperature of the free rotator, of the same inertia moment. Still neglecting any interaction between rotation and vibration one can write

$$f'(T) = (1-\exp\left[-\vartheta/T\right])^{-1} f(T)\,,$$

and using the $f(T)$ above derived for the rigid rotator, one derives:

$$P_E = (2E/RT)^{\frac{1}{2}}(E/R\vartheta + 1)(1-\exp\left[-\vartheta/T\right])\mathcal{J}^{-1}(E/RT)\,,$$

and taking the first term of the expression in ϑ/T

$$P_E = (2E/RT)^{\frac{1}{2}}(E/RT + \vartheta/T)\mathcal{J}^{-1}(E/RT)\,. \tag{28}$$

RIASSUNTO

Sono state effettuate misure di autodiffusione in stagno ed indio liquidi in un largo intervallo di temperatura, ed è stata rilevata una piccola ma sistematica deviazione dalla ordinaria equazione di Arrhenius. Dopo la usuale discussione in termini delle equazioni di Stokes-Einstein e di Eyring, sono ricavate nuove espressioni nell'approssimazione quasi cristallina dello stato liquido, seguendo l'analoga trattazione dei processi di diffusione nello stato solido. Viene allora dimostrato come della deviazione dalla equazione di Arrhenius si possa rendere conto mediante un meccanismo di scambio di atomi vicini, con un moto ad anello di due atomi.

IL NUOVO CIMENTO Vol. II, N. 3 1° Settembre 1955

The Formalism of Second Quantization in Quantum Statistical Mechanics.

R. Gatto

Istituto Nazionale di Fisica Nucleare - Sezione di Roma
Istituto di Fisica dell'Università - Roma

(ricevuto il 24 Luglio 1955)

Summary. — The advantage is pointed out of using an invariant formulation of quantum statistical mechanics with respect to unitary transformations of the hilbertspace. Second quantization allows one to give an invariant formulation of the quantummechanical grand ensemble. It provides a simpler framework for the use of transformation theory, and perturbation theory can be developed most conveniently in a way independent from the representation. The summations over the virtual intermediate states are, in a certain sense, absorbed into the c-numbers which arise by the commutations, a formal procedure which is largely used in quantum electrodynamics. The method is applied to a field-theoretical example, and some thermodynamical points are discussed.

1. – Introduction.

The thermodynamics of a system, as is physically clear, in general involves a smaller number of details than its mechanics. This point is sometimes obscured by the more common presentation in a particular frame of reference of the hilbertspace, usually that in which the hamiltonian is diagonal. One of the advantages of the invariant formulation is that of showing in a clear form how a previous diagonalization of the hamiltonian is, in principle, not necessary. We would like to point out that, even for problems of quantum statistical mechanics of particles (as opposed to the statistical mechanics of fields), there is an advantage in using the formalism of second quantization, which mainly lies in the possibility of giving an invariant formulation to the quantum statistical mechanics of grand ensembles with respect to unitary transformations in the hilbertspace. It seems that this advantage is of a fundamental nature,

so that one may consider that second quantization is the natural framework for dealing with grand ensembles. For the more restricted formulation with petit ensembles, the formalism is at any rate a wider framework for a simple use of the quantummechanical transformation theory.

In the development of pertubation theory the main stress will be put on the invariance of the formalism with respect to unitary transformations in the hilbertspace. The viewpoint is similar to that of recent quantum electrodynamics. The summations over the virtual intermediate states are, in a certain sense, absorbed into the c-numbers which arise in the course of the commutation of the factors in the product of operators which expresses the n-th term of the perturbative expansion. These developments may be of use in problems of quantum statistical mechanics of particles, which can conveniently be put in a second quantized form. In this connection we want again to stress the point that second quantization permits an invariant formulation of the quantummechanical grand ensembles.

2. – Transformation Theory.

We shall first give some formal developments which follow immediately from tranformation theory.

To be definite let us consider the case of a boson field, or of a system of Bose particles. We consider a representation in which the basic kets for one particle are the eigenkets $|X^\nu\rangle$ of a complete set of one-particle observables X. For this choice of the representation we can define the creation operators $x_\nu^\dagger$, the destruction operators x_ν, and the occupation numbers operators $n_\nu^X = x_\nu^\dagger x_\nu$. Suppose that the total hamiltonian H can be written in the form $H = \sum n_\nu^X H^\nu$. For another generic representation the symbols $|Y^\mu\rangle$, $y_\mu^\dagger$, y_μ, n_μ^Y will have the similar meaning. The transformation laws between the operators x and y are the same as those of the corresponding basic kets $|X\rangle$ and $|Y\rangle$

$$y_\nu^\dagger = \sum_\mu x_\mu^\dagger \langle X^\mu | Y^\nu \rangle , \tag{1}$$

$$y_\nu = \sum_\mu \langle Y^\nu | X^\mu \rangle x_\mu . \tag{1'}$$

Let us consider the thermodynamical mean values $\overline{x'x''}$ of the products $x'x''$, where x' and x'' are destruction or creation operators. With the density operator ρ of our stationary ensemble we have

$$\overline{x_\mu^\dagger x_\nu^\dagger} = 0 \qquad \overline{x_\mu^\dagger x_\nu} = \overline{n_\nu^X}\delta_{\mu\nu} \qquad \overline{x_\mu x_\nu^\dagger} = (\overline{n_\nu^X} + 1)\delta_{\mu\nu} \qquad \overline{x_\mu x_\nu} = 0 . \tag{2}$$

Thus we obtain the very simple relation between the thermodynamical mean

values $\overline{n^Y}$ and $\overline{n^X}$

$$n_\nu^{\bar{Y}} = \sum_\mu \overline{n_\mu^X} |\langle X^\mu | Y^\nu \rangle|^2 . \tag{3}$$

Consider a one-body operator of the form

$$F^{(1)} = \sum_{\boldsymbol{a}} F(\boldsymbol{a}) , \tag{4}$$

where $\boldsymbol{a}$ denotes the coordinates of the a-th particle. We use the representation

$$F^{(1)} = \sum_{\mu\nu} x_\nu^\dagger \langle \nu | F | \mu \rangle x_\mu , \tag{5}$$

where $\langle \nu | F | \mu \rangle = \langle X_{\boldsymbol{a}}^\nu | F(\boldsymbol{a}) | X_{\boldsymbol{a}}^\mu \rangle$. Using eq. (2) we obtain

$$\bar{F}^{(1)} = \sum_{\mu\nu} \langle \nu | F | \mu \rangle \overline{x_\nu^\dagger x_\mu} = \sum_\nu n_\nu^{\bar{X}} \langle F \rangle_\nu . \tag{6}$$

For the general case of a n-body operator

$$F^{(n)} = \sum_{\boldsymbol{a}} F(\boldsymbol{a}^{(1)}, \boldsymbol{a}^{(2)}, \ldots \boldsymbol{a}^{(n)}) , \tag{7}$$

one can similarly use the representation

$$F^{(n)} = \sum_{\mu\nu} x_{\nu^{(1)}}^\dagger x_{\nu^{(2)}}^\dagger \ldots x_{\nu^{(n)}}^\dagger \langle \nu^{(1)} \nu^{(2)} \ldots \nu^{(n)} | F | \mu^{(1)} \mu^{(2)} \ldots \mu^{(n)} \rangle x_{\mu^{(1)}} x_{\mu^{(2)}} \ldots x_{\mu^{(n)}} . \tag{8}$$

Of particular interest are quadrilinear couplings. Indeed, any interaction potential among pairs can be written in the form

$$V = \sum a_{\boldsymbol{p}_f}^\dagger a_{\boldsymbol{q}_f}^\dagger \langle \boldsymbol{p}_f \boldsymbol{q}_f | V | \boldsymbol{p}_i \boldsymbol{q}_i \rangle a_{\boldsymbol{p}_i} a_{\boldsymbol{q}_i} . \tag{9}$$

A simplification occurs, due to the fact that $V(i, k)$ will depend on the relative coordinates only

$$\langle \boldsymbol{p}_f \boldsymbol{q}_f | V | \boldsymbol{p}_i \boldsymbol{q}_i \rangle = \langle \boldsymbol{p}_f - \boldsymbol{q}_f | V | \boldsymbol{p}_i - \boldsymbol{q}_i \rangle \delta_{\boldsymbol{p}_f + \boldsymbol{q}_f, \boldsymbol{p}_i + \boldsymbol{q}_i} . \tag{10}$$

The interest of these expressions for the thermodynamical mean values lies in the circumstance that the first order perturbation formulae may be expressed with the thermodynamical mean value of the perturbation hamiltonian.

The above results (for instance the derivation of the formula (3)) show the convenience of using the formalism of second quantization also in the statistical mechanics of systems of particles. A fundamental point in this con-

nection is that the formalism of second quantization is particularly suitable for the introduction of grand ensembles. We would like to point out that the formalism of second quantization allows an invariant formulation of the statistical mechanics of grand ensembles with respect to unitary transformations in the hilbertspace.

3. – Perturbation Theory.

We can formally derive the perturbative expansion starting from Schwinger's expansion [1] for the trace of an exponential. Let us consider the case of a petit ensemble. We call $H^{(0)}$ the unperturbed hamiltonian and H' the perturbation term.

Using the formal properties of the trace, we can write Schwinger's expansion as

$$(11)\quad \text{trace}\ \{\exp[-\eta(H^{(0)}+H')]\} =$$

$$= \text{trace}\ \exp[-\eta H^{(0)}] - \eta\ \text{trace}\ \{H'\exp[-\eta H^{(0)}]\} -$$

$$+\frac{\eta^2}{2}\int_0^1 d\xi_1\ \text{trace}\ \{\exp[\xi_1\eta H^{(0)}]H'\exp[-\xi_1\eta H^{(0)}]H'\exp[-\eta H^{(0)}]\} + \dots +$$

$$+\frac{(-\eta)^{n+1}}{n+1}\int_0^1 d\xi_1\xi_1^{n-1}\int_0^1 d\xi_2\xi_2^{n-2}\dots\cdot$$

$$\cdot\int_0^1 d\xi_n\ \text{trace}\ \{\exp[\xi_1\eta H^{(0)}]H'\exp[-\xi_1(1-\xi_2)\eta H^{(0)}]\dots\cdot$$

$$\cdot H'\exp[-\xi_1\xi_2\dots\xi_{n-1}(1-\xi_n)\eta H^{(0)}]H'\exp[-\xi_1\xi_2\dots\xi_n\eta H^{(0)}]\,H'\exp[-\eta H^{(0)}]\} + \dots$$

The meaning of η is in our case $(kT)^{-1}$.

We can introduce the unperturbed density operator $\rho^{(0)}$, which is supposed to be normalized to unity, and put the above expression in the form

$$(12)\quad \text{trace}\ \{\exp[-\eta(H^{(0)}+H')]\} = \exp[-\eta F^{(0)}]\{1-\eta H' +$$

$$-\frac{\eta^2}{2}\int_0^1 d\xi_1\,\overline{\exp[\xi_1\eta H^{(0)}]H'\exp[-\xi_1\eta H^{(0)}]H'} + \dots + \frac{(-\eta)^{n+1}}{n+1}\int_0^1 d\xi_1\xi_1^{n-1}\int_0^1 d\xi_2\xi_2^{n-2}\dots\cdot$$

$$\cdot\int_0^1 d\xi_n\,\overline{\exp[\xi_1\eta H^{(0)}]H'\exp[-\xi_1(1-\xi_2)\eta H^{(0)}]\dots H'\exp[-\xi_1\xi_2\dots\cdot}$$

$$\overline{\cdot(1-\xi_n)\eta H^{(0)}]H'\exp[-\xi_1\xi_2\dots\xi_n\eta H^{(0)}]H'} + \dots,$$

[1] J. SCHWINGER: *Phys. Rev.*, **82**, 664 (1951); G. V. CHESTER: *Phys. Rev.*, **93**, 606 (1954).

where the thermodynamical mean values are taken with respect to the density operator $\rho^{(0)}$. In (12) we have introduced the unperturbed free energy $F^{(0)}$. The expansion (12) may be used to evaluate the perturbed free energy up to any order of the coupling constant. Up to the second order of the coupling constant, the expansion of the perturbed free energy reads

$$F = F^{(0)} + \overline{H'} + \frac{1}{2}\overline{H'}^2 - \frac{\eta}{2}\int_0^1 d\xi_1 \overline{\exp[\xi_1\eta H^{(0)}]H' \exp[-\xi_1\eta H^{(0)}]H'} , \tag{13}$$

To exhibit the meaning of the multiple integrals appearing in (12) it will perhaps be instructive to evaluate the last term of eq. (13), in the representation in which the unperturbed hamiltonian is diagonal. Let us denote with A, B the generic basic kets of this representation. We easily obtain for the last term of eq. (13)

$$\begin{aligned} &-\frac{\eta}{2}\int_0^1 d\xi_1 \overline{\exp[\xi_1\eta H^{(0)}]H' \exp[-\xi_1\eta H^{(0)}]H'} = \\ &= \frac{1}{2}\exp[\eta F^{(0)}] \sum_{AB} \langle A|H'|B\rangle\langle B|H'|A\rangle \frac{\exp[-\eta H_A^{(0)}] - \exp[-\eta H_B^{(0)}]}{H_A^{(0)} - H_B^{(0)}} = \\ &= \exp[\eta F^{(0)}] \sum_{AB} \langle A|H'|B\rangle\langle B|H'|A \frac{\exp[-\eta H_A^{(0)}]}{H_A^{(0)} - H_B^{(0)}} . \end{aligned} \tag{14}$$

where we have put

$$\langle A|H_A^{(0)}|A\rangle = H_A^{(0)}, \qquad \langle B|H^{(0)}|B\rangle = H_B^{(0)} . \tag{15}$$

The expression (14) can be simply written as

$$\sum_A \mathcal{E}_A'' \rho_A^{(0)} = \overline{\mathcal{E}''} ,$$

where $\mathcal{E}_A''$ is the second order energy perturbation for the state A. A similar procedure may be applied to evaluate any term in the expansion (12). However, the main advantage of the expansion formula (12) is its invariance with respect to unitary transformations in the hilbertspace. If we use a particular representation we are faced with the formal difficulty of carrying out the summations over the virtual intermediate states. A better procedure which avoids the appearance of these summations is to work directly with the operators without specifying the choice of the representation. When the interaction hamiltonian H' is given, one can change the order of the various operators in the integrands in eq. (12), by taking due account of the factors (c-numbers) which arise in the course of the commutation. The unperturbed hamiltonian will be in general a function of the occupation numbers operators n_ν of the

unperturbed system. The same holds for each exponential of the form

$$\exp\left[-cH^{(0)}\right], \tag{16}$$

in the integrands in eq. (12). Let us denote such a function of the n_ν's by $F(n_\nu)$. The interaction hamiltonian H_0 can generally be expanded as a sum of simple products of production and destruction operators $a_\nu^\dagger$ and a_ν. We can change the order of the operators in each integrand of eq. (12) by repeated use of the commutation rules

$$a_\nu F(n_\nu) = F(n_\nu + 1)a_\nu \ , \tag{17}$$

$$a_\nu^\dagger F(n_\nu) = F(n_\nu - 1)a_\nu^\dagger \ . \tag{17'}$$

Generally $F(n_\nu - 1)$ will be expressible as a product of the form $F(n_\nu)G_\nu^{(\pm)}$, where $G_\nu^{(\pm)}$ is a c-number. The net result of the commutation will be the appearance of these c-numbers in the integrands. Once the exponentials in the integrands in eq. (12) have all been put together, they cancel each other by virtue of the identity

$$\xi_1 - \xi_1(1-\xi_2) \ldots - \xi_1\xi_2 \ldots \xi_{n-1}(1-\xi_n) - \xi_1\xi_2 \ldots \xi_n = 0 \ , \tag{18}$$

which is satisfied for any $n \geq 2$. Thus, the final result will be directly expressed through the thermodynamical mean values of products of creation and annihilation operators, which can be readily evaluated. A particular case are the thermodynamical mean values

$$\overline{a_\nu^\dagger a_{\nu'}^\dagger} = 0 \quad \overline{a_\nu^\dagger a_{\nu'}} = \overline{n}_\nu \delta_{\nu\nu'} \quad \overline{a_\nu a_{\nu'}^\dagger} = (\overline{n}_\nu + 1)\delta_{\nu\nu'} \quad \overline{a_\nu a_{\nu'}} = 0 \ , \tag{19}$$

for the case of bosons, and

$$\overline{a_\nu^\dagger a_{\nu'}^\dagger} = 0 \quad \overline{a_\nu^\dagger a_{\nu'}} = \overline{n}_\nu \delta_{\nu\nu'} \quad \overline{a_\nu a_{\nu'}^\dagger} = (1 - \overline{n}_\nu)\delta_{\nu\nu'} \quad \overline{a_\nu a_{\nu'}} = 0 \ , \tag{19'}$$

for the case of fermions. One can say that the summations over the virtual intermediate states are, in a certain sense, absorbed into the c-numbers which arise by the commutations, a formal procedure which is largely used in electrodynamics.

Let us consider the formal extension to the case of a general grand ensemble. In the expansion (11) we can imagine to substitute for $H^{(0)}$ the expression $\zeta N + H^{(0)}$ (or a corresponding one for the more general cases), where ζ is the partial thermal potential and N the operator for the total number of particles. The principal

property of $H^{(0)}$ of being a function of the occupation numbers operators only is again valid for the new expression. Accordingly we interpret $\rho^{(0)}$ as the unperturbed density operator of our general grand ensemble, and substitute for $F^{(0)}$ and F the potentials $\Omega^{(0)}$ and Ω of Gibbs respectively (or corresponding potentials for the more general cases). The Ω-potential of Gibbs is related to the grand potential of Kramers by the relation $q = -\eta\Omega$ [2].

In the next section we shall give an example of application of the method by deriving the first terms of the perturbative expansion of the free energy of the system consisting of two scalar boson fields scalarly coupled. This system can be solved exactly in finite terms. Therefore we can compare the perturbative result with the exact one. For simplicity we consider a field-theoretic example: however, the method developed may be applied equally well to other cases. A field-theoretic example leads to the appearance of divergent terms. The discussion of the related questions will not be given here. In the following our discussion will only be limited to formal aspects. A discussion on the divergent features of field theory from a thermodynamical viewpoint will be given in a next work.

4. – A Solvable Example.

We consider the example of two scalar neutral boson fields interacting through a scalar coupling. This example has the advantage of being exactly solvable by means of a simple canonical transformation. Moreover it corresponds to a plausible physical system.

The Hamiltonian density is given by

$$H(\boldsymbol{x}) = H_1(\boldsymbol{x}) + H_2(\boldsymbol{x}) + H'(\boldsymbol{x}) , \tag{20}$$

where

$$H_j(\boldsymbol{x}) = \tfrac{1}{2}\{\pi_j(\boldsymbol{x})^2 + c^2(\nabla\varphi_j(\boldsymbol{x}))^2 + c^2\mu_j^2\varphi_j(\boldsymbol{x})^2\} , \qquad j = 1, 2 \tag{21}$$

$$H'(\boldsymbol{x}) = g\varphi_1(\boldsymbol{x})\varphi_2(\boldsymbol{x}) . \tag{21'}$$

With the usual notations

$$\varphi_j(\boldsymbol{x}) = V^{-\frac{1}{2}} \sum_{\nu} q_j(\boldsymbol{\nu}) \exp[i\boldsymbol{\nu}\cdot\boldsymbol{x}] \qquad \pi_j(\boldsymbol{x}) = V^{-\frac{1}{2}} \sum_{\nu} p_j(\boldsymbol{\nu}) \exp[-i\boldsymbol{\nu}\cdot\boldsymbol{x}], \tag{22}$$

$$p_j(-\boldsymbol{\nu}) = p_j(\boldsymbol{\nu})^\dagger \qquad q_j(-\boldsymbol{\nu}) = q_j(\boldsymbol{\nu})^\dagger \qquad \omega_j(\boldsymbol{\nu}) = c(\mu_j^2 + \nu^2)^{\frac{1}{2}} , \tag{22'}$$

[2] See D. TER HAAR: *Elements of Statistical Mechanics* (New York, 1954), p. 140.

the total hamiltonian, H, takes the form

$$H = \tfrac{1}{2} \sum_{\nu} \sum_{j,l} \{\delta_{jl} p_j(\nu)^\dagger p_l(\nu) + \alpha_{jl}(\nu) q_j(\nu)^\dagger q_l(\nu)\} , \tag{23}$$

where

$$\boldsymbol{a}_{jl}(\nu) = g + \{\omega_j(\nu)^2 - g\}\delta_{jl} . \tag{24}$$

Consider the transformation

$$q_j(\nu) = \sum_{\alpha} \xi_{j\alpha}(\nu) q_\alpha(\nu) , \qquad \alpha = +, - , \tag{25}$$

$$p_j(\nu) = \sum_{\alpha} \xi_{j\alpha}(\nu) p_\alpha(\nu) , \tag{25'}$$

where the coefficients $\xi_{j\alpha}(\nu)$ are taken to be real and to satisfy the relations

$$\sum_{j} \xi_{j\alpha}(\nu)\xi_{j\beta}(\nu) = \delta_{\alpha\beta} \qquad \sum_{\alpha} \xi_{j\alpha}(\nu)\xi_{l\alpha}(\nu) = \delta_{jl} . \tag{26}$$

This transformation is canonical. If we choose $\xi_{j\alpha}(\nu)$ to satisfy the equations

$$\sum_{l} \{g + [\omega_j(\nu)^2 - \omega_\alpha(\nu)^2 - g]\delta_{jl}\}\xi_{l\alpha}(\nu) = 0 , \tag{27}$$

the total hamiltonian H reduces to the form

$$H = \tfrac{1}{2} \sum_{\nu} \sum_{\alpha} \{p_\alpha(\nu)^\dagger p_\alpha(\nu) + \omega_\alpha(\nu)^2 q_\alpha(\nu)^\dagger q_\alpha(\nu)\} . \tag{28}$$

From the condition

$$\text{Det } |g + [\omega_j(\nu)^2 - \omega_\alpha(\nu)^2 - g]\delta_{jl}| = 0 , \tag{29}$$

we find

$$\omega_\pm(\nu)^2 = \frac{\omega_1(\nu)^2 + \omega_2(\nu)^2}{2} \pm \left\{\left(\frac{\omega_1(\nu)^2 - \omega_2(\nu)^2}{2}\right)^2 + g^2\right\}^{\frac{1}{2}} . \tag{30}$$

For $g \to 0$, $\omega_+(\nu) \to \omega_1(\nu)$, $\omega_-(\nu) \to \omega_2(\nu)$. To have a positive definite hamiltonian we impose the condition

$$|g| \leqslant \mu_1\mu_2 . \tag{31}$$

If this condition is satisfied $\omega_\alpha(\nu)^2 \geqslant 0$ for any ν. We may introduce the creation operators $a_\alpha(\nu)^\dagger$ and the annihilation operators $a_\alpha(\nu)$, and the corresponding occupation numbers operators $n_\alpha(\nu)$. The total hamiltonian then takes the form

$$H = \frac{\hbar}{2} \sum_{\nu} \sum_{\alpha} \omega_\alpha(\nu)\{2n_\alpha(\nu) + 1\}\,, \tag{32}$$

with commutation rules

$$[a_\alpha(\nu), a_\beta(\nu')]_- = 0 \qquad [a_\alpha(\nu), a_\beta(\nu')^\dagger]_- = \delta_{\alpha\beta}\delta_{\nu\nu'}. \tag{33}$$

If we introduce the creation operators $a_j(\nu)^\dagger$ and destruction operators $a_j(\nu)$ of the free fields we may give the hamiltonian the form

$$H = H^{(0)} + H' = \frac{\hbar}{2} \sum_{\nu} \omega_1(\nu)\{a_1(\nu)^\dagger a_1(\nu) + a_1(\nu)a_1(\nu)^\dagger\} + \tag{34}$$

$$+ \frac{\hbar}{2} \sum_{\nu} \omega_2(\nu)\{a_2(\nu)^\dagger a_2(\nu) + a_2(\nu)a_2(\nu)^\dagger\} +$$

$$+ g\frac{\hbar}{2} \sum_{\nu} [\omega_1(\nu)\omega_2(\nu)]^{-\frac{1}{2}}\{a_1(\nu)^\dagger a_2(\nu) + a_1(\nu)a_2(\nu)^\dagger + a_1(\nu)a_2(-\nu) + a_2(\nu)^\dagger a_2(-\nu)^\dagger\}\,.$$

We introduce a macrocanonical petit ensemble of fields, all having the same hamiltonian density (20). This ensemble at equilibrium is described by a density operator ρ. It follows that the thermodynamical mean values of $n_\alpha(\nu)$, $\overline{n_\alpha(\nu)}$ are given by

$$\overline{n_\alpha(\nu)} = \text{trace } [\rho n_\alpha(\nu)] = \sum_m \langle \rho n_\alpha(\nu)\rangle_m = \frac{1}{\exp[\eta\varepsilon_\alpha(\nu)] - 1}\,, \tag{35}$$

where we have put $\varepsilon_\alpha(\nu) = \hbar\omega_\alpha(\nu)$. It must be noted that the result does not depend upon the value of the additive constant in the hamiltonian. We could subtract from the total hamiltonian the zero point energy of the coupled fields

$$\frac{\hbar}{2} \sum_{\nu} \sum_{\alpha} \omega_\alpha(\nu)\,, \tag{36}$$

so as to attribute zero energy to the vacuum state; or, alternatively, we could subtract the sum of the zero point energy of the free fields

$$\frac{\hbar}{2} \sum_{\nu} \sum_{j} \omega_j(\nu)\,. \tag{37}$$

Equation (35) would still mantain the same form. This is a consequence of the normalization condition for the density operator ρ.

We see from (35) that the thermodynamical equilibrium state of the field at $T = 0$ is a pure state. It is that state of the field in which the operators $n_\alpha(\nu)$ all have eigenvalue 0. We see, from (32), that this state of the field is exactly the vacuum state, the ket of which we denote by $|0\rangle$. At $T = 0$ the density operator of our Gibbs ensemble coincides with the projection operator relative to the state $|0\rangle$.

The calculation of the thermodynamical potentials may be performed in the representation in which the $n_\alpha(\nu)$ are diagonal. For the density of the free energy we obtain

$$F = F_- + F_+ = \eta^{-1} V^{-1} \sum_\nu \{\log(1 - \exp[-\varepsilon_-(\nu)]) + \log(1 - \exp[-\eta\varepsilon_+(\nu)])\} + \tag{38}$$
$$+ V^{-1} \sum_\nu \{\tfrac{1}{2}\varepsilon_-(\nu) + \tfrac{1}{2}\varepsilon_+(\nu)\} .$$

The infinite constant, independent of the temperature, is the zero point term in the hamiltonian (32)

$$F_0 = (U + TS)_0 = U_0 . \tag{39}$$

To obtain $F_0 = 0$ we must subtract the vacuum energy (36) from the total hamiltonian (not the energy (37) of the uncoupled vacua).

We now derive the first two terms in the expansion of F in powers of the coupling constant g. We first expand $\varepsilon_-(\nu)$ and $\varepsilon_+(\nu)$ in powers of g

$$\varepsilon_-(\nu) = \hbar\omega_2(\nu) - \frac{1}{2}\hbar \frac{g^2}{\omega_2(\nu)[\omega_1(\nu)^2 - \omega_2(\nu)^2]} + 0(g^4) = \varepsilon_2(\nu) + \varepsilon_2'(\nu) + 0(g^4) , \tag{40}$$

$$\varepsilon_+(\nu) = \hbar\omega_1(\nu) + \frac{1}{2}\hbar \frac{g^2}{\omega_1(\nu)[\omega_1(\nu)^2 - \omega_2(\nu)^2]} + 0(g^4) = \varepsilon_1(\nu) + \varepsilon_1'(\nu) + 0(g^4), \tag{40'}$$

and we note that, for instance,

$$\log\{1 - \exp[-\eta\varepsilon_+(\nu)]\} = \log\{1 - \exp[-\eta\varepsilon_1(\nu)]\} + \tag{41}$$
$$+ \frac{\eta\varepsilon_1'(\nu)}{\exp[\eta\varepsilon_1(\nu)] - 1} + 0(g^4) = \log\{1 - \exp[-\eta\varepsilon_1(\nu)]\} + \eta\varepsilon_1'(\nu)\overline{n_1(\nu)}^{(0)} + 0(g^4) ,$$

where we have introduced the unperturbed distribution law for the thermodynamical mean values of $n_1(\nu)$, $\overline{n_2(\nu)}^{(0)}$. Thus, the result reads

$$F = F^{(0)} + V^{-1} \sum_\nu \varepsilon_1'(\nu)\overline{n_1(\nu)}^{(0)} + V^{-1} \sum_\nu \varepsilon_2'(\nu)\overline{n_2(\nu)}^{(0)} + \tag{42}$$
$$+ V^{-1} \sum_\nu \tfrac{1}{2}\varepsilon_1'(\nu) + V^{-1} \sum_\nu \tfrac{1}{2}\varepsilon_2'(\nu) + 0(g^4) ,$$

where $F^{(0)}$ is the free energy density of the unperturbed fields.

We can show that equation (42) has a more general validity. This may be seen by the following thermodynamical argument. Let us consider one of the two decoupled fields, to be definite the field having hamiltonian density $H_1(x)$. The effect of its interaction with the other field is, to the first order, a displacement of the one particle levels $\varepsilon_1(\nu)^{(0)}$ by the small quantity $\varepsilon_1'(\nu)$, up to $\varepsilon_1(\nu)^{(0)} + \varepsilon_1'(\nu) = \varepsilon_1(\nu)^{(1)}$. Now we imagine this change in the nature of the system to be accomplished very slowly, by some reversible transformation. During the transformation we assume that the system is always mantained in a large heat-bath at a fixed temperature. Therefore the total change in the free energy $F_1 - F_1^{(0)}$ must be the negative of the external work done by the system. This work is given by

$$(43) \qquad -\sum_{\nu} \overline{n_1(\nu)}^{(0)} \varepsilon_1'(\nu) \,,$$

since the level $\varepsilon_1(\nu)$ has been lifted up from its old value to the new value $\varepsilon_1(\nu)^{(0)} + \varepsilon_1'(\nu)$. So the proof is completed.

The perturbative expansion of the free energy up to terms of the second order in g, equation (13), will be written

$$(44) \qquad F = F^{(0)} - \frac{\eta}{2} \int_0^1 \mathrm{d}\xi_1 \, \overline{\exp\,[\xi_1 \eta H^{(0)}] H' \exp\,[-\xi_1 \eta H^{(0)}] H'} \,.$$

In fact, the thermodynamical mean value of the interaction hamiltonian is zero in our case. We must evaluate the thermodynamical mean value of the operator

$$(45) \qquad \exp\,[\xi_1 \eta H^{(0)}] H' \exp\,[-\xi_1 \eta H^{(0)}] H' =$$

$$+ \frac{g^2 \hbar^2}{4} \sum_{\nu\nu'} [\omega_1(\nu)\omega_2(\nu)\omega_1(\nu')\omega_2(\nu')]^{-\frac{1}{2}} \exp\,[\xi_1 \eta H^{(0)}] \{a_1(\nu)^\dagger a_2(\nu) + a_1(\nu) a_2(\nu)^\dagger +$$

$$+ a_1(\nu) a_2(-\nu) + a_1(\nu)^\dagger a_2(-\nu)^\dagger\} \exp\,[-\xi_1 \eta H^{(0)}] \{a_1(\nu)^\dagger a_2(\nu') + a_1(\nu') a_2(\nu')^\dagger +$$

$$+ a_1(\nu') a_2(-\nu') + a_1(\nu')^\dagger a_2(-\nu')^\dagger\} \,.$$

The commutation rules (17) and (17′) give the relations

$$(46) \qquad a_1(\nu)^\sharp a_2(\nu) \exp\,[-\xi_1 \eta H^{(0)}] = \exp\,[-\xi_1 \eta H^{(0)}] \cdot$$

$$\cdot \exp\,[-\xi_1 \eta(-\varepsilon_1(\nu) + \varepsilon_2(\nu))]\, a_1(\nu)^\dagger a_2(\nu) \,,$$

$$(46') \qquad a_1(\nu)\, a_2(\nu)^\sharp \exp\,[-\xi_1 \eta H^{(0)}] = \exp\,[-\xi_1 \eta H^{(0)}] \cdot$$

$$\cdot \exp\,[-\xi_1 \eta(\varepsilon_1(\nu) - \varepsilon_2(\nu))]\, a_1(\nu)\, a_2(\nu)^\sharp,$$

$$(46'')\quad a_1(\nu)\, a_2(-\nu)\, \exp\,[-\xi_1\eta H^{(0)}] = \exp\,[-\xi_1\eta H^{(0)}]\cdot$$
$$\cdot\exp\,[-\xi_1\eta(\varepsilon_1(\nu)+\varepsilon_2(\nu))]a_1(\nu)\,a_2(-\nu)\ ,$$

$$(46''')\quad a_1(\nu)^\dagger a_2(-\nu)^\dagger \exp\,[-\xi_1\eta H^{(0)}] = \exp\,[-\xi_1\eta H^{(0)}]\cdot$$
$$\cdot\exp\,[-\xi_1\eta(-\varepsilon_1(\nu)-\varepsilon_2(\nu))]a_1(\nu)^\dagger a_2(-\nu)^\dagger,$$

where use has been made of $\varepsilon_j(-\nu) = \varepsilon_j(\nu)$. We use the relations (46) to change the order of the factors in (45) so as to put together the two exponentials, which cancel each other. We can readily obtain the thermodynamical mean value of (45) using the equations (19). We make use of $\overline{n_j(-\nu)} = \overline{n_j(\nu)}$ and we carry out the summation over ν'. After performing the integration over ξ_1 we get for the last term in eq. (44), omitting for brevity the index ν

$$(47)\quad -\frac{\eta}{2}\int_0^1 \mathrm{d}\xi_1\, \overline{\exp\,[\xi_1\eta H^{(0)}]H'\exp\,[-\xi_1\eta H^{(0)}]H'} =$$
$$= \frac{g^2\hbar^2}{8}\sum_{\mathbf{w}}\frac{1}{\omega_1\omega_2}\Big\{\frac{\exp\,[-\eta(-\varepsilon_1+\varepsilon_2)]-1}{-\varepsilon_1+\varepsilon_2}\,\overline{n}_1^{(0)}(\overline{n}_2^{(0)}+1)+$$
$$+\frac{\exp\,[-\eta(\varepsilon_1-\varepsilon_2)]-1}{\varepsilon_1-\varepsilon_2}(\overline{n}_1^{(0)}+1)\overline{n}_2^{(0)}+\frac{\exp\,[-\eta(\varepsilon_1+\varepsilon_2)]-1}{\varepsilon_1+\varepsilon_2}\cdot$$
$$\cdot\,(\overline{n}_1^{(0)}+1)(\overline{n}_2^{(0)}+1)+\frac{\exp\,[-\eta(-\varepsilon_1-\varepsilon_2)]-1}{-\varepsilon_1-\varepsilon_2}\,\overline{n}_1^{(0)}\overline{n}_2^{(0)}\Big\},$$

which is the final result. It still remains to verify that our result (47) is the same as that of eq. (42). This follows immediately from the algebraic identities

$$(48)\quad \exp\,[-\eta(-\varepsilon_1+\varepsilon_2)]\overline{n}_1^{(0)}(\overline{n}_2^{(0)}+1) = (\overline{n}_1^{(0)}+1)\overline{n}_2^{(0)},$$

$$(48')\quad \exp\,[-\eta(\varepsilon_1-\varepsilon_2)](\overline{n}_1^{(0)}+1)\overline{n}_2^{(0)} = \overline{n}_1^{(0)}(\overline{n}_2^{(0)}+1),$$

$$(48'')\quad \exp\,[-\eta(\varepsilon_1+\varepsilon_2)](\overline{n}_1^{(0)}+1)(\overline{n}_2^{(0)}+1) = \overline{n}_1^{(0)}\overline{n}_2^{(0)},$$

$$(48''')\quad \exp\,[-\eta(-\varepsilon_1-\varepsilon_2)]\overline{n}_1^{(0)}\overline{n}_2^{(0)} = (\overline{n}_1^{(0)}+1)(\overline{n}_2^{(0)}+1).$$

which will be of use in these kind of problems. Thus we have seen that perturbation theory up to the second order furnishes the result derived from the exact solution. We think that the above example of the method makes it clear the advantage of the invariant formulation. No use has been made, throughout the calculation, of any particular choice of the representation.

* * *

I take pleasure in expressing my thank to prof. B. Ferretti for his interest in the work.

RIASSUNTO

Viene messo in evidenza il vantaggio di usare una formulazione invariante della meccanica statistica quantica rispetto a trasformazioni unitarie dello spazio di Hilbert. La seconda quantizzazione permette di dare una formulazione invariante ai grandi ensembles quantistici e permette un semplice uso della teoria delle trasformazioni. Inoltre la teoria delle perturbazioni può venire sviluppata in maniera indipendente dalla rappresentazione. Le somme sugli stati virtuali intermedi sono, in un certo senso, assorbite nei numeri c che compaiono ad ogni commutazione: questa procedura formale è largamente usata in elettrodinamica quantistica. Il metodo è applicato ad un esempio di teoria dei campi e vengono inoltre discussi alcuni punti a carattere termodinamico.

IL NUOVO CIMENTO Vol. II, N. 3 1° Settembre 1955

Mesonic Decay of a Singly Charged Fragment.

F. Anderson, G. Lawlor and T. E. Nevin

Physics Department, University College - Dublin

(ricevuto il 25 Luglio 1955)

Summary. — The results of measurements on a meson-active fragment event found in photographic emulsions are given. The event can be interpreted as the mesonic decay of either a $^3H_1$ or $^4H_1$ nucleus, containing a bound Λ^0-particle in place of a neutron. In either case, the binding energy of the Λ^0-particle is found to be -0.7 ± 0.8 MeV.

During systematic scanning in the *G*-stack an event has been observed in which a slow singly charged particle is emitted from a five prong star and comes to rest after 248 μm producing a three prong star. No useful mass measurement on the interacting particle can be made but it appears straighter than might be expected for a K^--meson.

One of the prongs (*a*) from the interaction is a meson which comes to rest after a range of 14.21 mm in eleven plates. Although no visible interaction occurs at the end the meson is identified as a π^--meson, the probability of a π^--meson stopping without visible interaction being about 30%. The second prong (*b*), singly charged, has a range of 399 μm in a single plate. The third prong (*c*) has a dip of 38° in the unprocessed emulsion and a range of 4.4 ± 0.4 μm. The angle between the planes (*ab*) and (*ac*) is difficult to estimate accurately because of the shortness and dip of the prong (*c*). The angle may be zero but the best estimate based on repeated measurements is $10° \pm 10°$.

If the event represents the mesonic decay of a singly charged fragment containing a bound Λ^0-particle a number of possible interpretations must be considered since, of the three particles involved in the decay, only the meson (*c*) can be directly identified. To conserve momentum, even approximately,

(*b*) must be a proton and interpretations of the event in which (*b*) is identified as a deuteron can be discarded. The different possible interpretations with the resulting Q-value, the binding energy of the Λ^0-particle and the momentum balance are shown in Table I. In (3) and (4) the neutron energy has been calculated from the momentum unbalance.

TABLE I.

N.	Track (*c*)	Decay Scheme	Q (MeV)	Binding energy (MeV)	Momentum unbalance (MeV/*c*)
1	p	$^2H_1^+ \rightarrow p + p + \pi^-$	37.5	-0.6 ± 0.8	24 ± 10
2	$^2H_1$	$^3H_1^+ \rightarrow {}^2H_1 + p + \pi^-$	37.6	-0.7 ± 0.8	9.6 ± 10
3	p	$^3H_1^+ \rightarrow p + p + n + \pi^-$	37.7	-3.0 ± 0.8	..
4	$^2H_1$	$^4H_1^+ \rightarrow {}^2H_1 + p + n + \pi^-$	37.6	-7.0 ± 0.8	—
5	$^3H_1$	$^4H_1^+ \rightarrow {}^3H_1 + p + \pi^-$	37.6	-0.7 ± 0.8	10.0 ± 10

The Range Energy relation given by G. BARONI *et al.* (CERN B. S. Bulletin No. 9) has been used. The Binding Energy of the Λ^0-particle has been taken to be 3.609 MeV.

The first interpretation of the event as the decay of a meson-active deuteron is unlikely. Apart from the unsatisfactory momentum balance no other examples of excited deuterons have been reported. It would seem reasonable to expect many more excited deuterons than tritons to be present in photographic emulsions if the proton and Λ^0-particle can form a bound system. Interpretations (3) and (4) seem very unlikely since the large negative binding energy of the Λ^0-particle, particularly in the case of (4), seems to be outside the range of possible errors on the measurements. The Q-value of an event similar to (3) found by YAGODA [1] was 31.5 ± 1 MeV. The binding energy of the Λ^0-particle in the $^4H_1$ event found by the Bristol group was 1.2 ± 0.8 MeV.

From the binding energies and the dynamics of the decay it does not seem possible to decide between (2) and (5). An example of (2) found by the Paris group was reported by CRUSSARD at the Pisa Conference. Altogether five examples of $^3H_1$ and three examples of $^4H_1$ have been reported.

The primary star of the event, not fully analysed, has two short black prongs, a grey proton track and a light unidentified track in addition to the track and a light unidentified track in addition to the excited nucleus. One

(1) H. YAGODA: *Phys. Rev.*, **98**, 153 (1955).
(2) Bristol Group: *Pisa Conference* (June 1955).

of the black prongs of length 1 μm gives rise to an interaction with three black prongs and a relatively slow electron.

* * *

We wish to thank Dr. FRIEDLANDER for tracing the π^--meson in the Bristol portion of the stack. We are indebted to our colleagues in Bristol particularly Mr. D. KEEFE for discussion of the event.

RIASSUNTO (*)

Si riportano i risultati delle misure eseguite su un evento provocato da un frammento dotato di attività mesonica rinvenuto in emulsione fotografica. L'evento si può interpretare come il decadimento mesonico di un nucleo $^3H_1$ o $^4H_1$ contenente al posto di un neutrone una particella Λ^0 legata. In ambo i casi l'energia di legame della particella Λ^0 risulta essere 0.7 ± 0.8 MeV.

(*) *Traduzione a cura della Redazione.*

Unusual Decay of a χ-Meson.

F. Anderson, G. Lawlor and T. E. Nevin

Physics Department, University College - Dublin

(ricevuto il 25 Luglio 1955)

Summary. — An event is described in which a χ-meson decays at rest to three charged particles, two of which are electrons. Details of the measurements are given and are consistent with the interpretation of a χ-meson decay involving a π^0-meson which undergoes anomalous decay to two electrons and a photon.

During systematic scanning in the *G*-stack a K-meson (K-Du UC3) has been observed which originates in a three prong star and comes to rest after traversing 9.84 mm in three plates. The mass of the K-meson by range-scattering with constant sagitta using the τ-meson tables of Fay *et al.* [1] is $896 \pm 150\ m_e$.

Three particles *A*, *B*, and *C*, originate at the end of the K-meson track. *A* leaves the stack through the end plate after 7.99 cm in 30 plates. *B* and *C* form a narrow pair of tracks just resolved in the plate in which the event originates. The space angle between *A* and the axis is $134° \pm 1°$. Observations on the event show that *A* is a π-meson and that *B* and *C* are an electron pair. Accordingly the K-particle can be interpreted as a χ-meson decaying according to the scheme

$$\chi \to \pi + \pi^0\,, \qquad \pi^0 \to e^+ + e^- + \gamma\,.$$

1. – Measurement on Track *A* (π-Meson).

Scattering measurements on *A* have been made over the first four centimetres of track in 13 plates using 100 μm and 200 μm cell sizes. The method

[1] H. Fay, K. Gottstein and K. Hain: *Suppl. Nuovo Cimento*, **2**, 234 (1954).

of second differences with $\overline{4D}$ cut-off gives $\bar{\alpha} = 0.190 \pm 0.022$ degrees/100 μm and the method of third differences using the relation [2]

$$\overline{D}'' = \frac{1}{1.07} \left| \frac{\overline{2}}{3} \overline{D}''' \right.$$

gives $\bar{\alpha} = 0.160 \pm 0.020°/100$ μm. With the value of the scattering constant given by GOTTSTEIN *et al.* [3] the corresponding values of $p\beta C$ are $129 \pm \pm 15$ MeV ($\bar{\alpha}''$) and 154 ± 15 MeV ($\bar{\alpha}'''$).

Assuming A to be a π-meson the corresponding values of $p\beta C$ at emission

$$\text{are} \quad 149 \pm 15 \text{ MeV } (\bar{\alpha}'')$$

$$\text{and} \quad 174 \pm 15 \text{ MeV } (\bar{\alpha}'''),$$

which are to be compared with the value 169 ± 4 MeV determined [4] from the energy of emission 108.4 ± 3 MeV of the π-meson from χ-decay.

Measurements of $p\beta C$ and g^* have also been made on the last available 1.02 cm of track in five plates. For the scattering measurements 50 μm and 100 μm cells were used. The method of second differences gives $\bar{\alpha} = 0.255° \pm \pm 0.022°$ and $p\beta C = 93 \pm 8$ MeV at a mean distance from the event of 7.54 ± 0.15 cm. The residual range for a π-meson is 4.0 ± 0.6 cm and the total range 11.5 ± 0.7 cm. Local calibrations of plateau ionization were made in the individual plates in the neighbourhood of the track and corrections made for development gradient. The value of g^* found was 1.52 ± 0.08, defined in the way described by FOWLER and PERKINS [5] corresponding to a residual range of $3.95 \, {}^{+.62}_{-.43}$ cm giving an estimate of $11.6 \, {}^{+0.7}_{-0.5}$ cm for the range at emission. This is in satisfactory agreement with the figure 11.71 ± 0.15 given in [4] determined from the stopping π-meson secondaires from χ-decay.

On the basis of preliminary g^* v. $p\beta C$ calibrations in the stack the estimate of the mass of particle A is:

$$m = 320 \pm 44 \text{ m}_e$$

where the error quoted is the statistical error on the ionization and scattering measurements.

---

[2] Genoa-Milan Group: private communication.

[3] K. GOTTSTEIN, M. G. K. MENON, G. H. MULVEY, C. O'CEALLAIGH and O. ROCHAT: *Phil. Mag.*, **42**, 708 (1951).

[4] *Results obtained in G-stack collaboration Experiment* (May 18, 1955).

[5] P. H. FOWLER and D. H. PERKINS: *Phil. Mag.*, **46**, 587 (1955).

Combining all the results it seems reasonably safe to identify the meson secondary as a π-meson from a χ-decay.

2. – Measurement on B and C (Electron Pair).

Scattering measurements have been made on track B over a total available length of 9.06 mm in seven plates using 25 μm and 50 μm cells. The dip gradually decreases from the origin in $221A$ to $212A$ where the particle undergoes a sharp scatter, the track becomes very steep and cannot be traced further. The data on the measurements are given in Table I.

TABLE I. – *Scattering measurements on electron track B.*

Plates	Length of track (mm)	$\bar{\alpha}''$	$\bar{\alpha}'''$	Distance from decay (mm)
$220A$-$217A$	3.81	0.56 ± 0.05	0.76 ± 0.05	2.09
$216A$	1.30	0.68 ± 0.12	1.00 ± 0.18	2.70
$215A$-$213A$	3.90	0.89 ± 0.08	1.15 ± 0.13	4.64

The observations suggest the occurrence of a loss of energy by radiation in plate $216A$. The value of $p\beta C$ obtained by a linear extrapolation back to the point of emission is found to be 46 ± 4 MeV (second differences) or 36 ± 3 MeV (third differences). The normalised blob density is $b^* = 1.12 \pm \pm 0.09$.

The dip of C gradually increases with distance and the range per plate after $213A$ becomes less than 500 μm. The measurements over an available track length of 5.3 mm are

$$\bar{\alpha}'' = 0.538 \pm 0.045\,, \qquad \bar{\alpha}''' = 0.514 \pm 0.045$$

and the corresponding values of $p\beta C$ obtained by extrapolating back to the origin assuming an ionization loss of 6 MeV/cm, are 43 ± 4 MeV or 48 ± 4 MeV. The normalized blob density is $b^* = 1.03 \pm 0.09$.

On the basis of these observations B and C are identified as an electron pair of energy 89 ± 6 MeV (second differences) or 84 ± 6 MeV (third differences).

3. – Discussion.

The observations are [consistent with the decay scheme

$$\chi^+ \to \pi^+ + \pi^0 , \qquad \pi^0 \to e^+ + e^- + \gamma .$$

The first grain of the electron pair is observed less than one micron from the end of the K-meson track and the probability of a γ-ray materialising in a distance of this order is negligible. The probability of the decay of a π^0-meson to a γ-ray and two electrons has been calculated by DALITZ [6] as 1/80.

Assuming a value for the momentum of the π^0-meson equal to the known momentum, 204 ± 3 MeV/c, of the π^0-meson in the χ decay scheme the energy of the electron pair calculated fromt the conservation laws and the observed angle of emission of the electron pair is 88 ± 4 MeV in agreement with the observed value. Alternatively, using the measured momentum of the charged π-meson observed in the present event (203 ± 3 MeV/c) and assuming a two body decay the mass of the neutral particle which decays into one photon and two electrons of energy 87 ± 6 MeV at an angle of $46^0 \pm 1^0$ with the line of flight of the neutral particle can be calculated. The value found is $260 \pm 8\ m_e$ in agreement with the mass of the π^0-meson.

We are at present scanning along the calculated line of travel of the γ-ray for a possible electron pair resulting from the materialization of the γ-ray.

This event, the first of its type reported in photographic emulsions, is to be compared with the event observed by the Princeton group [7] in which a heavy meson was observed to decay to a light meson and two electron pairs. The event was interpreted according to the scheme

$$K^+ \to \binom{\pi^+}{\mu^+} + \pi^0 + Q$$

followed by the decay of the π^0-meson into four electrons. The event also provides confirmatory evidence for the nature of the neutral particle emitted in the χ-mode of decay alternative to that of the M.I.T. Cloud chamber group.

---

[6] R. H. DALITZ: *Proc. Phys. Soc.*, A **64**, 667 (1951).

[7] A. L. HODSON, J. BALLAM, W. H. ARNOLD, D. R. HARRIS, R. RONALD RAW, G. T. REYNOLDS and S. B. TRUMAN: *Phys. Rev.*, **96**, 1089 (1954).

* * *

We wish to express our thanks to Miss BRIGID MAHER who observed the event. We are indebted to our colleagues in Bristol, particularly Mr. D. KEEFE, and in the Institute for Advanced Studies for discussion of the event.

RIASSUNTO (*)

Si descrive un evento in cui un mesone χ decade a riposo in tre particelle cariche, due delle quali sono elettroni. Si danno dettagli delle misure che sono compatibili con l'interpretazione del decadimento di un mesone χ in cui si formi un mesone π^0 che a sua volta soggiace a un decadimento anomalo in due elettroni e un fotone.

(*) *Traduzione a cura della Redazione.*

Absolute Low-Energy Differential Range Spectrum of Cosmic Ray μ-Mesons at Sea-Level.

D. Brini, L. Peli, O. Rimondi and P. Veronesi

Istituto di Fisica dell'Università - Bologna

(ricevuto il 25 Luglio 1955)

Summary. — In this work we give the results of a measurement of the differential range spectrum of μ-mesons between 0 and ~ 1.5 m.w.e. at sea-level. The experimental apparatus used consists of two liquid scintillation counters, placed in coincidence with each other. Between them there is the lead absorber. The lower counter, of 5.64 g/cm^2 thickness, works as a death thickness. The event $\mu \to e$ is detected by photographing the two successive pulses, due to the meson and electron, on a sincroscope screen. The experimental results have been corrected for any possible cause of errors. The scattering correction has been valuated by the Monte Carlo method, and experimentally verified. The results correspondent to the scattering correction show how great this influence may be sometime. The absolute intensity at range of ~ 150 g/cm^2 of a.e. has resulted of $7 \cdot 10^{-6}$ (sterad$\cdot$g$\cdot$s)$^{-1}$. The behaviour of the spectrum between 0 and 180 g/cm^2 of a.e. has resulted to have a slope of 0.091 ± 0.006.

1. – Introduction.

We have at present a quite wide qualitative knowledge of the cosmic ray complex phenomenology in the atmosphere. However, the available experimental data are still inadequate to allow to connect the several different phenomena in a satisfactory quantitative scheme. Neither can we deal quantitatively with the chain of generative processes, where the primary component generates the secondary ones, nor with the chain of transformation and absorption processes, where the secondary components change one into another and are absorbed. Moreover, even the quantitative investigations, at a more generic stage, such as energy balances, are still unsatisfactory. An answer to these problems might be given by an improvement of the experimental data.

Our present investigation concerns the vertical spectrum of μ-mesons at sea-level. This datum has always been the best available and, at present, for what concerns the ranges higher than 1 m.w.e., it is rather well known, especially from the magnetic measurements of Manchester and Sydney group, and from measurements performed under ground and under absorbers. On the contrary, the results on the small ranges, between 0 and 1 m.w.e., although widely investigated, are still vague, because the measurements made by several different workers, with various experimental techniques, don't agree with one another.

As it is well known, the μ-meson spectrum at sea-level, is one of the most essential elements to know the production spectrum of π-mesons in the inelastic collisions of nucleonic component. It is therefore important that the spectrum be well defined because from the meson production spectrum and from the knowledge of the primary component, we shall have, in the future, the possibility of checking the productions theories.

We have performed a measurement of the differential range spectum of muons approximately between 0 and 1 m.e.w., by using a different detection technique. Our results concern the slope and the absolute value of the spectrum. In our conclusion we shall discuss separately these two problems, comparing ours to other author's results.

2. – Experimental Apparatus.

Fig. 1 shows the experimental apparatus used. C_1 and C_2 are two liquid scintillation counters delimitating the solid angle.

Counter C_1 is a parallelepiped of $18 \times 18 \times 2$ cm^3, with transparent plexiglas walls of 2 mm thickness. The light is collected on one of the smallest area wall, and is carried to the PM 5819 photocatodes by a suitable pipe light. The liquid scintillation is a solution of 3 g terphenil in one litre of phenylcyclohexane plus 10 mg of diphenylhexatriene. The detailed properties of counter C_1, which, however, are not all essential for the present experiment, have been fully described in a previous work, in print [1].

Counter C_2 is a parallelepiped of $18 \times 18 \times 6$ cm^3, with transparent plexiglas walls, and is filled with the same solution. In it, the light is collected on one of the smallest wall to which the three PM 5819 photocatodes are directly connected. In this counter the wall opposite the one collecting the light, is a reflecting surface. Each phototube has a 1 000 V tension, equally distributed on all the dynodes.

T is a tray of GM counters, of 43×40 cm^2, lying under counter C_2.

[1] D. BRINI, L. PELI, O. RIMONDI and P. VERONESI: *Suppl. Nuovo Cimento*. In the press.

Counters C_1 and C_2 are in coincidence and the coincidence signal is put in anticoincidence with the signal coming from the tray T. The coincidence signal, not anticoincided, triggers the sweep of the oscilloscope, in which

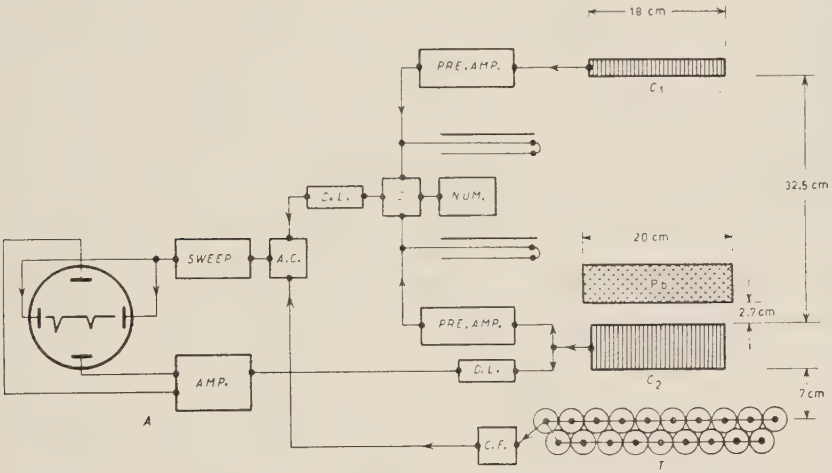

Fig. 1

the time sweep is 8.9 μs. Counter C_2 is the thickness of death (5.64 g/cm²). The resolving time of C_2 is quite sufficient to see the $\mu \rightarrow e$ decay. Such decay is shown by two distinct pulses: one due to μ-meson, which stops in the scintillator, the other one originated by the decay electron. Both pulses, formed at ~ 0.1 μs width by a reflection line, are sent to the vertical plates of the oscilloscope through the amplifier A. They are then photographed on a film. This film runs with constant speed. The range of the mesons is determined by a lead absorber of 20×20 cm² area, and of various thickness, which is placed between the two scintillation counters.

The two preamplifiers of counters C_1 and C_2 have a gain of ~ 7 and a rise time of few 10^{-8} s. The coincidence circuit is based on the Elmore circuit [2], and has a resolving time of 0.1 μs. Such resolving time has been chosen in order to get a good definition of the zero time of the sweep and in order to have a sufficiently low rate of chance coincidences. The anticoincidence is of conventional type and presents an inefficiency of 3%. The vertical amplifier A has been described in a previous work [3]. The oscilloscope time sweep has been calibrated by delay lines and by a quartz oscillator of known frequency. The measurements have been performed for about 3 months, with an amount of total hours $\simeq 1100$.

---

(2) W. C. Elmore: *Rev. Sci. Instr.*, **21**, 649 (1950).
(3) D. Brini, L. Peli, O. Rimondi and P. Veronesi: *Nuovo Cimento*, **11**, 651 (1954).

3. – Experimental Results.

The photographs have been observed separately by two observers. Their conclusions are not substantially different.

TABLE I.

Lead thick. (cm)	g/cm² of a.e.	$t_0(\mu s)$ 0.66 total n.	0.66 frequen. (min^{-1})	0.89	←	1.11	←	1.33	←	1.55	←
0	2	765	.0641 ±.0023	704	.0590 ±.0022	647	.0542 ±.0021	571	.0478 ±.0020	518	.0434 ±.0019
5.8	37	571	.0731 ±.0031	521	.0667 ±.0030	476	.0609 ±.0028	432	.0553 ±.0027	397	.0508 ±.0026
15.8	104	514	.0770 ±.0034	463	.0694 ±.0032	429	.0643 ±.0031	396	.0593 ±.0030	357	.0535 ±.0029
25.8	180	577	.0791 ±.0033	539	.0739 ±.0032	499	.0684 ±.0031	445	.0610 ±.0029	406	.0557 ±.0028

The measurements have been performed at four different lead thicknesses, namely 0 cm, 5.8 cm, 15.8 cm, 25.8 cm. At least 400 events, for each lead thickness, have been recorded to have a statistical error not greater than 5%. Each experimental point is the result of measurements performed in several different time intervals, and for a total time of about 110 hours. The frequencies determined in any time interval, at a certain thickness, have been found to be in agreement with one another. Table I reports the frequencies relative to the different lead thicknesses. These frequencies have been measured for different time values; the time is measured from the moment in

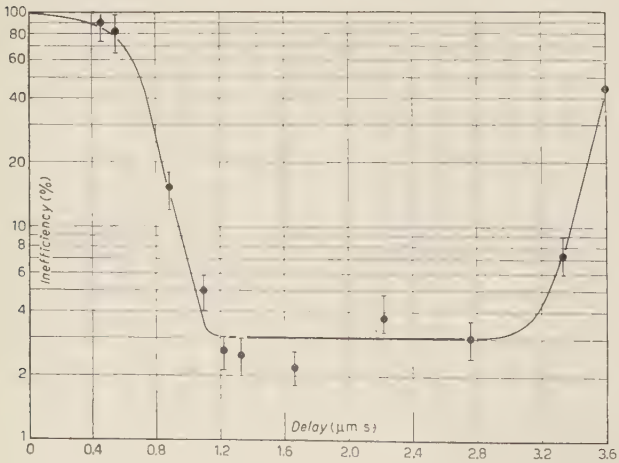

Fig. 2.

which the mesons come to rest. t_0 has been estimated with an error of about 0.1 μs. The minimum value of $t_0 = 0.66$ μs, has been suggested by the following considerations. We observe in Fig. 2 the experimental behaviour of the inefficiency of AC, versus the delay between C and AC; the minimum inefficiency is corresponding to a delay of ~ 1.2 μs. In the experimental apparatus used, the delay between C and AC has been adjusted at 1.33 μs. This means that the decay electrons emitted downward, penetrating the tray T, have a probability included between 97% and 70% of starting off AC in the first 0.66 μs. The corresponding events have the same probability of being cancelled. For this reason the number of events recorded between 0 and 0.6 μs is certainly not correct; therefore we did not take them into consideration. In a strict sense, events should be taken into account only starting from $t_0 = 1.1$ μs, because after that time the AC inefficiency is $\sim 97\%$. However, we have considered also the events, between 0.66 μs and 1.1 μs, because the frequency of the events, within this time interval, may be reasonably corrected by taking into account the geometry of the experimental arrangements. This correction will be described later.

The previous assumptions have been experimentally controlled as follows: it has been measured the number of events occurring in the intervals $0 \div 0.6$ μs and $0.6 \div 1.1$ μs in two different conditions, with or without AC. It has been observed that, even considering the chance coincidences which without AC were not negligible, the number of events falling in the first interval, is much higher ($\sim 40\% \pm 15\%$) than the number of the events recorded in the same conditions with AC. In the second interval the variations were within the statistical errors.

4. – Correction of the Experimental Results.

Different causes influence the experimental results. It is necessary, therefore, to consider the corrections that must be performed on the results. We have found the following causes and made the corrispondent corrections.

a) After pulses;
b) Causal events;
c) Showers;
d) AC efficiency (A);
e) Muons decay under counter C_2 with upward electron emission (U);
f) Extrapolation to $t_0 = 0$ and capture of μ^- within the scintillator (K);
g) Geometry and efficiency of the arrangement (G);
h) Scattering (S);
i) Barometer effect (B);

l) Detection efficiency of $\mu \to e$ decay (E);
m) Coincidences loss of counter C_2 (P).

Some of these corrections concern only the absolute values, and not the relative ones, because they influence every measurement percentually in the same way. We shall investigate now every type of correction, and try to establish quantitatively its weight. At the end we shall apply the corrections to the experimental values.

a) *After pulses.* – For the particular detection method of $\mu \to e$ event, the results may be influenced by the PM after pulses. The after pulses of PM 5819 ([4-6]) are essentially distributed within a few μs time interval, after the main pulses. In the present experiment, we think that this effect does not practically occur for the following reasons:

1) Sometimes, observing the traces, as many as 3 or 4 small pulses have been seen. They actually had constant height, and were distributed, averagely, within the interval from 0 to 5 μs. We have considered these pulses as after pulses. According to this consideration, we have established this criterion of choosing the events: we have omitted those traces where the secondary pulses had an amplitude inferior to the double height of the single after pulses. This bias, obviously, influences the detection efficiency of the $\mu \to e$ event, and therefore, the absolute intensity estimation.

The scintillation generates in the three PM, three correspondent current pulses, which overlap one another, because they are in phase. On the contrary, other after pulses result distributed at random. If we assume that the pulses are uniformely distributed in the interval $0 \div t$ μs, and that every PM averagely originates n after pulses, each one of Δt width (due to the forming delay-time)

$$P = 3\left(\frac{n}{t/\Delta t}\right)^3 \frac{t}{\Delta t} = 3n^3\left(\frac{\Delta t}{t}\right)^2,$$

gives the probability that three of them, coming from the three different PM, overlap. As it may be seen, for $\Delta t \simeq 0.1$ μs and $n = 2 \div 3$, the probability is very small and we did not take into consideration this event.

A proof of the validity of this estimation is the following fact: no more than two pulses of an amplitude higher than the bias have been observed in any trace. Obviously, if the probability was indicative, many more pulses should have been observed in a photogram.

([4]) P. W. DAVIDSON: *Nucleonics*, **10**, n. 3, 33 (1952).
([5]) F. B. HARRISON, T. N. K. GODFREY and J. W. KEUFFELL: *Nucleonics*, **10**, n. 3, 33 (1952).
([6]) D. W. MUELLER: *Nucleonics*, **10**, n. 3, 33 (1952).

2) Moreover, the presence of after pulses would have had a sensitive weight on the determination of the average lifetime of the muons: this did not occur as will be pointed out later. We did not think, therefore, our measurements should at all be modified for this reason.

b) *Casual events.* – Two distinct particles, passing through counter C_2 at a distance from each other of a time interval from 0.66 μs to 8.9 μs, simulate the decay of a muon. The frequency of these casual events is given by:

$$N = N_1 N_2 \sigma ,$$

where N_1 is the sweep per second, N_2 the pulses, coming from counter C_2, per second, with an amplitude higher than the bias, σ is the useful time sweep. Assuming the orders of magnitude:

$$N_1 \approx 0.1 \text{ sweep per min}$$

$$N_2 \approx 10^2 \text{ pulses per s}$$

$$\sigma \approx 10 \text{ μs}$$

we have:

$$N \approx 10^{-4} \text{ per min} .$$

Obviously, the casual events influence the obtained results in a negligible way.

c) *Showers.* – Some muons decaying in counter C_2 might belong to penetrating showers, made in the lead. We are not going to take into account corrections due to such events for the following reasons:

1) only a small percentage of μ, belonging to the showers, decay in the scintillator;

2) the frequency of such showers at sea-level is, by our arrangement, at least an order of magnitude inferior to the μ intensity in air;

3) other ionizing particles capable to start off AC are present very often in the penetrating showers.

Similar considerations may be made for the estensive air showers.

d) *Anticoincidence efficiency.* – Let us calculate the corrections to be made on the frequencies relative to the time values 0.66 μs, 0.89 μs and 1.11 μs as to what we said in the previous paragraph, about the anticoincidence efficiency. The mean solid angle, according to which, from any point of counter C_2 the plate T can be seen, is $\Omega \simeq 4$ sterad. As the decay electrons are isotropically emitted, the percentage of the ones hitting the plate T is given by $\simeq 32\,\%$.

If we take into account the anticoincidence efficiency, we obtain the corrections shown in Table II for the various t_0 values.

TABLE II.

t_0 (μs)	Eff (%)	Correction (%)	Factor A
0.66	40	$\sim 13 \pm 1.3$	1.010 ± 0.004
0.89	10	~ 3	1.002
1.11	12	~ 0.3	1

e) Decay of muons underneath counter C_2, with upward emission of the electron. – Condensed materials (such as wood table, GM counters, etc.), are placed underneath counter C_2, at a mean distance of about 20 cm. We estimated the absorbing thickness of these materials to be about 9 g/cm² with a total mass of ~ 25000 g. The muons decaying in such materials are ~ 15 times the number of muons decaying in counter C_2. Because our experimental apparatus might record one of these events, it is necessary:

1) AC be not working at the crossing of the muons;
2) the decay electron be emitted upward so that it may penetrate C_2;
3) AC be not working at the crossing of the decay electron.

Event 1) has a probability of 3%.

In event 2) we observe that the mean solid angle, under which C_2 may be seen, from any point of the medium where the muon might decay, has been calculated to be about 0.7 sterad. Therefore the electron percentage capable to cross through C_2, is $\sim 5\%$. Consequently, it can be recorded a number of these electrons equal to $\sim 70\%$ of the ones coming from muons decayed in the scintillator.

AC is inefficient to the muons decayed after 1.1 μs. Their probability of being considered decayed in the scintillator is $0.7 \cdot 0.03 = 2\%$. The muons decayed between 0.66 and 1.11 μs have a probability of generating a recordable electron similar, more or less, to the probability that AC be not working either at the arrival of the meson or at the passage of the electron directed upward. Besides, all the muons decayed within this time interval are fewer than the muons decayed after 1.1 μs. Obviously, the probability of recording such events may be disregarded, and we think that the only correction to be performed is the one related to the mesons decayed after 1.1 μs, starting from the instant in which they came to rest. Their corrective factor, is as we saw, $U = 0.980 \pm 0.001$.

f) Extrapolation to $t_0 = 0$ and μ-meson capture in the scintillator. – We are going to estimate now the total number of muons decayed in C_2, consi-

dering also the negative muons captured by nuclei in the scintillator. Be N^+ and N^-, respectively, the number of positive and negative μ-mesons, decayed after instant t_0. Be N_0^+ and N_0^- the μ-mesons present at $t_0 = 0$, τ^+ and τ^- be the mean lifetimes of the differently signed muons, f their ratio τ^-/τ^+. From the expression:

$$N^+ = N_0^+ \exp[-t_0/\tau^+] \; ; \qquad N^- = N_0^- \exp[-t_0/\tau^-]$$

remembering that $N_0^+/N_0^- = r$ at sea-level, and that our experimental apparatus has recorded decays as late as the instant $T = 8.9$ μs, we get:

$$(1) \qquad N_\infty(t_0) = N_T(t_0) + N_\infty(T) = \frac{N_0}{1+r}\{r \exp[-t_0/\tau^+] + f \exp[-t_0/\tau^-]\},$$

for the total number of muons decayed from t_0 on.

Consequently,

$$(2) \qquad N_0 = K_T(t_0) N_T(t_0)$$

gives the total number of muons decayed in our counter from instant $t_0 = 0$, which we indicate with $N_0 = N_0^+ + N_0^-$.

Even if we consider the different values given by several authors for the ratio f in the carbon (in our death thickness the capture is mostly due to carbon) the (1) may be rightly considered an exponential with decay constant expressed by:

$$\tau_m = \frac{\tau^- + \tau}{2} .$$

By this assumption $K_T(t_0)$ appearing in the (2) may be well expressed approximately by:

$$(3) \qquad K^T(t_0) = \frac{1+r}{r\{\exp[-t_0/\tau^+] - \exp[-T/\tau^+]\} + f\{\exp[-t_0/\tau^-] - \exp[-T/\tau^-]\}},$$

where

$$\tau^+ = 2\tau_m/(1+f) \quad \text{and} \quad \tau^- = 2f\tau_m/(1+f) .$$

In order to tabulate the (3) for the various values of t_0, we have deduced τ_m from our experimental results, using PEIERLS (7) formula, opportunely adjusted (see Appendix) because we have considered that the event computation is

(7) R. PEIERLS: *Proc. Roy. Soc.*, A **149**, 473 (1935).

made after a time t_0. In this manner we get the value $\tau_m = 2.08 \pm 0.03$ μs. Fig. 3 reports the experimental decay curve corrected for the decays occurred from T on. The straight line corresponds to the mean life τ_m.

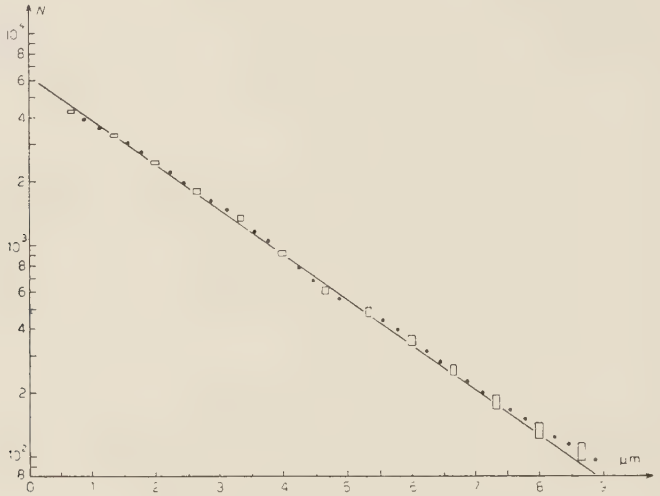

Fig. 3.

As may be seen, considering also the abscissa errors, the agreement is good. The theoretical value of f evaluated by WHEELER [8] and expressed by:

$$f = \frac{Z_0^4}{Z_0^4 + Z_{\text{eff}}^4}, \tag{4}$$

where

$$Z_{\text{eff}} = Z\left[1 + \left(\frac{Z}{37.2}\right)^{1.54}\right]^{-1/1.54}, \tag{5}$$

depends from constant Z_0 whose value must be deduced from the experimental values. They were found by several Authors and reported in Table III. These values have been used to calculate the Z_0 value with the least square method. Fig. 4 shows the experimental points and the continuous line curve, which has, as its parameter, the most probable value of Z_0. The other two dashed lines show Z_0 influence. In Table III there are also Z_0 values deduced from (4) according to several Authors. The weighted average of these values, gives $Z_0 = 10.57$. Then the f value, for carbon, assuming $Z_0 = 10.6$, becomes 0.92, in agreement to the value found by MOREWITZ ($f = 0.92 \pm 0.02$). Table IV

---

[8] F. A. WHEELER: *Rev. Mod. Phys.*, **21**, 133 (1949).

reports the numerical values of (3) estimated with reference to the following values 0.66, 0.89, 1.11, 1.33, 1.55 μs of t_0.

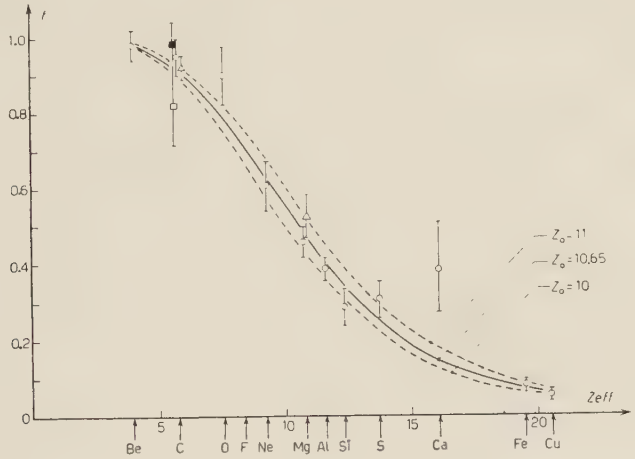

Fig. 4.

g) Geometry and efficiency of the detection apparatus. The geometry and efficiency of the experimental apparatus influence differently the results in connexion with the minimum range prefixed. In fact, when between C_1 and C_2, there are at least 5.8 cm of lead, the mesons μ crossing C_1 are practically relativistic; but they are not so, when between C_1 and C_2 there is no absorber. So the minimum mean track of the muons in counter C_1, sufficient to trigger the coincidence, is different in the two cases, namely with 5.8 cm of lead, it is twice the minimum mean track with 0 cm of lead. In other words, the telescope geometry must be differently evaluated, according to the different lead thickness. We will do so, by varying the solid angle; the distance between the two counters shall be virtually increased, so that the reduction of the recorded coincidences is corrispondent to the coincidences lost for the inefficiendy of the counters.

Counter C_2 is practically insensible to the two different circumstances above described, because the muons decaying in it, have always the same range distribution. In order to take into account the above facts, we have considered the entrance counter, with an area 18×18 cm², and placed it at a different distance from C_2 according to the two actual cases. Obviously, this distance must never be smaller than $L = 32.5$ cm, which is the distance between the lower base of C_1 and the upper one of C_2. To estimate how much L should be increased in the various cases, we have measured the hard component frequency ν_t (with ~ 15 cm of lead). Such frequency, taking into account the rather large solid angle considered, is related to the apparatus

TABLE III.

Year	Authors	Z	Z_{eff} (*)	τ^- (μs)	τ^+ (μs)	f	Z_0
1952	HINKS-BELL [9]	4	3.93	2.05 ± 0.06	2.09 ± 0.02	0.98 ± 0.04	10.2 ± 5
		6	5.78	1.98 ± 0.08	»	0.95 ± 0.05	12 ± 4
1953	MOREWITZ-SAMOS [10]	6	»	1.92 ± 0.04	»	0.92 ± 0.03	10.7 ± 1.5
1952	ALBERIGI-PANCINI [11]	6	»	2.18 ± 0.07	2.22 ± 0.06	0.98 ± 0.06	15 ± 10
1954	BISHOS-SINHA [12]	6	»	1.93 ± 0.24	2.35	0.82 ± 0.11	8.5 ± 2
1948	TICHO [13]	8	7.56	1.89 ± 0.15	2.09 ± 0.02	0.90 ± 0.08	10.3 ± 0.8
		10	9.25	1.28 ± 0.12	»	0.61 ± 0.07	10.3 ± 0.8
		12	10.83	0.96 ± 0.06	»	0.46 ± 0.04	10.4 ± 0.4
1949	VALLEY [14]	12	»	1.1 ± 0.20	»	0.53 ± 0.06	1.1 ± 0.7
		13	11.58	0.81 ± 0.06	»	0.39 ± 0.03	10.4 ± 0.4
1948	TICHO [13]	13	»	0.82 ± 0.05	»	0.39 ± 0.03	10.4 ± 0.4
1952	CATHEY [15]	14	12.33	0.60 ± 0.09	»	0.29 ± 0.05	9.9 ± 0.6
1948	TICHO [13]	16	13.7	0.66 ± 0.05	»	0.31 ± 0.05	11.2 ± 0.6
1952	CONFORTO [16]	20	16.1	0.81 ± 0.24	»	0.39 ± 0.12	14.4 ± 2
1952	KEUFFEL [17]	26	19.5	$.163 \pm .027$	»	$.078 \pm .014$	10.5 ± 0.5
		29	20.5	$.116 \pm .009$	»	$.055 \pm .005$	10.1 ± 0.3

(*) Z_{eff} calculated by (5).

geometry by:

$$(6) \qquad r_t = I_t \int \cos^2\theta \, d\Omega \cos\theta \, dS = I_t \int \cos^2\theta \sin\theta \, d\theta \, d\varphi \, dS = I_t A(L) ,$$

where $A(L)$ is the value resulting from the numerically performed integration on the solid angle, defined by the two counters, both considered with two plane surfaces of 18×18 cm area, at a distance L from each other. It is evident

TABLE IV.

t_0	0.6	0.89	1.11	1.33	1.55
$K_T(t_0)$	1.47	1.645	1.84	2.04	2.29

[9] *A. B.* HINCKS and *V. B.* BELL: *Phys. Rev.*, **88**, 168 (1952); **88**, 1424 (1952).
[10] H. A. MOREWITZ and M. H. SHAMOS: *Phys. Rev.*, **92**, 138 (1953).
[11] A. ALBERIGI and E. PANCINI: *Nuovo Cimento*, **9**, 959 (1952).
[12] D. E. BISHOP and M. S. SINHA: *Phys. Rev.*, **94**, 1400 (1954).
[13] H. A. TICHO: *Phys. Rev.*, **74**, 1337 (1948).
[14] G. E. VALLEY: *Phys. Rev.*, **73**, 1251 (1948).
[15] LE CONTE CATHEY: *Phys. Rev.*, **87**, 169 (1952).
[16] A. M. CONFORTO: *Phys. Rev.*, **86**, 465 (1952).
[17] T. W. KEUFFELL *et al.*: *Phys. Rev.*, **87**, 942 (1952).

that $A(L)$ depends from the distance L only. We calculated $A(L)$ for different values of L. The behaviour of A versus L, is reported in Fig. 5.

Assuming $I_t = 0.82 \cdot 10^{-2}$ sterad^{-1}s^{-1} cm^{-2} and for the frequency the measured value $\nu_t = 37.1 \pm 0.5$ counts/min, we have $A = 0.46 \cdot 10^4$ which gives $L = 32.5 + 2.8$ cm. We have repeated the measurements of ν_t after taking off the forming line, firstly from one counter, secondly from the other one, eventually from both. We have done so, because the forming lines, by cutting the pulses, diminish the efficiency. The obtained frequencies have been corrected for the chance coincidences, experimentally measured. With the relation (6), we have determined the actual value of L corresponding to several conditions. The obtained results are shown in Table V. These data demonstrate that the maximum efficiency is obtained when both counters are without the forming line. The corresponding value of L is in perfect agreement with the distance between the lower base of counter C_1 and the upper base of C_2. Taking into account the errors of Table V, we assumed the following values: $\Delta L_1 = 1.3$ cm and $\Delta L_2 = 1.7$ cm,

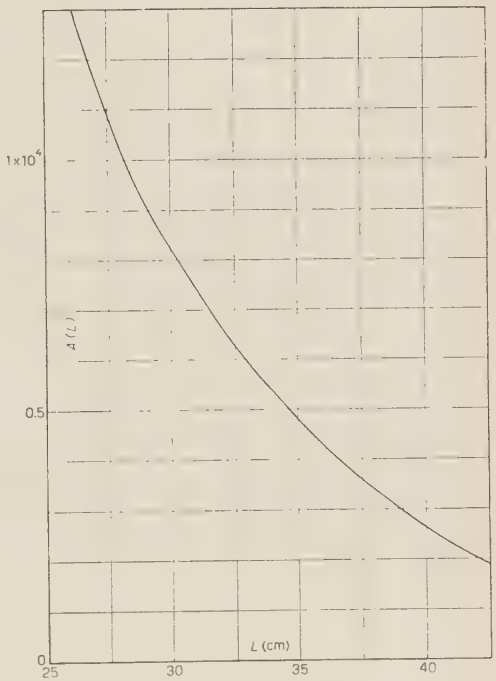

Fig. 5.

TABLE V.

	ν_t (*)	L_{eff} (cm)	ΔL (cm)
With forming line in C_1 and C_2	37.1 ± 0.5	35.3 ± 0.2	2.8 ± 0.2
Without forming line in C_1	41.3 ± 0.7	34.4 ± 0.2	1.9 ± 0.2
Without forming line in C_2	43.0 ± 1.0	34.0 ± 0.2	1.5 ± 0.2
Without forming line in C_1 and C_2	51.2 ± 0.9	32.5 ± 0.2	0 ± 0.4

(*) Corrected by chance coincidences.

respectively for counter C_1 and C_2. Other similar proofs, made with different ticknesses of lead, (> 15 cm) have again given good results, especially for the absolute values of $\Delta L = \Delta L_1 + \Delta L_2$.

Considering the differential spectrum, we observe that

$$(7) \qquad \nu_d = I_v \int \varrho \cos^3\theta \sin\theta \, d\theta \, d\varphi \, dh \, dS = I_v \varrho \sum_1^n {}_{\Delta h} A_{\Delta h}(L) \Delta h \,,$$

where Δh is the thickness of n layers, in which counter C_2 has been divided, ϱ is the scintillator liquid density, $\cos^3\theta$ is the zenital dependence ([18]).

From what we have been saying, so far, it is understood, that the $A_{\Delta h}(L)$ in (7) must be different if there is 0 cm of lead between C_1 and C_2 or more than 6 cm of lead. Considering that counter C_2 is actually whole efficient, because in it the muons die, we can draw the following considerations:

1) When between C_1 and C_2 there is at least 5.8 cm of lead, $L = 32.5 + 1.3$ cm is the minimum value of L correspondent to a perfect efficiency of the coincidence.

2) When between C_1 and C_2 there is no lead, we have already seen that the μ-mesons coming to rest in C_2 are not relativistic; therefore in C_1 they loose an amount of energy double the energy of the relativistic μ-mesons. This leads to: $L = 32.5 + 1.3/2$ cm.

Table VI, reports the value of:

$$G = \varrho \sum_1^{10} {}_{\Delta h} A_{\Delta h}(L) \Delta h$$

related to the two cases mentioned above where $n = 10$ and $\varrho = 0.94$ g/cm^3.

h) *Scattering.* – The scattering influence has been estimated with Monte Carlo method. The organisation was the following:

1) The position coordinates x_1 and y_1 of the muons incident, on counter C_1 (still considered as a horizontal plane surface) are all of equal probability.

TABLE VI.

Thickness of lead (cm)	0	> 5.8
$G\left(\frac{\text{sterad}\cdot\text{g}}{60}\right)$	$2.39 \cdot 10^4 \pm 0.02$	$2.297 \cdot 10^4 \pm 0.02$
G_{relative} (*)	1	1.040 ± 0.01

(*) $G_{\text{rel}} = 2.39 \cdot 10^4/4$.

([18]) J. J. KRAUSHAAR: *Phys. Rev.*, **76**, 1045 (1949).

2) All the values of azimutal angle φ has the same probability in the interval $0 \div 2\pi$.

3) The probability that the zenital angle α of an incident muon direction, might be between α and $\alpha + \mathrm{d}\alpha$, is espressed by:

$$\mathrm{d}P(\alpha) = K \cos^3\alpha \, \mathrm{d}\Omega \,,$$

where $\mathrm{d}\Omega$ is the unit solid angle in the zenital direction. The amplitude from 0° to $\pi/2$ has been divided in 20 angular intervals $\Delta\alpha$ having the same probability. The values of the estracted angles α, every one coupled to its own angle φ, have been projected in two planes normal to each other perpendicular to the plane $x_1 y_1$ to which counter C_1 belongs. In such way projections α_x, α_y have been obtained.

4) Counter C_2 has been divided in 10 layers of equal thickness, whose mean plane has been assumed as the decay plane of the mesons. The division has been suggested by the following considerations: the total death thickness is sufficiently small (5.64 g/cm²), therefore the mesons have the same probability of coming to rest anywhere in the counter, and of decaying there. The exact death depth is essential for the estimation of the residual range of the mesons, from which we get the mean square angle $\langle\theta^2\rangle$ of scattering. The valuation of the mean square angle has been performed by [19]:

$$(8) \qquad \langle\theta_x^2\rangle = \langle\theta_y^2\rangle = \frac{E_s^2}{2X_0} \int_{x_1}^{x_2} \frac{\mathrm{d}x}{(pc\beta)^2} \,,$$

where $E_s = 21$ MeV, $X_0 = 6.5\,\mathrm{g/cm^2}$ and $p\beta$ has been considered variable because the muons, particularly before coming off the scatterer, are no longer relativistic. The behaviour of the several different $\sqrt{\langle\theta_x^2\rangle}$ in function of the residual range and for several thicknesses of the scatterer, is shown in Fig. 6.

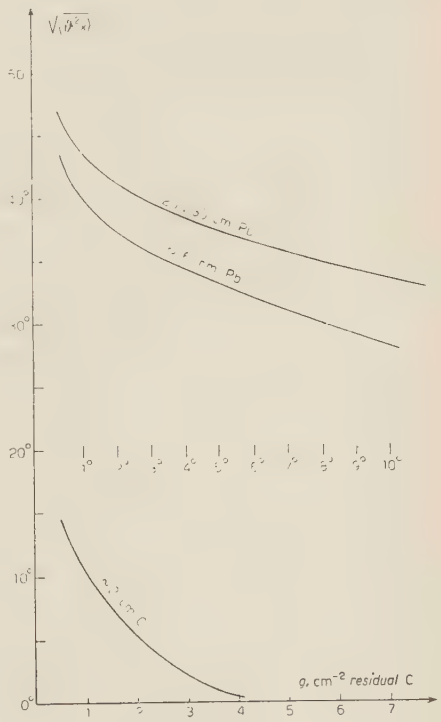

Fig. 6.

[19] B. Rossi: *High Energy Particles*, p. 68.

To perform the Monte Carlo method we have made these assumptions:

1) The meson trajectory is straight. Actually, there is a lateral displacement, but it varies from about 1 mm to 3 mm (for the lead thickness crossed and for the residual ranges). Taking into account the compensation effect and that the surface covered by the absorber is larger than the surface covered by counter C_2, we can consider the lead absorber with a plane surface, of equal area, placed at about 3 mm above the lower actual base; in this surface the scattering occurs around the incidence direction.

2) The range in the scatterer have been all increased of about 10% with respect to the geometrical vertical range. It has been done so, to valutate the longer range due to the zig-zag ([20]) trajectory for the multiple scattering, and due to the inclined incidence direction of the particles. It must, however, be pointed out that such longer range is practically not influencing $\langle\theta^2\rangle$, because of the small contribution of the scattering in the first centimetres of the scatterer. With these assumptions it is possible to establish the coordinates x and y on the scattering plane for the muons coming from counter C_1. Knowing that the distribution of the scattering angles projected θ_x and θ_y is gaussian, we have divided the angle from $-\pi/2$ to $\pi/2$ in 40 angular intervals $\Delta\theta_x$ and $\Delta\theta_y$ having the same probability.

This operation has been made for every value of $\langle\theta_x^2\rangle$ and $\langle\theta_y^2\rangle$.

6) It is possible to see whether the μ-meson falls into counter C_2 by knowing the following data, with the help of a simple mechanical device:

1) coordinate x (y) on the scattering plane;
2) distance of x (y) point from the upper base of counter C_2;
3) death depth in C_2;
4) value of the angle $\delta_x = \alpha_x + \theta_x$ ($\delta_y = \alpha_y + \theta_y$) made by the direction of the meson coming off the scattering plane with respect to the vertical line.

We calculated the ratio S of the number of mesons coming off C_1 which fall into counter C_2, by considering the scattering, and the number of the same mesons (from C_1) falling into C_2 without considering the scattering. The Monte Carlo method was performed on 2000 particles incident on counter C_1: among these particles, those reaching C_2, without considering the scattering, are $N = 298$.

Table VII reports the S values. In Fig. 7 is plotted the S ratio versus the progressive number of incident particles. From this curve we obtain the assimptotič values of S with the corresponding errors.

The scattering influence related to 15.8 of lead has been calculated by interpolation among the data calculated for 5.8 cm of lead and 25.8 cm of

([20]) H. P. KOENIG: *Phys. Rev.*, **69**, 590 (1946).

lead. We have also performed an experimental proof ([20]) of these evaluations. First of all, we have estimated, with Monte Carlo method, the scattering

TABLE VII.

Scatterer	C_1	5.8 cm of lead	25.8 cm of lead	15.8 cm of lead (*)
$S = N/N_S$	1.050 ± 0.013	1.185 ± 0.010	1.212 ± 0.013	1.20 ± 0.015

(*) Evaluated.

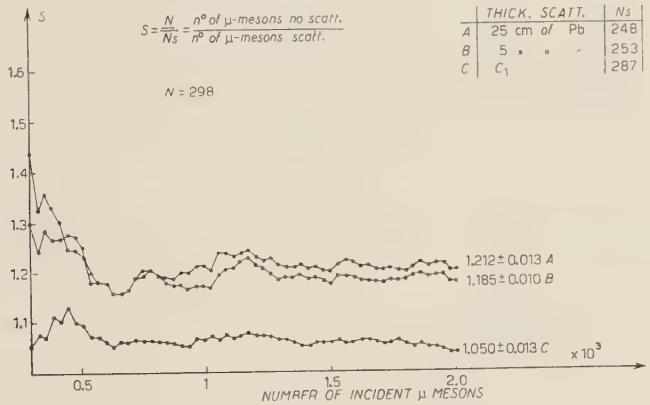

Fig. 7.

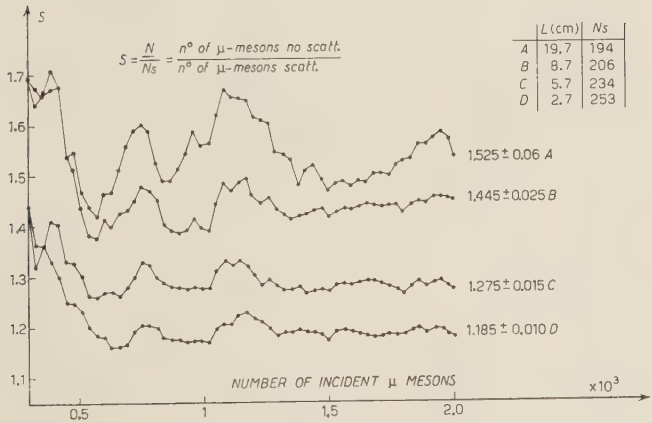

Fig. 8.

influence due to 5.8 cm of lead, when it is placed at different distances from counter C_2; exactly at 2.7, 5.7, 8.7, 19.7 cm respectively. These results can be obtained from Fig. 8.

Secondly we have measured the frequencies corresponding to the distances 2.7, 4.9, 7.7, 12.7, 22.7 cm. The obtained values, corrected for the barometer

effect, and the values above calculated, are reported in Fig. 9. In this is made the comparison between the experimental results and the ones deducted by the Monte Carlo method; these last results have been normalized at the distance $L = 0$ at 0.096.

The agreement is good. It may be observed that the scattering influence varies quickly from $L = 7 \div 8$ cm. Regarding higher values of L, the scat-

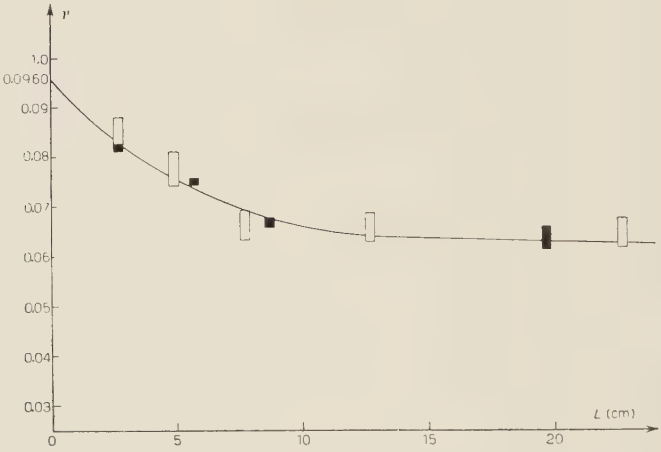

Fig. 9.

tering influence does not change much, at least, within the statistical errors and with our geometry ([20]).

i) *Barometer effect.* – For this correction, during the whole time of the measurement, we have taken the mean pressure values from the Meteorological Observatory of the University of Bologna. These values related to every experimental point, are reported in Table VIII.

TABLE VIII.

cm Pb	0	5.8	15.8	25.8
P average (torr)	755.5	755.5	754.0	753.5
B	0.992	0.992	0.990	0.989

Assuming as barometer coefficient of the intensity of slow μ-mesons the value $C = 1.75\%$ per mm of Hg ([21]), we get the correspondent correction factors B for every experimental point. They are reported in the same Table VIII.

([21]) D. C. ROSE: *Canad. Journ. Phys.*, **29**, 97 (1951).

l) Detection efficiency of the $\mu \to e$ *decay.* – To estimate the detection efficiency of the $\mu \to e$ decay in counter C_2, it is essential to know the relation between the energy lost by a particle in the scintillator and the relative pulse-height recorded in the photograph. With the same experimental apparatus without AC and with 15.8 cm of lead thickness between C_1 and C_2 we have photographed the pulses coming from counter C_2, and generated by the crossing μ-mesons which are mostly relativistic. Fig. 10 reports the istogram of the pulse-height distribution, of the photographs; the height in this figure is measured in arbitrary units.

The istogram of Fig. 10 would represent the Landau curve, due to the fluctuation in muon energy loss in the scintillator, if:

1) every particle had the same energy;
2) every particle had the same path in the scintillator;
3) amplifier were strictly uniform;
4) counter C_2 were strictly uniform.

Discussing the 1) condition, it must be noted that in Landau curves there is a remarkable difference in the most probable value of the energy loss, only between relativistic and slow μ-mesons ([22]). Our istogram contains also the slow meson contribution, but they represent percentually only a small fraction unable to change the most probable value of the energy loss. Therefore we may actually affirm that, for the prefixed range bias, the meson energy does not practically affect the value of the most probable energy loss.

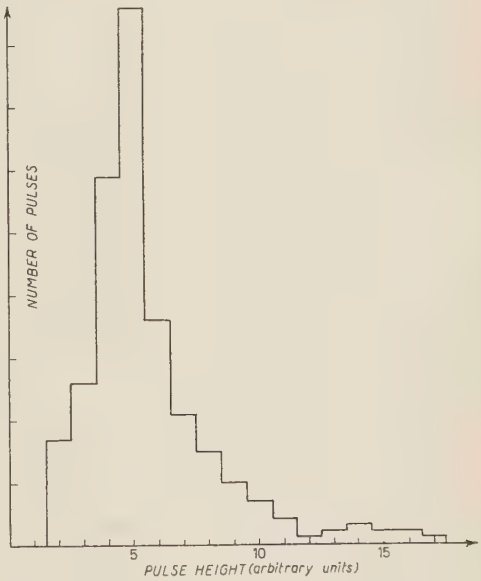

Fig. 10.

To estimate how important the second condition is, we have drawn the istogram of Fig. 11. In it, we reported the zenithal distribution of the coincidence muons, obtained by Monte Carlo method. The gravity center of this distribution falls around $\alpha \simeq 14^\circ$. To this value corresponds a path 3% longer than the vertical one. Furthermore there are μ-mesons capable to give a pulse height sufficient to trigger the coincidence circuit and coming off from the lateral walls.

([22]) T. Bowen and F. X. Roser: *Phys. Rev.*, 85, 992 (1952).

These are about 30% of the total number of mesons, and have a density practically constant in every point of such walls. Consequently we estimated at ~ 5.5 cm the mean path of all the crossing muons.

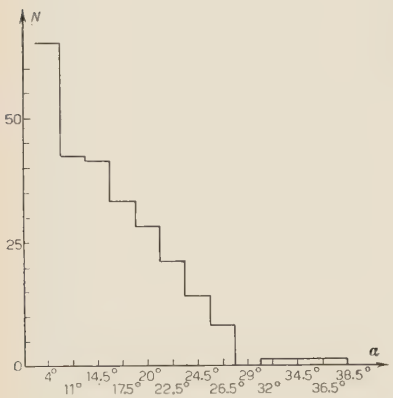

Fig. 11.

The influence of condition 3) is negligible. In fact, the amplifier is linear within 10% and in the conditions in which the istogram of Fig. 10 was obtained, most pulses were inadequate to saturate the amplifier.

Finally, let us see the influence of the C_2 disuniformity. Estimated according to the criterions shown in previous papers [1], it resulted to be $\pm 25\%$ in respect to the mean value. The pulse-height spread, due to such disuniformity, is much less than the statistical fluctuations in the energy loss. Its influence is marked by a small smoothing of the Landau curve. In our case, we have estimated that the disuniformity influence on the most probable value of the pulse-height in Fig. 10, is within $10 \div 20\%$.

Concluding this discussion, we think we may affirm that the istogram in Fig. 10 agrees with Landau curve, to an approximation good enough to perform a correct evaluation of the pulse-height with respect to the mean range. Actually the spread in the mean range distribution is much more remarkable towards the lower pulses of the mean path than towards the higher one. This fact leads to an enlargement of Landau curve towards the values of smaller energy losses; this enlargement is partially cut by the bias put by the coincidence. This fact may be clearly seen by observing the inferior cut in the istogram. We wish also to point out that the istogram extreme tail, towards the higher pulses, is perhaps due to the presence of slow μ-mesons, as we have already said. The most probable pulse-height, in the arbitrary units used, results of ~ 5.5 divisions and corresponds actually to the relativistic μ-meson mean path of ~ 5.5 cm in the scintillation. The correspondent energy loss is $\simeq 10$ MeV.

As we have considered a minimum amplitude ~ 1 division (for the already mentioned reasons on the after pulse influence), this amplitude corresponds ro an energy of ~ 1.8 MeV dissipated in the scintillator. For the decay electron, which are always relativistic, this energy represents its loss in a path of ~ 0.9 g/cm^2 $\simeq 1.0$ cm of scintillator. We are now able to determine the detection efficiency of the event $\mu \to e$ of our apparatus.

Let us indicate with a the minimum range of electron detection now estimated, with N_τ the total number of muons decaying in counter C_2; $l \times l \times h$

be its dimensions; the number of muons decaying in the layer between R and $R+\mathrm{d}R$ and emitted in the whole solid angle is

$$\frac{N_T}{h}\,\mathrm{d}R\,.$$

For $R<a$ the decay electrons emitted upward in a direction within the solid angle

$$\Omega = 2\pi\left(1-\frac{R}{a}\right),$$

are no detected.

Their relative number is clearly expressed by:

$$\frac{1}{N_T}\,\frac{2\pi}{4\pi}\,\frac{N_T}{h}\int_0^a\left(1-\frac{R}{a}\right)\mathrm{d}R = \frac{a}{4h}\,.$$

The same thing can be said for the electrons emitted downward.

The relative number of the non detected decay electrons calculated for the two bases is given by $a/2h$.

Taking into account also the influence of the lateral walls, the percentage of the detected decay electrons is:

$$\varepsilon = a\left(\frac{1}{2h}+\frac{1}{l}\right)\cdot 100 \simeq 13.9a\,\% \qquad (a \text{ in cm}).$$

This value is certainly slightly overestimated. In fact on estimating the partial losses on the single surface of the parallelepiped representing counter C_2 an amount of electrons is computed two times. However, these electrons concern a scintillator which is $\sim 10\,\%$ of the total volume. So we think that the experimental data should be corrected, according to this effect influence in the following way:

$$\varepsilon \simeq 13a\ \%\,.$$

The correction factor is, then, $E = 1.13 \pm 0.04$.

m) *Coincidence losses in counter* C_2. – Not the whole counter C_2 is efficient. When we discussed on the geometry of the apparatus, we saw that a relativistic muon, must cross at least ~ 1.7 cm to produce a signal adequate to trigger the coincidence. This path is equal to a mean energy loss of ~ 2.3 MeV. Consequently the coincidence will be triggered only by the mesons stopping in C_2 with a residual range of about 0.75 mm. We may, therefore, conclude that the percent of lost coincidence is $1.3\,\%$. The correction factor is then $P = 1.012 \pm 0.003$.

5. – Corrected Results.

Now we want to give the behaviour and absolute value of the differential range spectrum of slow μ-mesons according to our experimental results and to the considered corrections. As we have already pointed out, some corrections do not affect the spectrum behaviour, but only the absolute value; so we shall consider the two problem separately.

a) Differential spectrum behaviour. – Corrections G_{rel}, S and B influence the determination of the slope of the differential spectrum. The frequencies ν lf Table I are related to the experimental ones by:

$$\nu = \nu_{meas} G_{rel} SB \,. \tag{9}$$

The correction factors G_{rel}, S, B, with relative errors, are reported in Table IX. The Table X reports the frequency corrected values together with their errors. In a logarithmic diagram ν depends linearly from the range.

TABLE IX.

Thickness of lead (cm)	0	5.8	15.8	25.8
G_{rel}	1	1.04 ± 0.01	1.040 ± 0.010	1.04 ± 0.01
S	1.050 ± 0.013	1.185 ± 0.010	1.200 ± 0.015	1.212 ± 0.013
B	0.992 ± 0.002	0.992 ± 0.002	0.990 ± 0.002	0.989 ± 0.002
$G_{rel} SB$	1.042 ± 0.015	1.222 ± 0.024	1.236 ± 0.030	1.247 ± 0.029

TABLE X.

Lead thick. (cm)	g/cm² of a.c.	t_0 (μs) 0.66	0.89	1.11	1.33	1.55
		frequency (min⁻¹)	←	←	←	←
0	2	0.0670 ± 0.0033	0.0615 ± 0.0032	0.0565 ± 0.0030	0.0498 ± 0.0028	0.0452 ± 0.0027
5.8	37	0.0893 ± 0.0053	0.0815 ± 0.0052	0.0744 ± 0.0050	0.0676 ± 0.0046	0.0621 ± 0.0044
15.8	104	0.0936 ± 0.0064	0.0858 ± 0.0059	0.0795 ± 0.0056	0.0733 ± 0.0053	0.0661 ± 0.0049
25.8	180	0.0986 ± 0.0063	0.0922 ± 0.0061	0.0855 ± 0.0058	0.0761 ± 0.0054	0.0694 ± 0.0051

In Table XI we have reported the slopes calculated with the least square method, for different values of t_0.

Considering these data and performing a weighted average, the value of the slope results of 0.091 ± 0.006.

TABLE XI.

t_0 (μs)	0.66	0.89	1.11	1.33	1.55
slope	0.0857 ± 0.0069	0.0884 ± 0.0059	0.0898 ± 0.0048	0.0958 ± 0.0047	0.0959 ± 0.0046
Weight mean 0.0912 ± 0.0054					

b) *Absolute intensity.* – The experimental data to obtain the absolute vertical intensiti I_v must be corrected by all the factors, previously calculated. Namely

$$I_v = \alpha \nu_{\text{meas}} \qquad \left(\text{where } \alpha = \frac{AUKSBEP}{4}\right). \tag{10}$$

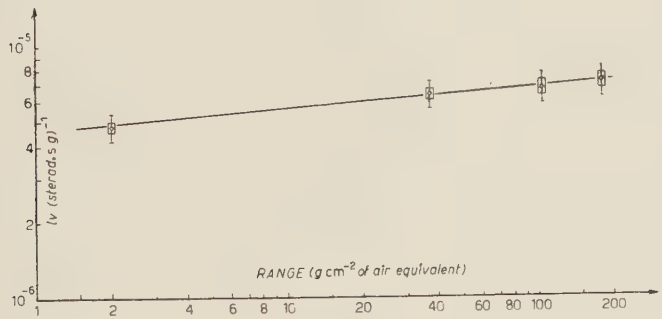

Fig. 12.

The values of (10) corresponding to different range, are reported in Table XII. They were obtained by making the weighted average on the values of I_v related to different values of t_0, and are reported in Fig. 12. The straight line has the slope calculated above.

TABLE XII.

g/cm² of a.e.	2	37	104	180
$I_v(10^{-6})$	4.8 ± 0.6	6.4 ± 0.8	6.8 ± 0.9	7.2 ± 1.0

6. – Conclusions.

In regard to the spectrum slope, our values is in good agreement with the ones of Rossi curve ([33]), and with recent Fafarman measurement ([34]).

We do not consider the results of measurements made by the cloud-chambers on the lower part of the spectrum. In fact they have large statistical errors and they are not correct for the well known limitation of this technique.

TABLE XIII.

Coincidence		Delay coincidence		Anticoincidence		Cloud-chamber	
EHMERT ([23])	6.5	STEIMBERGER ([27])	4.4	KOENIG ([20])	3.7	WILSON ([29])	3.6
ROSSI ([24])	4.8	SANDS ([26])	3.4	KELLERMAN ([28])	2.0	GERMAIN ([30]) (*)	8.4
NIELSEN ([25])	6.5			KRAUSHAAR ([18])	5.5	YORK ([31])	6.9
SANDS ([26])	5.6			SANDS ([26])	4.1	LICHTENSTEIN ([32])	6.0

(*) This value is obtained after the second correction by factor $\sqrt{2\pi}$ which YORK referred to.

Actually ours is slightly higher than Rossi's slope. This may be attributed to the scattering influence, which varies with the range. In our case, from ~ 10 to ~ 100 g/cm^2 of a.e., such influence increase of about 3%. Taking into account these order of magnitude corrections, both ours and Rossi's slope agree exactly. However there is not doubt that the spectrum behaviour, at least in the range from ~ 0 to ~ 180 g/cm^2 of a.e., is approximately straight and increase with the range, without any irregularity.

For the absolute value, to make a comparison with other Authors' results, let us consider their absolute values at ~ 150 g/cm^2 of a.e. For lower ranges, the experimental results may be affected by greater errors. Our value at ~ 150 g/cm^2 of a.e. is $(7 \pm 1) \cdot 10^{-6}$ 1/ster.s.g.

Table XIII reports other Authors' values, and their experimental methods.

([23]) C. EHMERT: *Zeits. f. Phys.*, **106**, 751 (1937).
([24]) B. ROSSI *et al.*: *Phys. Rev.*, **57**, 461 (1940).
([25]) W. M. NIELSEN *et al.*: *Phys. Rev.*, **59**, 547 (1941).
([26]) M. SANDS: *Phys. Rev.*, **77**, 180 (1950).
([27]) J. STEINBERGER: *Phys. Rev.*, **75**, 1137 (1949).
([28]) E. W. KELLERMAN: *Proc. Phys. Soc.*, A **62**, 356 (1949).
([29]) J. G. WILSON: *Nature*, **158**, 415 (1946).
([30]) L. GERMAIN: *Phys. Rev.*, **80**, 616 (1950).
([31]) C. M. YORK: *Phys. Rev.*, **85**, 998 (1952).
([32]) P. G. LICHTENSTEIN: *Phys. Rev.*, **93**, 858 (1954).
([33]) B. ROSSI: *Rev. Mod. Phys.*, **20**, 537 (1948).
([34]) A. FAFARMAN and M. H. SHAMOS: *Phys. Rev.*, **96**, 1096 (1954).

Rossi [33] assumed the value of $5.6 \cdot 10^{-6}$ 1/ster.s.g. York emphasised that the normalisation point of Rossi curve is lower because of the scattering influence. This fact leads to consider particularly the scattering corrections. The above results obtained by us confirm the exactness of York's conclusions. In fact, in our geometry, the only distance of the scatterer from the detector, can change the scattering influence from the $\sim 18\,\%$ to the $\sim 60\,\%$. For this reason we believe that our high value is right, considering also the actual agreement to the last results obtained with cloud-chamber.

* * *

We wish to thank Prof. G. Puppi for all his useful advice and discussions. We thank also Mr. C. Maroni who followed the experiment, Mr. R. Degli Esposti, who mounted the electronic devices, and Mr. L. Parisini, for his help in the calculation.

Appendix

We remember the expression of Peierls [7]:

$$w = \int_0^t w(t)\,\mathrm{d}t\,, \tag{1}$$

where w represents the probability that the event might occur within the time interval $0 \div t$ and $w(t)$ the probability that the same event might fall within the interval t and $t + \mathrm{d}t$. As we consider events occurred only within t_0 and T, we shall integrate the (1) within these limits. Considering that

$$w(t)\,\mathrm{d}t = \frac{1}{\tau} \exp\left[-t/\tau\right]\mathrm{d}t\,,$$

our integral leads to the espression:

$$w = \exp\left[-\frac{T}{\tau}\right] - \exp\left[-\frac{t_0}{\tau}\right]. \tag{2}$$

With the same considerations developed by Peierls one finds that the link

between $s = \sum t_\nu n_\nu / m$ and τ is given by:

$$S = \tau + \frac{t_0 - T \exp\left[-(T - t_0)/\tau\right]}{1 - \exp\left[-(T - t_0)/\tau\right]}, \tag{3}$$

of which the relation of Peierls:

$$S = \tau + \frac{T \exp\left[-T/\tau\right]}{\exp\left[-T/\tau\right] - 1},$$

represents a particular case. Eq. (3) has been tabulated assuming $T = 8.9$ μs and for the values: 0.66, 0.89, 1.11, 1.33, 1.55 μs.

RIASSUNTO (*)

In questo lavoro diamo i risultati di una misura dello spettro del range differenziale dei mesoni π tra 0 e ~ 1.5 m.a.e. al livello del mare. L'apparecchiatura sperimentale impiegata consiste di due contatori a scintillazione a riempimento liquido posti in coincidenza fra di loro. Tra essi si trova un assorbitore di piombo. Il contatore inferiore di spessore 5.64 g/cm² lavora come spessore di decadimento. L'evento $\pi \to e$ è stato rivelato dalla fotografia dei due impulsi successivi, dovuti al mesone e all'elettrone, sullo schermo di un sincroscopio. I risultati sperimentali sono stati corretti per ogni possibile causa di errore. La correzione di scattering è stata valutata col metodo di Monte Carlo e verificata sperimentalmente. I risultati corrispondenti alla correzione di scattering mostrano quanto grande possa essere alle volte questa influenza. L'intensità assoluta al range di ~ 150 g/cm² di aria eq. è risultata di $7 \cdot 10^{-6}$ (sterad·g·s)$^{-1}$. Il comportamento dello spettro tra 0 e 180 g/cm² di aria eq. è risultato con una pendenza di 0.091 ± 0.006.

(*) *Traduzione a cura della Redazione.*

Influenza di un campo magnetico trasversale sulla tensione d'innesco della scarica in un gas in alta frequenza.

L. Ferretti e P. Veronesi

Istituto di Fisica dell'Università - Bologna

(ricevuto il 25 Luglio 1955)

Riassunto. — Nel presente lavoro si riferiscono i risultati di alcune misure condotte in alta frequenza, per studiare l'influenza di un campo magnetico trasversale sulla tensione di innesco della scarica in un gas. Tali misure sono state eseguite per l'aria, alle pressioni di 0,1; 0,5; 1,0 mm Hg e con frequenze di 10; 15; 20; 25; 30 MHz. Il campo magnetico è stato fatto variare da 0 a 650 gauss ed il tubo da scarica usato era ad elettrodi cilindrici. I risultati mostrano una forte influenza del campo magnetico sulla tensione d'innesco della scarica; essi vengono discussi e confrontati con quelli ottenuti da S. C. Brown *et al.* e da J. S. Townsend *et al.* che sono i soli che si trovano nella letteratura.

1. – Introduzione.

È nota l'importanza che ha assunto lo studio delle scariche elettriche in alta frequenza in questi ultimi anni. Un esame generale delle scariche elettriche in alta frequenza, dei fenomeni ad essi connessi e delle loro principali applicazioni fisiche e tecniche è stato fatto recentemente da S. C. Brown [1] e da Llewellyn Jones [2]. In questi lavori, specialmente in quello ampio e completo di Llewellyn Jones è riportata una abbondante bibliografia sull'argomento. Da questa è possibile vedere che poche sono state le ricerche condotte per studiare il comportamento delle scariche in alta frequenza sotto l'influenza di un campo magnetico. Un confronto diretto dei risultati ottenuti dai vari autori, se può considerarsi buono sotto l'aspetto qualitativo, non

---

(1) S. C. Brown: *P.I.R.E.*, **39**, 1493 (1951).

(2) F. Llewellyn Jones: *Rep. Prog. Phys.*, **16**, 216 (1953).

può essere ritenuto tale per quello che riguarda i risultati quantitativi. Ciò è principalmente dovuto alle diverse condizioni sperimentali nelle quali hanno lavorato i vari ricercatori. Nel seguito, distingueremo tali diverse condizioni sperimentali con le lettere « *E* » ed « *H* », secondo il criterio di BABAT [3] riportato nel lavoro già citato di LLEWELLYN JONES.

Un primo gruppo di lavori [4,10] riguarda il comportamento della scarica elettrica in alta frequenza e campo magnetico, mentre un secondo gruppo si riferisce a ricerche sulla tensione d'innesco nelle medesime condizioni.

GILL [11] usando un dispositivo « E » con elettrodi esterni e campo magnetico trasversale ha notato una forte influenza di quest'ultimo sulla tensione d'innesco. Con una frequenza di 50 MHz ed un campo di circa 18 gauss, in un tubo contenente aria, questa influenza comincia a farsi sentire per pressioni inferiori a 10^{-4} mm_{Hg}. La tensione di innesco si riduce di un fattore 5 e di un fattore 10, rispettivamente, per pressioni di $2 \cdot 10^{-2}$ mm_{Hg}, e $2 \cdot 10^{-3}$ mm_{Hg}, rispetto alla tensione d'innesco in assenza di campo magnetico. GILL e TOWNSEND [12] hanno ripreso queste osservazioni, facendone una trattazione teorica ed eseguendo alcune misure con aria secca, contenuta in un pallone sferico di 13 cm di diametro ed un dispositivo ad « E » con elettrodi esterni e campo magnetico trasversale. Le frequenze usate erano 30 e 50 MHz e l'intensità del campo veniva veniva fatta variare da 0 a 40 gauss. Successivamente BROWN [13], con lo stesso dispositivo ha studiato il fenomeno con Azoto ed Elio. In particolare i risultati di questo autore mostrano che per basse pressioni $5 \cdot 10^{-2}$ mm_{Hg} esiste, per ciascuna pressione, un intervallo di valori del campo magnetico in corrispondenza del quale si ha un abbassamento della tensione d'innesco e di mantenimento della scarica, in accordo con le previsioni teoriche. POSIN [14] ha verificato lo stesso effetto, in aria, in un « gap » entro una guida d'onda, con microonde da 10000 MHz. Infine ALLIS ,BROWN e LAX [15] hanno studiato sperimentalmente e teoricamente l'azione di un campo magnetico trasversale

---

([3]) G. BABAT: *Journ. Instr. Elect. Eng.*, **94**, Pt. III, 27 (1947).

([4]) T. V. IONESCU e C. MIHUL: *Compt. Rend.*, **194**, 70 e 1330 (1932); **195**, 765 e 1008 (1932).

([5]) T. V. IONESCU e I. MIHUL: *Compt. Rend.*, **196**, 1292 (1933).

([6]) Y. ASAMI e M. SAITO: *I.E.E. Japan Journ.*, **56**, 882 (1936).

([7]) H. NEUERT: *Zeits. Naturfor.*, **3** A, 310 (1948); **4** A, 449 (1949).

([8]) B. KOCH e H. NEUERT: *Zeits. Naturfor.*, **4** A, 456 (1949); *Ann. Phys. Lpz.*, **7**, 97 (1950).

([9]) A. LINDBERGH H. NEUERT e H. WEIDNER: *Naturwissenschaften*, **39** 374, (1952).

([10]) M. U. CRIILOVIČ e M. B. NIKOLIČ: *Bull. Inst. Nucl. Sci.*, **3**, 29 (1953).

([11]) E. W. B. GILL: *Nature* **140**, 1061 (1937).

([12]) E. W. B. GILL e J. S. TOWSENDN: *Phil. Mag.*, **26**, 290 (1938).

([13]) A. E. BROWN: *Phil. Mag.*, **29**, 302 (1940).

([14]) D. Q. POSIN: *Phys. Rev.* **69**, 541 (1946).

([15]) W. P. ALLIS, S. C. BROWN e B. LAX: *Journ. App. Phys.*, **21**, 1197 (1950).

sulla tensione d'innesco della scarica in alta frequenza operando con Elio ed Idrogeno a pressione da 1 a 30 mm_{Hg}, campi fino a 3000 gauss e frequenza costante di 3000 MHz.

Come si vede dai lavori citati, soltanto tre di essi ([12,13,15]) riportano risultati quantitativi i quali consentono di apprezzare il ruolo giocato dal campo magnetico in questo tipo di fenomeni.

Noi abbiamo condotto una serie di misure analoghe, limitatamente all'aria, che possono essere di un certo interesse e che comunque estendono il quadro delle conoscenze sperimentali attuali.

2. – Dispositivo sperimentale e risultati.

Il tubo da scarica da noi usato era ad elettrodi cilindrici coassiali, di alluminio, della lunghezza di 10 cm, con cilindro esterno di diametro 2.2 cm e cilindro interno di diametro 0.2 cm. Il tubo da scarica era contenuto in un tubo di vetro connesso al sistema di vuoto. La pressione del gas veniva misurata mediante un manometro a mercurio, con un errore non superiore al 2%. L'elettrodo esterno era connesso a terra e quello interno alla sorgente di tensione alternata. Questa veniva fornita da un circuito E.C.O., le cui caratteristiche sono stabilità e purezza di frequenza, e prelevata mediante un circuito traslatore accordato. La tensione anodica alla valvola amplificatrice veniva fornita con una alimentazione indipendente e con possibilità di ampie variazioni, partendo da zero. Tutti i circuiti erano schermati con schermature poste a terra ed i collegamenti tenuti più corti possibile.

Per la misura della tensione abbiamo utilizzato un dispositivo analogo a quello descritto da Llewellyn Jones e Morgan ([16]) e tarato nella stessa maniera. L'errore di misura, nel nostro caso è stato stimato più forte di quello del dispositivo degli autori su citati; circa il 3% alle frequenze da noi usate. Il campo magnetico trasversale era ottenuto con una bobina cilindrica, coassiale col rubo da scarica. Il campo fornito è stato valutato con la formula riportata da Bozorth ([17]); si è visto che la disuniformità massima nella regione interessante la scarica (fra il punto di mezzo dell'asse del tubo e gli estremi) era del 7% circa. La lettura della tensione d'innesco è stata fatta col criterio Llewellin Jones e Morgan secondo il quale l'innesco coincide con l'apparizione del bagliore nel tubo da scarica (fra gli elettrodi) e la tensione d'innesco corrisponde al valore massimo segnato dal voltmetro a valvola, prima della brusca diminuzione che accompagna l'apparire del bagliore.

Le nostre misure sono state eseguite con cinque frequenze diverse e preci-

---

([16]) F. Llewellyn Jones e G. D. Morgan: *Proc. Phys. Soc.*, B **64**, 560 (1951).
([17]) R. M. Bozorth: *Ferromagnetism* (New York, 1951), p. 840.

samente 10, 15, 20, 25 e 30 MHz. Per ogni frequenza sono state ricavate le tensioni d'innesco corrispondenti a tre valori della pressione, cioè 0.1, 0.5, 1 mm_{Hg}.

I risultati sperimentali sono riassunti in fig. 1 in un diagramma semilogaritmico. In ordinate sono riportate le tensioni efficaci d'innesco V_s ed in ascisse il campo magnetico in gauss. Le curve sperimentali sono state ricavate da più

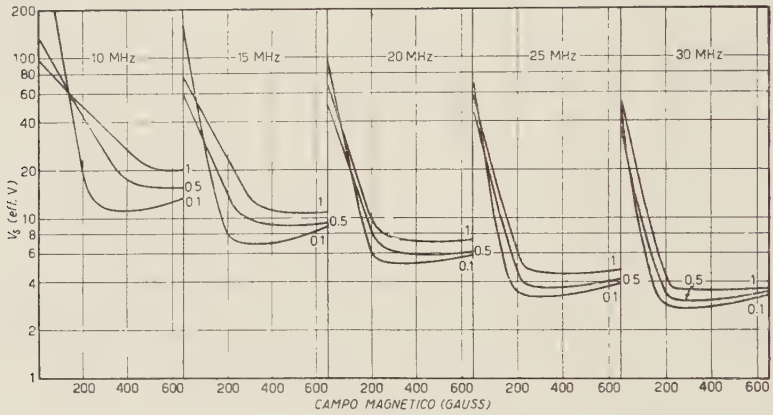

Fig. 1.

misure facendo, per ogni punto la media dei risultati ottenuti. Poichè le misure si sono mostrate abbastanza bene riproducibili noi stimiamo i nostri valori precisi entro il 5%. I punti sperimentali sono stati ricavati in corrispondenza dei seguenti valori del campo magnetico: 100, 200, 300, 400, 500, 600 e 650 gauss. Per chiarezza di rappresentazione non abbiamo riportato in figura i punti sperimentali ed i relativi errori.

3. – Discussione.

Come si vede dalla fig. 1 i nostri risultati confermano la forte influenza del campo magnetico sulla tensione d'innesco della scarica in alta frequenza. C'è da osservare che, rispetto ai risultati degli altri autori, nel nostro caso non abbiamo trovato il tipico minimo di risonanza che si ha quando è verificata la relazione

$$\omega = \frac{eB}{m}$$

dove ω è la pulsazione della tensione alternata e B il valore del campo magnetico. Ciò può essere imputato ai particolari valori di ω da noi usati in corri

spondenza delle pressioni del gas con le quali abbiamo operato. Gli autori che hanno lavorato con le nostre frequenze hanno usato pressioni di quasi due ordini di grandezza inferiori alle nostre, mentre gli autori che hanno sperimentato con pressioni dell'ordine di quelle da noi usate operarono con frequenze di circa due ordini di grandezze superiori alle nostre. Inoltre le misure sono state condotte in condizioni sperimentali notevolmente diverse.

Abbiamo tentato anche di inquadrare i nostri risultati utilizzando le conclusioni teoriche e sperimentali degli altri autori, in particolare del gruppo del M.I.T. ([15]).

I risultati di questi autori affermano che l'azione del campo magnetico trasversale sull'innesco della scarica in alta frequenza si traduce in una apparente aumento di tutte le dimensioni normali al campo magnetico nel rapporto

$$(\omega_b^2 + \nu_c^2)^{\frac{1}{2}}/\nu_c ,$$

dove $\omega_b = eB/m$ e ν_c è la frequenza di collisione degli elettroni liberi con le molecole del gas. In base a questa conclusione abbiamo eseguito i calcoli basandoci sulla teoria sviluppata da Brown e Herlin ([18]), che poggia sul concetto di coefficiente di ionizzazione in alta frequenza, staiblita per elettrodi cilindrici coassiali e verificata sperimentalmente per l'aria. Le conclusioni a cui siamo giunti non si accordano sufficientemente con i risultati sperimentali e non abbiamo creduto opportuno riportarle. È molto probabile che il disaccordo sia dovuto sia alle drastiche schematizzazioni da noi formulate sia al fatto che ci siamo serviti dei coefficienti di ionizzazione, stabiliti per frequenze nel delle microonde.

([18]) S. C. Brown e M. A. Merlin: *Phys. Rev.*, **74**, 291 e 911 (1948).

SUMMARY (*)

In this paper are reported the results of some high frequency measurements, carried out in order to study the influence of a transversal magnetic field on the breakdown voltage of a gas discharge. These measurements were performed in air at 0,1, 0,5; 1,0 mm_{Hg} pressure and at 10; 15; 20; 25; 30 MHz. The magnetic field was made to vary from 0 to 650 gauss and the emploied discharge tube had cylindrical electrodes. The results show a strong influence of the magnetic field on the breakdown voltage of the discharge. Our results are discussed and compared with those of S. C. Brown *et al.* and of J. S. Townsend *et al.* which are the only ones published.

(*) *Editor's Translation.*

A Sufficiently Fast and Economical Sweep Circuit.

D. Brini, L. Peli, O. Rimondi e P. Veronesi

Istituto di Fisica dell'Università - Bologna

(ricevuto il 2 Agosto 1955)

Summary. — We have built a sweep circuit, employing a very low number of secondary emission tubes (EFP 60). The sweep times of this circuit are within 40 and 3 000 mμs, on 10 cm of track. The linearity curves are also reported.

In the fast electronic, for the testing of the apparatus, are needed syncroscopes whose sweep circuits can detect the mμs. We have built a sweep circuit, which, compared to the conventional types, employes a rather low number of tubes, therefore needs a low power dissipation; it has good features of speed and linearity. The circuit is shown in Fig. 1.

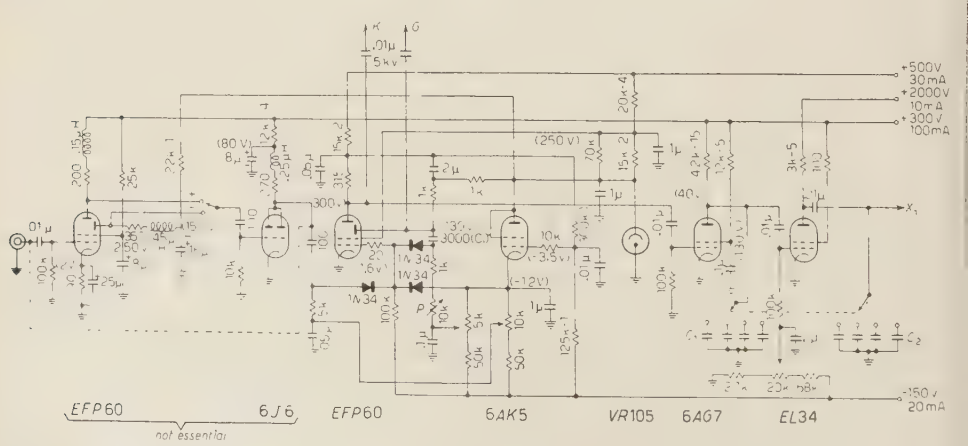

Fig. 1.

It is based on the well known fast discriminator (1), with secondary emission tubes. This circuit gives a rectangular negative pulse at 6AG7. The first part of the rise tension is amplified by the output EL34. Several different sweep times are obtained by the various C_1 and C_2 capacitances, placed at the input and output of EL34. The push-pull pulses taken at the dynode and anode of the EFP60 are used as intensifiers. The widths of these pulses, folloving the sweep speed, are controlled by potentiometer P. With only one C_i capacitance, and potentiometer P the obtained range between $4 \cdot 10^{-8}$ and $3 \cdot 10^{-6}$ s is covered. The first EFP60 is an amplifier-inverter stage which triggers the discriminator through another amplifier stage. The system has a gain of ~ 10 and a total rise time of about 10 mμs. It must be noticed that this system is not essential. Of course, if it does not exist, the pulses, which trigger the discriminator, must be positive only.

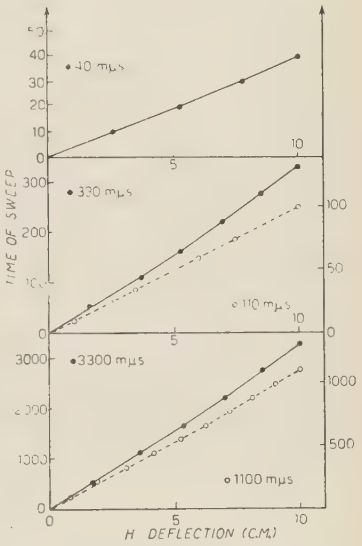

Fig. 2.

The features of this syncroscope are essentially bound to the possibilities of the fast discriminator. It is triggered by pulses of 0.1 V $\sim$ 10 mμs wide. The rise time of the intensifier pulses is of some mμs. The maximum speed sweeps are actually limited by the interelectrodic capacitances of the two output tubes. Table I shows the values of C_1 and C_2 capacities corresponding to the sweep speeds, which we have obtained. The delay time of the sweep circuit is about 30 mμs. In order to get a good linearity at every speed, it is necessary to delay more the output to the vertical plates, with respect to the start of the sweep. In the same Table I are reported the best delays obtained for the several sweep speeds.

TABLE I.

Sweep time (mμs)	C_1 (pF)	C_2 (pF)	Best delay (mμs)
40	0	0	70
$\sim$ 100	10	58	100
$\sim$ 330	22	290	120
$\sim$ 1100	200	1150	260
$\sim$ 3300	280	2500	320

(1) M. O. DEIGHTON, G. J. R. MCLUSKY, N. F. MOODY: *Electronic Eng.*, **24**, 214 (1952).

With these delays, the linearity is the different speeds at evaluated. This linearity can be seen in Fig. 2, where the deflection laws are reported. Our apparatus contains also the fast generator of very short pulses which is a mercury-contact sealed high pressure relay (1), triggered by a multivibrator for the two frequencies 1 and 100 s^{-1}. Fig. 3 shows some examples of pulses seen at the syncroscope. We used for these testing a C.R.T. Du Mont 5XP, with accelerations of 300 V and post accelerations of 15000 ÷ 20000 V.

Pulse 10 mμs wide.

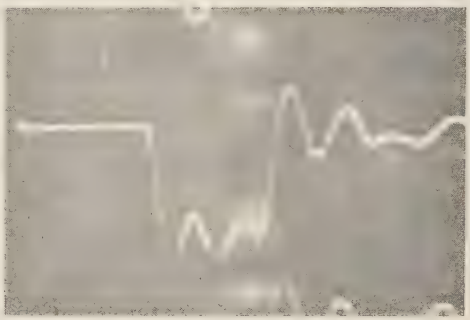

Damped oscillations - Period; 10 mμs.

Fig. 3. – Time sweep: 40 mμs.

Although the secondary emission tubes are used, the life of such circuit is rather long. This circuit has been used in an experiment (2) and in various testing which lasted about 2000 hours.

* * *

We thank Mr. R. Degli Esposti for having built the circuit described above.

(2) D. Brini, L. Peli, O. Rimondi and P. Veronesi: *Nuovo Cimento*, **2**, 613 (1953).

RIASSUNTO (*)

Abbiamo costruito un circuito di spazzamento impiegando un numero assai ridotto di tubi ad emissione secondaria (EFP 60). I tempi di spazzamento di tale circuito vanno da 40 a 3000 mμs su 10 cm di traccia. Si riportano anche le curve di linearità.

(*) *Traduzione a cura della Redazione.*

IL NUOVO CIMENTO Vol. I, N. 3 1° Settembre 1955

Analysis of Properties of Secondary Particles in Nucleon-Nucleon Collisions at Very High Energy (*).

M. Schein, R. G. Glasser and D. M. Haskin

Department of Physics, University of Chicago - Chicago, Illinois

(ricevuto il 16 Agosto 1955)

Summary. — Momentum measurements were made on the individual secondary particles emitted in the « outer » cone of the *S*-star. A lower limit to the momentum of the particles in the « inner » cone was obtained. The transformation from the laboratory system to the center-of-mass system can be made, using suitable approximations, on the assumption that all charged secondaries are pions. This leads to a symmetrical angular and energy distribution with all particles included in a forward or backward cone of half-angle 20°. The results are compared with various multiple production theories. It is possible to infer that there is no more than one pair of particles of protonic mass among the secondaries and that even the presence of one pair would violate symmetry. The number of K-mesons must also be small. The methods of analysis should be useful on other events in this energy range.

1. – Introduction.

The problem of analyzing stars caused by high energy cosmic ray particles in nuclear emulsions is, in general, quite complicated. However, if the incident particle is a nucleon and the target is a nucleon also, the analysis is considerably simplified since it is then possible to postulate bilateral symmetry in the center

(*) Paper presented at the International Congress on Elementary Particles held at Pisa, Italy, June 1955.

Supported in part by the joint program of the U. S. Office of Naval Research and the U. S. Atomic Energy Commission.

of mass system (1). Even is cases where the target nucleus is more complicated but where there is some evidence that the principal interaction was with a peripheral nucleon, it is possible to analyze the star on the basis of a nucleon-nucleon interaction since the energy transferred to the rest of the target nucleus may be negligibly small. It is possible to make a real distinction here between low and high energies. At low energies it is possible to have an appreciable fraction of the energy emitted from the « first nucleon-nucleon collision » in the form of secondary particles at relatively large angles. It is then quite probable that these secondaries will strike another nucleon inside the nucleus and that a nuclear cascade may develop. In the case of the very high energies ($E_p > 10^{13}$ eV), the secondaries from a given nucleon-nucleon collision are known to be very strongly collimated in the direction of motion of the incident nucleon and hence, it is quite possible that a collision with a peripheral nucleon will result in almost all the energy being transferred into a cone so narrow that it intersects no other nucleons. This is the same phenomenon which takes place in central collisions and produces the so-called « tunnel effect » (2). A simple computation shows that peripheral collisions are rather probable if the target nucleus is a light nucleus of the emulsion (C, N, O),

A number of authors have presented stars of varying degrees of complexity with primary energies of the order of 10^{13} eV or greater, generally with no possibility of analysing the energy of the secondaries (3).

In the present paper a careful analysis of the « S » star (1) is reported which illustrates the advantage of being able to measure the multiple scattering on several of the shower tracks. The « *S* » star is shown in Fig. 1. It occurred in a 200 μm Ilford G-5 emulsion flown at above 90000 feet for over 16 hours from Chicago, Illinois.

The fact that the only two secondary tracks (B and C) which are not closely collimated (within 5° in space) with the original direction of the primary track are gray tracks indicates that only an insignificant proportion of the original energy was transferred to the residual nucleus. It is thus reasonable to make an analysis on the assumption of a nucleon-nucleon collision. It will be shown that the event has bilateral symmetry in the center of mass system which is then confirming evidence of the nucleon-nucleon character of the event.

The energy of the incident singly charged particle (assumed to be a proton) has been determined previously by a method which uses not only the information from the angular distribution but also the available information on

(1) LORD, FAINBERG and M. SCHEIN: *Phys. Rev.*, **80**, 970 (1950).

(2) F. C. ROESLER and C. B. A. MCCUSKER: *Nuovo Cimento*, **10**, 127 (1953).

(3) ENGLER, U. HABER-SCHAIM and WINKLER: *Nuovo Cimento*, **12**, 930 (1954). Contains references to earlier work.

the energy of the secondaries (4). Now measurements have been made on the multiple scattering and the energies of the secondaries have been re-evaluated. The re-evaluation of these energies does not change the previous estimate of the primary energy.

The angles and energies of the individual secondary particles are calculated in the center of mass system of the colliding nucleons. The details of this analysis are described in section 2. This is important since it is possible to draw from this analysis some conclusions about the character of the secondaries.

The main interest of the present analysis is to indicate that it would be very profitable to investigate in greater detail the mechanism of collisions at these very high energies. It is of importance at the present time to learn something more of the nature of the collision process and of the secondaries produced. The first is of fundamental interest since it may indicate whether present theoretical attacks on the problem are likely to be fruitful. In particular, it should throw light on the validity of the statistical theories of the high energy collisions. The second is of interest since it is important to determine the role of heavy mesons and of nucleon-antinucleon pairs in high energy collisions. If heavy mesons are really elementary particles and are strongly coupled to the nucleon then one would expect their probability of production, relative to pions, to approach approximate equality at these high energies. If these mesons are merely composite states of other fundamental particles this conclusion would not necessarily hold (5). Certainly if nucleon-antinucleon pairs can be produced at all one would expect to see them in collisions of this energy (6). Finally these collisions should provide evidence on the interaction between free mesons; since mesons in the meson cloud around the nucleon extend far enough and since due to the Lorentz contraction of the cloud the collisions are of such short duration, some of the collisions, at least, are effectively meson-meson collisions.

2. – Transformation from Laboratory to Center of Mass System.

The formular for the Lorentz Transformation can be conveniently applied to the analysis of high energy stars in the following form:

$$E_i = \gamma(E_i' - \beta P_i' c \cos\theta_i') \tag{1}$$

$$P_i \cos\theta_i = \gamma(P_i' \cos\theta_i' - \beta(E_i'/c)) \tag{2}$$

$$P_i \sin\theta_i = P_i' \sin\theta_i' \tag{3}$$

---

(4) R. G. Glasser and M. Schein: *Phys. Rev.*, **80**, 970 (1950).

(5) G. Cocconi: *Phys. Rev.*, **93**, 1107 (1954).

(6) See *Proceedings of the Duke University Conference on Cosmic Rays* (Dec. 1953) (Unpublished), Session I.

where E_i, P_i, θ_i are the energy, momentum, and angle with the direction of motion, respectively, of the i-th particle and primed quantities are in the laboratory (L) system of coordinates, unprimed in the center of mass (c) system of coordinates. As usual, c is the velocity of light and βc the relative velocity of the C and L systems and $\gamma = (1 - \beta^2)^{-1/2}$. Dividing (3) by (2) one gets the trasnformation for angles:

$$\text{tg}\,\theta_i = \frac{\text{tg}\,\theta_i'}{\gamma[1 - \beta(E_i'/P_i'c)\sec\theta_i']}. \tag{4}$$

In the discussion of these formulae we will find it useful to introduce the following dimensionless quantities which will generally be very small compared to one:

$$\delta_\beta = 1 - \beta \tag{5}$$

$$\delta_{E_i} = \frac{E_i'}{P_i'c} - 1\,, \tag{6}$$

$$\delta_{\theta_i} = 1 - \cos\theta_i'\,. \tag{7}$$

Introducing these quantities into equations (1) and (4), the following expressions can easily be obtained:

$$E_i = \gamma E_i'\left[1 - \frac{(1 - \delta_\beta)(1 - \delta_{\theta_i})}{(1 + \delta_{E_i})}\right], \tag{8}$$

$$\text{tg}\,\theta_i = \frac{\text{tg}\,\theta_i'}{\gamma[1 - (1 - \delta_\beta)(1 + \delta_{E_i})(1 - \delta_{\theta_i})^{-1}]}. \tag{9}$$

Under the assumption that one can neglect δ_β, δ_{θ_i}, and δ_{E_i} and all products of these compared to one, (8) and (9) reduce to:

$$E_i = \gamma E_i'(\delta_\beta + \delta_{\theta_i} + \delta_{E_i}) \tag{10}$$

$$\text{tg}\,\theta_i = \frac{\text{tg}\,\theta_i'}{\gamma(\delta_\beta - \delta_{E_i} - \delta_{\theta_i})}. \tag{11}$$

These formulae are in a convenient form to derive the energy and angle in the C system from the measurements in the L system for the high energy collision we are treating.

The assumptions that these quantities, δ_β, δ_{θ_i}, δ_{E_i}, are small compared to one will be briefly discussed. If δ_β is small compared to one, this means

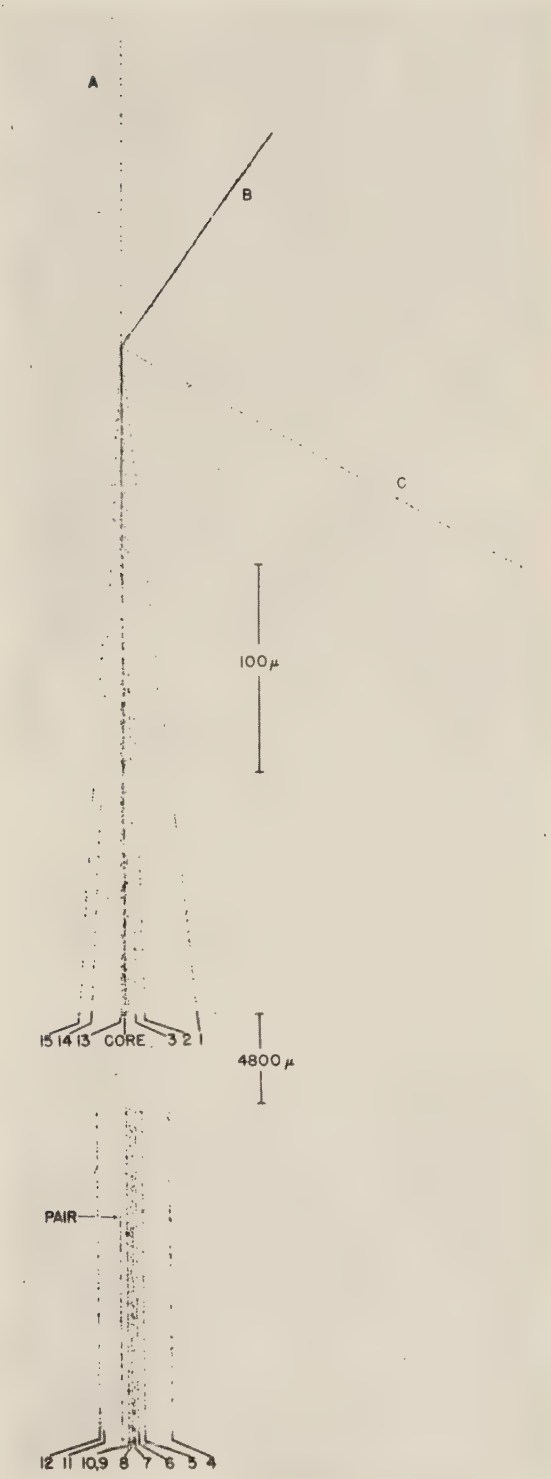

Fig. 1. – Projected view of the « *S* » star. A is the incident proton, B and C evaporation tracks. The core is shown at a distance sufficient to separate all except tracks 9 and 10. The pair is the only electron pair observed in the available distance.

that the relative velocity of the C and L system is nearly equal to that of light and hence corresponds to a very high energy primary. To the same order of accuracy as is used in neglecting δ_β compared to one, we can derive from (3) and the definition of γ:

$$\delta_\beta \approx \frac{1}{2\gamma'^2} . \tag{12}$$

The smallness of δ_{θ_i} means that the laboratory angle is itself very small, and hence we can write from (7):

$$\delta_{\theta_i} \approx \frac{\theta'^2}{2} . \tag{13}$$

If δ_{E_i} (in (6)) is small compared to one, this means that the laboratory energy of the secondaries is high. In this case we can write:

$$\delta_{E_i} \approx \frac{M_i^2 C^4}{2E_i'^2} . \tag{14}$$

The conditions that δ_β, δ_{θ_i}, δ_{E_i}, be small compared to one are well fulfilled in some high energy stars as will be shown in the next section.

3. – Analysis of the « S » Star.

The energy of the primary proton of the « S » star has previously been determined by the quantile method [1]. This method is valuable for stars where some multiple scattering data is available, since it makes use of this information which can greatly affect the energy determination. In the determination of the primary energy, it was assumed that all the secondaries are pions. The energy estimate would not be affected appreciably if a few of the secondaries had heavier mass. The energy was shown to be $(2^{+1.45}_{-0.85})\cdot 10^{13}$ eV.

The secondary tracks of the « S » star have been measured on the precision scattering stage in this laboratory. The $p\beta$ of the tracks in the outer cone (Fig. 1, tracks 1-4, 11-15) was measured directly by using the sagitta method of multiple scattering. The multiple scattering was definitely above noise in the largest cell length used on each track. The energies quoted should be accurate within a factor of two.

For the fast tracks of the inner cone (tracks 5-10) a track to track measurement of the multiple scattering was made. This method is the only one which can be used on these very fast tracks since it eliminates the small emulsion distortions and stage motion which contribute to the noise. This showed

definite scattering on one of the tracks (track 8). But the other five all showed no scattering sagitta as large as 250 Å, which was the limit of detection for the track position, in the 8000 μm observable track length. This corresponds to a $p\beta$ value of over 250 GeV/c for these tracks. They were treated in the rest of the computations as though this lower limit were a true, measured value.

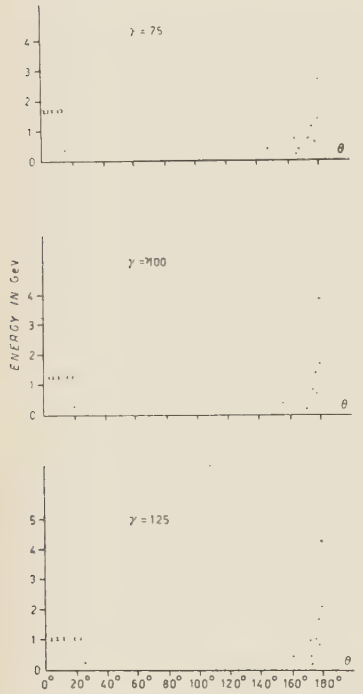

Since scattering measurements are thus available on all but the fastest tracks, it is possible to apply the analysis outlined in the preceding section to this event. For the purpose of this computation, all particles have been assumed to be pions. The calculations have been carried through for values of $\gamma = 100$ ($E_p = 2 \cdot 10^{13}$ eV), $\gamma = 125$ ($E_p = 3.1 \cdot 10^{13}$ eV), and $\gamma = 75$ ($E_p = 1.1 \cdot 10^{13}$ eV). Table I gives the results of this calculation for $\gamma = 100$. The results of the energy-angle correlation in the center of mass system for all three values of γ are shown in Fig. 2.

Fig. 2. – Energy vs. angle correlation for three values of γ. These correspond to the most probable value and values one standard deviation away. Points marked with a X represent particles for which only a lower limit to the energy can be obtained.

It should be noted that the points marked with crosses in Fig. 2 and for which it is possible to obtain only a lower limit to the energy by scattering measurements are relatively insensitive to the actual energy determination. That is, a change in the L-system energy does not affect the C-system angle, as can be seen from Table I. This is in distinction to the situation for the slow particles in the outer core where a change in measured energy affects both the C-system angle and energy.

Two facts show up very clearly in Fig. 2. One is that the shower particles are clearly divided into two cones of half angle approximately 20°. The fact that the forward cone contains six charged particles and the backward cone 9, is presumably due merely to statistical fluctutaions (*). The other fact is that

(*) In the original publication (reference (1)), track number 4 was placed in the forward cone since its energy was estimated to be much higher than the value now believed to be correct.

TABLE I. - *Transformation from L-system to C-system for three values of γ. $\gamma = 100$ is the most probable value. Auxiliary quantities have been included also for $\gamma = 100$ to illustrate their magnitude.*

Track	E' (GeV)	tg θ'	δ_E ($\cdot 10^{-6}$)	δ_θ ($\cdot 10^{-6}$)	$\gamma = 75$				θ	$\gamma = 100$		$\gamma = 125$	
					$\delta_\beta+\delta_\theta+\delta_E$ ($\cdot 10^{-6}$)	$\delta_\beta-\delta_\theta-\delta_E$ ($\cdot 10^{-6}$)	E (GeV)	tg θ		E (GeV)	θ	E (GeV)	θ
1	0.30	0.1733	--	—	—	—	2.6	— 0.0156	179.1°	3.9	179.3°	4.3	179.4°
2	1.5	0.0517	4360.	1340.	5790.	— 5610.	0.65	— 0.1229	173.0	0.86	174.8	1.07	175.8
3	6.0	0.0268	97°.	359.	720.	- 542.	0.32	— 0.6593	146.6	0.41	155.2	0.50	160.3
4	5.5	0.00047	324.	11.	424.	— 246.	0.17	— 0.2547	165.7	0.21	170.6	0.25	172.9
5	> 250.	0.00013	0.16	0.8	90.0	88.0	1.69	0.1970	11.1	1.28	14.9	1.03	18.5
6	> 250.	0.00008	0.16	0.3	89.5	88.5	1.68	0.1205	6.9	1.26	9.2	1.02	11.5
7	> 650.	0.0016	0.16	1.3	90.5	87.5	1.70	0.2438	13.7	1.29	18.3	1.05	22.8
8	50.	0.0016	3.9	1.3	94.2	83.8	0.35	0.2546	14.3	0.28	19.6	0.23	25.5
9	> 250.	0.0005	0.16	0.13	89.3	88.7	1.67	0.0752	4.3	1.26	5.7	1.01	7.2
10	> 250.	0.0002	0.16	0.04	89.2	88.8	1.67	0.0300	1.7	1.26	2.3	1.01	2.9
11	3.0	0.0200	1090.	200.	1378.	— 1200.	0.31	— 0.2222	167.5	0.40	170.8	0.50	172.7
12	1.5	0.0212	4360.	225.	4670.	— 4500.	0.53	0.0629	176.4	0.70	177.3	0.87	177.9
13	0.6	0.0397	28000.	788.	28800.	28700.	1.30	0.0185	178.9	1.71	179.2	2.16	179.4
14	3.0	0.0590	1090.	1740.	2920.	— 2740.	0.66	0.2870	164.0	0.86	168.0	1.07	172.0
15	1.0	0.0908	9800.	4120.	14000.	— 13900.	1.05	0.0873	175.0	1.40	176.3	1.75	177.0

the points plotted as crosses (for which only a lower limit to the energy was measured) corresponding to fast particles in the forward cone are probably very nearly at that lower limit, since if one assumed the actual energy were much higher the symmetry would be completely destroyed, although one would expect symmetry in such a nucleon-nucleon collision. This would seem to be supported by the fact that the one track in the forward cone whose energy is measured has an energy of the same order of magnitude as this lower limit.

The average energy of the secondaries in the backward cone is 0.84 GeV, 1.2 GeV, or 1.4 GeV for $\gamma = 75$, 100, or 125, respectively. Since symmetry between forward and backward cones should prevail, this can be considered as the best estimate of the average energy of all the secondaries. We observe fifteen charged secondaries; if we add one-half of this number for the neutral secondaries, the total energy carried away by the secondaries is about 25 GeV in the C-system. this should be compared with the total available energy in the C-system for the most probable values of γ ($\gamma = 100$) which is 200 GeV. On the basis of this comparison we conclude that only about one-eighth of the available energy is transferred to the secondaries in this collision. It should be emphasized that this conclusion is based on the assumption that the average energy of the neutral particles is the same as the energy of the charged pions as derived above, which in turn depends on the assumption of symmetry with respect to the plane perpendicular to the direction of motion of the primary.

These conclusions depend also on the identity of the charged particles which were assumed to be pions. If the assumption as to the nature of some of the particles were changed by assuming that they have mass M different from M_π, the principal effect would be to change δ_{E_i} by the factor M^2/M_π^2 as can be seen from (14), since the L-system energy is high enough that the measurement by multiple scattering can be considered a measurement of E'. If one assumes that some of the particles are of K-meson mass (about 1000 m_e) this factor is 13.3, and if one assumes particles of nucleonic mass it is 45. We will consider the effects with the estimate that $\gamma = 100$. The assumption that some of the particles are of K-meson mass would not affect the previous computations for the high energy forward particles (n. 5-7, 9-10 of Fig. 1) by more than five percent, but would for instance mean that if particle n. 8 were a K-meson instead of going at 20° with an energy of 0.3 GeV in the C-system, it would have been going at 100° with an energy of 0.5 GeV, an angle at which no pions are found according to the previous analysis. For the particles in the outher cone, this assumption would mean that they will be going almost straight backward in the C-system and with greatly increased energies. For example, we find that if particle n. 4 had K-meson mass it would be located in Fig. 2 at 179.5° instead of 170.0° with an energy of 2.4 GeV instead of 0.21 GeV, while all the others would have much higher energies.

In the case one assumes some of the particles to be of nucleonic mass the same qualitative features are observed but greatly intensified, there would even be a small effect on the high energy particles in the core, while the effect on the particles in the backward cone would be extremely large, giving energies up to 45 times that already estimated and all angles essentially backward (180°). Thus the assumption of more than one or two of the secondary particles being of either K-meson or nucleon mass would appreciably disturb the symmetry, since the forward cone is affected only slightly while the backward cone is completely distorted. The only theoretical possibility of restoring this symmetry approximately would be by making the radical assumption that essentially all of the secondaries were of a higher mass and as a consequence that the primary energy was appreciable lower. There is considerable evidence that pions are produced in these high energy collisions since they can sometimes be identified and since the large number of electron pairs can best be explained by neutral pions. Therefore, this would not seem to be a reasonable assumption.

4. – Discussion.

Under the assumption that all the charged particles are pions, the energy and angular distributions in the *C*-system show the following characteristic features: (1) symmetry under reflection in the plane perpendicular to the primary direction; (2) all the charged particles are included in two cones, one backward and one forward, of half angle approximately 20°; (3) the average energy of the charged particles is between 0.8 and 1.4 GeV; (4) the energies of the individual particles are not much different from the average.

Theories of multiple meson production have been presented by HEISENBERG [7], WATAGHIN [8], OPPENHEIMER *et al.* [9,10], FERMI [11], LANDAU [12], and BHABHA [13]. A comparison of the experimental facts presented in this

---

[7] W. HEISENBERG: *Zeits. f. Phys.*, **101**, 533 (1936); **113**, 61 (1939); **126**, 569 (1949); *Naturwiss.*, **39**, 69 (1952).

[8] G. WATAGHIN: *Phys. Rev.*, **63**, 137 (1943).

[9] L. OPPENHEIMER and WOUTHYUSEN: *Phys. Rev.*, **73**, 127 (1948).

[10] H. W. LEWIS: *Rev. Mod. Phys.*, **24**, 24 (1952). Contains also References to other Theoretical Work.

[11] E. FERMI: *Prog. Theor. Phys.*, **5**, 570 (1950); *Phys. Rev.*, **81**, 683 (1951); *Elementary Particles*, (New Haven, 1951) p. 84.

[12] L. D. LANDAU: *Izv. Akad. Nauk. SSSR* (Ser. Fiz), **17**, 51 (1953). The authors are indebted to Dr. M. HAMMERMESH of Argonne National Laboratory for his translation of this article.

[13] H. J. BHABHA: *Proc. Roy. Soc.* (London), A **219**, 293 (1953).

paper can be made with the theories of Fermi, Heisenberg and Landau. All these theories predict symmetry in the C-system. All of them predict the «two cone effect», although for different reasons. One on the essential differences is that Fermi's theories would predict a much higher average energy (about 10 GeV) in the C-system for a primary energy of $2 \cdot 10^4$ GeV since the available energy is about 200 GeV and the number of particles is about 25. On the other hand, Heisenberg's calculations on the S-star predict an average energy of about 1 GeV in the C-system in agreement with the observed values in the backward cone if the elasticity parameter (which he calls γ in his work) is about 8 (a value which would also be in agreement with our multiplicity on his theory). The two cone effect in Landau's theory is explained by the evaporation of particles from a comparatively flat surface. He gets an average angular spread of about 15° which fits well with our observations. The typical pion energy in his theory is also in general agreement with what we find, although he predicts the existence of some particles with extremely high energies, which however we have not observed.

If heavy mesons exist among the secondaries then the average energy in the C-system would be somewhat higher. On the assumption of approximate equipartition of energy pions in Fig. 2 could be heavy mesons since, for example, those which appear to be above 1 GeV considered as pions would turn out to have energies above 5 GeV considered as K-mesons and would thus have energies well above the pions. Since, as stated previously, the angles in the forward cone are relatively insensitive to mass while the angles in the backward cone are very sensitive, we cannot rule out K-mesons in the forward cone; however, we can safely assume that not more than one or two of the particles in the backward cone could be K-mesons.

For proton-antiproton pairs or hyperons the same argument holds only with much greater strength. If any of the particles in the backward cone are of protonic mass, then it is at a radically different energy (about 45 times higher) from all the pions and in addition is emitted essentially straight backward in the C-system. It is thus probable that none of these secondaries are of nucleonic mass on an assumption of approximate equipartition. Even if one does not assume equipartition if more than one of the charged secondaries in each of the two cones were of protonic mass the total energy of these particles would already be the total available energy in the C-system which would then leave no energy for the charged pions or for the neutral particles, and is thus not possible. This makes us believe that if nucleon-antinucleon pairs or hyperons are produced in collisions similar to the S-star their number must be at most about 10 percent of all charged particles. If such particles are produced at these energies, they certainly are not in equilibrium with the pions and statistical theories based on equilibrium cannot be applied.

5. – Conclusions.

1. Direct momentum measurements on the « S » star have yielded the energy and angular distributions in the C-system, assuming all particles to be pions.

2. The bilateral symmetry appears to be well verified for the angular distribution and is consistent with the energy distribution.

3. The average energy of the pions in the C-system is close to 1 GeV.

4. All the observed particles are emitted in the C-system within two cones of half-angle 20°.

5. The number of particles of protonic mass created in the collision is at most two and most likely none, on the assumption of equilibrium.

6. The results appear consistent with either Heisenberg's or Landau's theory.

7. In this collision, if all secondaries, are pions, the visible energy is small compared to the available energy in the C-system.

RIASSUNTO (*)

Si sono eseguite misure di quantità di moto sulle singole particelle secondarie emesse nel cono « esterno » della stella S. Si è ottenuto un limite inferiore per l'impulso delle particelle nel cono « interno ». La trasformazione dal sistema del laboratorio al sistema del centro di massa può esser fatta, servendosi di opportune approssimazioni, assumendo che tutti i secondari carichi siano pioni. Ciò porta a una distribuzione angolare simmetrica dell'energia con tutte le particelle contenute in un cono anteriore o posteriore di semiapertura 20°. Si confrontano i risultati con diverse teorie sulla produzione multipla. È possibile dedurre che fra i secondari non si ha più di una coppia di particelle con massa protonica e che anche la presenza di una sola coppia violerebbe la simmetria. Anche il numero di mesoni K deve essere basso. I metodi di analisi impiegati possono risultare utili anche per lo studio di altri eventi in questo intervallo di energia.

(*) *Traduzione a cura della Redazione.*

The Positive-Negative Difference of Cosmic-Ray Muons.

Y. YEIVIN

The Weizmann Institute of Science - Rehovoth, Israel.

(ricevuto il 20 Luglio 1955)

Results of accurate measurements of the ratio of the relative numbers of positive to negative sea level muons, as a function of the muon energy, were recently published by the Manchester [1] and the Padova [2,3] groups. These measurements, combined with sea-level muon spectrum data, yield the separate energy spectra of positive and negative muons. Cosmic-ray muons result mostly from the decay of pions produced in collisions of the primary particles with air nuclei (first-generation collisions), and in subsequent collisions of the secondary nucleons and pions. Any theory aiming to derive the observed sea-level spectra from a primary spectrum involves assumptions concerning the interactions of the primary and secondary particles in the atmosphere. Since the primary radiation is absorbed in the atmosphere in more than one collision, it is obviously profitable to concentrate on quantities which are directly related to the first-generation collisions, the derivation of which consequently involves fewer assumptions.

The purpose of this note is to suggest that the positive-negative muon difference is such a quantity (*), and to report preliminary results concerning its derivation on the basis of a simple, though quite general, collision model, as well as the comparison of the theoretical expression with experimental data. The positive value of the positive-negative difference is a consequence of the excess of protons over neutrons in the primary radiation. Since this proton excess very nearly disappears after the first generation collisions, the above difference should be a first generation effect within a good approximation. Moreover, this difference is also completely independent of any *primary* component consisting of equal numbers of protons and neutrons, such as α particles and heavier nuclei.

The analytical expression for the positive-negative muon difference was derived from a power spectrum for the primary protons on the basis of the following collision model:

a) primary proton-air nucleus col-

(1) B. G. OWEN and J. G. WILSON: *Proc. Phys. Soc.*, **64**, 417 (1951).

(2) F. BERRETTA, I. FILOSOFO, B. SOMMACAL, and G. PUPPI: *Nuovo Cimento*, **10**, 1354 (1953).

(3) I. FILOSOFO, E. POHL and J. POHL-RÜLING: *Nuovo Cimento*, **12**, 809 (1954).

(*) This was pointed out by A. DE SHALIT.

lisions are treated as « composite » collisions, in the sense of Cocconi's model (4),

b) the pion multiplicity rises as a given power of the collision energy,

c) in the centre of mass system all pions appear with the same energy.

We also assume the nucleon and pion collision mean free paths to be independent of energy, and equal.

Let us, then, approximate the primary (differential) proton spectrum by $n(E) \sim E^{-s}$ (*), and let the multiplicity be given by $m(W) \sim W^{x}$, where W is the collision energy in the c.m. system. Let us also measure the atmospheric depth x in units of the nucleon (or pion) collision path (≈ 70 g cm^{-2}), and the energy in such units that the pion path for decay is $\lambda_\pi = Ex$. Then the following differential positive-negative muon difference results:

$$\mu^+ - \mu^- = \mathrm{d}(E, x) \sim$$
$$\sim E^{-\beta} f_\beta(E) x^{-1/gE} \gamma(1 + 1/gE; x) \approx$$
$$\approx E^{-\beta} f_\beta(E) \{x^{-1/gE} \Gamma(1 + 1/gE) - e^{-x}\},$$

where

$$\beta = \frac{2s - \alpha}{2 - \alpha}, \quad g = \frac{m_\pi}{\tau_\pi} : \frac{m_\mu}{\tau_\mu} = 104.3,$$

$$f_\beta(E) = \int_1^r \frac{t^{-\beta-1}\,\mathrm{d}t}{1 + Et} \qquad \left[r = \left(\frac{m_\pi}{m_\mu}\right)^2 = 1.73\right],$$

and the incomplete - gamma - function, $\gamma(1 + 1/gE; x)$, is replaced by its approximate expression valid for $x \gg 1$ (at sea level $x \approx 14$).

Hence, the functional form of $\mathrm{d}(E, x)$ depends just on *one* parameter, β, which is a simple function of s and α. All other parameters involved in our model (namely, the coefficients of the primary spectrum and of the multiplicity-collision energy relation, a collision inelasticity factor, and the pion angular distribution in the c.m. system) affect only the normalization of $\mathrm{d}(E, x)$.

In order to compare our result with the experimental data, it is convenient to divide $\mathrm{d}(E, 14)$ by the observed sea-level muon spectrum, which is known very accurately (5). The β-family of curves, obtained for the ratio

$$\delta = 2 \frac{(\mu^+ - \mu^-)}{(\mu^+ + \mu^-)},$$

known as the muon positive excess, is then normalized to agree with the experimental point at the lowest energy, $\delta(1\ \mathrm{GeV}) = 0.192$. Fig. 1 shows these

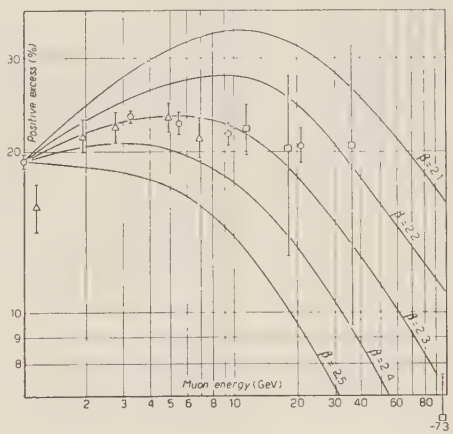

Fig. 1. – Positive-excess curves for different values of β (normalized to $\delta(1\ \mathrm{GeV}) = 19.2\,\%$), and experimental data. ○ Padua (2,3), △ Manchester (1), □ Manchester (unpublished) (6).

curves for $\beta = 2.1 - 2.5$, together with the Manchester and Padua data. Some recent, unpublished, results are also given (6). The best fit is with $\beta \approx 2.3$. Recalling that $\beta = (2s - \alpha)/(2 - \alpha)$, and noting that $0 \leqslant \alpha \leqslant 1$ ($\alpha = 0$ is the case of constant multiplicity, as in plural-

(4) G. Cocconi: *Phys. Rev.*, **93**, 1107 (1954).
(*) All energies are total energies.

(5) B. Rossi: *Rev. Mod. Phys.*, **20**, 537 (1948).
(6) J. G. Wilson: private communication to K. Sitte. I am indebted to Prof. Sitte for his kindness in showing me this letter.

production theories for instance, while for obvious reasons α cannot exceed unity) we may immediately conclude that $1.65 \leqslant s \leqslant 2.3$. Furthermore if we choose to adhere to the Fermi theory of pion production ([7,8]) and put $\alpha = \frac{1}{2}$ we find for s the value 1.98.

It is generally accepted at present ([9]) that the primary spectrum is represented by $n(E) \sim (E+B)^{-\gamma}$, rather than by the power law, E^{-s}, that we have assumed. This is equivalent to stating that instead of the power spectrum with a constant exponent s, we actually have a variable s continually increasing with the primary energy: $s(E) = \gamma E/(E+B)$. Using the accepted values of $B = 4.4$ GeV and $\gamma = 2.75$, it is found that 1.98 is the average exponent of the primary proton spectrum up to about 30 GeV. This primary energy range should, therefore, be mainly responsible for the $1 \div 10$ GeV first-generation muons at sea level. These considerations may also explain the indicated deviation of the experimental points above 10 GeV from the $\beta = 2.3$ curve. Assuming a certain collision model (i.e., fixing a certain value of α) the different curves correspond to different values of s. It can be shown that at very high energies, where practically all muons come from first-generation collisions, the positive excess is independent of the value of s; therefore all curves should coincide in that region. As a matter of fact, it is obvious that once the curves become parallel (on a log scale, as in Fig. 1) we shall have reached this « very high energy » region. It is in this region where the curves should really be normalized. With this normalization, the lower a curve appears on the graph the smaller is the value of s to which it correponds. This means, of course, than as we pass to higher energies the experimental points deviate toward higher values of s, as should be expected.

Another possible effect which may contribute to the observed deviation of the experimental points above 10 GeV was suggested by EISENBERG ([10]). It is known that K^+-mesons have a much higher production cross-section than the K^- do ([11]). If a considerable fraction of the energy in the high-energy collisions goes into the K-meson component, one might expect a higher positive excess than that obtained above assuming pion production only. A further investigation into this possibility is now in progress in this laboratory.

The detailed derivation of the expression for $d(E, x)$, its absolute normalization, and its sensitivity to the assumed collision model and to the form of the primary spectrum will be discussed in a further publication.

* * *

The subject of this note was extensively discussed with Drs. A. DE SHALIT and Y. EISENBERG, to whom the author wishes to express his gratitude.

([7]) E. FERMI: *Progr. Theor. Phys.*, **5**, 570 1950).

([8]) E. FERMI: *Phys. Rev.*, **84**, 683 (1951).

([9]) B. ROSSI: *High Energy Particles* (New York, 1952), p. 6.

([10]) Y. EISENBERG: private communication.

([11]) S. GOLDHABER: *Berkeley Bevatron preliminary results* (private communication).

Angular Correlation of Scattered Annihilation Radiation.

G. Bertolini, M. Bettoni and E. Lazzarini

(*Istituto di Fisica Sperimentale del Politecnico – Milano*)

(ricevuto il 25 Luglio 1955)

According to pair theory, the polarization planes of the two quanta emitted in the annihilation of a positron-electron pair with zero relative angular momentum should be perpendicular to each other. The experiment verifying the prediction of the theory was first proposed by Wheeler [1]; let two annihilation quanta strike two scatterers and let the resulting Compton scattered quanta be recorded in coincidence. Since Compton scattering is more probable in directions perpendicular to the electric vector of a gamma ray than parallel to it, the rate of coincidences will depend on the relative azimuthal angle $\Phi = \Phi_1 - \Phi_2$ of the two detectors, if there is a correlation between the polarization planes of the two quanta.

The ratio ϱ between the coincidence counts when the two detectors are at right angles to each other and the coincidence counts when the detectors are coplanar has been calculated by Snyder, Pasternack and Hornbostel [2] for different scattering angles θ. Moreover they calculated the ϱ ratio for a finite geometry of the detectors about $\theta = 82°$ which is the approximate location of the maximum of ϱ. Several investigators [3-5] measured this ratio without evaluating it theoretically in accordance with their experimental geometry. Only Wu and Shaknov [6] give the calculated asymmetry ratio ($\varrho = 2.00$) and the experimental ($\varrho = 2.08 \pm 0.08$) for Al scatterers and anthracene detectors.

We have measured the ratio ϱ with

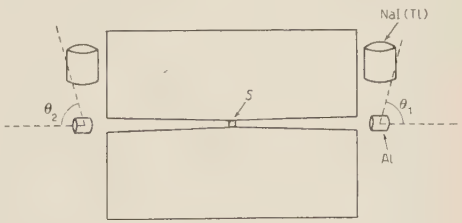

Fig. 1.

the experimental arrangement schematically shown in Fig. 1. A source of

(1) J. A. Wheeler: *Ann. N. Y. Acad. Sci.*, **48**, 219 (1946)..

(2) H. S. Snyder, S. Pasternack and J. Hornbostel: *Phys. Rev.*, **73**, 440 (1943).

(3) E. Bleuler and H. L. Bradt: *Phys. Rev.*, **73**, 1398 (1943).

(4) G. C. Hanna: *Nature*, **162**, 332 (1948).

(5) F. L. Hereford: *Phys. Rev.*, **81**, 482 (1951).

(6) C. S. Wu and I. Shaknov: *Phys. Rev.*, **77**, 136 (1950).

^{22}Na packed in a small Al capsule was placed in the center of a lead block $20 \times 15 \times 15$ cm and the annihilation radiation was collimated by two conical channels of 1 cm external diameter. effect of the multiple scattering was also decreased. Fig. 2 shows the complete γ spectrum detected by each crystal without scatterer (*a* curve) and with Al scatterer (*b* curve).

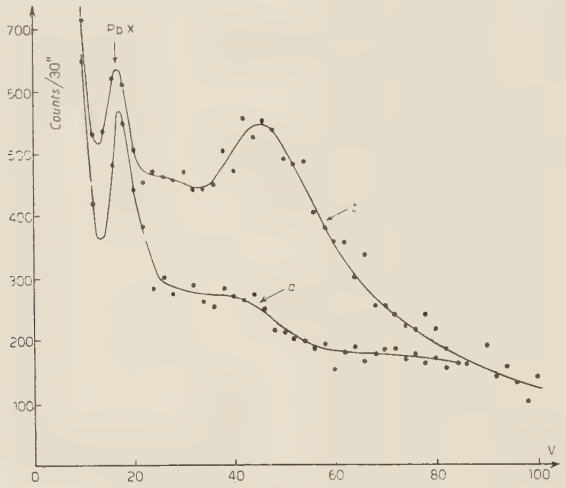

Fig. 2.

Cylindrical Al scatterers $\frac{1}{2}''$ dia $\times$ $\frac{1}{2}''$ long were placed in front of the holes and cylindrical NaI(Tl) crystals $1''$ dia $\times$ $1''$ long in optical joint with 5819 phototubes revealed the Compton scattered quanta. The phototubes were shielded with mu-metal. The pulses were sent to a coincidence with 0.5 μs resolving time through a discriminator with the bias so located (175 keV) as to cut out the Pb X-rays. In such a way the

Two different runs were made with different distance between scatterers and detectors: 10 mm, and 34 mm. The observed asymmetry ratios ϱ are respectively 1.32 ± 0.07 and 2.18 ± 0.09.

The ϱ ratio for the distance of 34 mm has been calculated for our geometrical arrangement and it is $\varrho = 2.32$. In such evaluation we have supposed a point scatterer placed on the axis of the crystal.

On the Associated Production of a Meson-Active $^4H_1$ Fragment and a K-Meson in a Nuclear Disintegration (*).

M. W. Friedlander, D. Keefe and M. G. K. Menon

H. H. Wills Physical Laboratory - University of Bristol

(ricevuto il 9 Agosto 1955)

During the course of scanning carried out in the G-stack, an event was observed which has been interpreted as the ejection of an unstable $^4H_1^+$ nucleus from a nuclear disintegration.

The parent star is of type $22 + 3p$; the slow unstable particle was emitted in the forward hemisphere and appeared to come to rest in the emulsion after a range of 268 μm, thereupon giving rise to a two-prong star. One of these prongs is due to a negative π-meson which stops after 38.61 mm in 48 strips and produces a three-prong sigma star. The range of this particle as quoted includes a correction of 1.0% for traversal of the tissue paper spacers between strips and for the small layer of emulsion removed from the surface of each strip during the cleaning of the plates after processing (see footnote). The other prong, in the opposite direction, is a short saturated recoil track, 8.5 μm in length, and is collinear with the π-meson track within the errors of measurement (± 3°). The π-meson which carries away practically all of the visible energy release, has an energy at emission of ~ 53 MeV.

Because of the short length of the primary track available, no useful mass measurements could be made. It was certainly due to a singly-charged particle and is straighter than a proton track of comparable range. Apart from that of a chance coincidence, one interpretation of the event is in terms of the capture at rest of a negative heavy unstable particle. Because of the wide variety of such capture stars it is never possible in a case like the present to exclude this as a possibility. The collinearity of the two prongs was, however, indicative of a two body process.

It has recently been pointed out by Dalitz [1] that if the assignment of isotopic spin zero to the Λ^0-particle is indeed correct then a meson-active iso-

(*) Provisional details of this event have been quoted in the mimeographed report — 18th May 1955 — of the « G-Stack Collaboration Experiment, 1954 ». Some of the figures and errors given in the present Communication differ slightly from the preliminary ones since in the meantime extensive calibration work has been carried out in this stack. A full discussion of the calibration measurements is presented elsewhere (*Nuovo Cimento*, 1955, in course of publication).

(1) R. H. Dalitz: Mimeographed preprint, (April 1955).

tope of hydrogen, $^4H_1^+$, should exist, in which a Λ^0-particle takes the place of a neutron and that the binding energy of the hyperon should be close to that observed in the case of $^4He_2^+$. The most likely mode of disintegration of such a $^4H_1^+$ nucleus is

$$^4H_1^+ \rightarrow {}^4He_2^+ + \pi^- + Q\,,$$

with

$$Q \sim 55 \text{ MeV}\,.$$

The close similarity between the Q-value for such a disintegration and the total visible energy release in the event described herein, as well as the collinearity already mentioned, strongly suggest that the observed phenomenon corresponds in fact to the breakup of a meson-active $^4H_1^+$ nucleus as first envisaged by Dalitz.

The experimental observations are in very good agreement with the rigorous demands of such a two-body decay scheme. Using the observed ranges the energies of the α-particle and π-meson are 2.55 ± 0.08 MeV and 53.1 ± 1.0 MeV respectively. The corresponding momenta are 138 ± 2 MeV/c and $133 \pm \pm 1.2$ MeV/c and are in good agreement. At first sight it might appear that the most precise value for the energy release, Q, could be obtained by using the independent information from the ranges of *both* the α-particle and the π-meson to estimate the mean momentum, p^*, of the particles in the rest system of the disintegrating nucleus. However, this estimate of p^* is rather strongly influenced by errors in the measurement of the range of the α-particle, e.g. the uncertainty in selecting the correct initial and final grains of the track. Further, in using the experimental range-energy points to determine the energy from the range there is the additional uncertainty in the convention to employ; the range of short tracks has been measured sometimes between the extremities of the bounding grains and sometimes between their centres. On a track of 8.5 μm, the precision of the energy estimate is affected more by these causes alone than by straggling. We have chosen rather to use only the π-meson range in the estimation of Q. The resultant imprecision arising from the straggling of the π-meson can be reduced in time when more events have been observed. The α-particle energy has been deduced from the momentum required to balance that of the π-meson of 53.1 MeV. In calculating the binding energy of the Λ^0-particle in the $^4H_1$ nucleus we have used the following numerical data: Q-value of the Λ^0-particle $=$ $= 36.9$ MeV; $^4He_2$ binding energy $=$ $= 28.3$ MeV: and the range-energy relation of Baroni *et al.* [2] to obtain the π-meson energy, normalised to the mean range of μ-mesons from π^+-meson decay. The binding energy of the Λ^0-particle is given by the relation

$$\begin{aligned} BE(\Lambda^0) = Q(\Lambda^0) + BE(^4\text{He}) - BE(^3\text{He}_1) - \\ - (\text{total kinetic energy} \\ \text{of } ^4\text{He and } \pi^-) \\ = (36.9 + 28.3 - 8.5 \quad 55.5) \text{ MeV} \\ = 1.2 \pm 1.0 \text{ MeV}\,. \end{aligned}$$

At the Pisa Conference (June 1955) two further examples of the probable disintegration of $^4H_1^+$ nuclei in this mode have been reported by the Oslo and Paris groups and the values for Q found by them are in good agreement with the present example.

The tracks from the parent star of the excited fragment were traced through the emulsion stack and with the exception of two lightly ionising shower particles all were identified using measurements of range, ionisation, and multiple

[2] G. Baroni, C. Castagnoli, G. Cortini, C. Franzinetti and A. Manfredini: BS. 9, C.E.R.N. Bulletin.

scattering. One of these tracks, whose direction made an angle of 86° with that of the fragment, was found to be due to a heavy meson which was emitted with an energy of 270 MeV. It has an average length per plate exceeding 1 cm, and scattering and grain density measurements made along the available length of 18.74 cm yielded a mass estimate:

$$m_K = 960 \pm 90\ m_e .$$

The error quoted includes uncertainties due to normalisation of the scattering constant and of plateau ionisation in the plates concerned. Having traversed 18.74 cm of emulsion the K-particle interacted in flight to give a two prong star; one branch is a short recoil and the other either a proton or the emerging K-particle which was not arrested in the emulsion.

The most likely interpretation of this event, therefore, in the light of present ideas, is in terms of the associated production of a K-meson with a hyperon, — either a Λ^0-particle, or a Σ-particle which has transformed in a fast nuclear interaction into a Λ_0-particle. In either case the Λ^0-particle was of such low energy that it emerged bound to a triton to form the $^4H_1^+$ nucleus.

* * *

We wish to thank Professor C. F. Powell for the hospitality and facilities of his laboratory, and Mrs. J. Keefe who found the $^4H_1^+$ event. We are indebted to Dr. R. H. Dalitz for sending us a preprint of his paper. This work was carried out during the course of the « *G*-Stack Collaboration Experiment (1954) ».

The Production of a Pair of Heavy Mesons in a High-Energy Nuclear Interaction (*).

M. W. Friedlander, D. Keefe and M. G. K. Menon
H. H. Wills Physical Laboratory - University of Bristol

(ricevuto il 9 Agosto 1955)

Recently there have been reported several examples of nuclear interactions in which occur the associated production of a hyperon and a heavy meson; in those examples where an identification of the charge of the heavy meson has been possible it has always been shown to be positive or neutral. In this communication we describe an event in which *a negative* K-*meson*, $K^-(Br_4)$, *is produced in association with another heavy meson.*

The negative K-meson capture star was found in the course of scanning in photographic emulsion. The track of the incoming particle was traced back to its origin which was found to be a star of type 6 + 5p. The orientations of the remaining tracks from the star were such that, with one exception, reliable measurements could be made on all, and their nature defined. The details and results of the measurements on the tracks are shown in Table I. The total visible energy of the star was about 3.5 GeV.

Table I. – *Analysis of the Parent Star* (6 + 5p) *of* K^-Br4

Track No.	Appearance	Identity	Energy at Emission MeV
1, 2, 3	black	short evaporation tracks; p? p? Li?	~ 20 (from range)
4	grey	proton	200 » »
5	grey	proton	170 (from g^*)
6	grey	K^--meson	53 (from range)
7	light	π?	relativistic
8, 9	light	π-mesons	70, 440 (from $(g^*, p\beta)$)
10	light	proton	300 (from $(g^*, p\beta)$)
11	light	K-meson	220 ± 5 (from $(g^*, p\beta)$)

The negative K-meson (Track 6) had

(*) Preliminary details have been mentioned in the mimeographed Report (May 18, 1955) of the « *G*-Stack Collaboration Experiment, 1954 ».

a range of 18.67 mm and traversed 12 emulsion strips. Careful measurements of mean gap-length at several points along the track yielded a mass estimate of $1030 \pm 60\ m_e$. Upon coming to rest it produced a capture star of two branches, one a π-meson of 53 MeV and the other a charged hyperon whose direction made an angle of 160.5° with that of the π-meson. The hyperon, after traversing a distance of 1.668 mm, decayed when at rest or nearly at rest, to a π-meson of 82.4 ± 3 MeV in the backward direction. If one assumes that it had come to rest before decaying, the Q-value for the decay mode $Y \rightarrow n + \pi^{\pm} + Q$, is 98 ± 4 MeV. In view of the small errors of measurement it is probable that this is an example of the decay in flight of a Σ-particle, with $Q(n, \pi) \approx 109$ MeV, which still had a residual range of about 200 μm. Under the conditions of development in these emulsions, it is not possible to be certain from ionisation measurements whether a particle of this mass had come to rest or still had a residual range of a few hundred microns. When this is taken into account, one can state limits for the possible Q-value as being 98 MeV and 110 MeV.

The track of the other K-particle (Track 11) was 13.75 cm long contained in 8 strips and passed out of the edge of the stack. It had an average length per plate of two centimetres and measurements of scattering and ionisation were made along its entire length, with the exception of the final centimetre near the edge of the stack. The ionisation was measured by the method described by Fowler and Perkins [1] and varied from $g^* = 1.35$ near the star to $g^* = 1.90$ near the exit point. From the $(\bar{\alpha}, g^*)$ measurements a mass value,

$$m_K = 875 \pm 65\ m_e ,$$

is obtained, where the standard deviation $\pm 65\ m_e$ includes the normalisation errors and is in good agreement with the spread of the individual measurements.

The parent star had a charged primary, and the angle made with its direction by the K^- particle was 61°, by the other K-particle 22°, and by the plane of the K-meson pair 20°. The angle between the K-mesons was 68°.

It is interesting that in this event, the heavy unstable particle which has been produced in association with a negative K-meson, is found to be another heavy meson and not a hyperon.

There have been two examples already reported [2,3] in which a decaying K-meson has been observed to come from the same star as a negative interacting particle. Neither of these events can, however, be taken as evidence of the pair production of a positive with a negative K-meson since in each case the range of the negative interacting particle was insufficient for any definite identification; they could, for example, have been instances of the more familiar type of associated production involving a positive K-meson and a negative hyperon.

In order to account for the low frequency of negative compared to positive slow K-mesons in cosmic ray experiments [4,5], various theoretical proposals have been made by Nakano and Nishijima [6] and Gell-Mann and Pais [7]. One of the consequences of

---

[1] P. H. Fowler and D. H. Perkins: *Phil. Mag.*, **46**, 587 (1955).

[2] D. Lal, Yash Pal and B. Peters: *Proc. Ind. Acad. Sci.*, **38**, 398 (1953).

[3] M. W. Friedlander, D. Keefe and M. G. K. Menon: *Nuovo Cimento*, **1**, 482 (1955).

[4] M. W. Friedlander, G. G. Harris and M. G. K. Menon: *Proc. Roy. Soc.*, A **221**, 394 (1954).

[5] B. Gregory, A. Lagarrigue, L. Leprince-Ringuet, F. Muller and C. Peyrou: *Nuovo Cimento*, **11**, 292 (1954).

[6] T. Nakano and K. Nishijima: *Prog. Theor. Phys.*, **10**, 581 (1953).

[7] M. Gell-Mann and A. Pais: *Proc. Int. Nuc. Phys. Conf. Glasgow* (July, 1954).

these schemes is that the negative K-meson should be produced in association with another K-particle but not with a hyperon, thus requiring a higher threshold energy. Apart from the fact that it may often be produced with a neutral K-particle, it is not altogether surprising that the production of a negative K-meson in a pair process is not a more frequently observed phenomenon, since the higher value of energy involved will often result in the positive particle being very energetic (and thus difficult to identify) if the negative partner is slow enough to be brought to rest in an emulsion stack.

* * *

We are grateful to Professor C. F. POWELL for the hospitality and the facilities of his laboratory; we also wish to thank Miss M. WOOD who found the capture star of $K^-(Br_4)$. This work was carried out during the course of the « G - Stack Collaboration Experiment (1954) ».

IL NUOVO CIMENTO Vol. II, N. 3 1° Settembre 1955

Theory of the Effect of Nucleon-Nucleon Correlations on the Scattering of High Energy Electrons or Muons by Nuclei.

R. Gatto

Istituto di Fisica dell'Università - Roma
Istituto Nazionale di Fisica Nucleare - Sezione di Roma

(ricevuto il 10 Agosto 1955)

1. – The purpose of this note is to present a study of the influence of the correlations between the constituent nucleons on the scattering of a fast electron or muon by a nucleus. The simple description of such a scattering by means of a static nuclear charge distribution is, obviously, incomplete, since it ignores the internal degrees of freedom of the nucleus. Recently some work has been devoted to the evaluation of the effects which follow from the possibility of real transitions to excited nuclear states (inelastic scattering) [1], and of virtual transitions to and from excited nuclear states (dispersion effects) [2]. Dispersion effects are expected to be small [2] and will not be considered in this paper.

The correlations between the nucleons are essentially due, (i), to the operation of the Pauli principle, and, (ii), to the specific interactions (nuclear forces and coulomb forces) between the nucleons. In the following a consistent procedure for evaluating these effects will be developed.

In the present paper we shall give a general discussion of the effect. Only the limiting case of zero range nuclear forces will be discussed in full detail. In this nuclear model only one parameter having the dimensions of a length intervenes, namely the nuclear radius, or, equivalently, the mean nuclear separation. The relevant role is played in the theory by the angle η such that

$$\sin\frac{\eta}{2} = \left(\frac{9\pi}{4}\,\frac{Z}{A}\right)^{\frac{1}{3}}\frac{\lambda\!\!\!^{-}}{r_0} = \frac{p_F}{|\boldsymbol{k}_i|}$$

where $\lambda\!\!\!^{-} = 1/|\boldsymbol{k}_i|$ is the wavelength of the incident particle, r_0 is defined by the relation nuclear radius $= r_0 A^{\frac{1}{3}}$, and p_F is the Fermi momentum. The physical significance of the angle η is evident from its definition. If the scattering occurs at an

(1) L. I. Schiff: *Phys. Rev.*, **96**, 765 (1954) and earlier papers cited there.
(2) L. I. Schiff: *Phys. Rev.*, **98**, 756 (1955).

angle larger than η, the recoil momentum imparted to the nucleon struck is always large enough to push the nucleon out of the Fermi sphere.

2. – We use a relativistic description for the scattered particle (but ignoring spin for simplicity), and a non relativistic description for the nucleons. Let us denote with $\mathcal{R}$ the ratio between the scattering by a nucleus with Z protons and the scattering by the point charge Ze. We regard $\mathcal{R}$ as the sum of a coherent contribution, $\mathcal{C}$, and of an incoherent contribution, $\mathcal{I}$. If the interaction between the incident particle and the nucleons is treated in first order, and if the closure approximation is used to carry out the sum over all the possible transitions, a simple expression can be obtained for $\mathcal{R}$ [3]

$$\mathcal{R} = \langle Z^{-1} \sum_{jl} \Gamma_{jl} \cos \boldsymbol{k}\cdot\boldsymbol{r}_{jl} \rangle_0 \,. \tag{1}$$

In (1) we have denoted with $|\rangle_0$ the ket representing the nuclear ground state; $\boldsymbol{k}$ is the difference between the final and the initial wave vectors of the particle, $\boldsymbol{k} = \boldsymbol{k}_f - \boldsymbol{k}_i$; $\boldsymbol{r}_{jl}$ is the difference between the position vector of the j-th nucleon and that of the l-th nucleon, $\boldsymbol{r}_{jl} = \boldsymbol{r}_j - \boldsymbol{r}_l$; Γ_{jl} is a projection operator acting on the isotopic spin coordinates of the j-th and of the l-th nucleons, which is designed to give unity when j and l are both protons, zero otherwise; the summation in (1) is extended over all the values of the indices j and l. An equivalent expression for $\mathcal{R}$ is

$$\mathcal{R} = Z^{-2}\{Z + \langle \sum_{j \neq l} \Gamma_{jl} \cos \boldsymbol{k}\cdot\boldsymbol{r}_{jl} \rangle_0\} \,, \tag{1'}$$

where the summation excludes the values $j = l$.

It is seen from (1) that only a sufficient knowledge of the nuclear ground state is required to evaluate $\mathcal{R}$. This is a direct consequence of the closure approximation For the validity of the approximation it is required that the incident particle has sufficiently high energy.

We consider the representation in which the basic kets for the individual nucleons are the eigenkets of the momentum operator. We can represent the ket $|\rangle_0$ as a superposition of the form

$$|\rangle_0 = |\rangle + \sum_{\nu} c_\nu |\nu\rangle \,, \tag{2}$$

where $|\rangle$ is the ket representing the configuration in which the nucleons occupy all the states of the Fermi sphere, and $|\nu\rangle$ represents an excited configuration in which some or all of the nucleons occupy states not contained in the Fermi sphere.

For simplicity we assume that only two body interactions between the nucleons are present. It is easily seen that in this case the only excited configurations which may appear in the superposition (2) are those which differ from the ground configuration in having simply replaced in it two individual states with two others not already contained, and, moreover, so as to leave the total momentum unaltered.

Let us consider the expansion of the coefficients c_ν in ascending powers of the nuclear interactions

$$c_\nu \equiv \langle \nu | \rangle_0 = c_\nu^{(0)} + c_\nu^{(1)} + \dots \,. \tag{3}$$

---

[3] R. GATTO: *Nuovo Cimento*, **10**, 1559 (1953), referred to as (A).

A corresponding expansion is obtained for $\mathcal{R} = \mathcal{J} + \mathcal{C}$

$$\mathcal{R} = \mathcal{R}^{(0)} + \mathcal{R}^{(1)} + \ldots = \mathcal{C}^{(0)} + \mathcal{J}^{(0)} + \mathcal{C}^{(1)} + \mathcal{J}^{(1)} + \ldots . \tag{4}$$

3. – The zero order term $\mathcal{R}^{(0)}$ of this expansion has been evaluated in (A). Let us introduce the vector $\boldsymbol{\varkappa} = \boldsymbol{k}/p_F$ and, for a generic momentum $\boldsymbol{p}$, the vector $\boldsymbol{\pi} = \boldsymbol{p}/p_F$ where p_F is the Fermi momentum. After subtracting the coherent contribution $\mathcal{C}^{(0)}$, one simply gets

$$\mathcal{J}^{(0)} = N(\boldsymbol{\varkappa}) , \tag{5}$$

$N(\boldsymbol{\varkappa})$ denoting the total number of proton states the wave vector of which satisfies the inequality $|\boldsymbol{p} - \boldsymbol{k}| > p_F$. For such states the vector $\boldsymbol{\pi}$ lies in that zone of the unit radius sphere where the inequality $|\boldsymbol{\pi} - \boldsymbol{\varkappa}| > 1$ is satisfied; this zone of the unit radius sphere we call $\mathcal{F}_>$. The relevant angle in this theory is the angle defined by the equality

$$\sin \frac{\eta}{2} = \frac{p_F}{|\boldsymbol{k}_i|} . \tag{6}$$

Taking for p_F

$$p_F = \left(\frac{9\pi}{4}\frac{Z}{A}\right)^{\frac{1}{3}} \frac{1}{r_0} , \tag{7}$$

where r_0 is related to the nuclear radius by nuclear radius $= r_0 A^{\frac{1}{3}}$, it follows

$$\sin \frac{\eta}{2} = \left(\frac{9\pi}{4}\frac{Z}{A}\right)^{\frac{1}{3}} \frac{\lambda\!\!\!^{-}}{r_0} , \tag{8}$$

where $\lambda\!\!\!^{-}$ is the reduced wave length of the impinging particle.

It will be convenient to introduce the variable ξ defined by

$$\xi = \frac{\sin(\theta/2)}{\sin(\eta/2)} , \tag{9}$$

where θ is the scattering angle. The simple result (5) for $\mathcal{J}^{(0)}$ can be written [3]

$$\mathcal{J}^{(0)} = Z^{-1}\{-\tfrac{1}{2}\xi^3 + \tfrac{3}{2}\xi\} , \qquad \text{for } \xi \leqslant 1 \tag{10}$$

$$= Z^{-1} . \qquad \text{for } \xi \geqslant 1 \tag{10'}$$

The physical significance of the angle η is expressed by the fact that for scattering angles $\theta \geqslant \eta$ the restrictive effect of the exclusion principle is absent.

4. – Let us consider the next term of the power series expansion (4).

First we demonstrate that the coherent contribution $\mathcal{C}^{(1)}$ is exactly zero. This may be seen most easily as follows. A typical term in the expression of the total charge density, linear in the perturbing interactions among the nucleons, will consist

of an integral taken over all nucleon coordinates except *one* of the product of the representatives of the ground state configuration and of an excited state configuration. This integral is zero: in fact *two* states are contained in the ground configuration different from those of the excited configuration.

In consequence of the preceding result we can simply write

$$\mathcal{T}^{(1)} = \mathcal{R}^{(1)} = \langle Z^{-2} \sum_{jl} \Gamma_{jl} \cos \boldsymbol{k}\cdot\boldsymbol{r}_{jl} \rangle_0^{(1)} . \tag{11}$$

From a formal viewpoint, we may observe that the calculation of the mean value (11) is not very different from that of a second order calculation of an energy level. The only difference is that the two successive steps of the virtual transition are here performed through two different interactions. In fact we may regard the appearance of the excited configurations in the representation (2) of the ket $|\rangle_0$ to the first order as corresponding to the first step of the virtual transition. This first step is performed through the nuclear interactions. The second step will be performed through the interaction term explicity indicated in (11). In the second step the total momentum is conserved, and, moreover, the momentum acquired by a single nucleon must be equal to the recoil momentum imparted to it by the scattered particle. This last condition follows from the particular form of the interaction term $\cos \boldsymbol{k}\cdot\boldsymbol{r}$.

Let us assume the nuclear interaction of the form $J_0 v(\boldsymbol{r})\{a_0 + a_\sigma(\boldsymbol{\sigma}_1\cdot\boldsymbol{\sigma}_2) + a_\tau(\boldsymbol{\tau}_1\cdot\boldsymbol{\tau}_2) + a_{\sigma\tau}(\boldsymbol{\sigma}_1\cdot\boldsymbol{\sigma}_2)(\boldsymbol{\tau}_1\cdot\boldsymbol{\tau}_2)\}$, briefly written as $J_0 v(\boldsymbol{r}) O$ [4]. We denote with $\boldsymbol{p}_-$ a generic momentum contained in the Fermi sphere, with $\boldsymbol{p}_+$ a generic momentum not contained in the Fermi sphere. It can be shown that $\mathcal{T}^{(1)}$ is given by

$$\left\{\begin{aligned} &\mathcal{T}^{(1)} = Z^{-2} 4 M J_0 \Sigma^{(-)} \Sigma^{(+)} \langle \boldsymbol{p}_-^{(1)} \boldsymbol{p}_-^{(2)} | \cos \boldsymbol{k}\cdot\boldsymbol{r}_{12} | \boldsymbol{p}_+^{(1)} \boldsymbol{p}_+^{(2)} \rangle \{ |\boldsymbol{p}_-^{(1)}|^2 + |\boldsymbol{p}_-^{(2)}|^2 - \\ &- |\boldsymbol{p}_+^{(1)}|^2 - |\boldsymbol{p}_+^{(2)}|^2 \}^{-1} \cdot \{ \langle \boldsymbol{p}_-^{(1)} \boldsymbol{p}_-^{(2)} | v(\boldsymbol{r}_{12}) | \boldsymbol{p}_+^{(1)} \boldsymbol{p}_+^{(2)} \rangle \text{ trace } [O\Gamma] - \\ &- \langle \boldsymbol{p}_-^{(1)} \boldsymbol{p}_-^{(2)} | v(\boldsymbol{r}_{12}) | \boldsymbol{p}_+^{(2)} \boldsymbol{p}_+^{(1)} \rangle \text{ trace } [O P_\sigma P_\tau \Gamma] \} , \end{aligned}\right. \tag{12}$$

where M is the nucleon mass; $\Sigma^{(-)}$ and $\Sigma^{(+)}$ are taken over all momenta $\boldsymbol{p}_-$ and $\boldsymbol{p}_+$ respectively, P_σ and P_τ are the usual ordinary spin and isotopic spin exchange operators respectively. In (12) the term $\{|\boldsymbol{p}_-^{(1)}|^2 + |\boldsymbol{p}_-^{(2)}|^2 - |\boldsymbol{p}_+^{(1)}|^2 - |\boldsymbol{p}_+^{(2)}|^2\}^{-1}$ is the well known energy denominator which occurs in the usual way in second order perturbation theory.

The matrix element $\langle \boldsymbol{p}_-^{(1)} \boldsymbol{p}_-^{(2)} | \cos \boldsymbol{k}\cdot\boldsymbol{r}_{12} | \boldsymbol{p}_+^{(1)} \boldsymbol{p}_+^{(2)} \rangle$ expresses the momentum conservation, $\boldsymbol{p}_-^{(1)} + \boldsymbol{p}_-^{(2)} - \boldsymbol{p}_+^{(1)} - \boldsymbol{p}_+^{(2)} = 0$, and specifies the transition by means of the equalities $\boldsymbol{p}_+^{(1)} - \boldsymbol{p}_-^{(1)} = \pm \boldsymbol{k}$.

$$\boldsymbol{p}_-^{(1)} \boldsymbol{p}_-^{(2)} | \cos \boldsymbol{k}\cdot\boldsymbol{r}_{12} | \boldsymbol{p}_+^{(1)} \boldsymbol{p}_+^{(2)} \rangle = \delta_{\boldsymbol{p}_-^{(1)} + \boldsymbol{p}_-^{(2)}, \boldsymbol{p}_+^{(1)} + \boldsymbol{p}_+^{(2)}} \cdot \tfrac{1}{2} \{ \delta_{\boldsymbol{p}_+^{(1)} - \boldsymbol{p}_-^{(1)}, \boldsymbol{k}} + \delta_{\boldsymbol{p}_+^{(1)} - \boldsymbol{p}_-^{(1)}, -\boldsymbol{k}} \} . \tag{13}$$

Similarly, putting

$$v(\boldsymbol{r}) = \Omega^{-1} \sum_{\boldsymbol{p}} \tilde{v}(\boldsymbol{p}) \exp [-i\boldsymbol{p}\cdot\boldsymbol{r}] , \tag{14}$$

---

[4] L. ROSENFELD: *Nuclear Forces* (Amsterdam, 1948), pp. 160 and 243.

it follows

$$\langle \boldsymbol{p}_-^{(1)}\boldsymbol{p}_-^{(2)}|v(\boldsymbol{r}_{12})|\boldsymbol{p}_+^{(1)}\boldsymbol{p}_+^{(2)}\rangle = \Omega^{-1}\tilde{v}(\boldsymbol{p}_-^{(1)}-\boldsymbol{p}_+^{(1)})\delta_{\boldsymbol{p}_-^{(1)}+\boldsymbol{p}_-^{(2)},\boldsymbol{p}_+^{(1)}+\boldsymbol{p}_+^{(2)}}, \tag{15}$$

$$\langle \boldsymbol{p}_-^{(1)}\boldsymbol{p}_-^{(2)}|v(\boldsymbol{r}_{12})|\boldsymbol{p}_+^{(2)}\boldsymbol{p}_+^{(1)}\rangle = \Omega^{-1}\tilde{v}(\boldsymbol{p}_-^{(1)}-\boldsymbol{p}_+^{(2)})\delta_{\boldsymbol{p}_-^{(1)}+\boldsymbol{p}_-^{(2)},\boldsymbol{p}_+^{(1)}+\boldsymbol{p}_+^{(2)}}. \tag{15'}$$

Inserting into (12) and making the usual substitutions of the summations into integrals one finds the result

$$\mathcal{J}^{(1)} = Z^{-1}C\left\{\int d\boldsymbol{\rho}\exp[i\boldsymbol{\varkappa}\cdot\boldsymbol{\rho}]\,v(\boldsymbol{\rho}/p_F)G(\boldsymbol{\rho}|\boldsymbol{\varkappa})\ \text{trace}\ [OP_\sigma P_\tau\Gamma] - \right.$$
$$\left. - \int d\boldsymbol{\rho}\exp[i\boldsymbol{\varkappa}\cdot\boldsymbol{\rho}]\,v(\boldsymbol{\rho}/p_F)G(0|\boldsymbol{\varkappa})\ \text{trace}\ [O\Gamma]\right\}, \tag{16}$$

where C is a constant given by

$$C = \frac{1}{2}\frac{A}{2Z}(MJ_0r_0^2)\frac{1}{6\pi^5}\left(\frac{9\pi}{8}\right)^{\frac{1}{3}}\left(\frac{2Z}{A}\right)^{\frac{1}{3}}, \tag{17}$$

$\boldsymbol{\rho}$ is defined by $\boldsymbol{\rho} = p_F\boldsymbol{r}$; $G(\boldsymbol{\rho}|\boldsymbol{\varkappa})$ is a typical kernel function which occurs in the theory and which can most simply be expressed by the following integral representation

$$G(\boldsymbol{\rho}|\boldsymbol{\varkappa}) = \int_0^\infty d\omega\exp[-\omega x^2]\,F(\omega,\boldsymbol{\varkappa},\boldsymbol{\rho})F^*(\omega,-\boldsymbol{\varkappa},\boldsymbol{\rho}), \tag{18}$$

where

$$F(\omega,\boldsymbol{\varkappa},\boldsymbol{\rho}) = \int_{\boldsymbol{\pi}\subset\mathcal{F}_>} d\boldsymbol{\pi}\exp[(\omega\boldsymbol{\varkappa} - i\boldsymbol{\rho})\cdot\boldsymbol{\pi}]. \tag{19}$$

The region $\mathcal{F}_>$ of the unit sphere has, already been defined: it is that region of the unit sphere where the inequality $|\boldsymbol{\pi}-\boldsymbol{\varkappa}|>1$ is satisfied.

The traces of the products of ordinary spin and isotopic spin operators which occur in (16) may easily be evaluated rembering the definition of the projection operator Γ. In fact, denoting by S an invariant ordinary spin operator and by T an invariant isotopic spin operator, it can easily be shown that

$$\text{trace}\ [ST\Gamma] = \langle T\rangle_3\cdot(4)\text{-trace}\ [S]. \tag{20}$$

Here we denote by $\langle T\rangle_3$ the mean value of T in a triplet isotopic spin state and we use the prefix (4) to keep in mind that only the 4 dimensional ordinary spin subspace of the total 16-dimensional product space must be considered. One then gets immediately

$$\text{trace}\ [OP_\sigma P_\tau\Gamma] = 2(a_0+a_\tau) + 6(a_\sigma + a_{\sigma\tau}), \tag{21}$$

$$\text{trace}\ [O\Gamma] = 4(a_0+a_\tau). \tag{21'}$$

For the internal consistency of the model it will be convenient to choose the values of the parameters a of the nuclear interaction in such a way that certain requirements which follow from the general properties of heavy nuclei are satisfied. From a well known necessary saturation condition due to Breit and Wigner it follows that trace $[O\Gamma] \geqslant 0$. From the necessary saturation conditions, from Volz's condition for α-nuclei, and from the Breit and Wigner condition for the stability of isobars (these last conditions are however somewhat less rigorously established) it follows that trace $[OP_\sigma P_\tau \Gamma] \geqslant 0$. From the same properties it follows that $a_0 \cong 0$, $a_\sigma \cong 0$. For the ratio $a_\tau / a_{\sigma\tau}$ we shall make the assumption $a_\tau \cong 0.01$, $a_{\sigma\tau} \cong 0.23$ [4].

5. – In the following we shall limit our discussion to the limiting case of zero range nuclear forces. A more complete discussion will be reported later. We do not

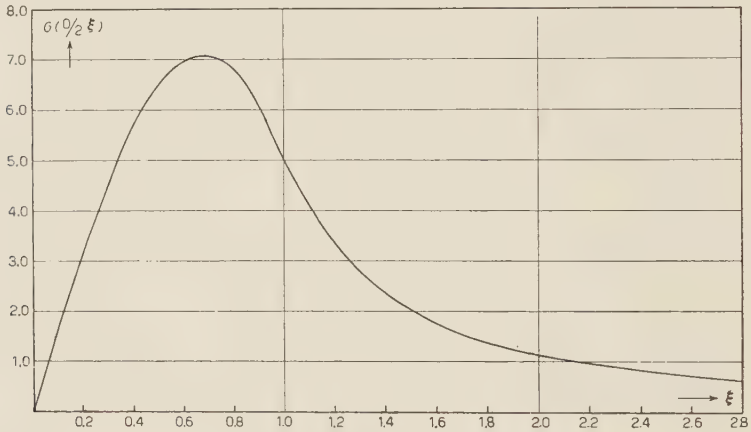

Fig. 1.

expect the zero range approximation to give entirely reliable results for the wavelengths λ which are of interest here, which are of the order of the nuclear dimensions. However, the zero range approximation should be useful to predict roughly the order of magnitude of the effect and some of its general features.

The nuclear model considered has only one parameter having the dimensions of a length, namely the nuclear radius, or equivalently the length r_0, defined by the relation, nuclear radius $= r_0 A^{\frac{1}{3}}$. A relevant role will be played in the theory by the angle η defined by (6), and it will be convenient to use the variable ξ defined by (9).

In the zero range approximation we substitute in (16) for $J_0 v(\boldsymbol{r})$ the expression

$$Q\delta(\boldsymbol{r}) = Q\delta(\boldsymbol{\rho}/p_F) = Qp_F^3\delta(\boldsymbol{\rho}) , \tag{22}$$

where Q has the physical dimensions of energy $\times$ volume. Putting $Q = Er_0^3$, after performing the integrations, we obtain

$$\mathcal{J}^{(1)} = Z^{-1}\tfrac{1}{2}(MEr_0^2)\frac{1}{6\pi^5}\left(\frac{9\pi}{8}\right)^{\frac{4}{3}}\left(\frac{2Z}{A}\right)^{\frac{1}{3}} G(0|\boldsymbol{\varkappa}) \text{ trace } [O(P_\sigma P_\tau - 1)\Gamma] . \tag{23}$$

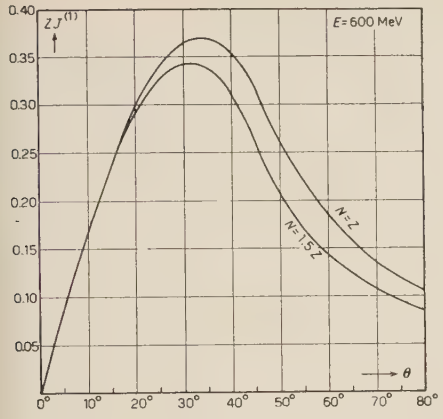

Fig. 2.

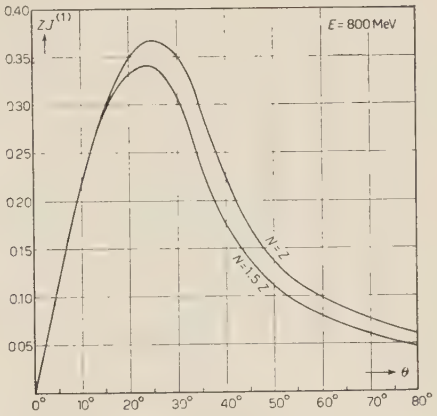

Fig. 3.

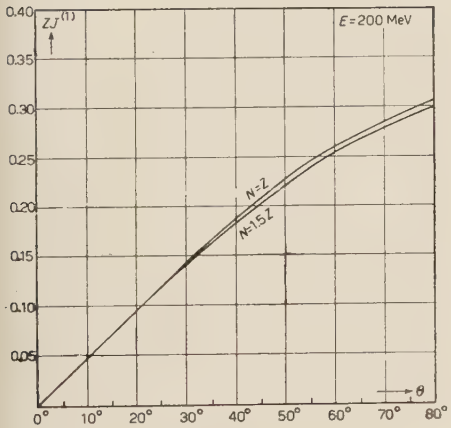

Fig. 4.

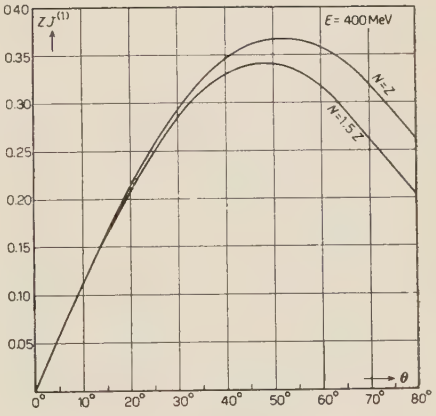

Fig. 5.

The integral in the expression of $G(0|\varkappa)$ may be reduced to a similar integral evaluated by EULER (5). We report the expression that one obtains for $G(0|\varkappa)$

$$(24)\qquad G(0|\varkappa) = \frac{2\pi^2}{15}\left[\left(\frac{4}{\xi} + \frac{15}{2} - 5\xi^2 - \frac{3}{2}\xi^4\right)\log(1+\xi) - 29\xi - 3\xi^3 + \right.$$

$$\left. - \left(\frac{4}{\xi} - \frac{15}{2} - 5\xi^2 - \frac{3}{2}\xi^4\right)\log(1-\xi) - 40\xi\log 2\right] \qquad \text{for } \xi \leqslant 1\,,$$

$$(24')\qquad = \frac{2\pi^2}{15}\left[\left(\frac{4}{\xi} - 20\xi - 20\xi^2 + 4\xi^4\right)\log(\xi+1) + 4\xi^2 + 22 + \right.$$

$$\left. - \left(-\frac{4}{\xi} + 20\xi - 20\xi^2 + 4\xi^4\right)\log(\xi-1) + (40\xi^2 - 8\xi^4)\log\xi\right] \qquad \text{for } \xi \geqslant 1\,.$$

(5) H. EULER: *Zeits. f. Phys.*, **105**, 553 (1937).

It can be seen that $G(0|\varkappa)$ is a continuos function and has a continuous derivative. The function $[G(0|\varkappa)$ is reported in the graph of fig. 1.

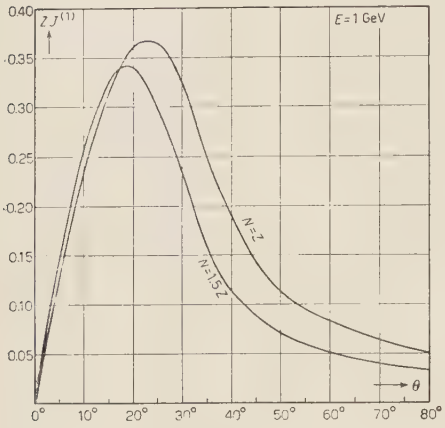

Fig. 6.

We have reported in the graphs of figs. 2-6 the values of $ZJ^{(1)}$ as given by (23) and (24) for different values of the energy of the incident particle, assumed to be a μ-meson. We have taken for Q a value of the order of the volume integral of the triplet neutron-proton potential, $Q = 1.3 \cdot 10^{-3}$MeV$\cdot$cm. Of coure no convincing argument can be given to justify such choice, and therefore the numerical results should not be taken literally. However, present experiments are still not enough accurate to permit a better comparison. The other parameter of the theory is r_0 which is related to the nuclear radius. We have chosen for it a value of $1.2 \cdot 10^{-13}$ cm. As to the value of the ratio $(2Z)/A$ which appears in (23) the graphs reported in figs. 2-6 correspond to the two extreme situations $(2Z)/A = 1$ (light nuclei) and $(2Z)/A = 4/5$ (heavy nuclei). The dependence on this parameter is however very weak.

5. – As is seen from the foregoing discussion, much uncertainty in the evaluation of the effect comes from the insufficiency of our knowledge of the nuclear interaction. Apart from the question of the validity of the zero range approximation, which is only a mathematical difficulty and will be resolved in a next work, the main assumption, that the phenomenological nuclear potential introduced here should be the same potential devised to explain the free nucleons scattering experiments, is, in our opinion, open to question.

As to the order of magnitude of the effect we can conclude that the previously obtained result expressed by the equations (10) and (10′) is not changed very much by the effects considered here. This could be taken, *a posteriori*, as a partial justification of the perturbation procedure employed.

Finally, with regard to the recent experiments on muon-nucleus scattering, which have been interpreted as demonstrating the existence of an appreciable muon-nucleon interaction, we may only confirm our conclusions expressed in a previous work [3]. A discussion on the question of the suggested anomalous muon-nucleon interaction can be found in a recent paper by FOWLER [6].

[6] C. N. FOWLER: *Proc. Phys. Soc.*, **86**, 482 (1955).

On the Purification of the Electron-Pulse Ionization Chamber.

C. Cernigoi and G. Poiani

Istituto di Fisica dell'Università - Trieste
Istituto Nazionale di Fisica Nucleare - Gruppo aggregato di Trieste

(ricevuto il 18 Agosto 1955)

One of the essential conditions which must be satisfied in order to have a properly working electron-pulse ionization chamber is that the gas used for filling up the chamber be sufficiently pure. Generally the degree of purification which is required is as higher as the gas pressure is higher.

Although the available data concerning this question are at the present rather poor, it is generally believed that an impurity of electronegative gas in the proportion of 1 to 10^5 begins, at atmospheric pressure, to favour a lowering of the pulse heights [1]. When argon is used as chamber filler, the purification technique generally adopted consists in letting the gas going over metallic calcium heated at about 250 °C. Few hours of circulation are sufficient for this purpose [2].

This procedure is useful when metallic calcium in the required conditions can be easily obtained or when the commercial argon is sufficiently pure and the chamber dimensions not very large. Since at the present we are setting up a fast pulse chamber having large dimensions (80 l) and filled with argon at 10 atm. of pressure, some difficulties have been met in pursuing the above mentioned procedure and to overcome them we have found as much more convenient to carry out the gas purification by letting the gas flowing over thin copper straps, heated to incandescence. A preliminary check of the efficiency of this method has been performed by purifying the gas of a Rossi chamber having standard dimensions. Then, to have a clear evidence that the device we have used is really effective, experiments have been made with nitrogen, which is sensible to very small proportion of impurities. The percentage of impurities we had in the gas were: O_2: 0.001%; H_2O: 10 mg/m^3 with a pressure of 4 atm.

The gas purifier we have used consists of a steel cylinder the upper and lower parts of which are connected to the ionization chamber, as it is seen in Fig. 1. The copper straps (1.4 cm thick and 0.01 cm thin) are stretched between two copper disks inside the cylinder, parallel to its axis. These two disks are fixed at the end of two large copper

(1) D. H. Wilkinson: *Ionization chambers and counters* (Cambridge, 1950).

(2) B. B. Rossi and H. H. Staub: *Ionization chambers and counters* (New York, 1949).

conductors, tightly fastened through the cylinder covers. The straps are heated by means of a high intensity alternating

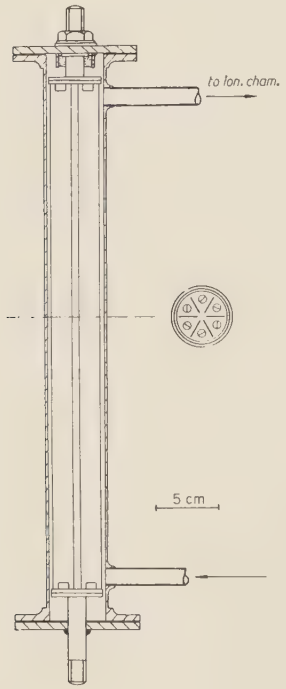

Fig. 1. – Design of the purifier.

current, obtained from a step down trasformer having a power of 2 kW. The chamber and the gas purifier are placed vertically in order to obtain, by heating a strong convective gas stream which favours an intense purification. The intensity of the current flowing through the straps can be varied to have variable temperatures. It has been noted that a temperature of about 500 °C (obtained with a current of 600 A) was sufficient to get a satisfactory purification of the gas.

The purification thus obtained has been experimentally cheked by detecting the integral spectrum of a Po α source placed on the inner walls of the chamber. At the beginning, operating with no purified gas, no pulses have been given by the electronic circuit. The first pulses were observed half an hour after the heating of the straps was started. Three hours of continuous heating has been found sufficient to get the integral spectrum of the α-particles. As an illustration we give in Fig. 2 the integral spectrum for various purification intervals.

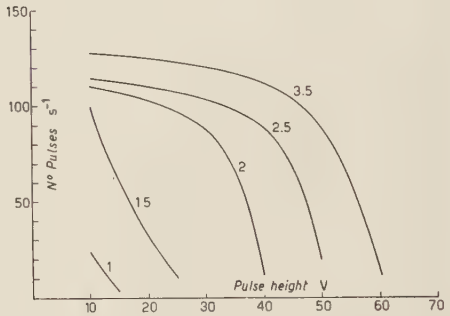

Fig. 2. – Integral spectrum of the α-particles for various time intervals, in hours.

A similar set-up, having dimensions proportionally enlarged and working with forced circulation, has been used also for purifying the argon of a 80 l ionization chamber at 10 atm. Also in this case the results have been found satisfactory.

LIBRI RICEVUTI E RECENSIONI

O. R. Frisch – *Progress in Nuclear Physics.* Pergamon press) London e New York, 1955, vol. IV, pp. 739 70 scellini.

Questo punto dell'opera che qui consideriamo, segue essenzialmente l'indirizzo dei tre precedenti presentando una raccolta di articoli che vanno dalla descrizione di tecniche sperimentali alla teoria pura. Ecco l'indice del volume: E. W. Titterton, Esperienze di fotodisintegrazione con emulsioni nucleari; E. Breitenberg, Statistica dello spettrometro a scintillazione; R. H. Dalitz, Fenomeni mesonici e teoria mesonica; T. G. Pickavance, Focheggiamento negli acceleratori per alte energie; W. E. Burcham, Spin isotopico e reazioni nucleari; D. Walker: Ioni pesanti di alta energia; J. O. Newton, Proprietà nucleari degli elementi pesantissimi; H. A. C. McKay e J. Milsted, Preparazione e chimica degli elementi transuranici; D. J. Hughes, Spettroscopia neutronica.

Dare un giudizio di un'opera del genere non è impresa facile poichè difficilmente il recensore è dotato di adeguata competenza in tanti campi diversi. Chi scrive si trova purtroppo in questa condizione e deve riconoscere che ad alcuni degli argomenti del volume si è accostato la prima volta attraverso le pagine di esso, e proprio per questo motivo può riconoscere l'efficacia dell'opera. È tuttavia proprio l'intento di questa serie di offrire al lettore non specializzato la possibilità di aggiornarsi su argomenti che non riguardano il suo campo specifico di lavoro. Questo scopo è raggiunto se i diversi articoli rappresentano un compromesso fra il metodo induttivo e quello deduttivo da cui risultino chiare le idee centrali di ciascun campo e la base sperimentale su cui esse riposano.

Giudicati sotto questo aspetto i vari articoli presentano meriti assai diversi. Cominciamo dai due lavori più specificamente tecnici. Il primo, di Breitenberg, sulla statistica dei contatori a scintillazione, risponde adeguatamente ai requisiti specificati più sopra. Forse sarebbe stato desiderabile, almeno per un teorico, uno sviluppo un po' più ampio della matematica delle funzioni generatrici la quale, come nota l'A. non si trova adeguatamente esposta che in lavori difficilmente accessibili. Tuttavia l'articolo riuscirà assai utile sia a chi vuole iniziarsi all'uso di questa tecnica, sia a chi già la conosce ma vuole studiarne criticamente l'applicazione. Su un piano diverso è invece l'articolo di Pickavance sul focheggiamento negli acceleratori di particelle. L'A. afferma esplicitamente di rivolgersi al fisico nucleare e non allo specialista di acceleratori, ma a giudizio di chi scrive, non tiene fede all'impegno. Manca una esposizione chiara dei principi fisici del focheggiamento, riassunti in maniera che può

piacere più ad un ingegnere costruttore che ad un fisico. Le utilissime analogie ottiche non sono neppure accennate, mentre vi si trovano diagrammi scarsamente perspicui. I principi del focheggiamento a gradiente alternato sono soltanto accennati e il famoso diagramma a « cravatta a quadretti scozzesi » apparso su tanti « preprints » e su tante lavagne delle aule dei seminari è riprodotto senza le spiegazioni necessarie a renderne chiaro il contenuto. Anche il paragrafo dedicato ai problemi economici è alquanto vago: vi si trova affermato che « una riduzione apprezzabile (delle oscillazioni delle particelle) farebbe risparmiare una gran quantità di denaro ». Dopo tutte le ricerche sul problema del focheggiamento si desidererebbe qualcosa di più preciso.

Veniamo ora agli articoli più prettamente fisici. Quello di TITTERTON sulle reazioni di fotodisintegrazione riassume brillantemente le ricerche recenti in questo campo al quale l'A. ha portato tanti contributi. Forse i dettagli sulla tecnica delle emulsioni nucleari sono un po' troppo condensati e forse la discussione sulle teorie di Goldhaber e Teller, e di Bethe e Levinger non è del tutto convincente. In compenso i processi di fotodisintegrazione diretta sono trattati con estrema chiarezza e così pure l'influenza delle regole di selezione derivanti dall'indipendenza dalla carica. Anche la discussione dei dati sperimentali è completa ed esauriente. Altrettanto lucida è l'esposizione che BURCHAM dà dell'importanza dello spin isotopico per la fisica nucleare. Il contenuto fisico del formalismo è esposto con estrema chiarezza e le diverse conferme sperimentali delle ipotesi dell'indipendenza dalla carica delle forze nucleari sono vagliate criticamente (livelli nucleari, interazione nucleone-nucleone, regole di selezione, interazione mesone-nucleone). Alcune poche inesattezze (per esempio a pag. 179 l'analogia dell'operazione di simmetria di carica con l'inversione spaziale) rappresentano gli unici appunti che lo scrivente trova da fare a questo articolo che per altro riuscirà certo utilissimo a chi voglia introdursi all'argomento.

Meno convincente sembra invece il capitolo di NEWTON sulle proprietà nucleari degli elementi pesantissimi. L'equilibrio, così notevole nei due precedenti articoli fra teoria e dati sperimentali, è qui rotto a scapito della teoria e insieme della chiarezza. I cenni sul modello di Bohr-Mottelson e su quello a shell sono insufficienti a chiarirne le idee fondamentali onde molti dei dati sperimentali perdono per il lettore non iniziato una parte del loro interesse mancando di un adeguato inquadramento teorico. Fatta questa riserva si deve però riconoscere che i dati sperimentali qui raccolti risulteranno certamente di grande utilità a chi voglia orientarsi nella fitta selva dei lavori originali. L'articolo di WALKER sull'accelerazione degli ioni pesanti è di lettura molto piacevole e offre un quadro preciso dello stato attuale dell'argomento. L'A. concentra la sua attenzione sui metodi di accelerazione (particolarmente interessante l'esposizione del metodo della terza armonica) mentre la discussione delle reazioni nucleari iniziate dagli ioni pesanti è forzatamente schematica principalmente a causa della scarsità dei dati oggi conosciuti.

L'ultimo dei lavori di fisica nucleare è quello di HUGHES sulla spettroscopia neutronica. In esso la chiara descrizione dei metodi sperimentali si accompagna ad una interessantissima discussione di come si ricavino dai dati sperimentali i parametri dei livelli nucleari. Infine questi parametri sono confrontati con quelli previsti dalla teoria riassunta in un paragrafo un po' breve seppure chiaro. Se un appunto si può fare a questo articolo è proprio la brevità con cui è accennato il così detto « cloudy crystal ball model » che pur sembra tanto promettente nell'interpretazione delle risonanze neutroniche. Comunque questo articolo

è senza dubbio utilissimo e riassume molto chiaramente l'enorme sviluppo che in questo campo si è avuto negli ultimi due anni.

L'articolo di DALITZ sulla teoria mesonica si stacca notevolmente dal tono generale del volume in quanto di lettura assai più difficile e rivolto palesemente ad un pubblico più specializzato. I paragrafi sulle proprietà sperimentali dei mesoni π (particolarmente efficace questo nel riassumere i vari metodi che hanno permesso di determinare tali proprietà), sullo scattering mesone-nucleone, e sulla fotoproduzione di mesoni costituiscono una rassegna di questi argomenti assai chiara. Meno convincente è il paragrafo sulla teoria dei campi, troppo condensato per chi non conosca l'argomento e forse superfluo per gli esperti.

L'ultimo articolo di cui dobbiamo occuparci è quello di MCKAY e MILSTED sulla chimica degli elementi transuranici. Data la scarsa competenza chimica di chi scrive gli è difficile valutarne il valore intrinseco: basterà dire che la lettura di alcune parti gli risultò assai più interessante e piacevole di quanto non avesse anticipato.

L. A. RADICATI

L. DE BROGLIE – *Théories Générales des particules a spin (Métodes de Fusion)*; Parigi, Gauthier-Villars, II edizione 1954.

LOUIS DE BROGLIE dedica questo volume alla teoria delle particelle con spin. I primi sei capitoli sono dedicati alla esposizione di premesse generali sulla meccanica ondulatoria e sui momenti angolari ed alla esposizione della teoria di Dirac per particelle a spin $\frac{1}{2}$. Nei restanti capitoli e nell'appendice viene trattata la teoria delle particelle a spin superiore, costruita con il metodo della fusione dovuto all'autore stesso. È fuori di dubbio l'interesse teorico del problema reso attuale in questi ultimi tempi dalla scoperta di nuove particelle, di cui, tra l'altro, non si sanno i valori degli spin.

Uno dei pregi del volume, che del resto si riscontra nelle altre opere didattiche di DE BROGLIE, è la chiarezza nella esposizione. Nei primi due capitoli vengono svolti i più semplici elementi della meccanica ondulatoria e ne viene discussa brevemente l'interpretazione fisica. Particolarmente riusciti sono il terzo ed il quarto capitolo. Il terzo capitolo contiene gli elementi della teoria quantistica dei momenti angolari, le cui relazioni di commutazione vengono riportate, in maniera intuitiva ed elementare alla geometria delle rotazioni spaziali. Il capitolo quarto è dedicato alla discussione dei momenti angolari dal punto di vista relativistico, che viene svolta in maniera semplice e con particolare accento su argomenti di carattere fisico. I due capitoli successivi comprendono la teoria dell'elettrone di Dirac e la sua interpretazione fisica.

Il resto del libro è dedicato alla teoria delle particelle con spin superiore. Due alternative sono, tra l'altro, a priori possibili per cercare una descrizione di particelle a spin superiore. La prima consiste nel cercare delle equazioni d'onda che descrivano solamente la particella di spin s; la seconda alternativa, cui l'autore è condotto dal suo metodo della fusione, consiste invece nel cercare delle equazioni per la particella « spin massimo s », che possiede diversi stati di spin totale, corrispondenti, a seconda che s sia intero o semintero, a tutti i valori interi o seminteri minori od uguali ad s. In assenza di interazioni si ottengono gruppi di equazioni indipendenti per i diversi stati di spin totale, che possono pertanto venire considerati ciascuno isolatamente. Perchè questo sia ancora lecito in presenza di interazioni, occorrono, come è chiaro, delle precise restrizioni sulla forma che queste interazioni possono avere. Non vogliamo qui discutere i successi e le difficoltà della

teoria della fusione per la descrizione di particelle a spin superiore. Come è noto, questo campo di ricerche sulle equazioni d'onda per particelle a spin superiore deve ancora ritenersi in fase di sviluppo e contributi indipendenti e diversi vi sono stati pure portati da DIRAC, FIERZ e PAULI, da CHANDRA e da BHABHA.

« Diverses raisons — riportiamo infine dal volume di DE BROGLIE — rendent assez vraisemblable que les corpuscules physiques véritablement élémentaires ont tout le spin $\frac{1}{2}$ et que, par suite, les particules de spin différent de $\frac{1}{2}$ sont complexes.... L'hypothèse que nous suggérons est évidemment, par sa nature même, aventureuse, mais l'histoire de la Physique a montré que ce genre d'hypothèse, qui tend à réduire le nombre des entités indépendantes, a souvent réussi en Physique ».

R. GATTO

F. LÖSCH – *Siebenstellige Tafeln der elementaren transzendenten Funktionen*, 1 vol. in-4°, pagg. VIII-335, Springer-Verlag, Berlin-Göttingen-Heidelberg, 1954, rilegato, DM 49.80.

Le presenti tavole sono le prime, dopo quelle di HAYASHI (1926), che raccolgono in un'unica opera di facile consultazione ed adatta a più tipi di calcoli la tabulazione con molti decimali delle funzioni trascendenti elementari. La materia è così ripartita: TAV. I: *Valori con nove cifre decimali delle funzioni trascendenti elementari per* $x = 0$ (0.0001) 0.1. - TAV. II: *Valori con sette cifre decimali delle funzioni trascendenti elementari per*: a) $x = 0.1$ (0.0005) 3.15; b) $x = 3$ (0.01) 10; c) $x = 10$ (0.1) 20; d) *valori di* tg x *per* x *prossimo a* $\pi/2$; e) *valori di* sett tgh x *e di* sett ctgh x *per* x *prossimo a* 1. - TAV. III: *Valori con sette cifre decimali di alcune funzioni elementari per* $x = 0$ (1) 100. - TAV. IV *Valori con dodici cifre decimali di* $(\pi/2)$ *per* $n = 0$ (1) 100. - TAV. V: *Valori con sette cifre decimali delle funzioni* $\sin(\pi/2)x$, $\cos(\pi/2)x$ *per* $x = 0$ (0.001) 0.5. - TAV. VI: *Valori con sette cifre decimali delle funzioni* $e^{(\pi/2)x}$, $e^{(\pi/2)x}$, $\sinh(\pi/2)x$, $\cosh(\pi/2)x$ *per* $x = 0$ (0.01) 2. - TAV. VII: *Valori con sette cifre decimali delle funzioni* $e^{\pi x/180}$, $e^{-\pi x/180}$, $\sinh \pi x/180$, $\cosh \pi x/180$ *per* $x = 0$ (1) 180. - TAV. VIII: *Trasformazione di radianti* (x) *in gradi* (φ). - TAV. IX: *Trasformazione di gradi* (φ) *in radianti* (x). - TAV X: *Alcuni valori numerici di uso frequente.*

(*N*.B. - Il simbolo $x = 0$ (1) 100 indica che x varia di unità in unità da 0 a 100).

La parte fondamentale dell'opera (che occupa 287 delle 335 pagine) è costituita dalla TAV. I e dalla sezione *a*) della TAV. II. In tale parte la tabulazione si svolge sulle coppie di pagine affacciate (pari-dispari); la prima colonna riporta i valori di x, la seconda i corrispondenti valori in gradi, primi e secondi, fino ai centesimi di secondo; i valori di x sono ripetuti nella prima colonna della pagina dispari. Le altre tredici colonne contengono i valori e le differenze tabulari delle funzioni $\sin x$, $\cos x$, $\sinh x$, $\cosh x$, $\tgh x$, $\log x$, e^x, e^{-x}, $\arc\sin x$, $\arc\tg x$, $\operatorname{sett}\sinh x$, $\operatorname{sett}\cosh x$, $\operatorname{sett}\tgh x$, $\operatorname{sett}\ctgh x$ (secondo l'uso tedesco, per le funzioni iperboliche e le loro inverse si usano i simboli: $\mathfrak{Sin}\, x$, $\mathfrak{Cof}\, x$, $\mathfrak{Tg}\, x$, $\mathfrak{Ar}\,\mathfrak{Sin}\, x$, $\mathfrak{Ar}\,\mathfrak{Cof}\, x$, $\mathfrak{Ar}\,\mathfrak{Tg}\, x$, $\mathfrak{Ar}\,\mathfrak{Cgt}\, x$, e per il logaritmo naturale il simbolo $\ln x$): s'intende che per $x < 1$ mancano le funzioni $\operatorname{sett}\cosh x$ e $\operatorname{sett}\ctgh x$, e, per $x > 1$, le funzioni $\arc\sin x$ e $\operatorname{sett}\tgh x$; ciò provoca un cambiamento di posto delle colonne dedicate alle funzioni $\arc\tg x$ e $\operatorname{sett}\sinh x$. Le funzioni e le differenze tabulari sono riportate col loro valore naturale, ivi compresa l'indicazione del segno, senza alcuna particolare convenzione; le prime cifre dei valori delle funzioni e delle differenze sono riportate in testa e in fondo alla relativa colonna; il loro eventuale cambiamento nella colonna stessa è indicato con uno o con due asterischi. L'ultima

cifra tabulata è arrotondata con le usuali convenzioni. Quando il passo è 0.0005 la differenza tabulare è raddoppiata, cioè riportata al passo 0.001, e ciò evidentemente per facilitare l'interpolazione lineare; occorre però tenerne conto nell'eventuale calcolo della differenza seconda. Inoltre il passo è scelto in modo che l'interpolazione lineare fornisca quasi ovunque un errore non superiore alle due unità dell'ultimo posto decimale tabulato; nei piccoli tratti di tavola dove ciò non accada se ne dà esplicito avviso scrivendo la differenza tabulare in caratteri corsivi ovvero omettendola; in questi casi è generalmente sufficiente l'interpolazione con la formula di NEWTON arrestata al termine del second'ordine. In alcune pagine si adottano talune convenzioni in aggiunta a quelle dette; esse sono indicate a piè di ciascuna pagina. La parte fondamentale dell'opera è completata dalle sezioni *d*), *e*) della TAV. II, che riportano al passo 0.0001 la tabulazione delle funzioni indicate, nell'intorno del loro punto singolare.

Per quanto riguarda il resto dell'opera, l'indice sopra riportato dà già un'esauriente spiegazione. Aggiungiamo che la TAV. III comprende le funzioni $\sin x$, $\cos x$, $\log x$, e^x, e^{-x}, sett $\sinh x$, sett $\cosh x$; le funzioni e^x, e^{-x} sono fornite, anzichè con sette posti decimali, con sette cifre significative (ad es. $e^{50} = 0.5184706 \cdot 10^{22}, e^{-50} = 0.1928750 \cdot 10^{-21}$). La TAV. VIII dà i valori in gradi, primi e secondi (con sette posti decimali per i secondi), ovvero in gradi (con dodici cifre decimali) delle varie unità degli ordini da 10^{-4} a 10^{1} (e, s'intende, dei loro multipli da 1 a 9).

La TAV. IX riporta con dodici decimali i valori in radianti degli angoli $\varphi = 0^\circ$ (1°) 90°, 0′ (1′) 60′, 0″ (1″) 60″. Nella TAV. X si trovano: *a*) i valori e gli inversi, con quindici decimali, delle costanti abituali (2, *e*, π, ecc.); *b*) i numeri di BERNOULLI (di indice pari) fino a B_{40}, in forma frazionaria (ad es. $B_{14} = 7 : 6$); *c*) i fattoriali e i loro logaritmi decimali, con quindici cifre decimali, nonchè i loro inversi con quindici cifre significative, fino a 15!; d) i coefficienti binomiali $\binom{n}{k}$, fino a $n = 15$.

Da quanto si è detto risulta evidente la facilità dell'uso di queste tavole; la loro lettura è resa ancor più agevole dall'accurata disposizione tipografica, dalla perfezione della stampa e dalla bellezza dei caratteri. La separazione delle cifre è fatta in gruppi di quattro ovvero di cinque cifre (a partire dalla virgola decimale) a seconda del numero dei posti adottati nella tavola. L'opera è preceduta da una prefazione e da un'introduzione; in questa si danno alcune norme per l'uso; nè, data la chiarezza del testo, sarebbero necessarie spiegazioni più particolareggiate.

M. BENEDICTY

Table de fonctions de Legendre Associées; I° fascicolo. Editore « La Revue d'Optique » Paris 1952, pagg. 292 + XXIII.

Il Centre Nationale d'études des Télécommunications ha programmato una estesa tabellazione delle funzioni associate di Legendre $P_n^m(\cos\theta)$ per valori non interi di n, funzioni che intervengono in numerosi problemi applicativi, in particolare nel calcolo delle antenne. Il fascicolo qui recensito costituisce il primo passo verso la realizzazione di tale programma.

Oltre che colmare le lacune esistenti nella conoscenza numerica di tali importanti funzioni, il Centro si propone anche di rendere le tabelle stesse accessibili al più vasto pubblico possibile, compresi i cultori isolati e a questo scopo la pubblicazione sfrutta gli accorgimenti di stampa e di legatura che riducendo il costo, non compromettono la maneggevolezza e nitidezza del fascicolo.

Le funzioni ora tabellate dànno i valori di $P_n^m(\cos\theta)$ per θ compreso tra 0° e 90° (col passo di 1°) e per i valori di $m=0, 1, 2, \ldots, 5$; n crescente da $-0{,}5$ a 10 col passo di 0.1.

I calcoli sono stati eseguiti dal Service Mécanographique de l'Armée de Terre. Poichè il procedimento di tabellazione fa largo uso delle catene di relazioni di ricorrenza per ottenere i valori delle funzioni a partire dai valori calcolati dagli sviluppi in serie, il numero di cifre significative riportate decresce con l'allungarsi delle catene, da 10 a 4, nelle peggiori condizioni. Mediante verifiche effettuabili non son stati rilevati errori di stampa.

Lo sviluppo del programma prevede in primo luogo di estendere le tabelle al secondo quadrante dell'angolo θ.

A. Borsellino

Direttore responsabile: G. Polvani Tipografia Compositori - Bologna

Questo fascicolo è stato licenziato dai torchi il 30-VIII-1955